Glucocorticoid Regulation of Lung and Kidney Organogenesis During Mouse Fetal Development

By Kelly Louise Short

Bachelor of Science (Honours in Biochemistry)

A thesis submitted for the degree of *Doctor of Philosophy* at

Monash University in 2020

Monash Biomedical Discovery Institute

Monash University, Clayton

Faculty of Medicine, Nursing & Health Science

Copyright notice

Declaration

I hereby declare that this thesis contains no material which has been accepted for the award of any other degree or diploma at any university or equivalent institution and that, to the best of my knowledge and belief, this thesis contains no material previously published or written by another person, except where due reference is made in the text of the thesis.

This thesis includes one original paper published in peer reviewed journals and one un-submitted narrative. The core theme of the thesis is "Glucocorticoid signalling in the developing lung and kidney". The ideas, development and writing up of all the papers in the thesis were the principal responsibility of myself, the student, working within the Biochemistry Department, Monash University, Clayton, Melbourne, Australia under the supervision of A/Prof Timothy. J. Cole.

The inclusion of co-authors reflects the fact that the work came from active collaboration between researchers and acknowledges input into team-based research. In particular, the following should be noted: Supporting ideas, experimental direction, manuscript revision were provided by Assoc. Prof. Timothy Cole, Prof. Stuart B Hooper, Assoc. Prof. Megan J Wallace, Dr Annie R A. McDougall and Dr Alexander N. Combes. RNA sequencing in chapter 3 and 4 was performed by Genewiz, Biotechnology, Suzhou, China. Single cell data used in chapter 4 was produced and analysed by Rachel Lam, Dr Julie Moreau and Dr Alexander N Combes. Technical assistance in chapter 2, 3 and 4 was provided by Judy Ng, Bennet Seow and Spencer Greatorex.

Thesis Chapter	Publication Title	Status *(published, in press, accepted or returned for revision, submitted)*	Nature and % of student contribution	Co-author name(s) Nature and % of Co-author's contribution*	Co-author(s), Monash student Y/N*
2	Glucocorticoid signalling drives reduced versican levels in the fetal mouse lung	Accepted	70% contribution Project direction, qPCR, immunohistochemistry, westernblotting and writing first draft	Dr A Daniel Bird supporting ideas, experimental direction 8%	N
				A/Prof Timothy J Cole Project design and manuscript editing 9%	N
				Dr Bennet K L Seow cell culture 3%	N
				Judy Ng Genotyping 2.5%	N
				Dr Annie R A McDougall manuscript editing 2.5%	N
				A/Prof Megan J Wallace manuscript editing 2.5%	N
				Prof Stuart B Hooper manuscript editing 2.5%	N

I have / have not renumbered sections of submitted or published papers in order to generate a consistent presentation within the thesis.

Student name: Kelly Lousie Short

Date: 2/06/20

I hereby certify that the above declaration correctly reflects the nature and extent of the student's and co-authors' contributions to this work. In instances where I am not the responsible author I have consulted with the responsible author to agree on the respective contributions of the authors.

Main Supervisor name: Assoc. Prof Timothy Cole

Date: 2/06/20

Contents

List of Abbreviations

11β-HSD1	11β-hydroxysteroid dehydrogenase 1
11β-HSD2	11β-hydroxysteroid dehydrogenase 2
ACAN	Aggrecan
ACTH	Adrenocorticophic hormone
ACVR2A	Activin receptor IIA
ADAMTS	A disintegrin and Metalloprotease with ThromboSondin Motifis
ADAMTS12	A disintegrin-like and metallopeptidase with thrombospondin type 1 motif, 12
ADAMTS18	A disintegrin-like and metallopeptidase with thrombospondin type 1 motif, 18
ADAMTSL2	ADAMTS-like 2
ADAMTSL4	ADAMTS-like 4
AEC	Alveolar epithelial cell
AIM	Anterior intermediate mesoderm
AR	Androgen receptor
ASDN	Aldosterone sensitive nephron
ASHSG	α-2-HS-glycoprotein
AVP	Arginine vasopressin
BMP4	Bone morphogenetic protein 4

BPD	Bronchopulmonary dysplasia
CAV1	Caveolin 1, caveolae protein
CBG	Corticosteroid binding globulin
CDH1	Cadherin 1
CEBPA	CCAAT/enhancer binding protein (C/EBP), alpha
CEMIP	Cell migration inducing protein, hyaluronan binding
CEP290	Centrosomal protein 290
CLD	Chronic lung disease
COL15A1	Collagen, type XV, alpha 1
COL7A1	Collagen, type VII alpha 1
COLA1	Collagen type III alpha 1
COPD	Chronic obstructive pulmonary disease
CRH	Corticotrophin releasing hormone
CRHR1	CRH receptor 1
CRISP1	Cysteine-rich secretory protein 1
CRISPLD2	Cysteine-rich secretory protein LCCL domain containing 2
DBD	Zinc-finger DNA binding domain
DCN	Decorin
DCT1	Early distal convoluted tubule
DCT2	Late distal convoluted tubule

DLK1	Delta like non-canonical Notch ligand 1
DOHaD	Developmental origins of health and disease
DPBS	Dulbecco's phosphate-buffered saline
DPPC	Dipalmitoylphosphatidylcholine
ECM	Extracellular matrix
ECM1	Extracellular matrix protein 1
ELN	Elastin
ENAC	Epithelial sodium channel
ER	Estrogen receptor
EYA1	EYA transcriptional coactivator and phosphatase 1
FACS	Fluorescence-activated cell sorting
FASN	Fatty acid synthase
FDR	False discovery rate
FGF10	Fibroblast growth factor 10
FGF2	Fibroblast growth factor 2
FGF9	Fibroblast growth factor 9
FGFR1C	Fibroblast growth factor receptor 1c
FGFR2C	Fibroblast growth factor receptor 2c
FIBIN	Fin bud initiation factor homolog
FKBP5	FK506 binding protein 5

FKBP5	FK506 binding protein 5
FN1	Fibronectin
FOXA2	Forkhead box A2
FPKM	Fragments per kilobase of transcripts per million
FPKM	Fragments per kilobase of transcript per million mapped reads
FZD2	Frizzled class receptor 2
GAGs	Glycosaminoglycans
GATA3	GATA binding protein 3
GATA6	GATA binding protein 6
GBP7	Guanylate binding protein 7
GC	Glucocorticoid
GDF1	Growth differentiation factor 1
GDNF	Glial cell line-derived neurotrophic factor
GFRA1	Glial cell line-derived neurotrophic factor
GILZ	Glucocorticoid-induced leucine zipper
GLI1	GLI-Kruppel family member GLI1
GLI2	GLI-Kruppel family member GLI2
GR	Glucocorticoid Receptor
GRcdKo	Mice lacking the GR in the collecting duct of the kidney
GRE	Glucocorticoid response element

GREM1	Gremlin 1, DAN family BMP antagonist
GRepikO	Mice lacking the GR in the epithelium
GRmesKO	Mice lacking the GR in the mesenchyme
GRnull	Total GR deficient mouse
HBA1-A1	Hemoglobin alpha, adult chain 1
HOP	HSP70-HSP90 organising protein
HPA	Hypothalamic-pituitary-Arenal axis
HSP	Heat shock protein
IFI203	Interferon activated gene 203, 2'-5'
IFIT1	Interferon-induced protein with tetratricopeptide repeats 1
IGFBP3	Insulin-like growth factor binding protein 3
IPF	Idiopathic pulmonary fibrosis
IVF	In Vitro Federalisation
KAP	Kidney androgen regulated protein
KIF3A	Kinesin family member 3A
LBD	Ling binding domain
LEFTY1	Left-right determination factor 1
LEFTY2	Left-right determination factor 2
LHX1	LIM homeobox protein 1
LPCAT	Lysophosphatidylcholine acltransferase

MATAN2	Matrilin 2
MC2R	ACTH receptor
MDS	Multidimensional scaling
mGR	Membrane-bound GR
MMPs	Matrix metalloproteinases
MNDAL	Myeloid nuclear differentiation antigen like
MR	Mineralocorticoid receptor
NCC	Thiazide-sensitive Na^+/Cl^- cotransporter
NDP	Norrie disease (pseudoglioma) (human)
NFATC1	Nuclear factor of activated T cells, cytoplasmic, calcineurin dependent 1
NFATC2	Nuclear factor of activated T cells, cytoplasmic, calcineurin dependent 2
NFATC3	Nuclear factor of activated T cells, cytoplasmic, calcineurin dependent 3
NGS RNA seq	Next generation RNA sequencing
NHE3	Sodium transport, sodium and hydrogen exchanger 3
NKCC2	Na-K-Cl cotransporter-2
NKX2.1	NK2 homeobox 1
Nr3c2	Nuclear receptor subfamily 3, group C, member 2

Nr3cl	Nuclear receptor subfamily 3, group C, member 1
NTD	N-terminal transactivation domain
OAS2	Oligoadenylate synthetase 2
OASL2	2’-5’ Oligoadenylate synthetase-like 2
PAS	Periodic acid-Schiff
PAX2	Paired box 2
PAX8	Paired box 8
PBS	Phosphate-buffered saline
PC	Phophatidycholine
PCYT1	Phospocholine cytidyltransferase
PENK	Preproenkephalin
PI	Propidium iodide
PIM	Posterior intermediate mesoderm
PITX2	Paired-like homeodomain transcription factor 2
POSTN	Periostin osteoblast specific factor
PPARG	Peroxisome proliferator activated receptor gamma
PR	Progesterone receptor
q-value	FDR adjusted p-value
RDS	Respiratory distress syndrome
RELN	Reelin

RPS29	Ribosomal protein 29
RSPO2	R-spondin 2
S100G	S100 calcium binding protein G
SALL1	Spalt like transcription factor 1
SGK1	Serum/glucocorticoid regulated kinase 1
SHH	Sonic hedgehog
SIX2	Sine oculis-related homeobox 2
SLC6A2	Norepinephrine transporter, Solute carrier family 6 (neurotransmitter transporter, noradrenalin), member 2
SMOC2	SPARC related modular calcium binding 2
SOX2	SRY (sex determining region Y)-box 2
SP	Surfactant protein
SPON1	Spondin 1
SPRY2	Sprouty RTK signalling antagonist 2
TGFβ1	Transforming growth factor beta 1
TGM2	Transglutaminase 2, C polypeptide
TIMPs	Inhibitors of metalloproteinases
TNC	Tenascin C
tRA	*Trans*-retinoic acid
TTF1	Thyroid transcription factor 1

VCAN	Versican
VEGFA	Vascular endothelial growth factor A
VIM	Vimentin
WNT	Wingless-related integration site
WNT1	Wingless-type MMTV integration site family, member 1
WNT11	Wingless-type MMTV integration site family, member 11
WNT2	Wingless-type MMTV integration site family, member 2
WNT9b	Wingless-type MMTV integration site family, member 9B
WT1	Wilms tumor 1 homolog

Publications

Kelly L. Short, A Daniel Bird, Bennet K.L Seow, Judy Ng, Annie R.A. McDougall, Megan Wallace, Stuart B Hooper, Timothy J Cole. (2020) Glucocorticoid signalling drives reduced versican levels in the fetal mouse lung. J Mol.Endo 64(3): 155-164.

Bennet K.L. Seow, Annie R.A. McDougall, **Kelly L. Short**, Megan J. Wallace, Stuart B. Hooper and Timothy J. Cole. (2019) Identification of Betamethasone-Regulated Target Genes and Cell Pathways in Fetal Rat Lung Mesenchymal Fibroblasts. Endocrinology 160(8): 1868-1884.

Timothy J. Cole, **Kelly L. Short**, Stuart B. Hooper. (2019) The Science of steroids Seminars in Fetal and Neonatal Medicine 24: 170-175.

Conference Presentations and Abstracts

Kelly L Short, A. Daniel Bird, Judy Ng, Timothy J Cole. 2016 Expression and Steroid Regulation of Alternative Splice Forms of the Extracellular Matrix Veriscan Gene in the mouse lung. Lorne genome. Victoria, AU (poster presentation)

Kelly L Short, A. Daniel Bird, Judy Ng, Timothy J Cole. 2016 Glucocorticoids Repress the Extracellular Matrix Proteoglycan Versican V1 Isoform During Lung Development. Endocrine Society of Australia. Gold Coast Queensland, AU (Oral presentation)

8th Australian Development Biology workshop

Kelly L short, A. Daniel Bird, Judy Ng, Timothy J Cole. 2017 Glucocorticoid-Mediated Regulation of Versican during Murine Lung Development. Lorne genome, Victoria, AU (poster presentation)

Kelly L short, A. Daniel Bird, Judy Ng, Timothy J Cole. 2017 Glucocorticoid-Mediated Regulation of Versican Cell Signalling During Mouse Lung Development. 18th International Congress of Developmental Biology. Singapore (poster presentation) 14

Kelly L Short, A. Daniel Bird, Judy Ng, Timothy J Cole. 2017 Glucocorticoid Receptor-Mediated Signalling Inhibits Cell Proliferation via Repression of the V1 Isoform of Versican during Mouse Lung Development. Endocrine Society of Australia. Perth Western Australia, AU (oral presentation, ESA Novartis Junior Scientist finalist

Kelly L Short, A. Daniel Bird, Bennet K.L Seow, Timothy J Cole. 2018 Glucocorticoid Receptor-Mediated Signalling Inhibits Mesenchymal Cell Proliferation via Repression of the V1 Isoform of Versican during Mouse Lung Development. Society for Endocrinology BES. Glasgow, Scotland (Oral presentation)

Acknowledgements

Firstly, I would like to sincerely thank my supervisor Assoc. Prof. Tim Cole for your guidance, support and encouragement over the last four years. I have learnt so much from you and developed a keen interest in the field of endocrinology. Thank you for encouraging me to present my work at conferences and for giving me the opportunity by covering travel expenses. Furthermore, thank you for all your help with preparing this thesis including correcting numerous drafts. I couldn't have asked for a more amazing supervisor.

To the other Cole lab members, past and present, Dr Spencer Greatorex, Dr Bennet Seow, Judy Ng, Bethany Campbell and Dr Daniel Bird thank you for your friendship, support, help, time, advice, coffee runs and all the laughs. To my panel members, Prof. Phil Bird, Assoc. Prof Megan Wallace, Dr Robert De Matteo, Assoc. Prof Craig Smith, Dr Natalie Lister and my co-supervisor Prof Ian Smyth thank you for all your time, guidance and feedback. I would also like to thank and acknowledge the whole Smyth lab, Lynelle Jones, Dr Denny Cottle, Dr Kerian Short, Dr Gloria Ursino, Ming Shen Tham and Allara Zylberberg for your generosity, help and kidney expertise.

I wish to also acknowledge the technical support and advice from the staff of Micromon Genomics, Monash Histology Platform, Monash Micro Imaging and the Biochemistry Imaging Facility. The work presented in this thesis was supported by the National Health and Medical Research Council (NHMRC) and my candidature was supported by a research training program (RTP) stipend funded by the Australian government.

To all my family and friends thank you for your support, friendship and continued encouragement over the last four years, a special mention to all the level 3 ADB PhD students thank you for the much-needed social distractions.

To my parents, Tammy and Alan Short thank you for all your support, encouragement, generosity and love. I am immensely grateful for everything you have done for me to make this possible. To my fiancé Peter Murphy, thank you for your continued support, love, friendship and patience.

Thesis Preface

The work presented in this thesis contains writings based on original work in requirement of the degree of the Doctor of Philosophy. Chapter 1 contains a current literature review, chapter 2 -4 contain writings based on the original work that was prepared as required for the degree. Chapter 5 is a general discussion and overview of the results presented in this thesis. This thesis is fewer than 80, 000 words in length.

Abstract

Mammalian lung development is a complex process that occurs over five overlapping stages termed the embryonic, pseudoglandular, canalicular, saccular and alveolar stages. Each stage is governed and regulated by a network of intrinsic transcriptional regulators and hormone-activated signalling pathways that coordinate the growth and development of the respiratory system. This thesis focuses on the role of glucocorticoid (GC) steroids for the transition from the canalicular stage to the saccular stage of development which is characterised by rapid tissue remodelling to mature the lung for efficient inflation at birth. This thesis also investigates GC actions in the fetal kidney close to birth. GC hormones acting via the glucocorticoid receptor (GR) are essential for normal lung maturation as mouse models deficient in the GR die shortly after birth due to respiratory failure. Furthermore, synthetic GCs such as dexamethasone and betamethasone are commonly used clinically to accelerate lung maturation in premature birth, although it is now recognised that they can have detrimental side-effects for the development of other organs that can persist into adulthood. There is therefore a need to understand the complex actions of endogenous GC signalling during fetal programming, that may inform on better treatments for the consequences of premature birth.

Despite the well-known importance of GCs in the maturation of the lung the underlying GC-regulated molecular mechanisms, gene networks and pathways regulated in the developing lung remains unclear. Conditional mouse knockout models of the GR have established that GR activity in the mesenchymal compartment of the lung is particularly crucial for survival at birth. Mice lacking the GR in the mesenchyme of the lung (GRmesKO) have a similar fate and phenotype to GRnull mice as they die at birth due to respiratory failure, with a hypercellular and thickened lung mesenchyme. Less is known about the actions of GCs via the GR in the developing fetal kidney.

The studies presented here investigate the gene targets and cell networks associated with GC hormone signalling in specific cells of the developing mouse lung and kidney by utilising conditional mouse GR knockout models. In the fetal lung my studies have shown that GCs regulate the expression of approximately 42 lung mesenchyme expressed genes associated with extracellular (ECM) remodelling and Wnt signalling that include Versican (*Vcan*), A disintegrin-like and metallopeptidase with thrombospondin type 1 motif 12 (*Adamts12*), Elastin (*Eln*), ADAMTS-like 2 (*Adamts-like 2*), R-spondin 2 (*Rspo2)*, Wingless-type MMTV integration site family, member 11 (*Wnt11*) and Cell migration inducing protein, hyaluronan binding (*Cemip*). Furthermore, I show that GC signalling drives the rapid reduction of VCAN protein from the mouse at E18.5 in part by the induction of the ECM protease ADAMTS12. In addition, I have shown that the GR is localised to restricted cell types in the fetal kidney from E13.5 with expanded localisation and expression of the GR to the renal proximal tubule, distal tubule, collecting ducts and stromal mesenchymal cells at E18.5. Finally, this thesis explored the role of the GR in the developing kidney by performing whole organ RNA-sequencing of the fetal kidney from mice with varying types of GR deficiency. I showed that complete absence of the GR has the most profound effect on the renal transcriptome with 454 genes differentially expressed including the primary cilia associated gene Centrosomal protein 290 (*Cep290*) and the tubule markers Kidney androgen regulated protein (*Kap*) (proximal tubule) and S100 calcium binding protein G (*S100g)* (distal tubule), with a more restricted set of genes altered in GRmesKO mice and very few changes in the fetal kidney from mice with collecting duct specific GR deletion (GRcdKO). In summary, my studies have identified GC target genes essential for ECM remodelling and Wnt signalling in the developing fetal mouse lung that warrant further studies, and investigated the role of the GR signalling during fetal kidney development. Understanding the complex actions of GC-GR hormone signalling will aid in the

development of new therapeutics to treat the complications of preterm birth and potentially avoid adverse effects from the use of synthetic GCs to treat prematurity.

List of Tables and Figures

Chapter 1

Chapter 2

Chapter 4

Chapter 1: Literature Review

1.1 Mammalian Lung Development

Mammalian lung development is composed of five over lapping stages referred to as the embryonic, pseudoglandular, canalicular, saccular and alveolar (Figure 1.1) (Herriges and Morrisey 2014; Post and Copland 2002). These stages encompass all the events required for life outside the aqueous environment of the womb. The stages of lung development differ slightly between humans and mice with the most notable difference being the timing of birth. Humans are born during the alveolar stage of development while mice are born during the saccular stage. Lung maturation is a complex process involving numerous transcription factors and mesenchymal cell - epithelial cell interactions (Table 1.1).

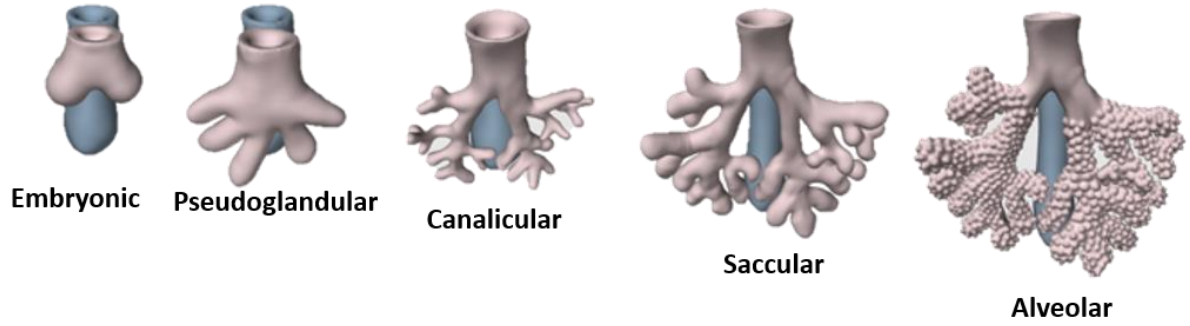

Figure 1.1 Schematic overview of lung development; Embryonic stage where two primary lung buds emerge from the forgut endoderm, the Pseudoglandular stage is characterised by extensive branching morphogenesis, the Canalicular stage involves remodelling of the distal regions of the developing lung, the Saccular stage is characterised by formation of sacculi by widening of the terminal ends of the respiratory tree and the Alveolar stage is when secondary septation occurs to form alveoli. Figure adapted from: (Beauchemin, et al. 2016)

Table 1.1: Timing, duration and transcription factors involved in mouse and human lung development

Stage of Lung Development	Duration	Transcription Factors and Growth Factors	References
Embryonic	Mouse: E9.5 – E12 Human: E26-E49 (4-7 weeks)	FGF10, FGF2, BMP4, SHH, Retinoic acid, TGFB1, GLI1, GLI2, NKX2.1 (TTF1)	(Herriges and Morrisey 2014; Kimura, et al. 1996; Sekine, et al. 1999)
Pseudoglandular	Mouse: E12-E16.5 Human: E35-E119 (5-17 weeks)	LEFTY1, LEFTY2, GDF1, PITX2, FGF10, FGF2, SPRY2, TGFB1, ACVR2A, SHH, BMP4, VEFGA, SOX2, NKX2.1, WNT1, ADAMTSL2, ADAMTS18	(Burri 1984; Cardoso and Lu 2006; Hubmacher, et al. 2015; Kitamura, et al. 1999; Meno, et al. 1998; Perl, et al. 2003; Rutledge, et al. 2019; Yin, et al. 2008)
Canalicular	Mouse: E16.5-E17.5 Human: E112-E182 (16-26 weeks)	GC, NKX2.1, CEBPA, GATA6, FOXA2, NFATC1, NFATC3	(DeFelice, et al. 2003; Martis, et al. 2006; Wan, et al. 2004; Yang, et al. 2002)

Saccular	Mouse: E17.5-P4 Human: E168-E266 (24-38 weeks)	GC, GR, GATA6, CEBPA, NFATC3, FOXA2, PPARG, VEGFA, CAV1, CDH1	(Cole, et al. 1995) (DeFelice et al. 2003; Martis et al. 2006; Wan et al. 2004; Yang et al. 2002)
Alveolar (stage 1)	Mouse: P4-P36 Human: E252 (36 weeks)- 21 years	TNC	(Burri 1974; Lindahl, et al. 1997)

1.1.1 The Embryonic Stage of Lung Development

The embryonic stage of lung development is characterised by the emergence of two primitive lung buds at E9.5 in the mouse or E26 in the human embryo from the ventral foregut endoderm, these buds will go on to form the right and left lung (Figure 1.1) (Cardoso and Lu 2006; Herriges and Morrisey 2014). The earliest marker of lung specification is the transcription factor NKX2.1 (TTF1) (Kimura et al. 1996; Minoo, et al. 1999) and high levels of expression have been detected at the position of lung bud formation on the ventral foregut endoderm. The lung buds are located on the left and right side of the emerging trachea (Schittny 2017). Through interactions with the surrounding mesenchymal tissue the lung buds become elongating into a bronchial tree. This process is driven by Fibroblast growth factor 10 (FGF10) in the surrounding mesenchyme, the importance of FGF10 is highlighted in the *Fgf10* null mouse where loss of *Fgf10* results in the cessation of branching (Sekine et al. 1999). In humans the left lung bud divides into two secondary bronchial buds that will form the two lobes of the left lung, the right lung bud divides into three secondary bronchial buds that will form the three lobes of the right lung (Merkus, et al. 1996). A similar process occurs in the rodent lung except

the right lung bud divides into four secondary bronchial buds that will give rise to the four lobes of the right lung, cranial, medial, caudal and accessory lobes while the left lung bud only gives rise to one lobe (Metzger, et al. 2008). The secondary bronchial buds undergo further dichromic branching and over generations of divisions result in the formation of the respiratory tree.

1.1.2 The Pseudoglandular Stage of Lung Development

The Pseudoglandular stage of lung development is characterised by the formation of the distal airways through a tightly regulated process of branching morphogenesis (Figure 1.1) (Herriges and Morrisey 2014). During this stage of lung development, the lung resembles a tubular gland. The epithelium branches out into the mesenchyme in a proximal to distal fashion by repeated dichotomous branching of the secondary lung buds (Merkus et al. 1996). Precise control of branching morphogenesis is essential to coordinate the patterning of the lung lobes. Additionally, most of the transcription factors essential to the embryonic stage of lung development are also important for branching morphogenesis, for example FGF10. FGF10 signalling in the mesenchyme directs the size and shape of the developing bronchial tree (Cardoso and Lu 2006). FGF10 activates Fibroblast growth factor 2 (FGF2) in the distal tips of the secondary lung buds promoting proliferation. FGF10 also activates Sprouty RTK signalling antagonist 2 (SPRY2) in the lung bud epithelium, SPRY2 is a FGF10-dependent inhibitor of FGF2 limiting proliferation and migration (Perl et al. 2003). Sonic hedgehog (SHH), Bone morphogenetic protein 4 (BMP4) and Transforming growth factor beta 1 (TGFβ1) also regulate FGF10 and FGF2 signalling (Cardoso and Lu 2006). SHH which is highly expressed in the distal epithelium of the lung buds negatively regulates FGF10 expression in the mesenchyme (Cardoso and Lu 2006). TGFβ1 which is also expressed in the adjacent mesenchyme stimulates synthesis of extracellular components required for branching including collagen I, collagen II and fibronectin (Cardoso and Lu 2006). Additionally, the

asymmetrical design of the lungs is highly dependent on various TGFβ-related transcription factors including Left-right determination factor 1 (LEFTY1), Left-right determination factor 2 (LEFTY2), Growth differentiation factor 1 (GDF1) and Paired-like homeodomain transcription factor 2 (PITX2) (Cardoso and Lu 2006; Kitamura et al. 1999; Meno et al. 1998). Together these molecules direct branching morphogenesis.

The epithelium also begins to differentiate into specialised cell types in a proximal to distal direction including; secretory cells which are involved in detoxification, ciliated cells which move debris along the airway, hormone-secreting neuroendocrine and goblet cells which produce mucus (Burri 1984; Herriges and Morrisey 2014). Additionally, α-smooth muscle cells start to form a layer around the future airways (Schittny 2017). These cells can spontaneously contract, and these spontaneous contractions are mechanical stimuli for branching morphogenesis and epithelial cell proliferation (Schittny, et al. 2000). Mechanical stimuli also activates the release of serotonin that promotes epithelial cell differentiation (Pan, et al. 2006). At the end of the pseudoglandular stage all the major conducting airways are formed.

1.1.3 The Canalicular Stage of Lung Development

The canalicular stage of lung development is characterised by extensive remodelling of the distal regions of the lung and the rapid expansion of the peripheral airways (Figure 1.1) (Herriges and Morrisey 2014). The mesenchyme tissue begins to decrease and an airway lumen starts to appear, coinciding with capillary growth in the surrounding mesenchyme (Herriges and Morrisey 2014). Airway widening triggers differentiation of cuboidal epithelia cells into type-1 and type-2 alveolar epithelial cells (AECs) (Flecknoe, et al. 2000). Type-1 AECs once differentiated start to cover the surface of the airway lumen (Schittny 2017). Once the lung is mature type-1 AECs will cover approximately 90% of the surface area and are responsible for gas exchange (Bolt, et al. 2001). Type-II AECs are found between the type -I AECs where the alveolar septa meet (Schittny 2017). At these locations the underlying capillaries come into

close contact with the epithelium forming the future blood-air barrier (Schittny 2017). Type-II AECs once differentiated start producing surfactant and store the surfactant in lamellar bodies (Harding, et al. 2003). The surfactant is secreted into the alveolar space by exocytosis and reduces surface tension. Type-II AECs cells unlike type I AECs that are terminally differentiated are primary progenitor for type I AECs. Many transcription factors are involved in the differentiation of alveolar cells including Glucocorticoid (GC) hormones (Cole, et al. 2004). Other molecules required for alveolar cell differentiation include TTF1, CCAAT/enhancer binding protein (C/EBP), alpha (CEBPA), Nuclear factor activated T cells, cytoplasmic, calcineurin dependent 1 (NFATC1), Nuclear factor activated T cells, cytoplasmic, calcineurin dependent 2 (NFATC2), GATA binding protein 6 (GATA6) and Forkhead box A2 (FOXA2) (DeFelice et al. 2003; Martis et al. 2006; Wan et al. 2004; Yang et al. 2002).

1.1.4 The Saccular Stage of Lung Development

The Saccular stage of lung development is when the terminal ends of the respiratory tree widen and form sacculi (Herriges and Morrisey 2014). These saccules then undergo further branching to form alveolar ducts, which are located at the outermost distal regions of the developing lung (Figure 1.1). The alveolar ducts go on to produce several alveolar sacs and the final dividing branches between the alveolar sacs are commonly referred to as “primary septum”. Also, during this stage of lung maturation, the mesenchymal tissue continues to thin and alveolar cells continue to differentiate into type I and type II AECs as sufficient production of surfactant and efficient gas exchange is required at birth. This is particularly important for rodents because they are born during the saccular stage (Amy, et al. 1977). Most of the transcription factors important for this stage of lung development overlap with the canalicular stage. In particular, GCs acting via the glucocorticoid receptor (GR) are essential for the thinning of the lung mesenchyme (Cole et al. 1995). The importance of GCs is well documented and GR-null mice

die shortly after birth due to respiratory failure as a result of an increased airway-blood barrier diffusion distance (Cole et al. 1995).

1.1.5 The Alveolar Stage of Lung Development

The alveolar stage of lung development is when the final gas exchange units are formed which are termed "alveoli". At the end of the saccular stage immature primary septa are present (Schittny 2017). These primary septa have a double-layered capillary network (Schittny 2017). During alveolarization secondary septa sprout from the walls of the primary septa with one of the capillary layers (Figure 1.2 b-c). The secondary septa form at locations where tenascin-C is highly expressed and myofibroblasts are present, to lay down elastic fibers and collagen (Figure 1.2) (Burri 1974; Lindahl et al. 1997). The space between two secondary septa forms the alveolus. Once the secondary septum has formed the two capillary layers fuse to form one efficient single layer, this process in known as microvascular maturation (Figure 1.2) (Caduff, et al. 1986). The mesenchymal tissue also continues to thin allowing the underlying capillaries to move into close proximity to the epithelium of the forming alveoli. To further reduce the diffusion distance the basement membranes of the capillary cells fuse with the epithelial cells (Schittny, et al. 1997). Until recently this process was thought to occur from P4 -P30 in the mouse and approximately 32 weeks till 2 years in humans however, it has now been demonstrated that alveolarization continues into young adulthood, reaching 200-300 alveoli in total (Pozarska, et al. 2017). This discovery has led to the proposed division of the alveolar stage into substages, and Schittny and colleagues have suggested dividing the alveolar stage into two stages; the classical alveolarization (mouse: P4-P21 and human E252 (36 weeks)-3 years) and continued alveolarization stages (mouse: P14-~P36 and Human: 2 years – young adult (17-21 years)) (Schittny 2017). While Beauchemin et al. based on transcriptome analysis have suggested that the alveolar stage should be divided into four substages (Beauchemin et al. 2016). A double-layered capillary network is still required in the continued /later stages of

alveolarization. This is achieved by upfolding of the capillary layer at sites of secondary septa formation. The gap in the capillary layer is swiftly filled via continued angiogenesis (Figure 1.2 e-h) (Schittny 2017).

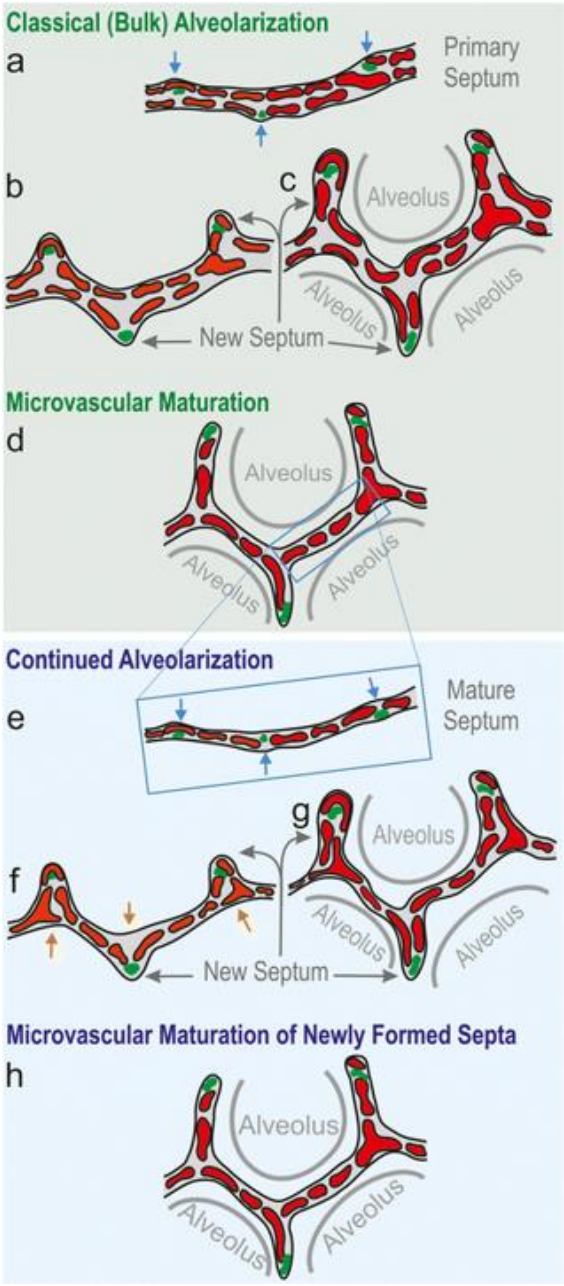

Figure 1.2 Schematic overview of alveolarization (A) Primary septum with a double layer of capillaries. (B-C) Secondary septa appear from places of high tenascin-C and where myofibroblasts are present (green areas). (D) During microvascular maturation the double capillary layer fuses to form one layer, the space between two septa creates the alveolus. (E) Mature septum with a single capillary layer. (F-G) The required double layer of capillaries is achieved by uplifting of the single layer; the gap is filled by angiogenesis (orange arrow). (H) Maturation of a newly formed septa Figure from (Schittny 2017).

1.1.6 The Developing Lung Mesenchyme

During all stages of lung development, the mesenchymal derived extracellular matrix (ECM) plays an important role in providing mechanical and structural support. However, it is now widely recognised that the mesenchyme also provides essential signalling cues that drive lung development, for example FGF10 signalling to promote lung bud formation in the embryonic stage of lung development, and later branching morphogenesis in the pseudoglandular stage (Cardoso and Lu 2006; Sekine et al. 1999). Proper lung development is also dependent on interactions between the mesenchyme, epithelium and mesothelium (McCulley, et al. 2015). This is highlighted in the mesothelial conditional-KO Fibroblast growth factor 9 (*Fgf9)* null mouse that has a reduction in airway branching as a result of loss of Wingless-type MMTV integration site family, member 2 (WNT2) expression in the mesenchyme (Yin, et al. 2011). The loss of FGF9 that normally signals to Fibroblast growth factor receptor 2c (FGFR2C) and Fibroblast growth receptor 1c (FGFR1C) in the mesenchyme reduces WNT2 expression leading to a reduction in β-catenin required for epithelial branching morphogenesis (Yin et al. 2011). Furthermore, epithelial deletion of Wnt Frizzled class receptor 2 (*Fzd2*) disrupts branch formation in the developing respiratory tree (Kadzik, et al. 2014). It is predicated that mesenchymal WNT signalling regulates new branch formation through the signalling with the epithelial localised FZD2 (Kadzik et al. 2014). Mesenchymal derived signalling also contributes to the differentiation of epithelial cells (McCulley et al. 2015). This was demonstrated in tissue recombination experiments that showed proximal tracheal mesenchyme could induce distal lung epithelium to express more of a proximal cell profile while, mesenchyme from the distal regions could induce proximal tracheal epithelium to take on a distal cell profile (Shannon, et al. 1998). The specific mesenchymal signalling molecules that drive epithelial cell differentiation remain elusive. The interactions of the mesenchyme and epithelium is a growing area of research in both fetal lung development and lung disease. The

ECM regulates cell differentiation, cell migration and helps guide the shape of the developing lung while, the lung epithelial cells control the production and breakdown of the ECM (Zhou, et al. 2018). Any alterations in this process can lead to abnormal lung development and may contribute to adult lung conditions including idiopathic pulmonary fibrosis (IPF), chronic obstructive pulmonary disease (COPD) and bronchopulmonary dysplasia (BPD) (Chanda, et al. 2016).

The composition of the ECM is very dynamic and changes over the course of lung development (Zhou et al. 2018). The ECM is also very heterogenous depending on the location in the lung for example, close to bronchi vs the outermost regions of the distal lung (Zhou et al. 2018). The developing fetal ECM is very distinct from the adult lung ECM. The fetal ECM tends to have more glycosaminoglycans (GAGs), proteoglycans and collagen in the pleura and alveolar septae compared to the adult lung (Bateman, et al. 1981). The developing fetal lung ECM also contains all five laminin γ chains while the adult ECM tends to only express three γ3, γ4 and γ5 (Nguyen, et al. 2005; Sorokin, et al. 1997). The developing ECM is constantly remodelling and adapting during lung development. In particular, GCs induced rapid thinning of the lung mesenchyme late in gestation to decrease the blood air barrier for efficient gas exchange (Bird, et al. 2007; Cole et al. 2004). Proteolytic enzymes including matrix metalloproteinases (MMPs) and their primary inhibitors known as tissue inhibitors of metalloproteinases (TIMPs) are responsible for the remodelling of the ECM during development. The adult lung has a more anti-proteolytic profile including higher expression of TIMPS than MMPS while the fetal lung is proteolytic with higher expression of MMPs than TIMPS (Ryu, et al. 2005).

1.2 Glucocorticoids and The Glucocorticoids Receptor

1.2.1 Glucocorticoid Hormones

GCs belong to the steroid hormone family and are synthesised from cholesterol in the adrenal gland (Acconcia and Marino 2016; Brown, et al. 1979). They are secreted from the adrenal cortex in response to adrenocorticotrophic hormone (Barnes 2011). Once in the circulation they can readily diffuse across the cell membrane due to their lipophilic nature and bind to nuclear receptors (Zhou and Cidlowski 2005). GCs have essential roles in various physiological processes including embryonic development, behaviour, metabolism and growth (Zhou and Cidlowski 2005). The major GC in humans is cortisol, while in rodents this is corticosterone (Buckingham 2006). Powerful synthetic GCs are commonly used clinically to treat conditions such as asthma, inflammation, allergic reactions and arthritis (Buckingham 2006). Synthetic GCs are also used clinically in situations of preterm birth to stimulate lung development and reduce the risk of Respiratory Distress Syndrome (RDS). Synthetic GCs tend to have a much higher potency for the GR and a longer half-life in vivo.

1.2.2 Regulation of Glucocorticoid Hormone Synthesis

GC synthesis is regulated by the hypothalamic-pituitary-adrenal (HPA) axis, one of the major neuroendocrine circuits of the stress response system (Acconcia and Marino 2016; Chung, et al. 2011). When stimulated by stress the hypophysiotropic neurons releases corticotrophin releasing hormone (CRH) which travels to the anterior pituitary (Rivier and Vale 1983; Vale, et al. 1981). Binding of CRF to its receptor on pituitary corticotropes stimulates the production and secretion of adrenocorticotrophic hormone (ACTH) into the circulation (Chung et al. 2011; Smith and Vale 2006). When ACTH reaches its target organ, the adrenal gland, it induces the production and release of GCs into the general circulation from the zona fasciculata (Chung et al. 2011). The HPA axis is regulated via negative feedback mechanisms for example; GCs can also act on the hypothalamus and anterior pituitary repressing the production of CRH

resulting in sequential reduction of ACTH and therefore inhibiting GC synthesis (Figure 1.3) (Chung et al. 2011).

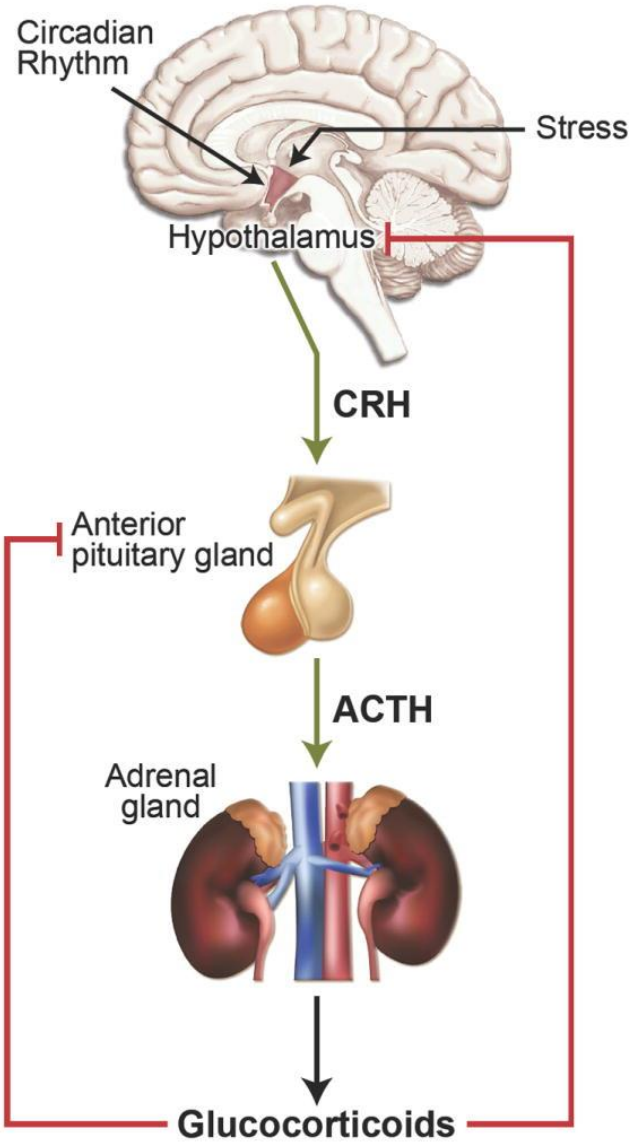

Figure 1.3 The hypothalamic-pituitary-adrenal axis. The synthesis of GCs is initiated by stress or circadian rhythm, this simulates the neuroendocrine cells in the hypothalamus to release corticotrophin releasing hormone (CRH) into the anterior pituitary gland, which results in the secretion of adrenocorticotrophic hormone (ACTH). ACTH travels to the adrenal gland and leads to the synthesis and release of GCs. The axis is controlled by negative feedback and as GCs can act on the hypothalamus and pituitary repressing the synthesis of CRH and ACTH. Figure from (Oakley and Cidlowski 2013).

1.2.3 Regulation of Glucocorticoid Signalling

The concentration of circulating cortisol and corticosterone varies widely throughout the day and night with a circadian rhythm or can become high during periods of stress or illness. Up to 80% of circulating GCs are tightly bound to Corticosteroid binding globulin (CBG), another 15% can be bound loosely to albumin, leaving around 5% of active free GCs that can diffuse across cell membranes and act on target cells through the GR or Mineralocorticoid Receptor (MR) (Chapman, et al. 2013; Lin, et al. 2010). The tissue/cell specific actions of GCs are controlled by two enzymes in both humans and rodents, 11β-hydroxysteroid dehydrogenase 1 (11β-HSD1) and 11β-hydroxysteroid dehydrogenase 2 (11β-HSD2). 11β-HSD1 is a reductase enzyme that utilises NADPH to convert inactive cortisone (or inactive 11-dehydrocorticosterone in rodents) into active cortisol (or corticosterone in rodents), while 11β-HSD2 converts active cortisol into inactive cortisone (Figure 1.4) (Chapman et al. 2013). The tissue specific actions of GCs are regulated by the expression of these two enzymes. 11β-HSD1 tends to be expressed in metabolic tissue including liver, adipose tissue, skeletal muscle and some glands while, 11β-HSD2 is expressed in tissues/organs that also express the MR for example; distal nephrons, sweat glands and colonic epithelium. 11β-HSD2 is also expressed in discrete regions of the brain, the developing fetus and in the placenta (Chapman et al. 2013).

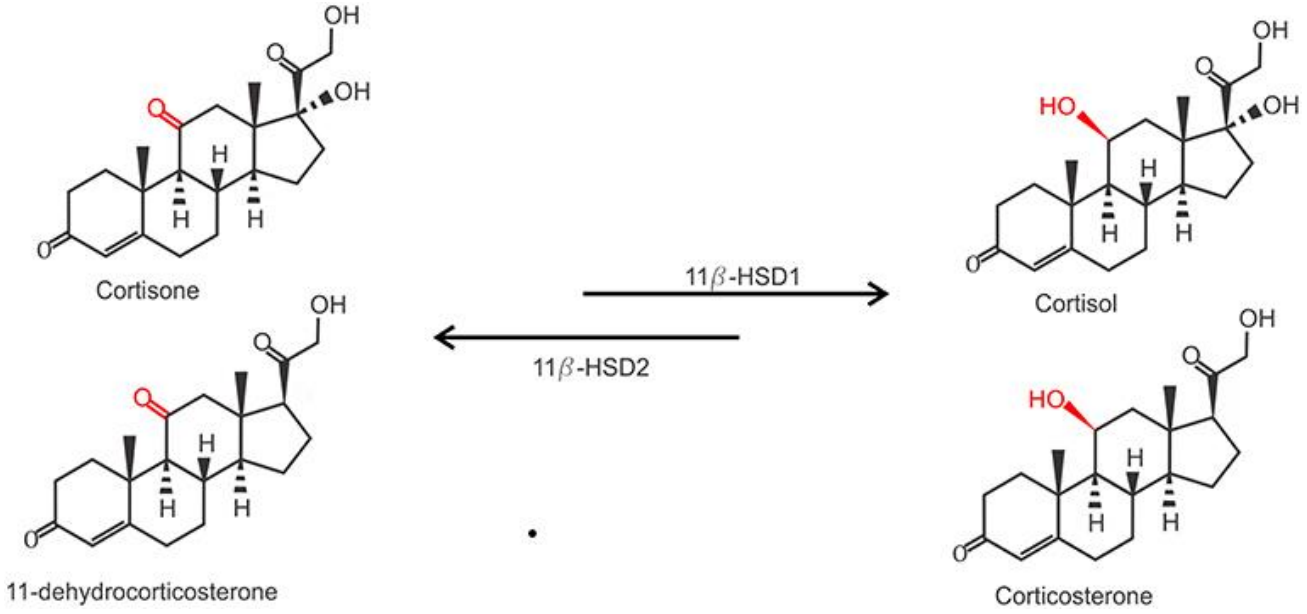

Figure 1.4 Interconversion of cortisone (11-dehydrocorticosterone in rodents) to cortisol (corticosterone in rodents) via 11β-HSD1 and 11βHSD2. From (Timmermans, et al. 2019)

1.2.4 The Glucocorticoid Receptor

GCs exert their effects through the intracellular GR (Zhou and Cidlowski 2005). The GR is a ligand-dependent transcription factor and is ubiquitously expressed in the body. The GR is a member of the nuclear receptor super family which is composed of 48 receptors including the GR, progesterone receptor (PR), MR, estrogen receptor (ER) and the androgen receptor (AR) (Robinson-Rechavi, et al. 2003). In humans, the GR is encoded by the nuclear receptor subfamily 3, group C, member 1 (*Nr3c1*) gene on chromosome 5, while in mice the *Nr3c1* gene is located on chromosome 18 (Schaaf and Cidlowski 2003). The GR is a modular protein consisting of three major domains including a N-terminal transactivation domain (NTD), a zinc-finger DNA binding domain (DBD) and a C-terminal ligand binding domain (LBD) (Kino 2000). The NTD is essential for communication between GR and other molecules required for the regulation of transcription (Almlof, et al. 1998). The DBD has two zinc finger motifs which are used to bind to glucocorticoid response elements (GRE) in DNA and the LBD as the name

suggests is required for glucocorticoid ligand binding and therefore activation of the GR (Bledsoe, et al. 2002; Howard, et al. 1990).

The *Nr3c1* gene has 9 exons and can be alternatively spliced at exon 1 and 9. Alternative splicing of exon 9 generates two isoforms GRα and GRβ which have been extensively studied. GRα and GRβ are identical until the last 50 amino acids, human GRα has an additional 50 amino acids while human GRβ has 15 nonhomologous amino acids (Chrousos and Kino 2005). Although the two forms share a similar sequence, they have different functions. GRα is the classical GR that functions as a ligand-dependent transcription factor and is ubiquitously expressed. GRβ doesn't bind to GCs and functions as an inhibitor of GRα's transcriptional activity (Bamberger, et al. 1995; Kino 2000). GRβ expression is more tissue specific, GRβ is highly expressed in epithelial cells of the terminal bronchioles of the lung, the Hassall's corpuscle in the thymus and the bile duct in the liver (Lu and Cidlowski 2006).

The GRα isoform can also generate at least 8 translational isoforms with shortened N termini, GRα-A, -B, -C_1, -C_2, -C_3, -D_1, -D_2 and -D_3 (Lu and Cidlowski 2005). These isoforms are created by translation reinitiation. In full length GRα translation begins at the first start codon and concludes when the ribosome reaches the stop codon generating a 777 amino acid polypeptide (Lu and Cidlowski 2006). The shorter N terminal isoforms are generated by the ribosome initiating translation at one of the seven other internal methionine start codons in the GRα transcript (Figure 1.5) (Lu and Cidlowski 2005, 2006). All the GRα isoforms are potentially functional because they all contain identically LBDs, however, their GRE-driven transcriptional activity varies. GR-C_3 has the highest transcriptional activity with a two-fold higher activity on GREs than the complete GRα isoform (Lu and Cidlowski 2005). The GR-D isoforms have the least amount of transcriptional activity with only half of the activity of full length GRα (Lu and Cidlowski 2005). The other isoforms have intermediate levels of translational activity (Lu and Cidlowski 2005). The GRα isoforms have different tissue

expression patterns. In rodents GRα-C isoforms are more highly expressed in the lung and pancreas while GRα-D isoforms are more abundant in the spleen and bladder (Lu and Cidlowski 2005). Mice exclusively expressing GR-C3 die at birth due to respiratory failure but interestingly these mice can be rescued from neonatal death by the administration of the synthetic glucocorticoid dexamethasone (Oakley, et al. 2018). This suggests that corticosterone activated GR-C3 and dexamethasone activated GR-C3 have different regulatory effects on key target genes involved in lung maturation (Oakley et al. 2018). The differences in isoform expression and activity may explain some of the differences in the tissue-specific actions of GCs. However, more research is required to explore the roles of the GR isoforms in fetal development and other physiological processes.

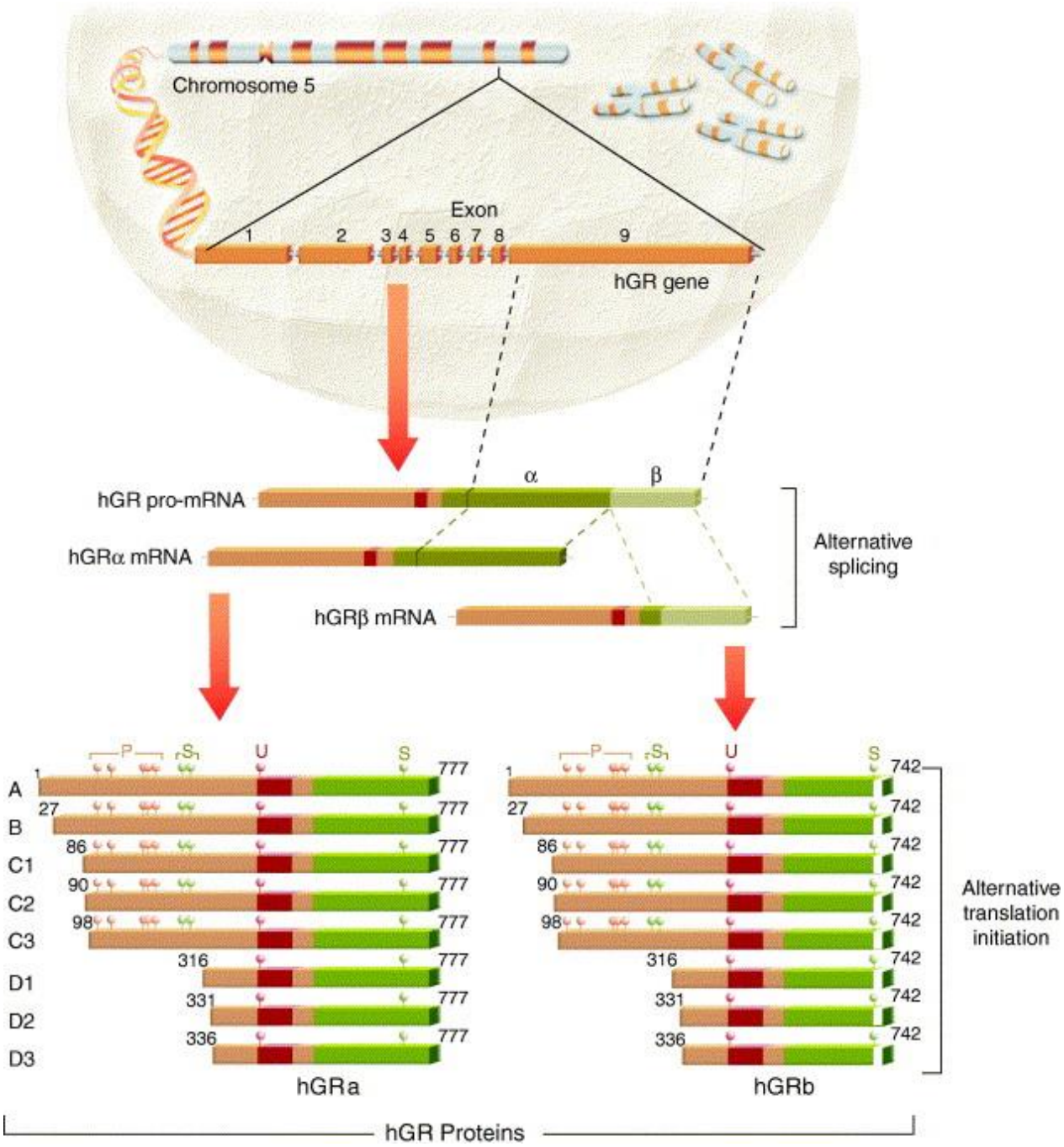

Figure 1.5 Alternative splicing of the *Nr3c1* gene in Humans. Alternative splicing of exon 9 generates GRα and GRβ. Additional isoforms of GRα and GRβ are generated by alternative translation initiation. Each GR protein is further modified by phosphorylation (P), ubiquitination (U) and sumoylation (S). From (Lu and Cidlowski 2006).

1.2.5 Mechanism of Glucocorticoid Receptor signalling

In the absence of GCs, the GR is localised to the cytoplasm and is maintained in an inactive complex with heat shock proteins (HSPs) and immunophilins (Quax, et al. 2013). A low affinity state is maintained by binding of HSP70, HSP40 and HSP70-HSP90 organising protein (HOP) which results in closing the GC ligand binding site, while binding of HSP90 and p23 results in the opening of the GC binding site directing GR towards a high affinity state (Grad and Picard 2007). Activation of the GR by GC binding results in dissociation of the HSPs, translocation to the nucleus and homodimerisation. The GR dimer then binds to DNA at specific GREs in the regulatory regions of target gene promoters leading to transrepression or transactivation of gene transcription (Figure 1.6) (Quax et al. 2013).

Interestingly, there is also evidence for non-genomic actions of GCs that are far more rapid than classical cytoplasmic GR binding. It is postulated that GCs may bind to membrane-bound GR (mGR) and stimulate intracellular signalling cascades (Strehl and Buttgereit 2014). It is relatively unknown if the mGR is an isoform of GR or a different protein all together. Some studies indicate that mGR is a GRα isoform (Deng, et al. 2015) while, others suggest that mGR is the GRγ isoform (Morgan, et al. 2016). The GR antagonist mifepristone (RU486) blocks many, not all of the described rapid responses of GCs, further supporting the hypothesis that the mGR is an isoform of GR (Chen, et al. 1991; Deng et al. 2015; Hua and Chen 1989; Vernocchi, et al. 2013).

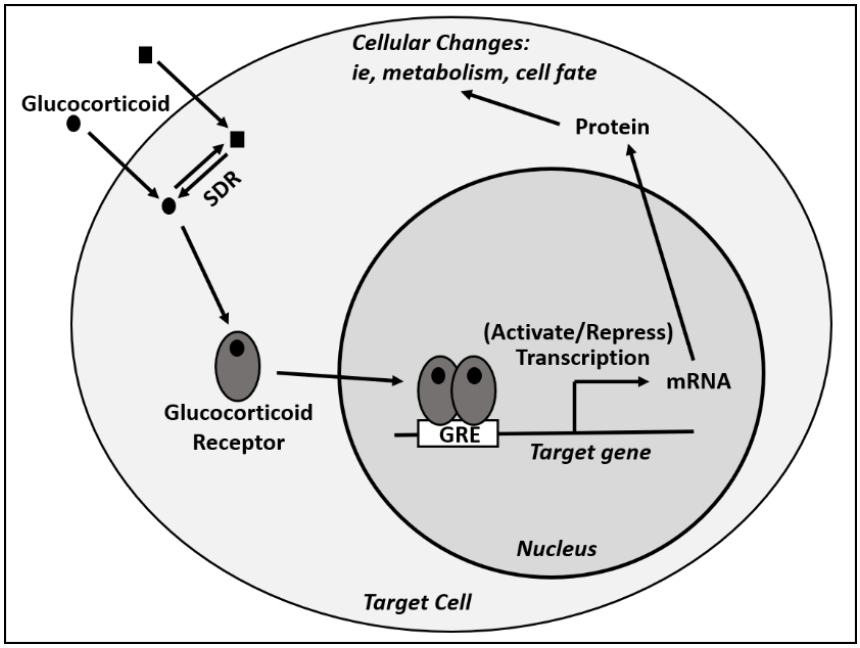

Figure 1.6 Mechanism of intracellular GC signalling. The GR binds to GCs in the cytosol initiating a conformational change. GR translocates into the nucleus, dimerise and binds to GREs on specific genes resulting in transactivation or repression of target genes. GCs may require activation by short-chain alcohol dehydrogenase reductase (SDR) enzymes to adopt their active state. Circle active GC, Dimond inactive GC. Adapted from (Cole, et al. 2019).

1.2.5 Mineralocorticoid Receptor

GCs are also able to bind to the closely related MR also known as the aldosterone receptor. The MR has an equivalent affinity for GCs as aldosterone and unwanted receptor activity stimulated by GCs is prevented by the inactivation of GCs via the enzyme 11β-HSD2 as described above (Buckingham 2006; Chapman et al. 2013). The MR is encoded by the nuclear receptor subfamily 3, group C, member 2 (*Nr3c2*) gene located on chromosome 4 in humans and chromosome 8 in rodents (Fan, et al. 1989). The MR and GR have nearly identical DBD's; this homology allows both receptors to interact with the same GRE's on target genes. The homology between GR and MR also results in a similar signalling pattern. Briefly, MR binds to aldosterone or GCs in the cytosol, translocates to the nucleus and dimerises before binding to target genes. Furthermore, there is evidence that MR and GR can form heterodimers and

interact with DNA however, the genes regulated by MR-GR complexes remain unknown (Pooley, et al. 2020) . The main difference between MR and GR is the expression pattern of the receptors while GR is ubiquitously expressed the MR has a more restricted expression pattern. MR is primarily localised to epithelial cells that regulate sodium and potassium homeostasis that include cells of the kidney, sweat glands, colon and specific regions of the brain (Buckingham 2006). Interestingly, the MR can also be localised in non-epithelial cells of the heart, brain and immune systems. In these tissues the MR is not protected by the expression of 11β-HSD2 and can be easily activated by aldosterone or by cortisol (Cole and Young 2017).

1.3 Preterm Birth

Preterm birth is defined as any birth that occurs before 37 weeks in gestation (Slattery and Morrison 2002; Suff, et al. 2019). The incidence of preterm birth is around 11% with 15 million infants born prematurely each year (Blencowe, et al. 2012). Preterm birth complications account for 44% of total under-5 year old deaths globally (Liu, et al. 2015). Preterm birth can be further characterised into groups dependent on the gestational age of the infant; extreme prematurity (< 28 weeks), accounting for ~5% of all preterm births, severe prematurity (28-31 weeks), accounting for ~15% of preterm births and moderate or late prematurity (32-37 weeks) accounting for 60%-70% of preterm births (Purisch and Gyamfi-Bannerman 2017). The classifications are required because there are many complications of preterm birth and the earlier the birth in gestation the more detrimental the direct consequences with extreme prematurity having the highest mortality rate. Preterm birth exposes the infant to the outside environment with immature organs and systems that must rapidly adapt for the infant to survive, and this can lead to life-long health consequences (Chehade, et al. 2018). Preterm birth is a complex condition with many factors involved making pinpointing the causes difficult in most cases. There are several known risk factors for the mother and fetus including but not

limited to; having a previous preterm birth, multiple births, diabetes, hypertension, stress, smoking, infection, In Vitro Fertilisation (IVF) and drug abuse (Goldenberg, et al. 2008).

1.3.1 Respiratory Complications of Preterm Birth

Preterm infants are born before the lungs are ready for life outside the womb, usually towards the end of the canalicular stage or during the saccular stage of human lung development. Lung immaturity is characterised by a thickened gas-exchange barrier, reduced surface area for gas-exchange and inadequate surfactant production as the result of decreased numbers of type II AECs and the retention of fluid (Reynolds, et al. 1968). These factors result in rapid breathing, chest restriction and cyanosis (bluish discoloration due to insufficient oxygenation of the blood), all classical characteristics of RDS. RDS is the most common cause of death in preterm infants and it affects ~50% of infants born before 28 weeks, ~33% of infants born before 32 weeks and ~42% of extremely low birth weight infants (<500g) (Hintz, et al. 2007). Treatments of RDS include synthetic surfactant to try and reduce surface tension and avoid airway collapse and mechanical ventilation. Unfortunately, mechanical ventilation commonly results in ventilator-induced lung injury which can be caused by high airway pressure, high or low lung volumes and high levels of inspired oxygen (Dreyfuss and Saumon 1998). Ventilator-induced lung injury can develop into chronic lung disease (CLD), referred to as bronchopulmonary dysplasia (BPD) (Allen, et al. 2003).

BPD was first recognised by Northway et al. in 1967 in a group of preterm infants, which after receiving ventilation and oxygen to treat RDS, developed chronic pulmonary disease (Northway, et al. 1967). Improved treatments of preterm birth and RDS also include administration of antenatal GCs, and together with the use of synthetic surfactant and modern ventilation techniques has resulted in a greater number of very premature infants surviving postnatally. These infants have less lung fibrosis, but they have evidence of arrested lung development and this is commonly referred to as “new BPD” (Davidson and Berkelhamer

2017). The long-term consequences of new BPD remain relatively unknown because the populations available for study represent survivors of now outdated care (Davidson and Berkelhamer 2017). Follow-up studies on children and young adult survivors of new BPD have raised concerns of potential life-time long consequences including compromised pulmonary function, asthma-like symptoms, pulmonary hypertension, exercise intolerance due to altered response to hypoxia and compromised pulmonary defences against environmental insults (Davidson and Berkelhamer 2017; Moss 2006).

1.3.2 Clinical use of Synthetic Glucocorticoids for Respiratory Distress Syndrome

Currently the standard clinical practice is to treat women at risk of preterm labour with antenatal GCs to accelerate lung maturation and reduced the risk of RDS in the infant. This stems from the pioneering work of Liggins and Howie, who showed that treating mothers at risk of preterm labour with betamethasone 2-7 days before delivery reduced the incidence of RDS and neonatal death (Liggins and Howie 1972). Following this landmark study more than 20 randomised clinical trials were published before 1993 all replicating Liggins and Howie's original finding (Roberts, et al. 2017). Liggins, original dosage and drug combination of two maternal intramuscular injections 24 hours apart of 6 mg of betamethasone phosphate and 6 mg of betamethasone acetate is still the most common GC drug regimen used today (Brownfoot, et al. 2013). The second most widely used GC is dexamethasone and is also given maternally by intramuscular injection; 6 mg of dexamethasone is injected four times, 12 hours apart to achieve continuous fetal exposure for 48 hours (Ballard and Liggins 1982). GC treatments have resulted in a ~40.5% increase in survival of extremely preterm infants (<28 weeks) (Blencowe, et al. 2013). Interestingly, the clinical importance of GCs is not matched by an understanding of the molecular mechanisms by which GCs mediate lung maturation. It is known that GCs induce increased thinning of the interstitial tissue, temporarily increase the production of surfactant and increase liquid clearance rate (Daniel Bird, et al. 2015). However,

there is concern that exposure to powerful synthetic GCs might have serious long-term side effects on the respiratory system and due to GR's uniform expression also on other body systems.

1.4 Endogenous Glucocorticoids and Fetal Lung Development

1.4.1 The Preparturition Cortisol Surge

The levels of circulating GCs in the fetus rapidly increase towards birth, which is known as the pre-parturition GC surge. The GC surge is essential for maturation of several organs including the lungs, liver, gastrointestinal tract, heart, thyroid gland, adrenals and kidneys (Fowden and Forhead 2015). The rise in GCs has been consistently observed in all animals and is essential for survival immediately after birth (Figure 1.7) (Fowden, et al. 2016). During the early stages of fetal development 70-80% of circulating GCs are of maternal origin due to the fetal adrenal cortex being relatively inactive (Huang, et al. 2012). The adrenal glands emerge at ~ 8 weeks in the human embryo and starts to produce cortisol from ~28 weeks (Mastorakos and Ilias 2003). In fetal mice corticosterone synthesis begins at ~E14.5 around 5 days prior to birth (Michelsohn and Anderson 1992). During most of gestation the levels of GC's in the fetus remain relatively low due to placental expression of 11β-HSD2 and P-glycoprotein-mediated transport of GCs from the fetus to the mother (Chapman et al. 2013). 11β-HSD2 is also expressed in several sensitive tissues to protect against any spill-over of GCs (Fowden and Forhead 2004). During late gestation the activity of placental 11β-HSD2 decreases, maternal GC rises, and fetal GC synthesis increases to amplify the GC surge prior to birth (Agnew, et al. 2018). Preterm infants are born before the natural surge in endogenous GCs and are at risk of neonatal death due to RDS. In order to reduce the risk of neonatal death and RDS synthetic GCs are administered to mimic the naturally occurring pre-parturition GC surge.

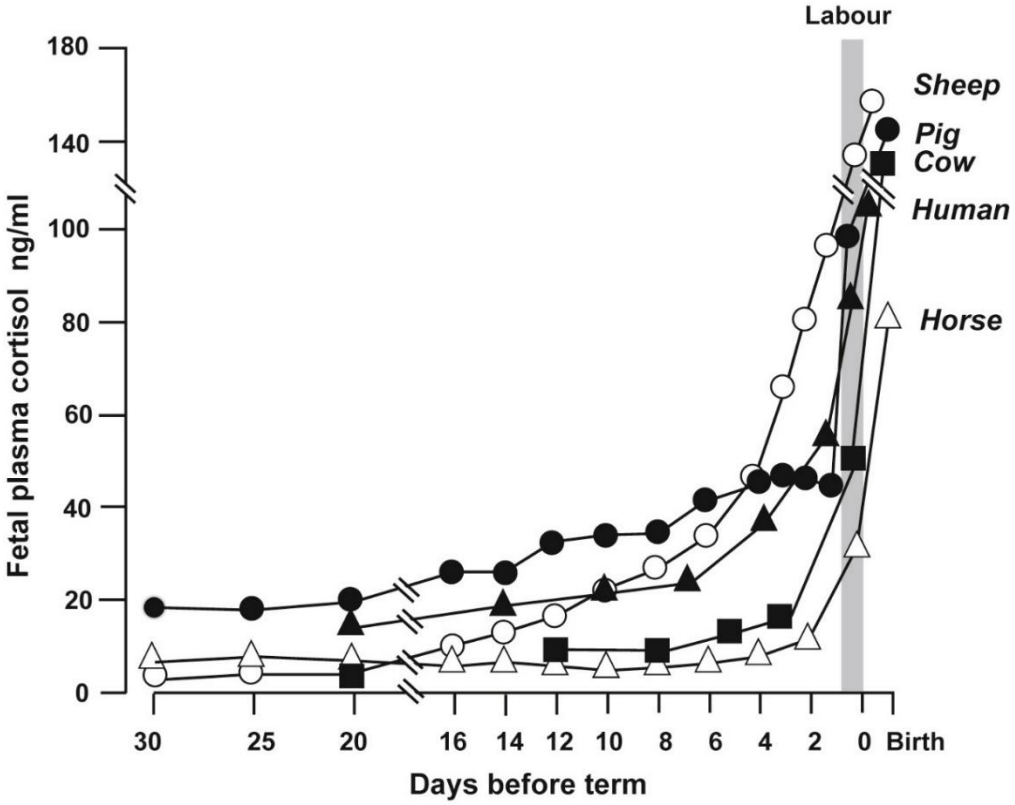

Figure 1.7 Fetal cortisol levels across several large species during late gestation. Gestational length: horse 335 days, cow 280 days, human 280 days, sheep 145 days and pig 115 days. From (Fowden et al. 2016)

1.4.2 The Respiratory Phenotype of Glucocorticoid Receptor Deficient Mice

To study the molecular mechanisms of GC signalling in the developing fetal lung, several GR deficient transgenic mouse models have been developed (Figure 1.8). Total GR deficient (GRnull) mice die shortly after birth due to respiratory failure (Cole et al. 1995). Closer examination of the GRnull mouse lung has shown lung development continues normally until ~E15.5, then begins to show defective alveolar epithelial cell differentiation and progressive hypercellularity due to unrestricted cell proliferation (Bird et al. 2007; Cole et al. 1995; Cole et al. 2004). This results in an thicken blood-air barrier increasing the diffusion distance and restricting gas exchange at birth. The timing of the phenotype coincides with the GC surge that occurs towards the end of the pseudoglandular stage of lung development. Histologically the lung of GRnull mice appears immature and resembles the canalicular stage of lung

development. The same phenotype is observed in mouse models in which the synthesis of GCs is disrupted by targeting of different stages of the HPA axis including CRH, CRH receptor 1 (CRHR1) and ACTH receptor (MC2R), but only when the pups are born from dams that are homozygous knockouts for the same HPA axis gene (Chida, et al. 2009; Muglia, et al. 1995; Smith, et al. 1998). This can be explained by the initiation of lung maturation by the transfer of maternal GCs across the placenta (Venihaki, et al. 2000). Interestingly, 11βHSD-1 deficient mice survive at birth and only show minor differences in surfactant synthesis (Hundertmark, et al. 2002; Kotelevtsev, et al. 1997).

To further characterise GC/GR signalling in the developing lung conditional GR knockout mice have been developed. Epithelial deletion of GR in mice (GRepiKO) has little effect on the lung phenotype or survival at birth (Bird, et al. 2014). In comparison mesenchymal-specific GR deletion in mice (GRmesKO) results in a severe lung phenotype that resembles the GRnull mouse lung (Bird et al. 2014; Habermehl, et al. 2011; Li, et al. 2013) (Figure 1.8). This suggests that GC/GR signalling in the mesenchymal compartment of the lung is of greatest importance and essential for normal lung development. It has been well established that GCs promote cell apoptosis however, it has been demonstrated that the hypercellular phenotype observed in both GRnull and GRmesKO mouse lung is due to an increase in cell proliferation rather than a reduction in cell apoptosis (Bird et al. 2014; Bird et al. 2007). This suggests that the GR is an inhibitor of cell proliferation in the developing lung. The complexity of mesenchymal tissue makes it difficult to identify the specific GC/GR signalling mechanisms that is responsible. There are many cell types within the mesenchyme and unlike the well investigated epithelium there is a lack of specific cell markers which makes selectively deleting GR in sub populations of mesenchymal cells more difficult.

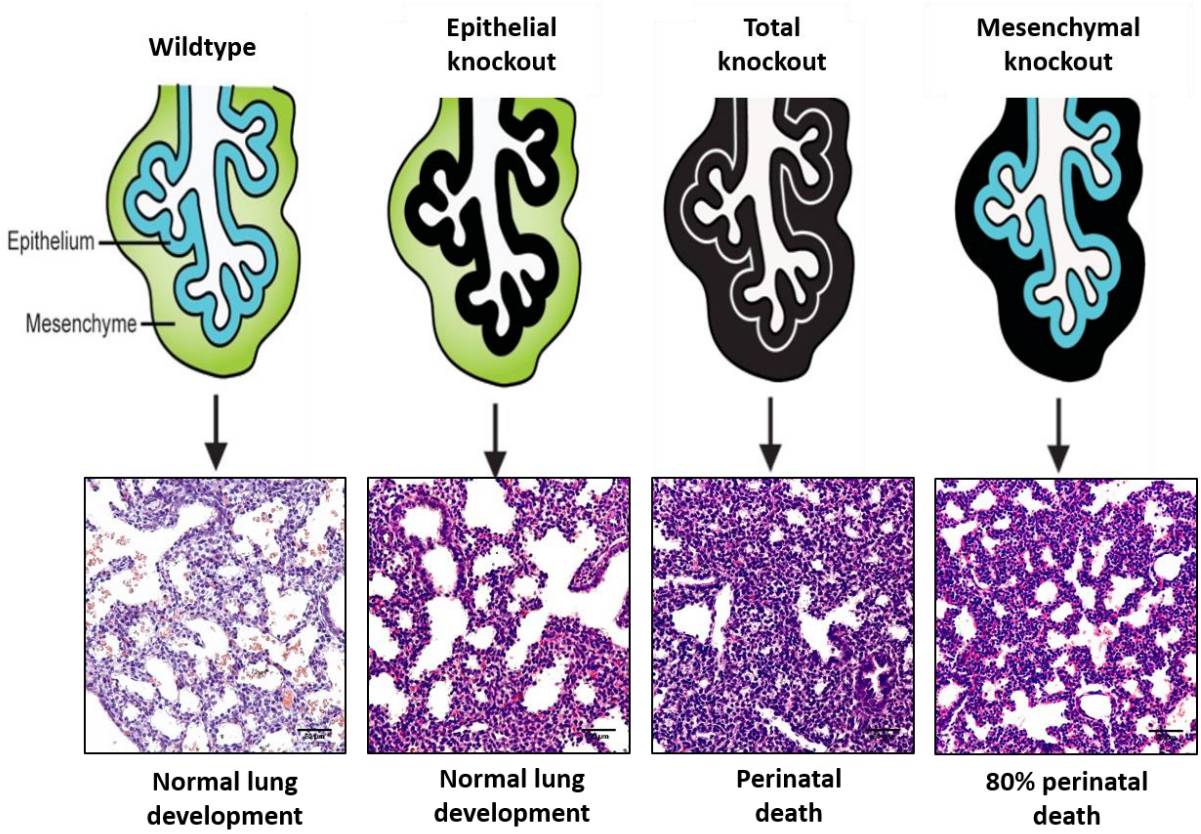

Figure 1.8 Lung morphology of conditional GR deficient mice. Black layers represent GR deletion. Lungs sections were stained with hematoxylin and eosin and imaged at E18.5 at 200x magnification. Scale bars= 50µm. Adapted from (Daniel Bird et al. 2015)

1.5. The Role of Versican in Lung Development

Studies utilising conditional mouse knockouts of the GR gene (*Nr3c1*) have established that mesenchymal GC signalling is essential for normal lung maturation (Bird et al. 2014). Screens for differently expressed genes in GRmesKO mouse lung have identified the strong overexpression of midkine and its large mesenchymal-localised ECM receptor Versican (VCAN) (Bird et al. 2014; Bird et al. 2007; Kaplan, et al. 2003). VCAN is a strong promoter of cell proliferation and an important component of the developing ECM during embryogenesis in mammals (Wight 2002). *Vcan* null mice known as hdf-mice (heart defect) die during

embryonic development around E10.5 due to severe cardiac defects including the absence of endocardial cushions and dilation of both the primitive atrium and ventricle (Mjaatvedt, et al. 1998). Due to the early lethality of *hdf* mice prior to the pseudoglandular stage of lung development the effect of total loss of *Vcan* on the lung is not known.

1.5.1 The Mammalian *Versican* Gene and VCAN protein

VCAN is part of the large proteoglycan family of ECM proteins which contain long repeating linear polymers of specific GAG disaccharides. VCAN has known roles in cell adhesion, proliferation, migration, angiogenesis and ECM assembly (Ricciardelli, et al. 2009; Wight 2002). The *Vcan* gene is located on chromosome 5 in humans and chromosome 13 in mice and consists of 15 exons (Iozzo, et al. 1992). VCAN has a core protein structure consisting of an N-terminal (G1) domain, a carboxy-terminal (G3) domain and two centrally located chondroitin sulphate GAG attachment domains, GAG α and GAG β. In mice, the GAG α domain is encoded by exon 7 and the GAG β domain is encoded on exon 8 (Wight 2002; Zimmermann and Ruoslahti 1989). The *Vcan* gene can be alternative spliced into five isoforms, *V0, V1, V2, V3* and *V4*, with the encoded proteins having molecular weights of 370 kDa, 263 kDa, 180 kDa, 74 kDa and 115 kDa, respectively (Dours-Zimmermann and Zimmermann 1994; Kischel, et al. 2010; Zako, et al. 1995). V0, the largest of the five isoforms contains both the GAG domains while V1 only contains the GAG β domain, V2 only contains the GAG α domain and V3 contains neither of the GAG domains (Figure 1.9) (Dours-Zimmermann and Zimmermann 1994; Kischel et al. 2010; Zako et al. 1995). A fifth isoform, V4 has only been identified in breast cancer and is similar to V1 except it contains a shortened GAG β domain (Kischel et al. 2010). The isoforms differ in function and expression, the V1 isoform is highly expressed in several developing tissues including the lung, heart and limbs (Snyder, et al. 2015), while, the V2 isoform has a more restricted expression and can be found in the nervous system (Snyder et al. 2015). The V1 isoform is known to promote cell proliferation and

mesenchymal-epithelial transitions, while the V2 isoform is thought to inhibit cell proliferation (Snyder et al. 2015).

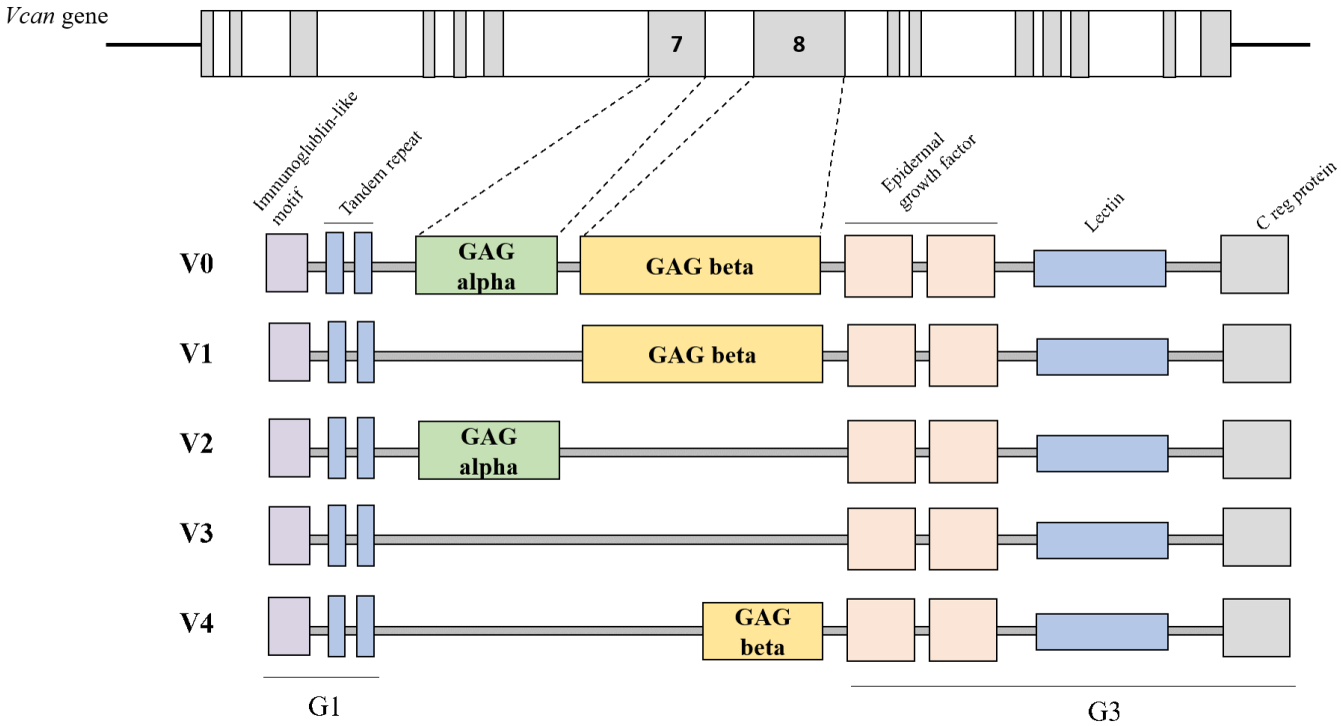

Figure 1.9 Domain structure of Versican isoforms V0, V1, V2, V3 and V4. V0 contains all exons, including exons 7 and 8 that encode GAG α and GAG β domains respectively. V1 lacks the GAG α domain, V2 lacks the GAG β domain, V3 contains neither of the GAG domains and V4 lacks GAG α and has a truncated GAG β domain.

1.5.2 Versican Degradation and Protein Clearance

Towards the end of embryogenesis there is a tightly regulated degradation and structural remodelling of the ECM in several tissues including the lung. Part of this remodelling is the rapid clearance of extracellular VCAN (Kelwick, et al. 2015). VCAN and other proteoglycans are cleared by members of the A Disintegrin and Metalloprotease with ThromboSondin Motifis (ADAMTS) proteinases family of enzymes (Kelwick et al. 2015). The ADAMTS family is continually expanding; to date there are 19 metalloproteinases and 7 ADAMTS-like members (Apte 2009) (Figure 1.10). Six of the members have been shown to cleave VCAN, including ADAMTS 1, 4, 5, 9, 15 and 20 (Nandadasa, et al. 2014). VCAN has cleavage sites in both the

GAG β domain at Glu^{405}-Gln^{406} and the GAG α domain at Glu^{1428}-Ala^{1429} (Sandy, et al. 2001; Westling, et al. 2004). Cleavage of V1 by ADAMTS 1, 4, 5 and 9 results in a 70kd fragment containing the neoepitope peptide sequence DPEAAE (Westling et al. 2004). It has been shown that a reduction in GAG β around the airways and periphery of the lung at E15.5 is co-localised to areas of high DPEAAE, suggesting ADAMTS proteases are actively degrading VCAN in the lung at this time point. Furthermore, VCAN and ADAMTS protein expression have been shown to overlap in the embryonic heart and lung in late gestation suggesting increased proteolysis (Snyder et al. 2015).

Several mouse knockout models of specific ADAMTS family members are available, with the severity of the phenotypes varying greatly depending on which *Adamts* gene was targeted (Dubail and Apte 2015; Kelwick et al. 2015). Knockdown of *Adsmts9* is lethal at E7.5 while deletion of *Adamts 4, 5, 12* and *13* results in no phenotype, unchallenged (Lee, et al. 2005; Llamazares, et al. 2007; Russell, et al. 2003; Stankunas, et al. 2008). Mice deficient in *Adamts4* develop normally and live into adulthood, indicating that other members of the ADAMTS family can compensate for the loss of *Adamts4* (Glasson, et al. 2004). For example; deletion of both *Adamats1* and *Adamts4* is lethal with mice dying within 72 h of birth due to severe kidney defects, including a dilated renal pelvis and thinned renal medulla (Boerboom, et al. 2011). Interestingly, knockdown of *Adamts5* protects against surgery-induced osteoarthritis and antigen-induced arthritis (Glasson, et al. 2005; Stanton, et al. 2005). While, deletion of *Adamts12* in mice exacerbates inflammation and airway dysfunction in allergen-induced airway disease (Paulissen, et al. 2012). Additionally, the phenotype of *Adamts13* null mice varies depending on the genetic background. *Adamts13* null mice breed on a CASA/Rc genetic background (a mouse strain with elevated plasma vWF) develop thrombocytopenia resulting in decreased survival (Motto, et al. 2005).

ADAMTS18 is essential for branching morphogenesis of the lung and kidney, coordinating the organisation of the two organs. The deletion of *Adamts18* in mice results in altered epithelial branching morphogenesis in both organs (Rutledge et al. 2019). *Adamts18* null mice have smaller misshaped lungs with reduced epithelial volume and shorter primary branches (Rutledge et al. 2019). Rutledge and colleagues also showed that 29% of *Adamts18* null mice developed double ureters that resulted in larger kidneys (Rutledge et al. 2019). A more detailed review of the phenotypes of *Adamts* knockout animals can be found here (Dubail and Apte 2015).

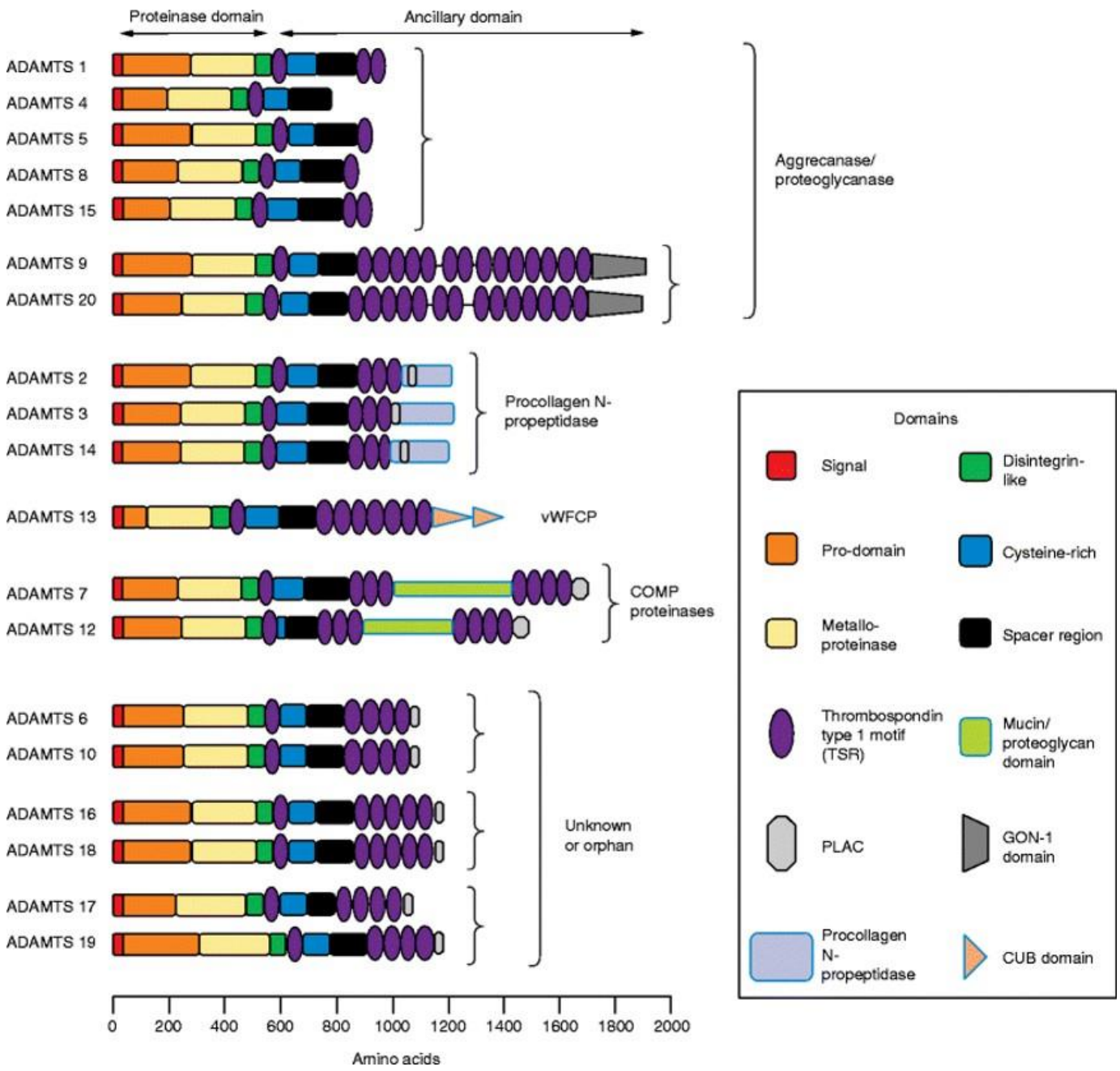

Figure 1.10 The ADAMTS family. Structurally ADAMTS proteins are divided into the proteinase domain and the ancillary domain. The proteinase domain is more conserved across the members while the ancillary domain is more variable. From (Kelwick et al. 2015)

1.6 The Effect of Synthetic Glucocorticoids and Lung Development

1.6.1 Synthetic Glucocorticoids and Lung Morphology

It is now widely accepted that GCs induce the rapid remodelling of the interstitial mesenchymal tissue in the developing lung to decrease the airway to capillary diffusion distance (Bird et al. 2007; Cole et al. 2004). This has been replicated in several models including fetal lung explant systems and by animal models of maternal GC treatments in rodents, rabbits and rhesus monkeys (Bunton and Plopper 1984; Kauffman 1977; Oshika, et al. 1998a; Snyder, et al. 1992). The effects of GCs on the lung are consistent across the models with arrest of normal proximal lung morphogenesis and accelerated structural maturation of the distal lung. GC treatment earlier in lung development may also influence branching morphogenesis. Dexamethasone treatments on rat lung explants early in the pseudoglandular stage showed distorted branching, dilated proximal tubules and a reduction in proliferation of distal tubule epithelial cells (Oshika et al. 1998a). GC treatments can also impair secondary setae formation resulting in a decreased alveolar surface area for gas exchange (Massaro and Massaro 1992). The impairment to secondary setae formation can be rescued by the administration of *trans*-retinoic acid (tRA), demonstrating an inhibitory effect of retinoic acid on GC signalling during alveolar development (Hind and Maden 2004; Massaro and Massaro 2000).

1.6.7 Synthetic Glucocorticoids and Surfactant Production

One of the first identified benefits of GC treatment is the increase in surfactant production. Mammalian pulmonary surfactant is composed of ~80-85% phospholipids, 5-10% neutral lipids and ~8-10% surfactant proteins (SP-A, -B, -C and -D) (Botas, et al. 1998). The most abundant phospholipid is phophatidycholine (PC) and the disaturated form, dipalmitoylphosphatidylcholine (DPPC) is the primary phospholipid responsible for lowering alveolar surface tension in vivo (Ballard, et al. 1997). The surfactant proteins SP-B and SP-C increase the rate of phospholipid spreading across the alveolar surface (Bolt et al. 2001). SP-B

also regulates surfactant metabolism by increasing the uptake of phospholipids by type II AECs (Rice, et al. 1989). The importance of SP-B is highlighted in the SP-B knockout mouse that has severe respiratory failure (Tokieda, et al. 1997). SP-A and SP-D are less essential to surfactant function but are important for host defence against pulmonary infections (Korfhagen, et al. 1996; LeVine, et al. 1997). Surfactant is synthesized by type-II AECs and stored in lamellar bodies (Bolt et al. 2001). GC treatment can increase levels of DPPC in tracheal fluid from lungs of fetal sheep and increase mRNA expression of SP-C and SP-B in human lung explants (Ballard et al. 1997; Ohashi, et al. 1991; Venkatesh, et al. 1993). Furthermore, GC treatment can stimulate expression of enzymes that control the production of PC and DPPC including fatty acid synthase (FASN), lysophosphatidylcholine acltransferase (LPCAT) and phospocholine cytidyltransferase (PCYT1) (Beneke and Rooney 2001; Chen, et al. 2006; Sharma, et al. 1993). However, the GC effects on surfactant synthesis are short lived and only temporary. There are other non-GC mechanisms that are more essential in the production of surfactant.

1.6.8 Synthetic Glucocorticoids and Lung Epithelial Cell Differentiation

Synthetic GC treatment is also known to influence the differentiation of epithelial cell populations in the developing lung. Antenatal GC treatment on fetal rabbits significantly increases the proportion of type-II AECs. Interestingly, dexamethasone treated human A549 cells (type-II like alveolar epithelial cell line) in culture show a shift towards a more type-I phenotype with increased expression of type-I markers including AQP5 and caveolin-1 (Barar, et al. 2007; Ben, et al. 2008; Snyder et al. 1992). Furthermore, fetal GRnull mice have altered epithelial cell populations in the lung including ~50% less type-I AECs, ~30% more type-II AECs and a ~17% increase in undifferentiated epithelial cells in comparison to wild type fetal mice (Cole et al. 2004). This may suggest that GC signalling is required for type-I AEC differentiation but not type-II AEC differentiation. This is supported by experiments with

RU486 (GR antagonist) treated rat lung explants that had no change in the number of type-II AECs (Guettari, et al. 1990). GCs also increase the synthesis of surfactant (discussed above) which is associated with increased type-II AEC differentiation. It is important to note that the GC induced change in alveolar epithelial cell populations is only transient as lung expansion can adjust the cell populations due to the ability of alveolar cells to trans-differentiate in response to stretch signals (Flecknoe, et al. 2002).

1.6.9 Synthetic Glucocorticoids and Lung Fluid Reabsorption

At birth the lungs must rapidly clear fluid to allow air to enter and gaseous exchange to occur. Prior to birth the lungs are filled with liquid to maintain an expanded state required for lung development (Nardo, et al. 1998). Lung expansion is a stimulus for lung growth and if the liquid is removed lung expansion decreases, and this may result in severe lung hypoplasia due to a reduction in fetal lung growth. The fluid is secreted into the lungs by osmosis facilitated by the transport of Cl^- and Na^+ across the epithelium and into the lumen via a Na^+-K^+-ATPase (sodium-potassium pump) (Olver, et al. 2004). Na^+ enters epithelial cells while Cl^- exits the cells via Cl^- channels on the cell membrane facing the lumen. The movement of Cl^- into the lumen creates the osmotic gradient for water movement in the same direction (Olver et al. 2004). At birth Na^+ is actively reabsorbed into the interstitium from the lung lumen by the activation of epithelial sodium channels (ENaCs) (Olver et al. 2004). ENaCs are activated by increased levels of intra-cellular cAMP caused by increased adrenaline during labour (Barker and Olver 2002). ENaCs are composed of three subunits α, β and γ and deletion of the individual subunits in mice results in differing degrees of fluid retention (Barker, et al. 1998; Hummler, et al. 1996; McDonald, et al. 1999). Deletion of the ENaC α subunit results in the most severe phenotype and these mice have the most difficulty removing lung liquid (Hummler et al. 1996). Synthetic GC treatment induces gene expression of Na^+-K^+-ATPase and the ENac subunits. Rats treated with maternal dexamethasone have increase mRNA expression of the

Na^+-K^+-ATPase β1 gene (Ingbar, et al. 1997). GREs have been identified in the promoter region of the Na^+-K^+-ATPase β1 gene in both humans and rats (Hao, et al. 2003). Furthermore, antenatal dexamethasone treatment in rabbits increases mRNA expression and levels of the α subunit of ENaC (Mustafa, et al. 2004). A GRE has also been found in the promotor region of the human α-ENaC gene however, no GREs have been found in either the β-ENaC or γ-ENaC genes (Bremner, et al. 2002; Chow, et al. 1999; Thomas, et al. 1999).

1.7 Effects of Synthetic Glucocorticoids on Other Body Systems

The benefits of antenatal GC treatment in preventing RDS and reducing neonatal death in preterm infants are well established. However, there are growing concerns that exposure to high concentrations of synthetic GCs is associated with detrimental side effects. Synthetic GCs have a much higher potency for GR and have longer half-life's *in vivo* than endogenous GCs. Synthetic GCs dexamethasone and betamethasone can also easily cross the placenta because they are not readily metabolised by 11βHSD2 due to the presence of an additional fluorine group (Garbrecht, et al. 2006). Potential side effects include reduced birth weight, altered HPA axis, neonatal sepsis, smaller head circumference, altered development of the neural cortex, restricted placental development, hypertension and adverse cardiovascular and metabolic effects (Fowden and Forhead 2015; Garbrecht et al. 2006; Kemp, et al. 2018; Sheen, et al. 2015). To reduce the potential side effects of antenatal GCs it is standard practice to administer a single course of synthetic GCs to a mother in preterm labour at 24-34 weeks gestation (Brownfoot et al. 2013). However, it is very challenging to predict when preterm labour will occur, and sometimes pregnant women receive multiple courses of GCs as they have not given birth during the effective window of 2 -7 days (Crowther, et al. 2015).

1.7.1 Effects of Synthetic Glucocorticoids on Placental Development and Function

The placenta is the site of nutritional and waste exchange between the fetus and mother. Adequate placental growth is essential for adequate fetal growth (Ozmen, et al. 2017). The placenta responds to a variety of endocrine signals including GCs (Murphy, et al. 2006). Endogenous GCs act through the placenta to influence development, maturation and survival of the fetus (Murphy et al. 2006). The main regulator of maternal endogenous fetal GC exposure is the expression of 11βHSD2 in the placenta (Chapman et al. 2013). However, as discussed above fluorinated synthetic GCs including dexamethasone and betamethasone are not readily metabolised by 11βHSD2 and therefore, can readily diffuse across the placenta *in utero*. Several animal studies have demonstrated that administration of exogenous synthetic GCs can result in reduced placental weight and fetal growth (Cottrell and Seckl 2009; Fowden and Forhead 2015; Vaughan, et al. 2011). Maternal administration of dexamethasone to rats late in gestation resulted in an 11% decrease in birth weight (Levitt, et al. 1996). A similar phenotype is observed when placental 11βHSD2 is inhibited by carbenoxolone treatment (Lindsay, et al. 1996). Furthermore, dexamethasone treatment in sheep can increase expression of apoptotic factors in the placenta and a decrease in proliferative markers (Braun, et al. 2015). Synthetic GCs can also affect the transport of nutrients across the placenta for example; fetal growth restriction is observed in betamethasone treated fetal sheep due to impaired placental transport of nutrients including calcium and lactate (Moss, et al. 2003). In humans betamethasone exposure has been linked to decreased placental width (~6%), reduced body length (~6%) and decreased birth weight (~18%) (Braun, et al. 2013).

1.7.2 Effects of Synthetic Glucocorticoids on the Developing HPA Axis

The fetal HPA axis is very sensitive to overexposure of GCs and excess levels can alter HPA function and regulation through GC-mediated fetal programming (Moisiadis and Matthews 2014). The fetal HPA axis is well developed by ~20 weeks of gestation and can mount a

response to stress (Noorlander, et al. 2006). A single or multiple courses of synthetic GCs antenatally rapidly suppresses both maternal and fetal plasma levels of ACTH and cortisol (Ballard, et al. 1975). Furthermore, infants born prematurely and exposed to synthetic GCs have decreased basal cortisol levels within hours of birth and reduced responsiveness of the HPA axis to stress through the first week of life (Arnold, et al. 1998; Davis, et al. 2004; Schaffer, et al. 2009). The effects of GCs on the HPA axis have also been studied in several animal models including sheep, rodents, guinea pigs and non-human primates (Moisiadis and Matthews 2014). Baboons exposed to multiple courses of betamethasone during gestational days 150-164 (term 185 days) have decreased levels of *Pomc* mRNA that encodes for proopiomelanocortin a precursor protein for ACTH and reduced adrenal levels of *Mc2r* mRNA that encodes for the adrenal-expressed ACTH receptor (Leavitt, et al. 1997). Similarly, guinea pigs exposed to multiple courses of synthetic GCs late in gestation reduces levels of CRH mRNA and POMC mRNA (McCabe, et al. 2001). Interestingly, fetal sheep exposed to either single or multiple courses of GCs during gestational days 106-127 (term 145 days) have increased ACTH and cortisol responses to hypoxic stress (Rakers, et al. 2013). The variation of GC effects on the HPA axis could be explained by sensitivity to GCs; for example pregnant sheep tend to be very sensitive to the labour inducing effects of GCs, while guinea pigs are more GC resistant relative to humans (Moisiadis and Matthews 2014). The effects of GCs on the HPA axis can extend into infancy; for example 18-day old guinea pigs exposed to a single course of synthetic GCs during gestation have a suppressed adrenocortical response to stress (Dean, et al. 2001). Furthermore, juvenile rhesus monkeys treated with multiple courses of synthetic GCs in utero have increased HPA function in response to stress (de Vries, et al. 2007).

1.7.3 Effects of Synthetic Glucocorticoids on Brain Development

The rapid increase in GCs towards the end of gestation is not only essential for lung maturation but also neurodevelopment. GCs initiate the terminal maturation of neurons and regulates the

growth of axons, dendrites and synapses (Adhya, et al. 2018; Meyer 1983). Synthetic GCs can pass the blood brain barrier by simple diffusion (Kajantie, et al. 2004). Although, GCs can have beneficial maturation effects on the brain during late gestation, overexposure of GCs can cause altered structural brain development, dysregulation of the HPA axis (see above) and behavioural problems later in life including learning impairments, anxiety, depression and enhanced sensitivity to drugs of abuse (Lupien, et al. 2009). The regions of the brain most sensitive to synthetic GCs also have the highest expression of GR including the hippocampus, medial prefrontal cortex and the anterior cingulate cortex (Cerqueira, et al. 2007; Shoener, et al. 2006). Antenatal synthetic GC administered to rhesus monkeys at 132 to 133 days of gestation (term 166 days) resulted in a ~ 30% reduction in hippocampus size at 9 months (Uno, et al. 1994). However, most of the animal studies on synthetic GCs and brain development use multiple courses of synthetic GCs. In humans a single course of GCs is generally associated with benefits to neurodevelopment while a multiple course is detrimental; for example; a single course of synthetic GCs decreases the risk of cerebral palsy while, multiple course of the same dosage is correlated with cerebral palsy (French, et al. 2004; Roberts and Dalziel 2006). Additionally, a single course of GCs in women at high risk for preterm birth decreases neurodevelopmental disability in infants born at 23, 24 and 25 weeks (Carlo, et al. 2011). However, emerging evidence has shown synthetic GCs can also be negatively associated with brain cortex development for example; 6-10-year-old children exposed to synthetic GCs *in utero* have greater cortical thinning in the rostral anterior cingulate cortex and increases in associated behavioural problems (Davis, et al. 2013). The effects of synthetic GCs on brain development are most likely associated with the stage of brain development, the duration of GC exposure and the dosage used.

1.7.4 Effects of Synthetic Glucocorticoids on the Renal System

In addition to promoting lung maturation synthetic GCs have also been shown to accelerate renal development resulting in both adequate and efficient tubular reabsorption at birth (Ervin, et al. 1996; Ervin, et al. 1998; Petershack, et al. 1999). Most studies investigating the effects of synthetic GCs on renal development have been on animal models and have focused on the short-term side effects of GCs. These studies have indicated that antenatal GC treatment increases arterial blood pressure, increases glomerular filtration rate and decreases sodium excretion in infants (Ervin et al. 1996; Hill, et al. 1988; Stonestreet, et al. 1983). At birth renal tubular sodium excretion decreases in response to improved function of renal sodium transporters and NA^+ K^+ -ATPase (Jahnukainen, et al. 2001). Animal studies have shown that synthetic GCs can increase NA^+K^+-ATPase mRNA in both rats and sheep (Celsi, et al. 1991; Jahnukainen et al. 2001). Furthermore, antenatal synthetic GC treatment increases renal sodium reabsorption in very preterm baboons (Ervin et al. 1998). Synthetic GCs can also alter renal cell proliferation, fetal rats exposed to high dosages of dexamethasone late in gestation have impaired renal cell proliferation and reduced total kidney cell numbers (Slotkin, et al. 1991). Interestingly, even low doses of dexamethasone result in a temporary reduction in total kidney cell number for the first three days after birth (Slotkin et al. 1991).

Synthetic GCs can also alter the renal transcriptome; antenatal dexamethasone treatment in rats alters 431 renal genes including key development genes, for example *Gfra1* that encodes glial cell line-derived neurotrophic factor (GDNF), which is essential to branching morphogenesis (Sheen et al. 2015) (discussed below). Additionally, dexamethasone treatment after adrenalectomy in adult rats increases expression of SGK-1, αENaC and GC-induced leucine zipper (GILZ) which are essential to renal sodium reabsorption (Muller, et al. 2003). Furthermore, synthetic GCs may also reduce nephron number in the kidney however, this seems to be dependent on the timing of GC exposure (Ortiz, et al. 2001). Rats exposed to

dexamethasone *in utero* on embryonic days 15 and 16 have a 20% reduction in nephron number, additionally rats exposed to synthetic GCs on days 17 and 18 have a 17% reduction in nephrons, but rats exposed on days 11-12, 13-14, 19-20 and 20-21 have similar numbers of nephrons to untreated controls (Ortiz et al. 2001). It has been postulated that low nephron numbers may increase the risk of developing chronic kidney disease and hypertension later in life.

1.8 The Developmental Origins of Health and Disease

The Developmental Origins of Health and Disease (DOHaD) hypothesis suggests that exposure to certain environmental challenges including poor nutrition, chemicals, infections, stress or hormones such as GCs during fetal development may impact an individual's health later in life. Early research into DOHad was focused on well-documented famines (Hoffman, et al. 2017). One of the most well-known and studied cohorts is the Dutch famine cohort composed of men and women who were born before, during and after the 1944-1945 Dutch famine (Ravelli, et al. 1998). Adults exposed to the famine during mid or late gestation had lower glucose tolerance compared to adults either never exposed to the famine or exposed earlier in gestation (Ravelli et al. 1998). Furthermore, adults exposed to the famine for any 10-week period of gestation had a 3 times higher risk of developing hypertension than unexposed adults (Stein, et al. 2006). These findings are consistent with the Chinese famine of 1958 where adults exposed to the famine during gestation were 4 times more likely to have hypertension than adults exposed to the famine postnatally (Huang, et al. 2010). Adults who were exposed to the Chinese famine antenatally also had a 50% higher risk of type II diabetes (Wang, et al. 2016).

The mechanisms driving DOHaD is a growing area of research, one hypothesis to explain DOHaD is fetal GC overexposure (Reynolds 2013). As discussed above GCs are essential for normal fetal development and tissue maturation. Antenatal treatment with synthetic GCs is

associated with lower birth weight and insulin resistance later in life (Dalziel, et al. 2005). GC exposure *in utero* has also been linked to alterations in brain development and behaviour. Furthermore, consequences of GC exposure extend into adulthood with higher risks of both cardiovascular and renal disease in adults exposed to GCs during gestation (Sheen et al. 2015).

1.9 Kidney Development

The kidney develops from the intermediate mesoderm, located between the lateral plate and paraxial mesoderm's (Saxen and Sariola 1987). In higher vertebrates three distinct kidney structures form successively, termed the pronephros, mesonephros and metanephros (Saxen and Sariola 1987) (Figure 1.11). Each organ is more advanced than its progenitor and they reflect the evolutionary past of the vertebrate lineage (Saxen and Sariola 1987). The three kidney structures migrate in a rostral to caudal direction forming the nephric duct (Short and Smyth 2016). The pronephros and mesonephros are transient structures in the human and mouse, they are non-functional and absorbed during development (Saxen and Sariola 1987). The metanephros is a more complex structure and goes on to form the functioning adult kidney. Most research has focused on the development of the metanephros that emerges from the nephric duct at ~E10.5 in mice or at ~E26 in the human embryo (4 weeks of gestation) (Osathanondh and Potter 1963). The emerging bud is known as the ureteric bud and this elongates towards a collection of mesenchymal cells known as metanephric mesenchyme and eventually invades (Saxen and Sariola 1987). Once in contact with the metanephric mesenchyme, tightly regulated rounds of branching morphogenesis occurs to form the epithelial collecting duct system (Short and Smyth 2016).

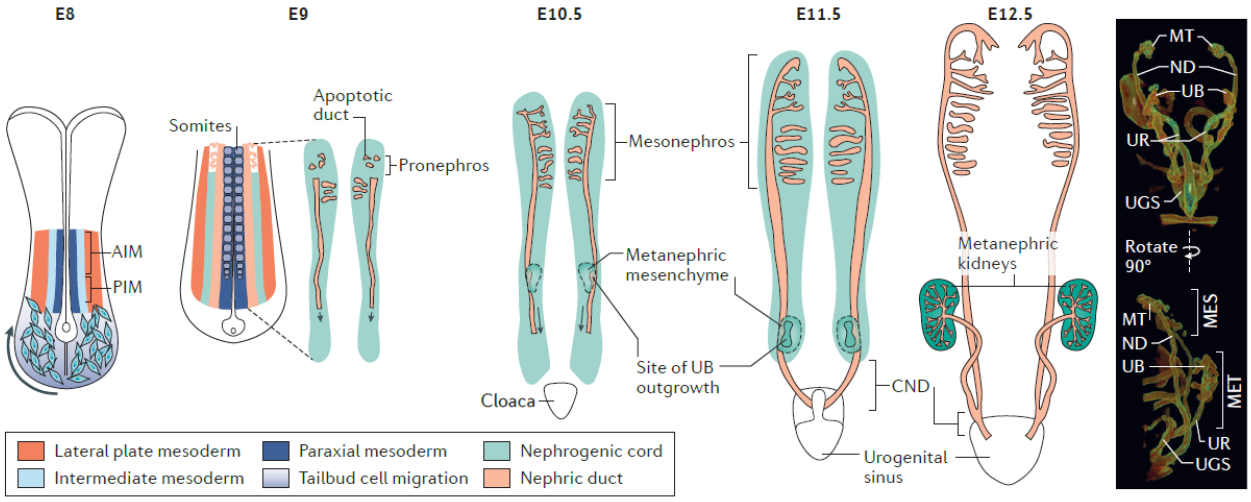

Figure 1.11 Schematic overview of kidney development. Kidney development occurs over three successive phases and involves the formation of three independent kidneys. The Pronephros is the earliest form of the kidney and emerges from the intermediate mesdoderm. The second form of the kidney the mesonephros appears at ~ E9.0 and consists of unbranched tubules. The third kidney the metanephros will go on to form the functioning adult kidney. The metanephros forms from an outgrowth of the nephric duct at ~E10.5. From (Short and Smyth 2016)

1.9.1 The Pronephros

The earliest form of the kidney, the pronephros first emerges at ~E8 in mice or ~E22 in the human embryo (Bouchard, et al. 2000; Vetter and Gibley 1966). The pronephros generates the nephric duct that migrates caudally and stimulates mesonephric tubule formation (Davidson 2009). The transcription factors controlling the formation of the pronephros include Paired box 2 (PAX2), Paired box 8 (PAX8), GATA binding protein 3 (GATA3) and LIM homeobox protein 1 (LHX1) (formerly LIM1) (Bouchard 2004). PAX2 and PAX8 are essential for the formation of the pronephros and persist in the nephric duct (Bouchard, et al. 2002). Curiously *Pax8* null embryos have a severe defect in thyroid development however, they develop normal

kidneys (Mansouri, et al. 1998). In comparison *Pax2* null embryos form a nephric duct but it later degenerates and never reaches the urogenital sinus (Torres, et al. 1995). A double *Pax8/Pax2* null mutant never forms a nephric duct and therefore no kidney structures arise and the intermediate mesoderm undergoes apoptosis by E9.5 (Bouchard et al. 2002). This is evidence that PAX8 and PAX2 are a compensatory mechanism to ensure that the intermediate mesoderm is committed to nephric duct formation (Davidson 2009).

GATA3 is expressed as early as E8.5 and is a direct target of PAX2 and PAX8. Targeted inactivation of GATA3 results in non-directional growth of the nephric duct and a lack of a metanephros due to incomplete extension of the nephric duct to the urogenital sinus (Grote, et al. 2006). LHX1 is also essential to the formation of the pronephros. LHX1 expression is first evident at E7.5 in the intermediate mesoderm and lateral plate mesoderm however it becomes localised to the nephric duct by E9.5 (Davidson 2009). *Lhx1* null mutants form a nephric duct but it undergoes necrotic degeneration indicating that LHX1 has a role in nephric duct survival (Kobayashi, et al. 2005; Shawlot and Behringer 1995). These defects result in abnormalities in the formation of the sequential kidney structures, the mesonephros and metanephros, with the most serve abnormality being the complete absence of the metanephros (Kobayashi et al. 2005).

1.9.2 The Mesonephros

The Mesonephros emerges at ~E9.0 in the mouse or ~E25 in the human embryo, the mesonephros consists of approximately 18 pairs of tubules that are generated from the anterior intermediate mesoderm (AIM) and posterior intermediate mesoderm (PIM) (Davidson 2009; Vetter and Gibley 1966). The tubules produced from the AIM are the rostral mesonephric tubules and will go on to form primary glomeruli; in contrast the PIM produces caudal mesonephric tubules which make up the bulk of the mesonephros and will go on to form the

primitive unbranched tubules (Sainio, et al. 1997). The caudal tubules are initially nephrogenic cord cells that undergo a mesenchymal-to-epithelial transition (Davidson 2009). At E14.5 the mesonephros begins degenerating rapidly, within 24 hours nearly all the tubules have undergone apoptosis (Sainio et al. 1997; Smith and Mackay 1991). In females, all the tubules are degraded, however in males a few of the rostral tubules go on to contribute to the formation of the testis (Vetter and Gibley 1966).

The molecular mechanisms governing the formation of the mesonephros are relatively unknown presumably because the mesonephros is a transitional kidney and has little function postnatally (Davidson 2009). It has been demonstrated that microsurgical disruption of the nephric duct in chick embryos results in failure of the mesonephros to form (Boyden 1927; Waddington 1938). It can therefore be speculated that signals from the nephric duct are essential in the formation of the mesonephros tubules (Davidson 2009). Wingless-type MMTV integration site family, member 9B (WNT9B) is expressed by the nephric duct during both mesonephros and metanephros kidney development (Carroll, et al. 2005). WNT9B has been found to promote the production of nephrons during mesonephros and metanephros development (Carroll et al. 2005). In support of this *Wnt9b* null mice lack both mesonephros and metanephros nephrons (Carroll et al. 2005).

1.9.10 The Metanephros

Metanephros formation begins with the formation of the ureteric bud which is an outgrowth of the nephric bud at ~E10.5-11 in mice or approximately the fifth week of human gestation (Osathanondh and Potter 1963). The ureteric bud is encapsulated within the metanephric mesenchyme (Saxen and Sariola 1987). Once the ureteric bud contacts the metanephric mesenchyme, the ureteric bud initiates branching morphogenesis through sequential divisions that lead to the formation of a complex ureteric tree (Short and Smyth 2016) (Figure 1.12). The

process of branching morphogenesis occurs over a short period. In mice, nearly all ~13 branching events occur within a 4-day period and this is consistent with human ureteric bud branching which consists of ~15 events that starts at ~5 weeks of gestation and ends at ~15 weeks of gestation (Short, et al. 2014). As the ureteric tree becomes more complex the cells within proximity to the tips of the tree differentiate into cap mesenchyme (Short and Smyth 2016). A small subpopulation of cap mesenchyme cells cluster together on either side of the main stem of the ureteric bud (Brunskill, et al. 2008). These cells undergo a mesenchymal-to-epithelial transition to form renal vesicles (Saxen and Sariola 1987). These renal vesicles proliferate and form a comma-shaped body followed by a S-shaped body which fuse with the collecting duct epithelium creating a nephron (Smith and Mackay 1991).

It is now widely recognised that the cap mesenchyme and ureteric tree outgrowth are dependent on each other. The failure of ureteric tree outgrowth results in apoptosis of the cap mesenchyme (Kreidberg, et al. 1993) and inactivation of genes associated with either cap mesenchyme differentiation or survival leads to disrupted ureteric tree outgrowth (Self, et al. 2006). This co-dependence leads to a tightly regulated balance between the formation of nephrons and branching morphogenesis (Short and Smyth 2016). This process is most likely going to have an impact on final nephron number and the avoidance of defects in kidney organogenesis (Short and Smyth 2016).

Ureteric bud outgrowth involves a complex signalling network. One of the most important factors and master regulators of outgrowth is GDNF which signals through the RET tyrosine kinase receptor (Costantini and Shakya 2006). GDNF is expressed throughout the nephrogenic cord at E9.5 but becomes localised to the metanephric mesenchyme by E10.5 (Costantini and Shakya 2006). The correct expression of GDNF is essential to kidney development and is controlled by several factors including the Homeobox-leucine zipper protein HOX11 (HOX11) gene family, FOXC1, FOXC2, BMP4 and Gremlin 1, DAN family BMP antagonist (GREM1),

reviewed in (Short and Smyth 2016) . The cap mesenchyme is essential to stimulating ureteric bud branching and provides the progenitor cells for nephron formation (Davidson 2009). Several molecular factors are involved in survival and proliferation of the cap mesenchyme including Spalt like transcription factor 1 (SALL1), Wilms tumor 1 homolog (WT1), Sine oculis-related homeobox 2 (SIX2), EYA transcriptional coactivator and phosphatase 1 (EYA1), and PAX2 reviewed in (Davidson 2009).

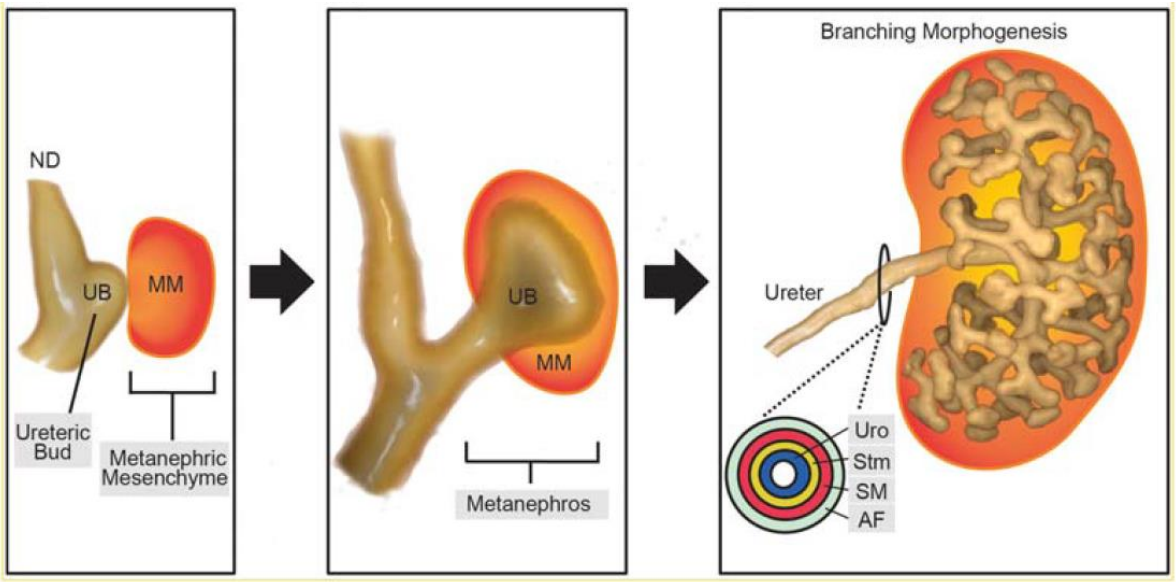

Figure 1.12 Schematic overview of metanephros development. The uteric bud (UB) emerges from the nephric duct (ND) at ~E10.5 and elongates towards a group of mesenchymal cells known as the metanephric mesenchyme (MM). Once the uteric bud contacts the metanephric mesenchyme branching morphogenesis occurs. The uteric bud outside the metanephric mesenchyme will form the ureter that develops into four layers of cells; urothlium (Uro), Stromal cells (Stm), Smooth muscle cells (SM) and adventitial fibroblasts (AF) From (Tham and Smyth 2019).

1.10 Endogenous Glucocorticoids and Fetal Kidney Development

Although studies have established a link between synthetic GC treatment and renal disease later in life the role of endogenous GCs in kidney development remains relatively unknown. It has been demonstrated that GR gene expression occurs in a specific pattern in the developing kidney. GR gene expression in the fetal mouse kidney increases from E9.5 to ~E14.5, which correlates with the start of GC biosynthesis in the fetal mouse at E14.5 (Speirs, et al. 2004). This is followed by a reduction in GR mRNA expression until ~E17, after which GR expression increases until birth (Speirs et al. 2004). This pattern of GR gene expression is evidence that correct GC/GR signalling is important in normal kidney development (Speirs et al. 2004). However, it is not entirely known when GR begins appearing in different structures within the developing mammalian kidney. Most of the studies on GR localisation have been in adult animal models. In the adult rat kidney GR and MR are expressed in the nuclei of cells in the aldosterone-sensitive distal nephron (ASDN) including in the thick ascending limb, distal convoluted tubule, connecting tubule, collecting duct, intercalated cells and proximal tubule cells (Ackermann, et al. 2010). Interestingly, GR expression in the kidney is altered by a high salt diet which reduces aldosterone secretion. In a low aldosterone state GR remains in the nuclei of cells of the proximal tubules and thick ascending limb but is removed from the nuclei of cells of the collecting tubule and collecting duct (Ackermann et al. 2010). Additionally, it has been demonstrated that in conditions of low aldosterone levels the specific cells where GR was present in the nuclei were segment-specific and corresponded to areas of low 11β-HSD2 expression, notably in the early distal convoluted tubule (DCT1) (Ackermann et al. 2010). The same study also showed that nuclei GR localisation in the low aldosterone state progressively disappears along the distal convoluted tubule and is almost absent in the late convoluted tubule (DCT2) where 11βHSD2 expression is high (Ackermann et al. 2010). This supports the idea that GR expression occurs in a gradient along the DCT.

The effects of the loss of GR on the developing kidney and postnatally is relatively unclear due to the early lethality of the global GRnull mice (Cole et al. 1995). A small number of studies have used mouse models of conditional kidney specific deletion of the GR. Conditional GR deletion in the distal nephron using the *Kspcre* results in slightly elevated blood pressure but on a whole these mice appear normal and have similar body weight, renal histology and nephron number to control animals (Goodwin, et al. 2010). A wider renal tubule deletion of GR in adult mice using an inducible *Pax8*-Cre driver alters the function and abundance of key sodium transports including thiazide-sensitive Na^+/Cl^- cotransporter (NCC), Sodium transport, sodium and hydrogen exchanger 3 (NHE3) and Na-K-Cl cotransporter-2 (NKCC2) (Canonica, et al. 2019).

1.11 Summary

In summary the importance of GC signalling for the functional maturation of many fetal tissues is well established, yet the underlying cellular mechanisms are not well understood. GCs rapidly mature the lung for gaseous exchange and prepare the kidney for efficient tubular absorption after birth. Furthermore, antenatal synthetic GCs are used routinely in situations of preterm birth and administration of antenatal synthetic GCs up to 24 hours prior to birth decreases the morbidity and mortality in preterm infants at risk of RDS. Surprisingly, the clinical use and importance of GCs in late development is not matched by an understanding of the GC-regulated molecular mechanisms and gene networks in the embryo. Use of conditional mouse knockout models have highlighted that GR-mediated signalling activity in the mesenchymal compartment of the lung is particularly crucial. Even less is known about the molecular signalling pathways of GCs in compartments of the developing kidney. This is of concern because it has been demonstrated that exposure to powerful synthetic GCs including betamethasone and dexamethasone is associated with reduced birth weight, increased risk of

high blood pressure and reduced total kidney cell number. With the increasing evidence supporting the DOHad theory, it is essential to understand the complex actions of GC/GR signalling during fetal programming and development, to avoid consequences of excessive and poorly timed exposure to GCs. This thesis aims to investigate both the gene networks that underpin GC regulation during late gestation lung development in the mesenchymal compartment of the lung and to further explore the role of GC/GR signalling during kidney development.

1.12 Research Aims

Aim 1: Define the GC/GR regulation of the ECM protein VCAN during lung development in the mouse

The severe lung phenotype in GR-null mice, as well as the beneficial outcomes in neonatal respiratory function gained from exogenous GC treatment is primarily due to altered expression of GR-regulated factors in the lung mesenchyme. Previous microarrays on GRmesKO mouse lung have identified the ECM protein VCAN as a potential GR regulated target. This thesis will aim to investigate the GC-regulation of VCAN during late lung development.

Aim 2: Identify and investigate the GC/GR regulation of specific target genes and cell pathways related to cell proliferation in the mesenchyme during lung development in the mouse

Despite a known role for mesenchymal GR signalling in lung morphological maturation, the underlying molecular mechanisms and gene networks remain elusive. This chapter will explore some of the GC/GR gene networks in the developing mouse lung mesenchyme utilising RNA sequencing.

Aim 3: Investigate the specific actions of glucocorticoids via GR signalling during kidney organogenesis via analysis of GR-null and GR-tissue-specific null fetal mice

GCs play important roles in the development of many organs in the embryo. However, the kidney specific actions of GC/GR signalling are not well characterised in the developing kidney. This chapter will investigate the effects of eliminating the GR in different compartments of the kidney including the collecting ducts and mesenchyme by utilising kidney conditional mouse GR knockout mouse models.

Chapter 2: Glucocorticoid Signalling Drives Reduced Versican Levels in the Fetal Mouse Lung

RESEARCH

Glucocorticoid signalling drives reduced versican levels in the fetal mouse lung

Kelly L Short[1], **A Daniel Bird**[1,2], **Bennet K L Seow**[1], **Judy Ng**[1], **Annie R A McDougall**[3], **Megan J Wallace**[3], **Stuart B Hooper**[3] and **Timothy J Cole**[1]

[1]Department of Biochemistry and Molecular Biology, Monash University, Melbourne, Vicoria, Australia.
[2]Centre for Endocrinology and Metabolism, Hudson Institute of Medical Research, Monash Medical Centre, Clayton, Victoria, Australia
[3]The Richie Centre, Hudson Institute of Medical Research, Monash Medical Centre, Clayton, Victoria, Australia

Correspondence should be addressed to T J Cole: tim.cole@monash.edu

Abstract

Glucocorticoid (GC) signaling via the glucocorticoid receptor (GR) is essential for lung maturation in mammals. Previous studies using global or conditional mouse model knockouts of the GR gene have established that GR-mediated signaling in the interstitial mesenchyme of the fetal lung is critical for normal lung development. Screens for downstream GC-targets in conditional mesenchymal GR deficient mouse lung (GRmesKO) identified Versican (*Vcan*), an important extracellular matrix component and cell proliferation regulator, as a potential GR-regulated target. We show that, of the five major VCAN isoforms, the VCAN-V1 isoform containing the GAGβ domain is the predominant VCAN isoform in the fetal mouse lung distal mesenchyme at both E16.5 and E18.5, whereas the GAGα-specific VCAN-V2 isoform was only localized to the smooth muscle surrounding proximal airways. Both *Vcan-V1* mRNA and protein levels were strongly overexpressed in the GRmesKO lung at E18.5. Finally, we investigated the GC regulation of the ECM protease ADAMTS 12 and showed that *Adamts 12* mRNA levels were markedly reduced at E18.5 in GRmesKO fetal mouse lung and were strongly induced by both cortisol and betamethasone in cultures of primary rat fetal lung fibroblasts. ADAMTS12 protein immunoreactivity was also strongly increased in the distal lung at E18.5, after dexamethasone treatment *in utero*. In summary, glucocorticoid signaling via GR represses GAGβ domain-containing VCAN isoforms in distal lung mesenchyme *in vivo* by repressing *Vcan* gene expression and, in part, by inducing the ECM protease ADAMTS12, thereby contributing to the control of ECM remodelling and lung cell proliferation prior to birth.

Key Words

- glucocorticoids
- glucocorticoid receptors
- versican
- lung development

Journal of Molecular Endocrinology
(2020) **64**, 155–164

Introduction

The final stages of mammalian lung development are characterised by a dramatic reduction in and remodelling of the mesenchymal compartment to provide a thinning of the distal airways. This process is, in part, regulated via the action of the glucocorticoid (GC) steroids acting via the glucocorticoid receptor (GR), a member of the nuclear receptor superfamily (Oshika *et al.* 1998, Cole *et al.* 2019). The importance of GCs in human lung development is highlighted by the now routine clinical administration of strong synthetic GCs, such as betamethasone, to mothers who are at risk of preterm birth to greatly reduce the morbidity and mortality of preterm infants at risk of developing respiratory distress syndrome (Liggins & Howie 1972, Roberts & Dalziel 2006).

https://jme.bioscientifica.com
https://doi.org/10.1530/JME-19-0235

There is, however, limited understanding of the important GC-regulated molecular mechanisms and gene networks in the developing lung required for normal development. Studies using global or conditional mouse knockouts of the GR gene (Bird *et al.* 2015) have established that GR signaling in the mesenchymal compartment of the lung is particularly crucial for normal lung maturation (Bird *et al.* 2014). Both global and mesenchymal conditional GR knockout (GRmesKO) mice die shortly after birth due to respiratory failure, as a result of lung mesenchymal cell hyperplasia which thickens the gas exchange barrier (Cole *et al.* 1995, Bird *et al.* 2014). Previous screens for differentially expressed genes in GRmesKO lungs have identified the mesenchyme-localised extracellular matrix (ECM) lectican protein Versican (VCAN) as strongly overexpressed in distal lung compartments (Bird *et al.* 2014).

VCAN has a core protein structure consisting of an N-terminal G1 domain and a carboxy-terminal G3 domain as well as two central chondroitin sulfate glycosaminoglycan (GAG) attachment domains, termed the GAGα and GAGβ domains (Wight 2002). The *Vcan* gene can be alternatively spliced into five isoforms *V0*, *V1*, *V2*, *V3*, and *V4*, and the encoded proteins have molecular weights of approximately 370, 263, 180, 74, and 115 kDa, respectively (Zimmermann & Ruoslahti 1989, Ricciardelli *et al.* 2009, Kischel *et al.* 2010). The VCAN-V1 isoform is expressed in the developing lung, heart, and limbs, while VCAN-V2 is the predominant VCAN isoform in the nervous system (Milev *et al.* 1998, Snyder *et al.* 2015). VCAN-V1 is known to promote cell proliferation and mesenchymal-epithelial transitions, whereas VCAN-V2 is known to inhibit cell proliferation (Sheng *et al.* 2005, 2006).

VCAN is an important ECM proteoglycan that, in the embryo, together with hyaluronan and fibronectin form a loose hydrated matrix to allow tissue hydration, solute permeability, appropriate cell proliferation, cell migration, and ECM assembly. This promotes cell growth and differentiation and tissue remodelling in a range of fetal tissues (Wight 2002, Ricciardelli *et al.* 2009, Nandadasa *et al.* 2014).Toward the end of embryogenesis there is a tightly regulated degradation and remodelling of ECM components in many tissues, including the fetal lung. The breakdown and clearance of VCAN involves a number of members of the A Disintegrin and Metalloproteinase with ThromboSpondin motifis (ADAMTS) proteinases family (Stanton *et al.* 2011). We have investigated the isoform-specific expression of *Vcan* in the mouse fetal lung and the GC/GR-mediated repression of VCAN during the late stages of lung development. This was assessed using isoform-specific qPCR, immunohistochemistry, and Western blot analysis in the GRmesKO and the normal fetal mouse lung. Finally, we assessed the expression levels and mode of GC regulation of three members of the ADAMTS ECM protease family.

Materials and methods

Animals

The care and use of all animals was approved by the Monash Animal Research Platform-1 Animal Ethics Committee at Monash University. Time-mated pregnant Sprague–Dawley rats were provided by Monash Animal Research Platform. Global GR-null fetal mice and mesenchymal-specific GR-null fetal mice (Mus musculus) were all of an isogenic C57BL/6 genetic background and generated using the Cre/LoxP gene recombination system and ,as previously described (Cole *et al.* 1995, Zhan *et al.* 2003, Bird *et al.* 2007, 2014) briefly, mice expressing Cre under the control of the Dermo1 promoter were crossed with $GR^{loxp/loxp}$ mice to generate $GR^{loxp/+}$, $Dermo1^{cre/+}$ mice. These mice were then time-mated with $GR^{loxp/loxp}$ to generate $GR^{loxp/loxp}$, $Dermo1^{cre/+}$ fetal mice. Pregnant dams were treated with dexamethasone (0.1 mg/kg) at E14.5 and E15.5, and fetal lung tissue were removed from pups at E18.5. The morning of a positive plug mating was designated as embryonic (E) day 0.5. Pregnant mice were killed according to approved guidelines of the Animal Ethics Committee at Monash University at E14.5, E16.5, E18.5, and PN 0.5, and the pups were killed by decapitation. The lungs of fetal pups (at least $n=4$ for each genotype collected from 2–3 litters) were isolated and either snap frozen in liquid N2 or fixed in 4% paraformaldehyde for further analysis as described subsequently. Tail snips from pups were collected at dissection for genotyping by PCR and gel electrophoresis as previously described (Bird *et al.* 2014).

Isolation of primary rat fetal lung fibroblasts

At E20, pregnant Sprague–Dawley rats were killed by CO_2, according to approved Animal Ethics Committee guidelines. Fetal lung fibroblasts (99% fibroblast cultures) were then isolated from pups via differential attachment as previously described (McDougall *et al.* 2011, 2013). Fibroblast cells from a single litter were pooled together and treated as one biological replicate ($n=1$). Cells were seeded onto six well dishes for RNA isolation in

https://jme.bioscientifica.com
https://doi.org/10.1530/JME-19-0235

Waymouth's MB 752/1 medium containing 10% heat-inactivated fetal calf serum (ThermoFisher), 50 U/mL penicillin, and 50 µg/mL streptomycin and were cultured for 6 h at 37°C in 5% CO_2.

Treatment of fetal lung fibroblasts

E20 primary rat lung fibroblasts were maintained in Waymouth's MB media containing 10% charcoal-stripped FBS, 50 U/mL Penicillin, and 50 µg/mL Streptomycin. The fibroblasts were treated with either corticosterone (1 µM in ethanol, Sigma-Aldrich), betamethasone (1 µM Celestone Chronodose, Schering-Plough, Australia), or 100% ethanol (vehicle control) for 6 h at 37°C at 5% CO_2.

Isolation of RNA, cDNA synthesis and qRT-PCR

Total RNA was obtained from embryonic mice and embryonic fetal rat lung fibroblasts using TRIzol (Invitrogen), and cDNA was prepared with a QuantiTech RT kit (Qiagen) (Moore *et al.* 2000). To measure mRNA levels of the four *Vcan* isoforms quantitative real-time PCR using SyBr green was performed following a previous protocol (Wong *et al.* 2007). *Vcan* DNA PCR primers were designed to overlap specific exon-exon junctions to amplify fragments representing the *V0* (exon 7–8), *V1* (exon 7–9), *V2* (exon 8–9), and *V3* (exon 6–9) specific *Vcan* isoform mRNAs (Fig. 1) and for *Adamts1*, *12*, and *15*. DNA primers to *Rps29* were also designed, and *Rps29* mRNA levels were used as a reference gene for normalisation of gene expression between samples. All qPCR products were verified by DNA sequencing. PCR DNA sequences (5′ to 3′) were: mouse *Vcan-V0* CAAGACAGGTCGATTGAGTG (forward) and GCAAACAGATCATGCAGTGG (reverse); *Vcan-V1* TGCTTTAAACGTCGATTGAGTG (forward) and CCTCTCCGTCTTCATCTTCC (reverse); mouse *Vcan-V2* GACAGGACCTGATCTCTGC (forward) and CCGACAAGG GTTAGAGTGAC (reverse); mouse *Vcan-V3* GACAGGACC TCTCTGC (forward) and CGACAAGGGTTAGTGACA (reverse); mouse *Rps29* GGACATAGGCTTCATTAAGTTGG (forward) and TCAGTCGAATCCATTCAAGGT (reverse); rat *Vcan-V0* CAAGACAGGT CGAATGAGTGA (forward) and ACAGTCCTCCTCTCCATCTT (reverse); rat *Vcan-V1* ATGCTTCCCTCTCCCTGATA (forward) and ACAGTCCTC CTCTCCATCTT (reverse); rat *Vcan-V2* CAGGACCTG ATCTCTGCAA (forward) and ACAGGTGCACAC ATAGGAAG (reverse); rat-*Gapdh* ACCATCTTCCAG GAGCGAGA (forward) and GTTCACACCC ATCACAAACA (reverse); rat *Rps29* GACATAGGCTTCATTAAGTTGGAC (forward) and GCATGATTGGTATCACAGGG (reverse); mouse *Adamts-1* CCTGTGAAGCC AAAGGCATTG (forward) and TGCACACAGACAGAGGTAGAGT (reverse); mouse *Adamts-15* GCTCATCTGCCGAGCCAAT (forward) and CAGCCAGCCTTGATGC ACTT (reverse); and mouse/rat *Adamts-12* CCGCTGGTTCCCAGTGTTTA (forward) and GTCACAGCCAACCCTCTTACA (reverse).

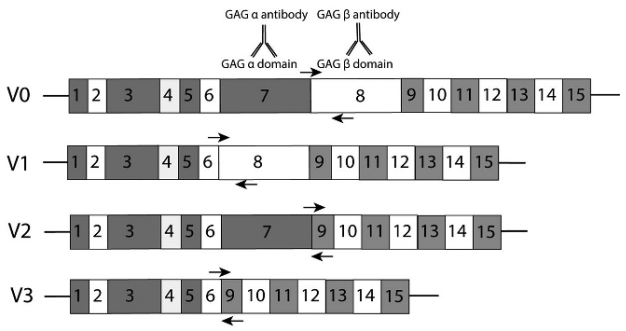

Figure 1
Schematic showing exon structure of the *Vcan* isoforms *V0*, *V1*, *V2*, and *V3*. *Vcan-V0* contains all exons, including exons 7 and 8 that encode the GAGα and GAGβ domains respectively. *Vcan-V1* lacks exon 7 (GAGα domain), *Vcan-V2* lacks exon 8 (GAG β domain), and *Vcan-V3* lacks both exon 7 and 8. Primer location for real-time qPCR are shown with black arrows and the exon epitope recognized by the two GAG antibodies is also indicated. Schematic diagram is not to scale.

Immunohistochemistry

Fetal mouse torsos were fixed in 4% paraformaldehyde (diluted in PBS) before they were processed and embedded in paraffin. Paraffin blocks were cut and 5 µM sections mounted on slides and used for immunohistochemistry. Sections were stained with either a rabbit anti-VCAN GAG β domain (1:200; Millipore, AB1033), rabbit anti-VCAN GAG α domain (1:300; Millipore, AB1032), or rabbit anti-ADAMTS12 (1:100; Abcam, ab203102) antibody. For VCAN antibody staining, slides were pre-digested with 0.1 U/mL Chondroitinase ABC (Sigma-Aldrich) in 50mM Tris pH 8.0, 60 mM sodium acetate, and 0.02% BSA for 1 h. Immunostaining was then performed following our previous protocol (Bird *et al.* 2014).

Immunohistochemistry analysis

Stained sections were imaged by light microscopy using Eclipse E400, Nikon. Three sections per animal were stained and the three photos per section were analysed using the image analysis software, Image-pro plus, Version 6.2, media cybernetics.

https://jme.bioscientifica.com
https://doi.org/10.1530/JME-19-0235

Western blot

Proteins were isolated from mouse lung tissue in urea buffer (4 M urea, 50 mM sodium acetate, 0.2 M NaCl, and 0.5% Trition×in H_2O). Briefly, 500 µL of urea buffer was added to each lung sample, and the samples were then homogenised and incubated on ice for 15 min. Lung samples were centrifuged for 20 min at 4°C and 14,000 ***g***, supernatants collected, and protein concentrations determined using a DC assay (BioRad). 40 µg of protein was pre-treated with 0.5 U of Chondroitinase ABC (Sigma-Aldrich) in 50 mM Tris pH 8.0 and 60 mM sodium acetate for 2 h before separation by electrophoresis on a TGX sain-free 7.5% fastcast SDS-PAGE polyacrylamide gel (BioRad). Following a standard protocol, the protein was transferred onto a nylon membrane and incubated with either VCAN GAG-β specific antibody (0.5 µg/mL; Millipore, AB1033), VCAN GAG alpha specific antibody (0.5 µg/mL; Millipore, AB1032), or VIMENTIN (1:200 dilution; Cell signalling, D21H3). After X-ray imaging, the membranes were stripped with 0.5 M NaOH and incubated with a BETA ACTIN antibody (1:100,000; Sigma-Aldrich) to control protein loading.

Statistical analysis

GraphPad Prism software was used for all statistical analysis, with statistical significance nominally set at $P<0.05$. Two groups were compared using an unpaired *t*-test, and multiple groups were compared by either a 1-way or 2-way ANOVA with a Tukey's post hoc test.

Results

Expression of *Vcan* isoforms in the developing lung during late gestation

The mRNA levels of specific *Vcan* isoforms were measured with isoform-specific primer pairs (Fig. 1) in total RNA samples from the fetal lung at various times during fetal lung development using qPCR ($n=4$/group). mRNA levels were measured from E14.5 to P0.5 and showed a large 11-, 8.5-, 6.6-, and 6.1-fold decrease of *V0*, *V1*, *V2*, and *V3* isoform mRNA levels from E14.5 to P0.5 ($P\leq0.05$) respectively (Fig. 2A, B, C and D). We also investigated VCAN protein levels with a VCAN GAG-beta-specific and a GAG-alpha-specific antibody at E16.5 ($n=3$) and E18.5 ($n=3$) in the mouse fetal lung via Western blot analysis (Fig. 2E, F and G) and detected a significant decrease in VCAN protein level from E16.5 to E18.5. These results show that *Vcan* expression at both the RNA and protein levels strongly decrease in the fetal lung shortly before birth.

Localization of GAGβ-containing VCAN-V1 and GAGα-containing VCAN-V2 in the mouse lung at E16.5 and E18.5

To determine the localization of GAGα- and GAGβ-containing VCAN proteins at the E16.5 and E18.5 fetal mouse lung, immunohistochemistry was performed using antibodies specific for the GAGβ and GAGα domains of VCAN (Fig. 3). Transverse sections of whole fetal mouse

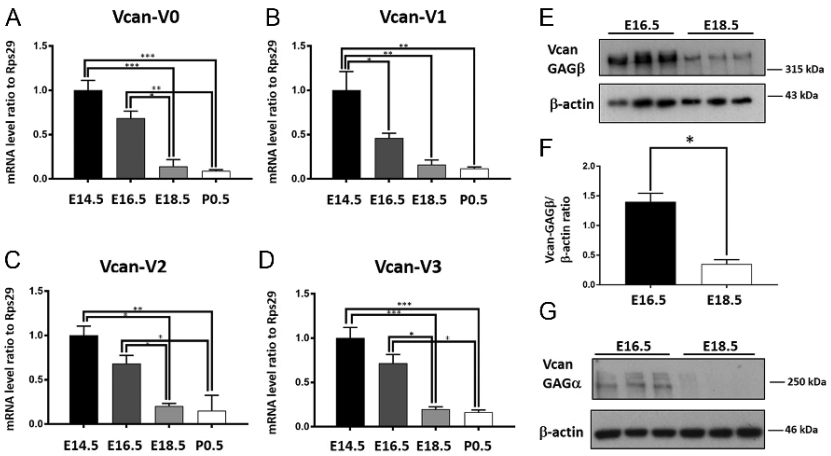

Figure 2
Expression of *Vcan* isoforms during late gestation of lung development. The mRNA levels (mean ± s.e.m.) of *Vcan* in C57/BL6 mice (Mus musculus) during late lung gestation were determined for (A) *V0*, (B) *V1*, (C) *V2*, and (D) *V3-Vcan* at E14.5 (black bars), E16.5 (dark grey bars), E18.5 (light grey bars), and P0.5 (white bars) fetal lung total RNA ($n=4$). The mRNA levels in all groups are expressed relative to mRNA levels of the housekeeping gene *Rps29*. Western blot analysis (mean ± s.e.m.) (E and F) for protein levels of GAGβ-containing VCAN (V0/V1) at E16.5 and E18.5 in the fetal mouse lung ($n=3$). Total protein levels were determined relative to β-ACTIN levels. Significant differences were analysed by 1-way ANOVA with Tukey's post hoc test (*V0*: $P\leq0.0001$, *V1*: $P=0.0004$, *V2*: $P=0.0004$, and *V3*: $P\leq0.0001$) or an unpaired *t*-test (F) and are all indicated by $*P<0.05$, $**P<0.001$, and $***P<0.0001$. (G) Western blot for protein levels of GAG alpha-containing VCAN (V0/V2) at E16.5 and E18.5 in the fetal mouse lung ($n=3$).

https://jme.bioscientifica.com
https://doi.org/10.1530/JME-19-0235

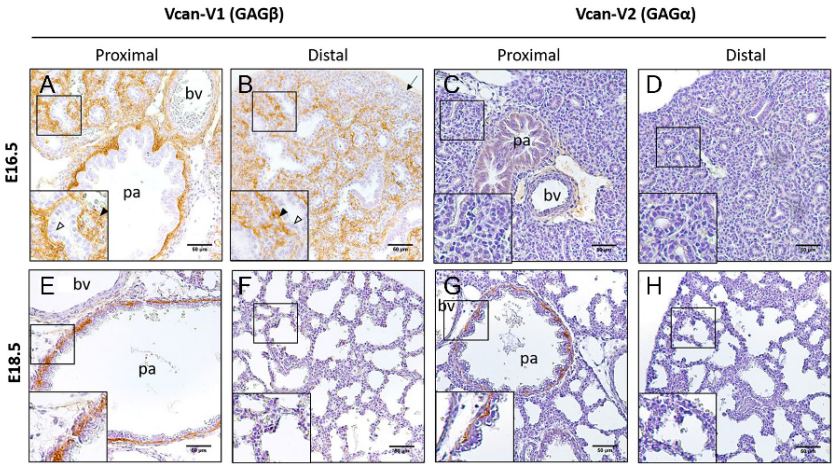

Figure 3
Localization of GAGβ- and GAGα-containing VCAN in the fetal lung at E16.5 and E18.5 of gestation. Immunohistochemistry was performed with antibodies specific for the VCAN GAGβ (V0/V1) and GAGα (V0/V2) domains at E16.5 and E18.5. Boxed regions are magnified in the bottom left corner of each image. All images were of the left lobe and are representative of three animals per age group. Arrow indicates mesothelium, arrowhead indicates mesenchyme, and empty arrowhead indicates epithelium; pa = proximal airway; bv = blood vessel.

torsos were used and the left lung lobes were chosen for all imaging. At E16.5, GAGβ-specific VCAN staining was observed in most mesenchymal compartments including the smooth muscle surrounding large proximal airways (Fig. 3A and E) and distal lung mesenchyme (Fig. 3B and F). Interestingly, GAGβ-specific staining appeared to show a gradient of expression. Qualitatively, staining appeared darker toward airways, compared to the distal regions of the lung. Indeed, GAGβ-specific VCAN-V1 staining was often virtually absent in the outermost regions of the lung, adjacent to the mesothelium (Fig. 3B, black arrow, $n=3$, one representative image is shown). At E18.5, GAGβ-specific VCAN protein staining was barely detectable in the distal lung mesenchyme (Fig. 3F) but instead was primarily restricted to the smooth muscle layer surrounding large proximal airways (Fig. 3E). In contrast GAGα-specific VCAN staining was only reliably detected in the smooth muscle layer surrounding the large proximal airways and was completely absent in the distal lung mesenchyme at both E16.5 and E18.5 (Fig. 3C, D, G and H). The VCAN immunostaining pattern observed in the distal fetal lung mesenchyme can be attributed to the GAGβ-specific VCAN-V1 isoform rather than VCAN-V0, as the latter also contains the GAGα domain that was not stained in this region of the lung by the GAGα-specific antibody. This demonstrates that, at E16.5, the VCAN-V1 isoform is the predominant isoform present in the fetal lung and that the levels of VCAN-V1 regress dramatically over 2 days just before birth.

Increased *Vcan* isoform mRNA and VCAN-V1 protein levels in the GRmesKO lung

We next investigated the influence of glucocorticoid signaling on *Vcan-V1* levels in the distal lung mesenchyme using GRmesKO mice, where the GR has been deleted using the Cre/loxp recombination system in the fetal lung mesenchyme (Bird *et al.* 2014). We first measured mRNA levels for the specific *Vcan* isoforms in GRmesKO mouse lungs by qPCR ($n=4$) (Fig. 4A, B, C and D). We detected a 2.3-, 1.6-, 1.8-, and 1.8-fold increase for *Vcan V0*, *V1*, *V2*, and *V3* mRNAs respectively in E18.5 GRmesKO lung relative to control lung ($P \geq 0.01$) (Fig. 4A, B, C and D). In comparison, we detected no difference in mRNA levels for all isoforms at E16.5 for GRmesKO lung vs controls (Fig. 4A, B, C and D). We then measured protein levels of GAGβ-specific VCAN in whole tissue extracts from E18.5 control and GRmesKO mouse lung ($n=7$) using Western blot analysis (Fig. 4E and F, 4 representative wells are shown). There was a significant 3-fold increase in GAGβ VCAN protein in the GRmesKO mouse lung. Immunohistochemistry was then used to investigate localisation of VCAN in the GRmesKO mouse lung using the GAGα-specific and GAGβ-specific VCAN antibodies. At E16.5, there appeared to be no difference in the level and localisation of either GAGα- or GAGβ-containing VCAN proteins between the GRmesKO and control lung (Fig. 5A). At E18.5, strong immunostaining of GAGβ-containing VCAN was again evident in the smooth muscle layer surrounding large airways in GRmesKO lungs (Fig. 5A), and in agreement with Fig. 4E, we detected a dramatic increase in GAGβ-specific staining in the distal lung mesenchyme in the E18.5 GRmesKO lung compared to aged-matched controls (Fig. 5A). Similar to Fig. 3, there was virtually no VCAN immunostaining detected in the distal lung with the GAGα-specific antibody in either the GRmesKO lung or controls (Fig. 5A). This indicates that in the absence of GR-mediated signaling there is no normal repression and clearance of VCAN V1 protein from the distal lung mesenchyme close to birth.

https://jme.bioscientifica.com
https://doi.org/10.1530/JME-19-0235

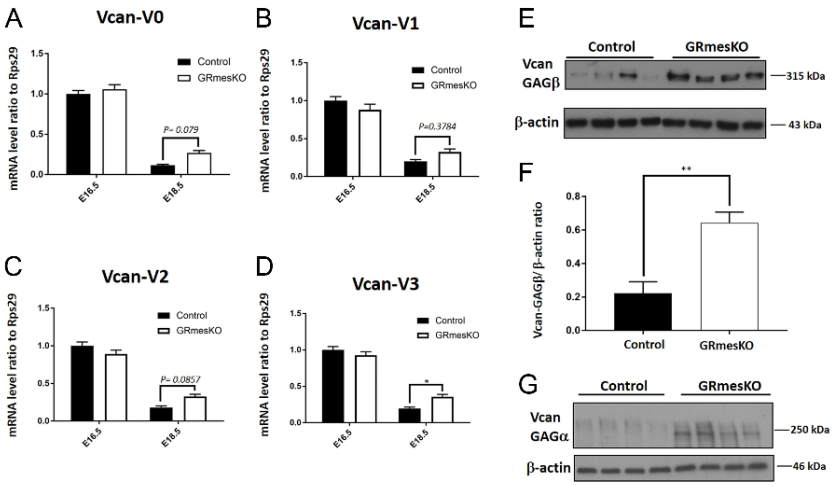

Figure 4
Vcan isoform expression levels in the GRmesKO fetal mouse lung. *Vcan* isoform mRNA levels (mean ± s.e.m.) at E16.5 and E18.5 in control (black bars) and GRmesKO (white bars) embryonic mouse lung ($n = 4$). (A) *V0* effect on embryonic age: $P \leq 0.0001$, effect on genotype: $P = 0.0177$, and interaction: $P = 0.2528$; (B) *V1* effect on embryonic age: $P \leq 0.0001$, effect on genotype: $P = 0.9918$, and interaction: $P = 0.0364$; (C) *V2* effect on embryonic age: $P \leq 0.0001$, effect on genotype: $P = 0.6458$, and interaction: $P = 0.0089$; and (D) *V3* effect on embryonic age: $P \leq 0.0001$, effect on genotype: $P = 0.2804$, and interaction: $P = 0.0097$. The mRNA levels in all groups are expressed relative to levels of *Rps29* mRNA. Western blot analysis (mean ± s.e.m.) (E and F) for protein levels of GAG β at E18.5 in control and GRmesKO embryonic mouse lung ($n = 7$). (F) Western blot quantitation representative of seven animals per group. Total protein levels are relative to β-ACTIN. Significance in A–D was assessed by a 2-way ANOVA with a Tukey's post hoc test and in F by an unpaired *t*-test. Significant differences are indicated by $*P < 0.05$ or by a specific *P* value. (G) Western blot for protein levels of GAG alpha-contain VCAN (V0/V2) at E18.5 in control and GRmesKO fetal mouse lung ($n = 4$).

Increased GAGβ-specific staining in distal lung areas were also quantitated and compared in GRmesKO and GR-null lung at E18.5 and shown to increase (Fig. 5B). To rule out that this increase did not just reflect on a greatly expanded distal area, Western blot analysis was performed with an antibody to the distal mesenchyme marker VIMENTIN (Fig. 5C). We observed a small but 1.3-fold increase in VIMENTIN protein level that was not unexpected, as GRmesKO mice have more lung mesenchymal tissue; however, we also observed a far greater increase in GAGβ protein levels with an increase of approximately 2-fold (Fig. 5D and E). This confirmed that there was increased GAGβ-specific protein content per mesenchyme area in the distal fetal lung.

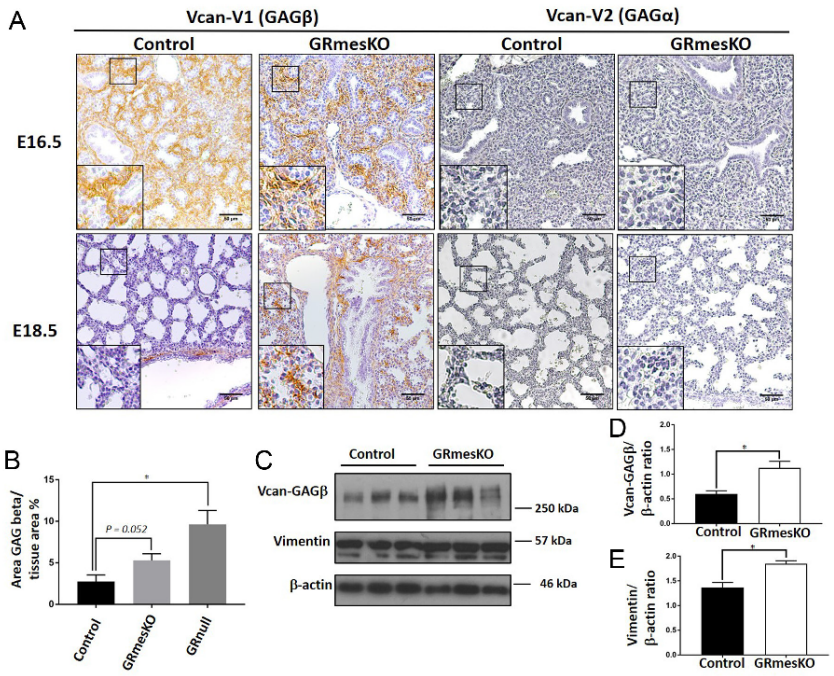

Figure 5
Localization of the V1 (GAGβ) and V2 (GAGα) isoforms of VCAN at E16.5 and E18.5 in the GRmesKO fetal mouse lung by immunohistochemistry. Immunohistochemistry was performed with antibodies specific for the VCAN GAGβ (V1) and GAGα (V2) domains at E16.5 and E18.5 for control and GRmesKO fetal mice (A). Boxed regions are magnified in the bottom left corner of each image. All images were of the left lobe and are representative of three animals per age group. GAG beta immunohistochemistry analysis (mean ± s.e.m.) on E18.5 control (black bar, $n = 8$), GRmesKO (light grey bar, $n = 6$), and GR-null (dark grey bar, $n = 7$) fetal mice (B). Three sections per an animal were stained with GAG beta, and three images from each section were analysed using Image-pro plus. Percentage of GAG beta staining is relative to total tissue in the image. (C, D, and E) Western blot analysis of protein levels of GAG beta containing VCAN (V1/V0) and VIMENTIN in E18.5 control and GRmesKO fetal lung ($n = 3$). Significance between the groups was assessed by 1-way ANOVA with a Tukey's post hoc test (B: $P = 0.0015$) or an un-paired *t*-test (D and E). Significant differences are indicated by $*P < 0.05$ or individual *P* value.

https://jme.bioscientifica.com
https://doi.org/10.1530/JME-19-0235

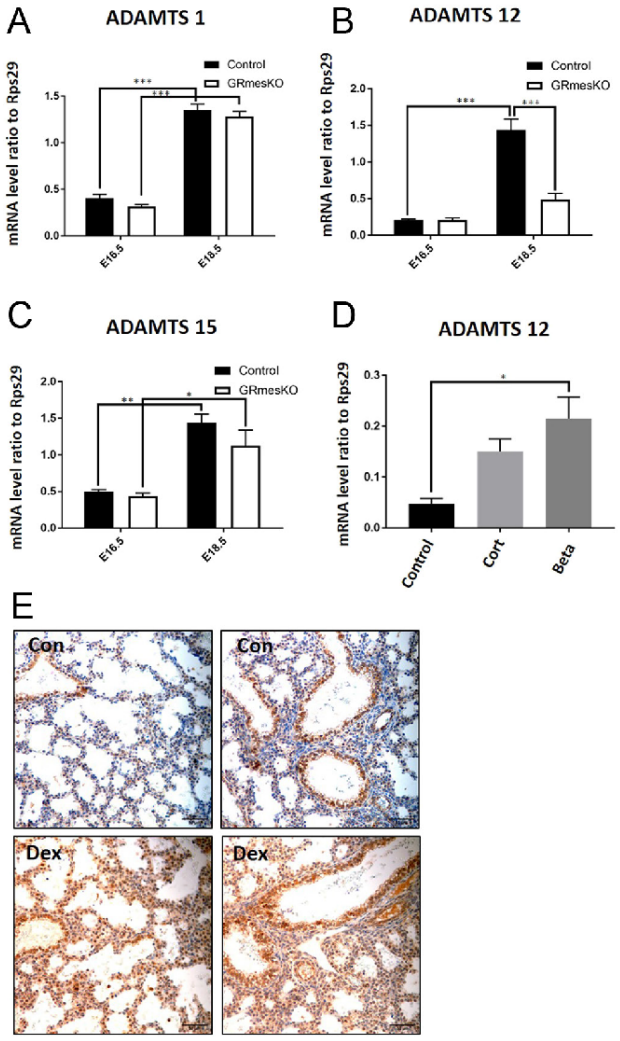

Figure 6

Expression of ADAMTS proteases in GRmesKO fetal mouse lung and in glucocorticoid treated primary rat fetal lung fibroblasts. mRNA levels determined by qPCR (mean ± S.E.M.) of three *Adamts* proteases at E16.5 and E18.5 control and GRmesKO mouse lung for (A) *Adamts 1* effect on embryonic age: $P \leq 0.0001$, effect on genotype: $P = 0.1239$, and interaction: $P = 0.8433$; (B) *Adamts 12* effect on embryonic age: $P \leq 0.0001$, effect on genotype: $P = 0.0002$, and interaction: $P = 0.0002$; and (C) *Adamts 15* effect on embryonic age: $P \leq 0.0001$, effect on genotype: $P = 0.1521$, and interaction: $P = 0.3341$ ($n = 4$). (D): *Adamts 12* mRNA levels (mean ± S.E.M.) for E20 primary rat lung fibroblasts treated with either control, corticosterone (cort), or betamethasone (beta) ($n = 5$). (E) Immunohistochemistry for ADAMTS 12 in mouse fetal lung at E18.5 following injection of pregnant dams at E14.5 and E15.5 with dexamethasone-21-phosphate (0.1 mg/kg). Lung sections (400× magnification) from a control (Con) and dexamethasone (Dex) treated E18.5 fetal mouse. Scale bar of 50 µM. Significance in A–C was assessed by a 2-way ANOVA with a Tukey's post hoc test. Significance in D was determined by a 1-way ANOVA with a Tukey's post hoc test. Significant differences between groups are indicated by $^*P < 0.05$, $^{**}P < 0.001$, $^{***}P < 0.0001$, or by a specific P value.

ADAMTS protease expression in the fetal mouse lung

Degradation and turnover of VCAN in embryonic tissues is facilitated by the presence and action of specific members of the ADAMTS protease family (Stanton *et al.* 2011). We assessed the mRNA levels of three *Adamts* proteases, *1*, *12*, and *15*, whose transcripts we detected in a recent RNA-sequencing analysis of GC-treated cultured fetal rat lung fibroblasts (Seow *et al.* 2019). *Adamts 1*, *12*, and *15* mRNA levels were measured by real-time qPCR in total lung RNA at both E16.5 and E18.5 in control and GRmesKO mouse lung. We observed an increase in *Adamts 1*, *12*, and *15* mRNA levels from E16.5 to E18.5 in control lung with fold changes of 3.3, 6.9, and 2.9, respectively (Fig. 6A, B and C). We also measured the effect of the loss of GR-signalling in the mesenchyme on *Adamts* mRNA levels at E16.5 and E18.5 in GRmesKO mice. At E18.5, we observed a significant loss of the normal increase in mRNA levels for only *Adamts 12*, with no significant effect on *Adamts 1* and *15* mRNA levels (Fig. 6A, B and C).

Glucocorticoids induce expression of ADAMTS12 in the fetal lung

We detected a rapid reduction in VCAN levels in the fetal lung for over 2 days between E16.5 and E18.5, and this decrease could be facilitated by increased activity of specific ECM proteases such as ADAMTS12. We next assessed direct glucocorticoid induction of *Adamts12* mRNA using real-time qPCR with primary cultures of E20 rat fetal lung fibroblasts stimulated with corticosterone and betamethasone for 6 h (Fig. 6D). We observed a strong 4.5-fold increase of *Adamts12* mRNA levels in betamethasone treated fetal lung fibroblasts relative to control cultures, clearly implicating *Adamts12* protease as a direct GC-induced target in the rodent fetal lung. To confirm induction of ADAMTS12 at the protein level *in vivo*, we analysed fetal mouse lungs at E18.5 from pups that had been treated *in utero* with dexamethasone (0.1 mg/kg) at E14.5 and E15.5. Immunohistochemistry using a rabbit anti-ADAMTS12 antibody showed a strong increase in ADAMTS12 immunoreactivity in distal lung regions compared to control treated pups (Fig. 5E). These results suggest that reduced expression and levels of VCAN in the fetal lung is coordinated by glucocorticoid signaling via a repression of *Vcan* expression and a possible increase

https://jme.bioscientifica.com
https://doi.org/10.1530/JME-19-0235

in VCAN degradation and clearance by induction of the ECM protease ADAMTS12.

Discussion

In this study, we have demonstrated that GR-mediated signaling regulates rapid repression and regression of VCAN during the late stages of mouse lung development and that, in the absence of GR-mediated cell signaling in the lung mesenchyme, the *Vcan* gene is overexpressed and the VCAN-V1 isoform proteoglycan persists in the distal lung prior to birth contributing to a state of ECM dysfunction and cellular over proliferation. We have shown here that the mRNA levels of the *Vcan V0*, *V1*, *V2*, and *V3* isoforms all normally decline rapidly during the latter stages of mouse lung development from E14.5 to P0.5, and using a GAGβ-specific VCAN antibody we also observed a rapid decrease in VCAN-V1 protein levels primarily in the distal regions of the developing mouse fetal lung. This is consistent with previous studies in the developing sheep and mouse lung that showed high levels of *Vcan* mRNA and VCAN protein at early- to mid-gestation stages and then a rapid decline in the days before birth (Faggian *et al.* 2007, Snyder *et al.* 2015). Studies in sheep observed a similar expression pattern and reported that there was an identical reduction in both V0 and V1 isoforms during late lung development (Faggian *et al.* 2007). We show for the first time that this rapid reduction in V0/V1 VCAN is, in part, driven by glucocorticoid receptor mediated cell signaling in the distal mesenchymal compartment of the fetal lung.

From approximately E16.5 in the mouse, there is extensive remodelling of the distal lung and capillary bed network that involves proteolytic breakdown of matrix proteins (Herriges & Morrisey 2014). At this stage of development, the GAGβ-containing VCAN-V1 isoform was localised to all mesenchymal compartments, yet by E18.5 this was restricted to the smooth muscle layer surrounding the large proximal airways. This coincides with a period of rapid remodelling of the mesenchyme, during which the lung mesenchyme dramatically thins allowing sufficient gas exchange at birth (Herriges & Morrisey 2014). We have previously reported that the reduction in mesenchyme tissue is associated with a decrease of cell proliferation rather than an increase in cell apoptosis (Bird *et al.* 2014). VCAN is a known promoter of cell proliferation, acting as a cell-surface receptor for growth factors such as the epithelial cell-growth factor midkine (Muramatsu 2014).

In comparison, GAGα-domain containing VCAN isoforms were only detected in the smooth muscle layer surrounding the large airways at both E16.5 and E18.5, and these levels were unchanged during fetal development. At earlier time points in lung development, the localisation of GAGα-containing VCAN to only the smooth muscle in the lung was also described by Snyder *et al.* (Snyder *et al.* 2015). The lack of GAGα-staining VCAN in the distal mesenchyme region of the lung suggests that V0 is not a predominant VCAN isoform in the fetal lung, as the V0 isoform contains both the GAGα and GAGβ domains. The V0 isoform could still potentially be expressed in the bronchial smooth muscle, where GAGα and GAGβ-specific antibody staining overlaps. Interestingly, we also observed a consistent proximal to distal gradient of high to low expression of GAGβ at E16.5. This leads us to speculate that the GAGβ domain plays an important role for recruitment of growth factors to stimulate cell proliferation of the more proximal mesenchymal tissue, particularly smooth muscle.

The importance of GC-signalling for lung maturation has been clearly demonstrated in GRnull mice which die shortly after birth due to acute respiratory distress (Cole *et al.* 1995). It has also been shown that GC-GR signaling in the mesenchymal compartment of the fetal lung is of greatest importance for normal lung development (Bird *et al.* 2014). Here we demonstrate that the *V0*, *V1*, *V2*, and *V3 Vcan* isoforms are all overexpressed in the GRmesKO mouse lung at E18.5, indicating a loss on normal GC-GR driven repression of *Vcan* gene expression. Although there is no significant difference between controls and GRmesKO at E16.5 this is somewhat expected, as the GRnull and GRmesKO lungs appear histologically normal until E15.5 but from E16.5 develop a progressive hypercellularity (Cole *et al.* 1995). The protein accumulation of GAGα was similar between controls and GRmesKO fetal lungs at both E16.5 and E18.5. However, we did observe variable mesenchymal GAGβ protein staining in E18.5 GRmesKO mouse lung. Furthermore, there was a significant increase in protein levels evident by Western blot. Further analysis of the distal mesenchyme compartment with VIMENTIN showed that there was a significant and higher content of GAG β-VCAN protein per area of distal mesenchyme.

The ADAMTS family of ECM proteases has 19 members, and to date 6 members, ADAMTS1, 4, 5, 9, 15, and 20, have been shown to cleave VCAN (Nandadasa *et al.* 2014). VCAN has ADAMTS cleavage sites in both the GAG beta and GAG alpha domains, Glu^{405}-Gln^{406} and Glu^{1428}-Ala^{1429}, respectively (Sandy *et al.* 2001, Westling *et al.* 2004). We have demonstrated that *Adamts 12* mRNA levels were greatly reduced in the GRmesKO lung, most likely due to a loss of normal GC-induced expression,

https://jme.bioscientifica.com
https://doi.org/10.1530/JME-19-0235

and this loss of ADAMTS 12 may contribute to the higher levels of VCAN protein observed in GRmesKO. Multiple ADAMTS proteases have been shown to cleave VCAN, and further studies are required to assess the localisation of specific ADAMTS at the protein level in the fetal lung. We have shown that both corticosterone and betamethasone can rapidly stimulate increased expression of ADAMTS 12 in fetal lung fibroblasts and that dexamethasone treatment *in vivo* stimulates strong ADAMTS 12 immunostaining in the distal mesenchyme prior to birth. Therefore, loss of normal GC-stimulated induction of ADAMTS 12 may strongly contribute to the lack of normal regression and clearance of VCAN just prior to birth. Respiratory studies in *Adamts12*-deficient mice provide evidence for a protective effect of ADAMTS 12 against bronchial inflammation that is in line with the anti-inflammatory actions of glucocorticoid steroids (Paulissen *et al.* 2012). Other studies have demonstrated that GCs can induce expression of *Adamts* enzymes, such as *Adamts1* in C2C12 myoblasts, following treatment with dexamethasone (McRae *et al.* 2017). We, therefore, suggest that GCs are stimulating increased ADAMTS 12 levels in the lung which, in turn, facilitates a lowering of the levels of VCAN. Further functional studies are required to investigate the direct genomic mechanisms involved between activated GC-GR signaling and regulation of the *Adamts 12* gene.

VCAN is able to interact with many binding partners (Nandadasa *et al.* 2014). One interaction, believed to be important, during lung development is of extracellular VCAN with MIDKINE, an epithelial-derived growth factor. MIDKINE is a heparin-binding growth factor, localised to the epithelium with roles in cell survival, migration, cytokine expression, and cell differentiation (Muramatsu 2014). We predict that GC/GR signaling late in lung development represses *Vcan* expression through either a direct or indirect mechanism, thereby preventing MIDKINE binding to VCAN and promoting cell proliferation. It has been shown that the major form of VCAN that binds to MIDKINE is VCAN-V1 (Zou *et al.* 2000), and we have demonstrated that VCAN-V1 is the dominant form expressed during fetal lung development.

In conclusion, we have shown that the GAGβ domain-containing VCAN-V1 isoform is the predominant VCAN proteoglycan present during the fetal stages of lung development in rodents. GCs, acting via the GR, drive the repression of *Vcan* gene expression and also the rapid reduction and potentially the clearance of VCAN from the fetal lung prior to birth. GCs do this, in part, by mediating induction of the ADAMT 12 protease that could then degrade and potentially mediate the clearance of VCAN from distal lung regions. Together, these results demonstrate that GC steroids acting via the GR co-ordinately regulate repression of *Vcan* gene expression and VCAN protein to contribute to the normal development of the fetal respiratory system in mammals.

Declaration of interest

The authors declare that there is no conflict of interest that could be perceived as prejudicing the impartiality of the research reported.

Funding

This work was funded by a Program Grant (384100) from the National Health and Medical Research Council of Australia and Grant-in-Aid from the Rebecca Cooper Foundation (10497).

Author contribution statement

T J C, A D B, and K L S designed the experiments and wrote the manuscript. K L S, A D B, B K L S, and J N performed the experiments. M W, A M, and S H helped finalise the manuscript.

Acknowledgements

The authors acknowledge the facilities and the scientific and technical assistance of Monash Histology Platform, Department of Anatomy and Developmental Biology, Monash University, and the Monash Animal Research Platform for their technical expertise.

References

Bird AD, Tan KH, Olsson PF, Zieba M, Flecknoe SJ, Liddicoat DR, Mollard R, Hooper SB & Cole TJ 2007 Identification of glucocorticoid-regulated genes that control cell proliferation during murine respiratory development. *Journal of Physiology* **585** 187–201. (https://doi.org/10.1113/jphysiol.2007.136796)

Bird AD, Choo YL, Hooper SB, McDougall AR & Cole TJ 2014 Mesenchymal glucocorticoid receptor regulates the development of multiple cell layers of the mouse lung. *American Journal of Respiratory Cell and Molecular Biology* **50** 419–428. (https://doi.org/10.1165/rcmb.2013-0169OC)

Bird AD, McDougall AR, Seow B, Hooper SB & Cole TJ 2015 Glucocorticoid regulation of lung development: lessons learned from conditional GR knockout mice. *Molecular Endocrinology* **29** 158–171. (https://doi.org/10.1210/me.2014-1362)

Cole TJ, Blendy JA, Monaghan AP, Krieglstein K, Schmid W, Aguzzi A, Fantuzzi G, Hummler E, Unsicker K & Schutz G 1995 Targeted disruption of the glucocorticoid receptor gene blocks adrenergic chromaffin cell development and severely retards lung maturation. *Genes and Development* **9** 1608–1621. (https://doi.org/10.1101/gad.9.13.1608)

Cole TJ, Short KL & Hooper SB 2019 The science of steroids. *Seminars in Fetal and Neonatal Medicine* **24** 170–175. (https://doi.org/10.1016/j.siny.2019.05.005)

Faggian J, Fosang AJ, Zieba M, Wallace MJ & Hooper SB 2007 Changes in versican and chondroitin sulfate proteoglycans during structural development of the lung. *American Journal of Physiology: Regulatory,*

Integrative and Comparative Physiology **293** R784–R792. (https://doi.org/10.1152/ajpregu.00801.2006)

Herriges M & Morrisey EE 2014 Lung development: orchestrating the generation and regeneration of a complex organ. *Development* **141** 502–513. (https://doi.org/10.1242/dev.098186)

Kischel P, Waltregny D, Dumont B, Turtoi A, Greffe Y, Kirsch S, De Pauw E & Castronovo V 2010 Versican overexpression in human breast cancer lesions: known and new isoforms for stromal tumor targeting. *International Journal of Cancer* **126** 640–650. (https://doi.org/10.1002/ijc.24812)

Liggins GC & Howie RN 1972 A controlled trial of antepartum glucocorticoid treatment for prevention of the respiratory distress syndrome in premature infants. *Pediatrics* **50** 515–525.

McDougall AR, Hooper SB, Zahra VA, Sozo F, Lo CY, Cole TJ, Doran T & Wallace MJ 2011 The oncogene Trop2 regulates fetal lung cell proliferation. *American Journal of Physiology: Lung Cellular and Molecular Physiology* **301** L478–L489. (https://doi.org/10.1152/ajplung.00063.2011)

McDougall AR, Hooper SB, Zahra VA, Cole TJ, Lo CY, Doran T & Wallace MJ 2013 Trop2 regulates motility and lamellipodia formation in cultured fetal lung fibroblasts. *American Journal of Physiology: Lung Cellular and Molecular Physiology* **305** L508–L521. (https://doi.org/10.1152/ajplung.00160.2012)

McRae N, Forgan L, McNeill B, Addinsall A, McCulloch D, Van der Poel C & Stupka N 2017 Glucocorticoids improve myogenic differentiation in vitro by suppressing the synthesis of versican, a transitional matrix protein overexpressed in dystrophic skeletal muscles. *International Journal of Molecular Sciences* **18** E2629. (https://doi.org/10.3390/ijms18122629)

Milev P, Maurel P, Chiba A, Mevissen M, Popp S, Yamaguchi Y, Margolis RK & Margolis RU 1998 Differential regulation of expression of hyaluronan-binding proteoglycans in developing brain: aggrecan, versican, neurocan, and brevican. *Biochemical and Biophysical Research Communications* **247** 207–212. (https://doi.org/10.1006/bbrc.1998.8759)

Moore XL, Hoong I & Cole TJ 2000 Expression of the 11beta-hydroxysteroid dehydrogenase 2 gene in the mouse. *Kidney International* **57** 1307–1312. (https://doi.org/10.1046/j.1523-1755.2000.00967.x)

Muramatsu T 2014 Structure and function of midkine as the basis of its pharmacological effects. *British Journal of Pharmacology* **171** 814–826. (https://doi.org/10.1111/bph.12353)

Nandadasa S, Foulcer S & Apte SS 2014 The multiple, complex roles of versican and its proteolytic turnover by ADAMTS proteases during embryogenesis. *Matrix Biology* **35** 34–41. (https://doi.org/10.1016/j.matbio.2014.01.005)

Oshika E, Liu S, Ung LP, Singh G, Shinozuka H, Michalopoulos GK & Katyal SL 1998 Glucocorticoid-induced effects on pattern formation and epithelial cell differentiation in early embryonic rat lungs. *Pediatric Research* **43** 305–314. (https://doi.org/10.1203/00006450-199803000-00001)

Paulissen G, El Hour M, Rocks N, Gueders MM, Bureau F, Foidart JM, Lopez-Otin C, Noel A & Cataldo DD 2012 Control of allergen-induced inflammation and hyperresponsiveness by the metalloproteinase ADAMTS-12. *Journal of Immunology* **189** 4135–4143. (https://doi.org/10.4049/jimmunol.1103739)

Ricciardelli C, Sakko AJ, Ween MP, Russell DL & Horsfall DJ 2009 The biological role and regulation of versican levels in cancer. *Cancer Metastasis Reviews* **28** 233–245. (https://doi.org/10.1007/s10555-009-9182-y)

Roberts D & Dalziel S 2006 Antenatal corticosteroids for accelerating fetal lung maturation for women at risk of preterm birth. *Cochrane Database of Systematic Reviews* Cd004454. (https://doi.org/10.1002/14651858.CD004454.pub2)

Sandy JD, Westling J, Kenagy RD, Iruela-Arispe ML, Verscharen C, Rodriguez-Mazaneque JC, Zimmermann DR, Lemire JM, Fischer JW, Wight TN, *et al.* 2001 Versican V1 proteolysis in human aorta in vivo occurs at the Glu441-Ala442 bond, a site that is cleaved by recombinant ADAMTS-1 and ADAMTS-4. *Journal of Biological Chemistry* **276** 13372–13378. (https://doi.org/10.1074/jbc.M009737200)

Seow BKL, McDougall ARA, Short KL, Wallace MJ, Hooper SB & Cole TJ 2019 Identification of betamethasone-regulated target genes and cell pathways in fetal rat lung mesenchymal fibroblasts. *Endocrinology* **160** 1868–1884. (https://doi.org/10.1210/en.2018-01071)

Sheng W, Wang G, Wang Y, Liang J, Wen J, Zheng PS, Wu Y, Lee V, Slingerland J, Dumont D, *et al.* 2005 The roles of versican V1 and V2 isoforms in cell proliferation and apoptosis. *Molecular Biology of the Cell* **16** 1330–1340. (https://doi.org/10.1091/mbc.e04-04-0295)

Sheng W, Wang G, La Pierre DP, Wen J, Deng Z, Wong CK, Lee DY & Yang BB 2006 Versican mediates mesenchymal-epithelial transition. *Molecular Biology of the Cell* **17** 2009–2020. (https://doi.org/10.1091/mbc.e05-10-0951)

Snyder JM, Washington IM, Birkland T, Chang MY & Frevert CW 2015 Correlation of versican expression, accumulation, and degradation during embryonic development by quantitative immunohistochemistry. *Journal of Histochemistry and Cytochemistry* **63** 952–967. (https://doi.org/10.1369/0022155415610383)

Stanton H, Melrose J, Little CB & Fosang AJ 2011 Proteoglycan degradation by the ADAMTS family of proteinases. *Biochimica and Biophysica Acta* **1812** 1616–1629. (https://doi.org/10.1016/j.bbadis.2011.08.009)

Westling J, Gottschall PE, Thompson VP, Cockburn A, Perides G, Zimmermann DR & Sandy JD 2004 ADAMTS4 (aggrecanase-1) cleaves human brain versican V2 at Glu405-Gln406 to generate glial hyaluronate binding protein. *Biochemical Journal* **377** 787–795. (https://doi.org/10.1042/BJ20030896)

Wight TN 2002 Versican: a versatile extracellular matrix proteoglycan in cell biology. *Current Opinion in Cell Biology* **14** 617–623. (https://doi.org/10.1016/s0955-0674(02)00375-7)

Wong S, Brennan FE, Young MJ, Fuller PJ & Cole TJ 2007 A direct effect of aldosterone on endothelin-1 gene expression in vivo. *Endocrinology* **148** 1511–1517. (https://doi.org/10.1210/en.2006-0965)

Zhan Y, Purton JF, Godfrey DI, Cole TJ, Heath WR & Lew AM 2003 Without peripheral interference, thymic deletion is mediated in a cohort of double-positive cells without classical activation. *PNAS* **100** 1197–1202. (https://doi.org/10.1073/pnas.0237316100)

Zimmermann DR & Ruoslahti E 1989 Multiple domains of the large fibroblast proteoglycan, versican. *EMBO Journal* **8** 2975–2981. (https://doi.org/10.1002/j.1460-2075.1989.tb08447.x)

Zou K, Muramatsu H, Ikematsu S, Sakuma S, Salama RH, Shinomura T, Kimata K & Muramatsu T 2000 A heparin-binding growth factor, midkine, binds to a chondroitin sulfate proteoglycan, PG-M/versican. *European Journal of Biochemistry* **267** 4046–4053. (https://doi.org/10.1046/j.1432-1327.2000.01440.x)

Received in final form 13 January 2020
Accepted 17 January 2020
Accepted Manuscript published online 20 January 2020

Chapter 3: Identification of Extracellular Matrix Remodelling and Wnt Signalling as Glucocorticoid-GR Regulated Processes using Transcriptome Sequencing of Isolated Fetal Lung Mesenchymal Cells

3.1 Introduction

The interstitial mesenchyme of the developing lung is constantly remodelling and undergoes rapid regression just prior to birth in response to mechanical and signalling cues. GCs are an essential signalling hormone in the latter stages of lung development. GCs act via the intracellular GR and contribute to the rapid thinning of the mesenchyme tissue to reduce the thickness of the blood-air barrier for efficient gas exchange at birth (Cole et al. 2019; Oshika, et al. 1998b). Preterm infants born before the endogenous GC surge have an underdeveloped lung characterised by reduced surfactant synthesis, immature alveolar development and an excess of mesenchymal tissue (Reynolds et al. 1968). Antenatal synthetic GC treatment reduces the risk of respiratory RDS in the infant by accelerating lung maturation (Liggins and Howie 1972). Furthermore, conditional mouse models have demonstrated that GC/GR signalling in the mesenchymal layer of the fetal lung is critical for this process (Bird et al. 2014). Similar to complete GR-null mice, mice deficient in mesenchymal-expressed GR die shortly after birth due to respiratory failure (Bird et al. 2014). Morphologically at E18.5 the lungs of these mice appear hypercellular with an thicken blood-air barrier increasing the diffusion distance for gaseous exchange (Bird et al. 2014). It is generally accepted that the hypercellular lung phenotype is the result of increased cell proliferation rather than a decrease in cell apoptosis (Bird et al. 2014; Bird et al. 2007). Despite the well-recognised importance of GCs in morphological lung maturation and the clinical use of synthetic GCs in the treatment of preterm birth, the underlying molecular mechanisms, GC-regulated gene targets and modulated gene pathways remain elusive.

To identify mesenchymal GC signalling regulated pathways and gene networks I have isolated lung mesenchymal cells from GRmesKO mice at E18.5 using fluorescent-activated cell sorting (FACS) and performed Next generation RNA sequencing (NGS RNA seq). Using this approach, I have identified a large number of genes with altered expression in lung

mesenchymal cells from GRmesKO mice. I identified 290 differentially expressed genes that included a large number of mRNAs encoding ECM associated genes. These included Elastin (*Eln)*, Fin bud imitation factor homology (zebrafish) (*Fibin)*, Preproenkephalin (*Penk)*, SPARC related modular calcium binding 2 (*Smoc2)* and *Adamts-like 2 (Adamtsl2).* I also showed that a small number of Wnt signalling associated genes were increased in mesenchymal cells isolated from GRmesKO mouse lung including R-spondin 2 (*Rspo2)*, Wingless-type MMTV integration site family, member 11 (*Wnt11)* and Cell migration inducing protein, hyaluronan binding (*Cemip)* with fold changes of 1.9, 1.7 and 1.6 respectively.

3.2 Materials and Methods

Animals

The care and use of all animals were approved by the Monash Animal Research Platform-1 Animal Ethics Committee at Monash University. GRmesKO mice (Mus musculus) were of an isogenic C57BL/6 genetic background. GRmesKO mice were generated using the Cre/Loxp gene recombination system as previously described (Bird et al. 2014). Briefly, mice expressing Cre under the mesenchymal specific promotor, dermo1 (mice provided by Prof. Wainwright, University of Queensland, Brisbane, Australia) were bred with $GR^{loxp/lxop}$ mice to generate $GR^{loxp/+}$, $Dermo1^{cre/+}$. These mice were then time-mated with $GR^{loxp/loxp}$ to generate 25 % of the offspring as $GR^{loxp/loxp}$, $Dermo1^{cre/+}$ mice that were used in the study with $GR^{loxp/+}$ control littermates. The morning of a positive plug mating was designated as embryonic (E) day 0.5. Pregnant mice were sacrificed according to approved guidelines of the Animal Ethics Committee at Monash University at E18.5, and pups were sacrificed by decapitation. The lung of GRmesKO fetal pups were isolated and processed into a single cell suspension for FACS analysis or snap frozen in liquid N_2. Tail snips from pups were collected at dissection for immediate genotyping by qPCR and analysis of PCR fragments by gel electrophoresis. $Dermo1^{cre/+}$ mice have two bands, one for the internal control and one for the cre band, while control animals have only the internal control band (Bird et al. 2014). Primer sequences can be found in Table 3.1.

Table 3.1: Primer sequences used to genotype GR targeted mice

Gene	Primer Sequence
GRloxp	GR forward: 5'-TTGCAAATAACTCAGTACAAATGG-3'
	GR reverse: 5'-TACTACTTCCAGTTCTTAACCCTCTC-3'
	Loxp forward: 5'-TGCGAGCTGTACTGATAACTTC-3'
Dermo1cre	Wild type Forward: 5'-AACTTCCTCTCCCGGAGACC-3'
	Wild type reverse: 5'-TGCCTCTCCAGCTCTTCCTC-3'
	Transgene: 5'-CCGGTTATTCAACTTGCACC-3'

Preparation of Cell Suspensions from Control and GRmesKO Fetal Lung Tissue

The entire lung was dissected from fetal control and GRmesKO pups at E18.5, chopped into very small pieces and washed 3 times with phosphate-buffered saline (PBS). The macerated lung tissue was then added to 200 µl of filter sterilised lung tissue digestion buffer containing 12.5% heat-inactivated chicken serum (Gibco, Australia), 32.5 mM HEPES (Gibco, Australia), 3.75 mg/ml of collagenase type 1 and 1A (Sigma-Aldrich, Australia) and 0.5 mg/ml of DNase (Sigma-Aldrich), diluted in DMEM media. Lung tissue samples in digestion buffer were incubated at 37°C in a heat-block. Every 5 min the incubating tubes were shaken vigorously, and the contents also slowly pipetted up and down until no clumps of tissue were visible for a maximum of 30 min. At the end of digestion period, the cells were filtered through a sterilised 100 µm cell strainer. The cell suspensions were then washed 3 times with PBS resuspension after centrifugation for 5 min at 1500 g-force, to ensure the complete removal of digestion buffer.

Isolation of Fetal Mouse Lung Mesenchymal Fibroblast Cells

The cell suspension was centrifuged for 5 min at 1500 g-force and cells were then resuspended with a multi-antibody incubation buffer containing; 1% fetal bovine serum, Epcam FITC (Biolegend 118208, 1:200), CD45 BV510 (BD 563891, 1:200) and CD31 PeCy7 (eBio, 25-0311-082, 1:200), diluted in PBS. The cells were then incubated for 20 min on ice in the dark. At the end of the incubation the cells were washed with PBS by centrifugation for 5 min at 1500 g-force. The cells were then resuspended in FACS buffer containing 5mM EDTA, 20% fetal bovine serum and 1 µl/ml of Propidium iodide (PI), diluted in PBS. Cells were sorted on a BD Influxer (Becton Dickinson – BD - Franklin Lakes, NJ, USA) and sorted populations of cells collected in DMEM media supplemented with 20% fetal bovine serum. Isolated triple negative cells ($Epcam^-$ (epithelial), $CD45^-$ (immune) and $CD31^-$ (endothelial) were pelleted by

centrifuging for 5 min at 1500 g-force and stored at -80°C for eventual RNA extraction and sequencing.

Isolation of Total RNA from Sorted Fetal Lung Mesenchymal Cells and Analysis by Next Generation RNA Sequencing

Total RNA was isolated from fetal lung mesenchymal cells using RNeasy mini RNA extraction kit (Qiagen, USA) according to the manufacturer's instructions. Purified total RNA was analysed using a Bioanalyzer 2100 (Agilent Technologies) by Micromon: Genomics, Biotechnology and Diagnostics (Monash University Platform Service, Melbourne Australia). NGS RNA seq was then performed on samples with a purity 'Rin' number of at least 7 by Genewiz Biotechnologies, Suzhou, China. Control sample 1 (C1) and GRmesKO sample 2 (K2) did not meet this Rin number requirement and therefore not sequenced. Briefly, sequencing (20 million reads) was performed on the Illumina Hiseq sequencing platform, in a 2 x 150bp paired-end format. The Raw sequence data was interpreted by Genwiz's bioinformatics team which included quality control, alignment to the reference mouse genome (ENSEMBL, version GRCm38.89), assembly and pathway enrichment and analysis. Gene differential expression analysis was performed using the Bioconductor package DESeq2 (V1.6.3) (Love, et al. 2014).

cDNA Synthesis and Analysis of mRNA Levels of Specific Genes by qPCR

Total RNA was isolated from GRmesKO fetal mouse lungs at E18.5 using TRIzol™ (Invitrogen, USA) and cDNA was prepared with a QuantiTech RT kit (Qiagen, USA) according to the manufacturer's instructions. RNA was quality checked by nanodrop for analysis of OD260/280 values and run out on a gel to check for degradation. mRNA levels were assessed for the following gene targets identified in the NGS RNA Seq data: *Eln*, *Fibin*, *Penk*, *Smoc2*, *Adamtsl2*, Adamts-like 4 (*Adamtsl4*), Extracellular matrix protein 1 (*Ecm1*),

Insulin-like growth factor binding protein 3 (*Igfbp3*), *Rspo2*, *Wnt11*, *Cemip* and Collagen, type XV, alpha 1 (*Col15a1*). qPCR analysis was performed using the QuantiNova® SYBR® green master mix (Qiagen, USA) on a CFX384 Touch Real-Time PCR Detection System (Biorad, USA), with the following cycling conditions: An initial hot start at 95°C for 10 min, followed by 40 cycles of 95°C for 15 sec and 60° for 45 sec, the fluorescence was measured at the end of each cycle. After the 40 cycles a melt curve was performed from 65°C to 95°C, increasing by 0.05°C increments followed by a final hold at 95°C for 5 sec. The relative mRNA level for each gene was normalised to the housekeeping gene Ribosomal protein 29 (*Rps29*) using the ΔΔCt method (Livak and Schmittgen 2001) and expressed relative to the mRNA levels of littermate control mice. Primer pair sequences for each target gene can be found in Table 3.2.

Table 3.2: DNA sequence of primer pairs used for qPCR analysis

Gene	Forward	Reverse
Eln	5’-AGTTCCTGGTGTTGGTCTTC-3’	5’-TTTGACTCCTGTGCCAGTG-3’
Wnt11	5’-CTACCTGTCAGCCACGAAG-3’	5’-TGTTGCACTGCCTGTCTT-3’
Rspo2	5’-GCAATAAGCGAGCTAGTTATGT-3’	5’-GACGCATTCCTTCTCTTCGA-3’
Fibin	5’-CTCTTCAGGGTGAGTGATCG-3’	5’-AGGTCGTAGGAGATGCTCTT-3’
Penk	5’-GACATCAATTTCCTGGCGTG-3’	5’-CCTCCGTACCGTTTCATGAA-3’
Smoc2	5’-TTGCAAAGATGTGTCCAGGT-3’	5’-CTGTAGGTGCCGTCATCATT-3’
Adamtsl2	5’-GAGCAGTGTGTCTCCTTCAA-3’	5’-CGTAGTCATCCGGGTAAAGG-3’
Adamtsl4	5’-TCAATGTGACTTCTCCCAGC-3’	5’-CAGGATCGAGAACACGGAC-3’
Ecm1	5’-CCAGCACCTCCATGAAGTAG-3’	5’-GGCTGCACTTCTCTTTGTTC-3’
Igfbp3	5’-ATCCACTCCATGCCAAGATG-3’	5’-GCAGGGACCGTATTCTGTC-3’
Col15a1	5’-GCTGGAGAGATTTACGGGTT-3’	5’-AGCTTCCATGATTTCAGCGA-3’
Cemip	5’-CCTTGGAGCTTCATCACTGT-3’	5’-CCATTCCACATCTTGAACCC-3’
Rps29	5’-GGACATAGGCTTCATTAAGTTGG-3’	5’-TCAGTCGAATCCATTCAAGGT-3’

3.3 Results

3.3.1 Isolation of E18.5 Mouse Fetal Lung Mesenchymal Cells by FACS

An enriched population of fetal lung mesenchymal cells (Epcam$^-$, CD45$^-$ and CD31$^-$) was isolated from control and GRmesKO fetal mice at E18.5 using FACS to remove cells from the epithelial, endothelial and immune cell compartments (Figure 3.1A) (*n*=3/group). To determine if these other cell populations had been effectively removed, I assessed the expression of cell markers within the NGS RNA seq data set. The cell markers were selected from LungGens a web-based tool exploring gene expression during lung development (Du, et al. 2015; Du, et al. 2017). As expected, we observed high expression of mesenchymal cell markers that included Vimentin (*Vim*), Fibronectin (*Fn1*) and *Eln* (Figure 3.1B). I observed very low expression of endothelial, immune and epithelial cell markers, indicating I had successfully isolated an enriched population of mesenchymal cells for analysis by whole cell transcriptome sequencing (Figure 3.1B). To validate that the cells lacked the GR we showed that four well-characterised and known GC-regulated target genes with previously identified GREs were downregulated as expected in GRmesKO fetal mice. These genes were the serum/glucocorticoid regulated kinase 1 (*Sgk1*) (fold change -2.3, FDR 1.07E-10), FK506 binding protein 5 (*Fkbp5*) (fold change -6.8, FDR 8.68E-54), Transglutaminase 2, C polypeptide (*Tgm2*) (fold change -4.7, FDR 1.11E-38) and Cysteine-rich secretory protein LCCL domain containing 2 (*Crispld2*) (fold change -2.6, FDR 9.39E-06) (Table 3.3) (Seow et al, 2019).

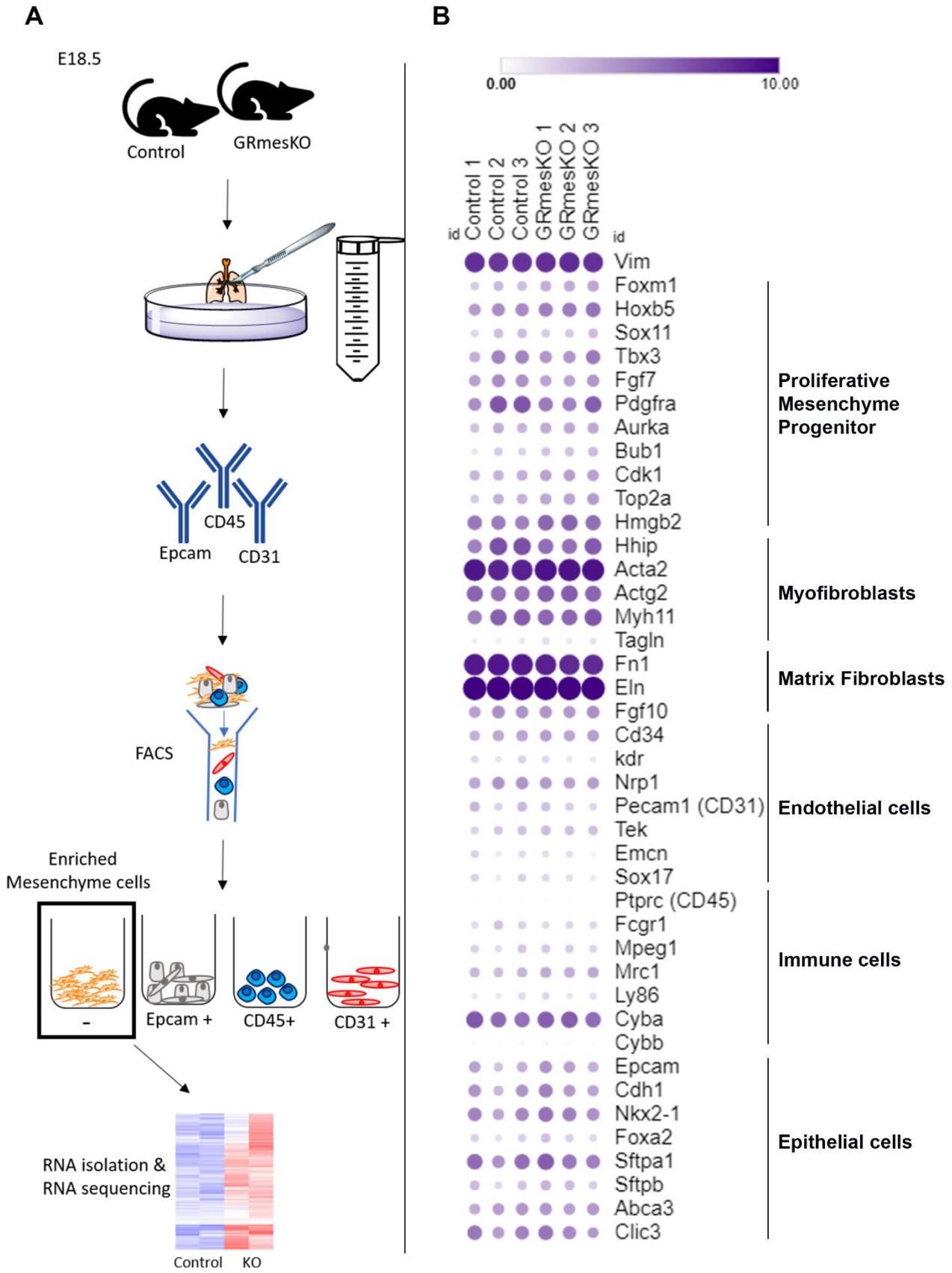
A
E18.5
Control
GRmesKO
CD45
Epcam
CD31
FACS
Enriched
Mesenchyme cells
-
Epcam +
CD45+
CD31 +
RNA isolation &
RNA sequencing
Control
KO
B
0.00
10.00
id
Control 1
Control 2
Control 3
GRmesKO 1
GRmesKO 2
GRmesKO 3
id
Vim
Foxm1
Hoxb5
Sox11
Tbx3
Fgf7
Pdgfra
Aurka
Bub1
Cdk1
Top2a
Hmgb2
Hhip
Acta2
Actg2
Myh11
Tagln
Fn1
Eln
Fgf10
Cd34
kdr
Nrp1
Pecam1 (CD31)
Tek
Emcn
Sox17
Ptprc (CD45)
Fcgr1
Mpeg1
Mrc1
Ly86
Cyba
Cybb
Epcam
Cdh1
Nkx2-1
Foxa2
Sftpa1
Sftpb
Abca3
Clic3
Proliferative Mesenchyme Progenitor
Myofibroblasts
Matrix Fibroblasts
Endothelial cells
Immune cells
Epithelial cells

Figure 3.1. Isolation of FACS sorted cell population from the E18.5 fetal mouse lung. (A) Experimental workflow; lungs were first isolated from control and GRmesKO fetal pups at E18.5 and processed by tissue digestion into a single cell suspension. Cells were then stained with different fluorescently-tagged antibodies to CD45, Epcam and CD31. After staining cells were sorted by FACS and Epcam$^-$, CD45$^-$ and CD31$^-$ cells were collected for RNA isolation and sequencing. (B) Cell type specific markers identified in the mesenchyme-enriched RNA-seq datasets. Scale indicates Log2(FPKM+1). FPKM = Fragments per kilobase of transcript per million mapped reads.

Table 3.3: mRNA fold change of four known GR-regulated and GRE-associated genes in enriched mesenchymal cells between control and GRmesKO fetal mice at E18.5. GRE binding sites identified by (Seow, et al. 2019) in rat primary fetal lung fibroblasts by CHIP-seq. GRE = Glucocorticoid response element, TSS = Transcriptional start site., FDR= False discovery rate

Gene ID	Gene name	GRE sequence 15bp inverted palindrome	GRE Location in gene	Distance from TSS (bp)	Fold change in GRmesKO	FDR
ENSMUSG00000019970	serum/glucocorticoid regulated kinase 1 (Sgk1)	AGAACATTCTGTCCT	Intronic	110207	-2.3	1.07E-10
ENSMUSG00000024222	FK506 binding protein 5 (Fkbp5)	AGAACAGGGTGTTCT	Intronic Intronic	19960 19929	-6.8	8.68E-54
ENSMUSG00000037820	transglutaminase 2, C polypeptide (Tgm2)	CGGACAGTTTGTCCT	Upstream	-50551	-4.7	1.11E-38
ENSMUSG00000031825	cysteine-rich secretory protein LCCL domain containing 2 (Crispld2)	AGAACAGACTGTCCT	Intronic	30720	-2.6	9.39E-06

3.3.2 Analysis of the Global Transcriptome Changes in mRNA Levels between E18.5 Control and GRmesKO Fetal Mice for the Enriched Mesenchymal Cell Population

Transcriptome datasets for the enriched mesenchymal cell populations from control and GRmesKO fetal lungs could be distinguished and as expected clustered together by genotype along the second principal component using a multidimensional scaling (MDS) analysis plot (Figure 3.2A). Bioinformatic analysis of genes with differential mRNA levels between control and GRmesoKO genotype identified 290 differentially expressed genes at a q-value (FDR adjusted p-value) less than 0.05 and a fold change greater than 2. A volcano plot shows that the majority of differentially expressed genes are significantly decreased in expression, with the mRNA level of 217 genes decreased in GRmesKO cells compared to 73 genes that were increased (Figure 3.2B). The different mRNA level changes for all genes are shown in a heatmap (Figure 3.2C), for genes with a fold change greater than 2 and a q-value less than 0.05. Hierarchical clustering analysis was used to group both the samples and 290 genes into groups with similar expression patterns. The genes clustered into 6 main groups that are colour-coded on the heatmap. The first main cluster on the heatmap includes 113 genes (green group), the second cluster (light blue group) includes 72 genes, the third cluster (red group) includes 6 genes, the fourth cluster (dark blue group) includes 26 genes, the fifth cluster (pink group) includes 10 genes and the last cluster (purple group) includes 63 genes. Genes in the pink and purple clusters were upregulated relative to controls while genes in all other clusters were downregulated. All differentially expressed genes can be found listed in supplementary table 3.1 within their gene cluster group.

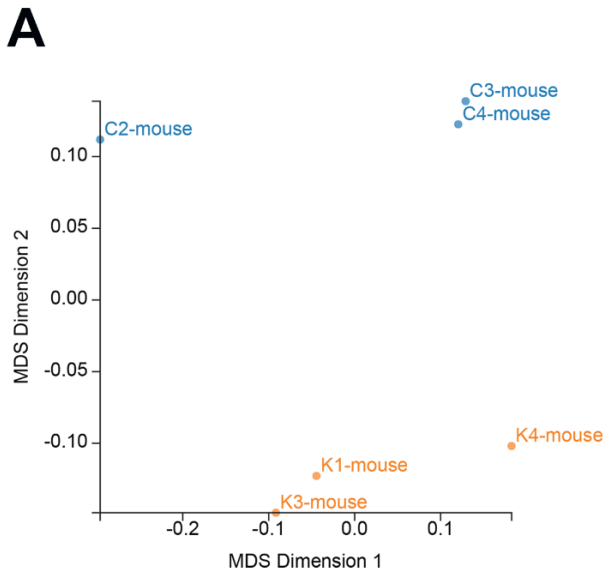
A
C3-mouse
C4-mouse
C2-mouse
K4-mouse
K1-mouse
K3-mouse
MDS Dimension 2
MDS Dimension 1
0.10
0.05
0.00
-0.05
-0.10
-0.2
-0.1
0.0
0.1

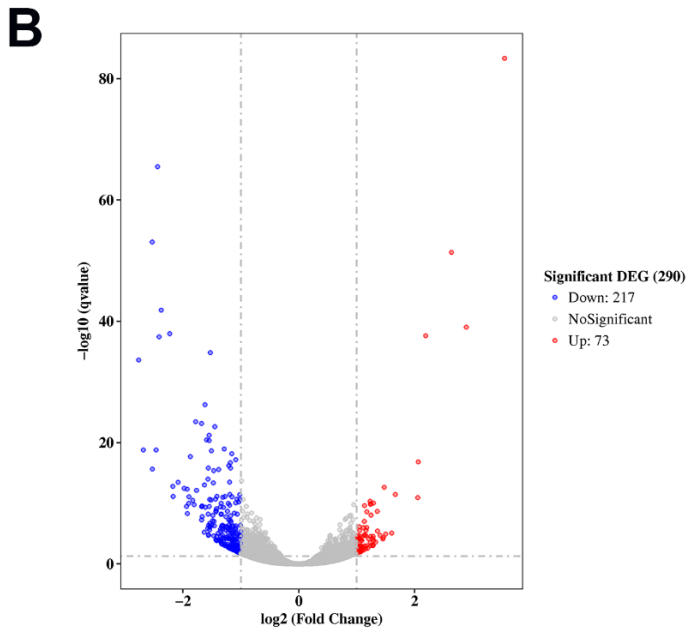
B
Significant DEG (290)
Down: 217
NoSignificant
Up: 73
−log10 (qvalue)
log2 (Fold Change)
80
60
40
20
0
−2
0
2

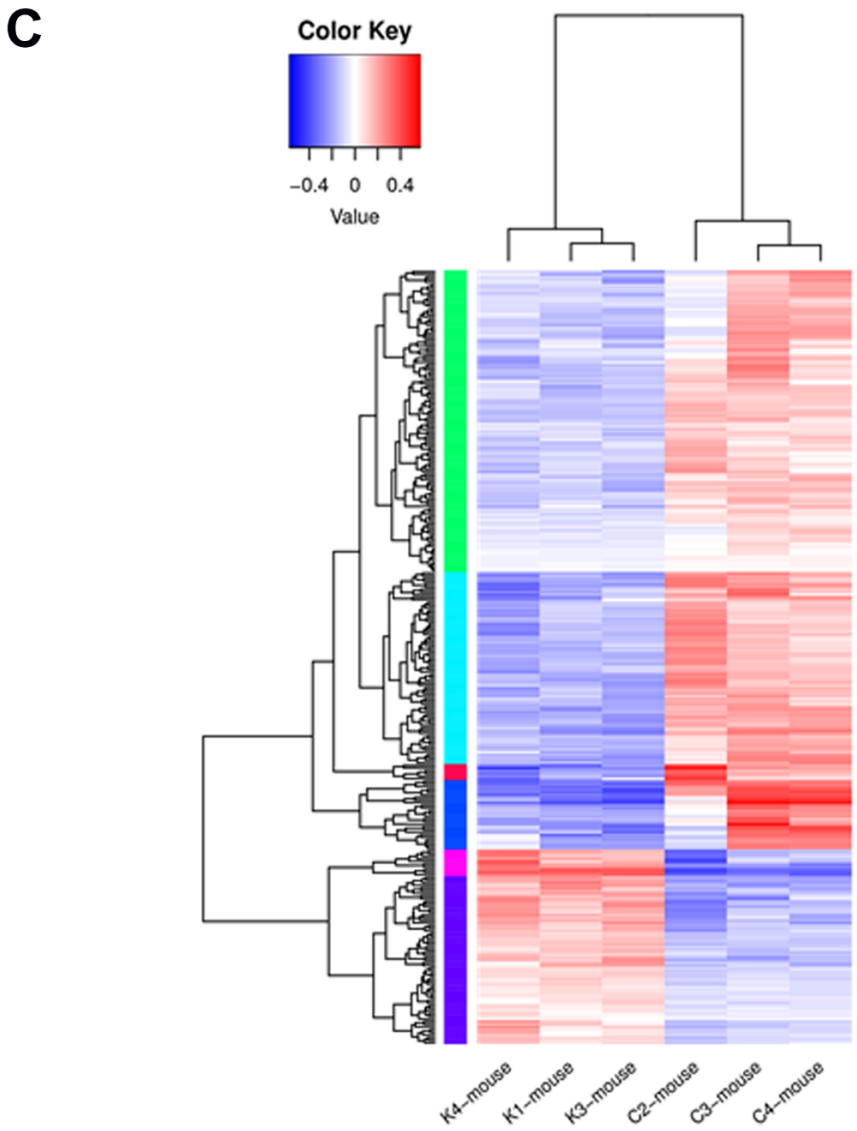
C
Color Key
−0.4
0
0.4
Value
K4−mouse
K1−mouse
K3−mouse
C2−mouse
C3−mouse
C4−mouse

Figure 3.2: Differential expression analysis of NGS RNA seq datasets between control and GRmesKO FACS-enriched mesenchymal cells isolated from E18.5 fetal mice. (A) Multidimensional scaling (MDS) plot showing clustered separation of control (C) and GRmesKO (K) lung mesenchymal cell samples (n=3). (B) A Volcano plot with log-fold changes on the x-axis and -log10 (q-value) (FDR adjusted pvalue) on the y-axis. Red dots represent gene mRNA levels that are significantly increased, and blue dots represent genes with significantly decreased mRNA levels with a significant q-value of less than 0.05 and a log-fold change greater than 2. (C) A heatmap with cluster analysis of the 290 differentially expressed mRNAs with a fold change greater than 2 and a q-value less than 0.05 were included. Log10 (FPKM+1) values were used for hierarchical clustering and generation of the dendrogram. The colours on the left represent different gene clusters.

3.3.3 Extracellular Matrix Associated Genes are Dysregulated in Fetal Lung GRmesKO Enriched Mesenchymal Cells

To identify the main biological process of genes regulated by the GR in the developing fetal lung mesenchyme we analysed the differentially expressed genes identified using GOSeq (v1.32.1) analysis. The top 30 biological process 'GOterms' related to the 290 gene set are shown in Figure 3.3. The GOterms with the most associated genes were related to the ECM that included 36 genes associated with the term 'extracellular space', 19 genes associated with the term 'extracellular region',17 genes associated with the term 'proteinaceous extracellular matrix' and 7 genes associated with the term 'extracellular matrix organisation'. The genes associated with these ECM terms are shown in a separate Heatmap (Figure 3.4). 42 ECM-associated genes were downregulated in GRmesKO mesenchymal cell mRNA and included ADAMTS-like 4 (*Adamts14*), *Ecm1*, *Col15a1*, *Eln*, Adamts*12*, *Tgm2* and *Crispld2*. 11 ECM-associated genes were upregulated and were related to Wnt signalling and included *Wnt11*, Norrie disease (pseudoglioma) (human) (*Ndp*), *Rspo2* and *Cemip*.

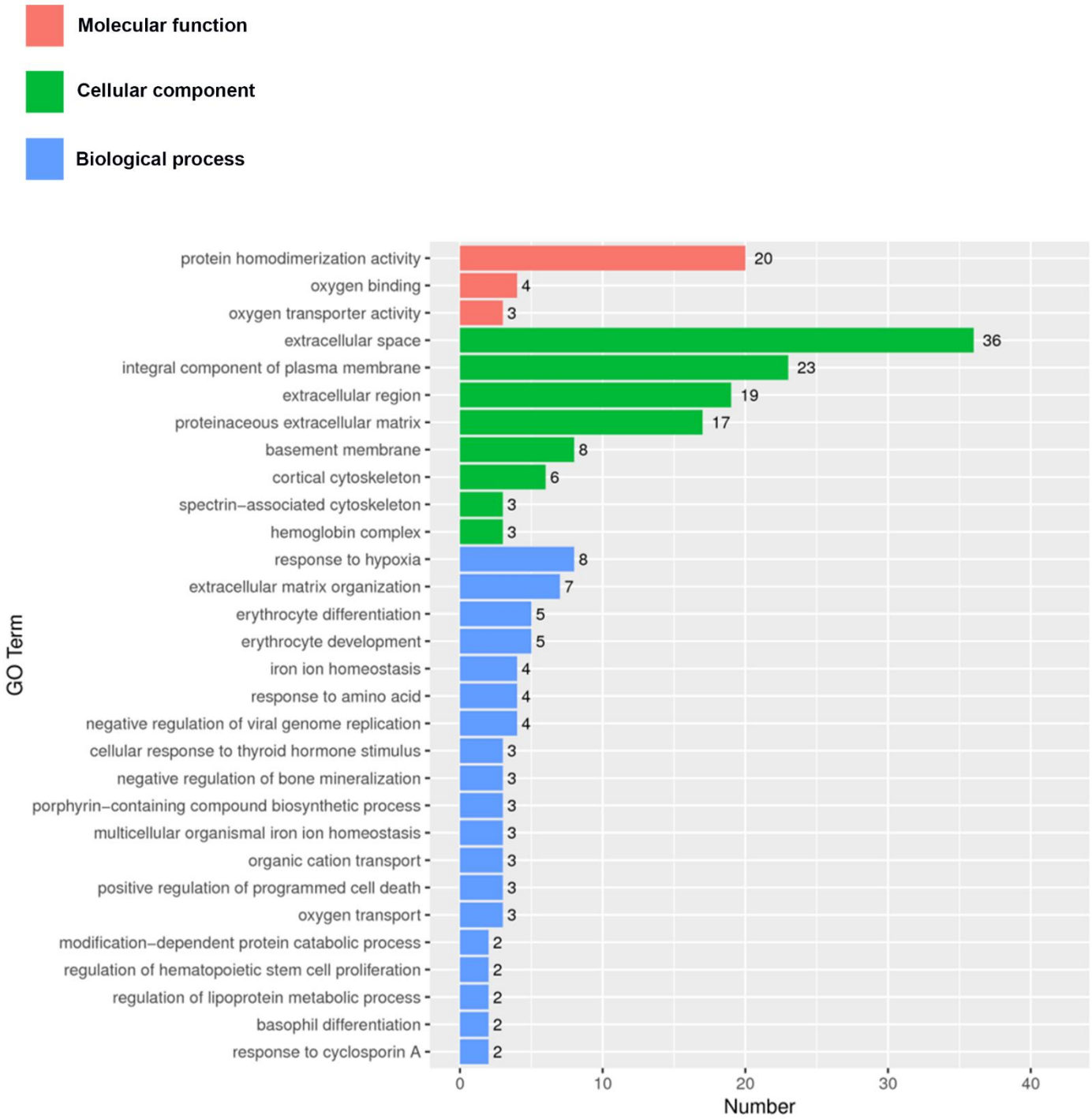

Figure 3.3: Analysis of biological process altered in GRmesKO versus control fetal lung mesenchymal cells using differential gene GO enrichment. X axis: number of differentially expressed genes associated with this GO biological process term. Colour coded to distinguish the categories; molecular function (pink), cellular component (green) and biological process (blue).

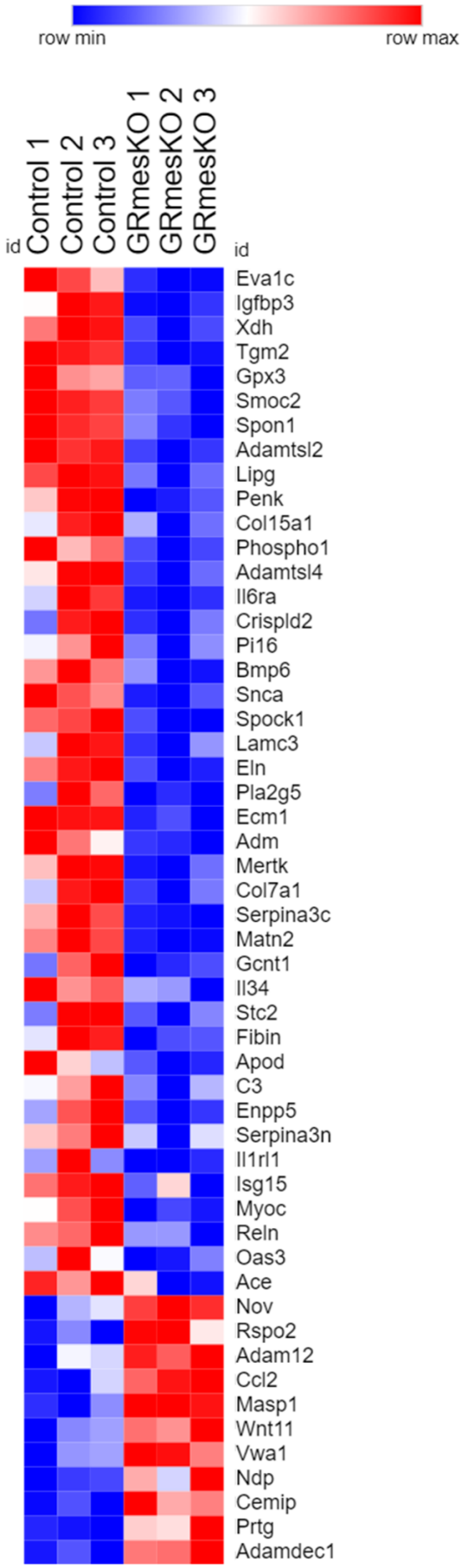
row min
row max
id
Control 1
Control 2
Control 3
GRmesKO 1
GRmesKO 2
GRmesKO 3
id
Eva1c
Igfbp3
Xdh
Tgm2
Gpx3
Smoc2
Spon1
Adamtsl2
Lipg
Penk
Col15a1
Phospho1
Adamtsl4
Il6ra
Crispld2
Pi16
Bmp6
Snca
Spock1
Lamc3
Eln
Pla2g5
Ecm1
Adm
Mertk
Col7a1
Serpina3c
Matn2
Gcnt1
Il34
Stc2
Fibin
Apod
C3
Enpp5
Serpina3n
Il1rl1
Isg15
Myoc
Reln
Oas3
Ace
Nov
Rspo2
Adam12
Ccl2
Masp1
Wnt11
Vwa1
Ndp
Cemip
Prtg
Adamdec1

Figure 3.4: Genes that had differential expression of mRNAs between control and GRmesKO mice that were associated with the extracellular matrix. Heatmap of 42 differently expressed genes related to the extracellular matrix with a fold change greater than 2 and a q-value (FDR adjusted pvalue) less than 0.05. Log10 (FPKM +1) values were used to construct the heatmap.

3.3.4 Extracellular Matrix Associated Gene Expression in the GRmesKO Fetal Lung by qPCR

The identified ECM-associated gene targets from the mesenchyme NGS RNA seq dataset were analysed for gene expression changes in whole fetal lung RNA. Total RNA was extracted from control and GRmesKO fetal lung at E18.5 and converted to cDNA for analysis by qPCR (*n*=4/group). Of the 42 ECM-associated genes identified we initially selected 12 for further analysis, with all targets to be analysed in the future. Similar to results obtained above we detected a decrease in the following ECM-associated genes in whole lung mRNA from GRmesKO fetal mice compared to control fetal mice; *Eln* (P=0.0371, 30% reduction), *Fibin* (p=0.0360, 20% reduction), *Penk* (p=0.0104, 40% reduction), *Smoc2* (p=0.0033, 40% reduction) and *Adamtsl2* (p=0.0024, 60% reduction) (Figure 3.5 A-E). This further suggests perturbations in ECM remodelling in the developing fetal lung of GRmesKO mice that may contribute to the phenotype of respiratory failure at birth. Wnt signalling associated genes were increased including *Rspo2* (p=0.0055, 1.9-fold increase), *Wnt11* (p=0.0009, 1.7-fold increase) and *Cemip* (p=0.0201, 1.6-fold increase) in GRmesKO lung relative to control fetal lung (Figure 3.6 A-C). A dysregulation of Wnt signalling may contribute to the hypercellular lung phenotype observed in GRmesKO mice. However, the following ECM-associated genes were not significantly altered in GRmesKO lung and included *Adamtsl4* (p=0.1890), *Ecm1* (p=0.1917) and *Igfbp3* (p=0.0946) (Figure 3.5F-H, and Figure 3.6D). In contrast, *Col15a1* mRNA levels were increased in mRNA from GRmesKO whole fetal lung that compared to a decrease in levels in isolated mesenchymal cells from GRmesKO lung (p=0.0342, 1.4-fold increase) (Figure 3.5 I). These putative GC-GR regulated gene targets in the fetal lung mesenchyme require further investigation and analysis.

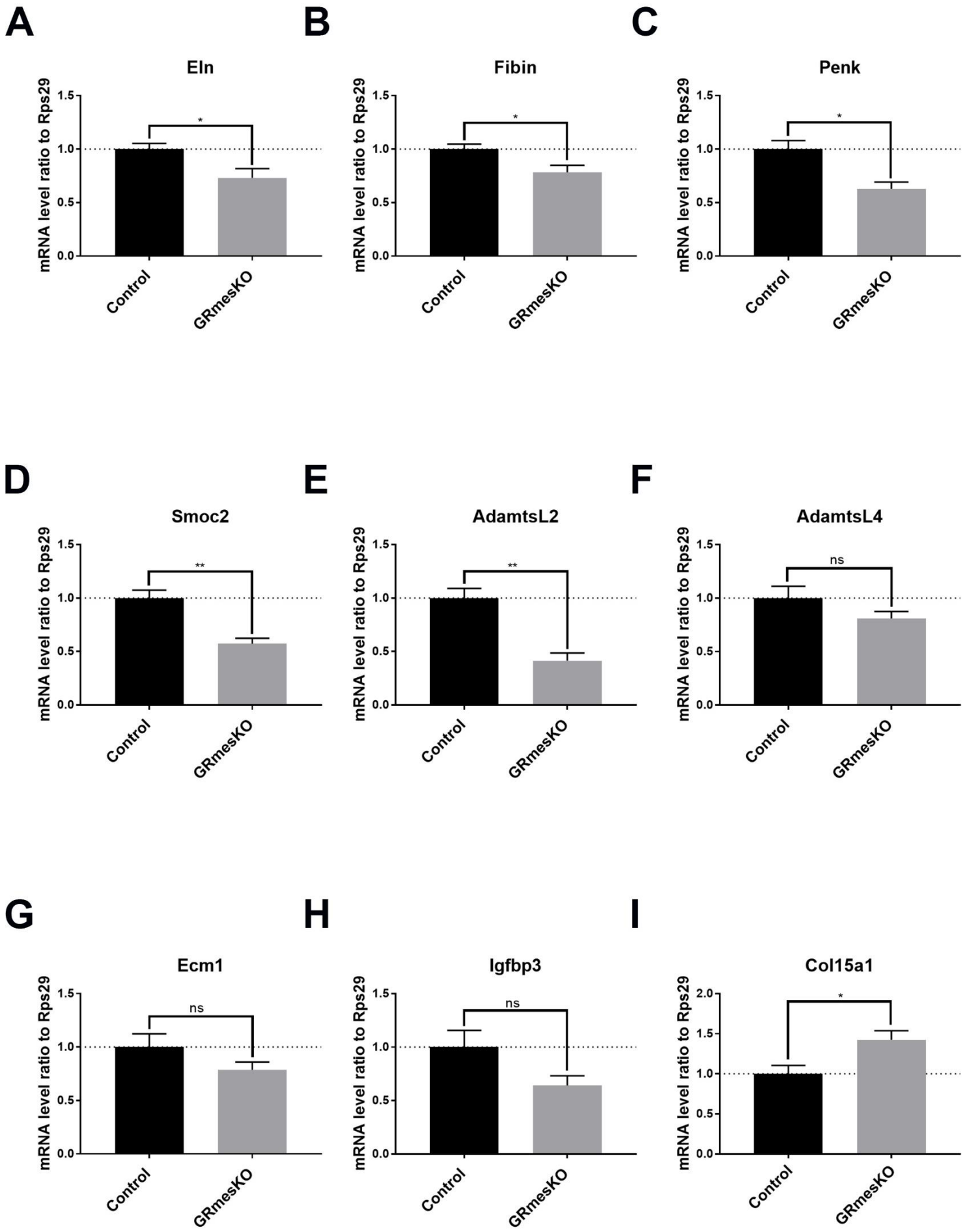
A
Eln
mRNA level ratio to Rps29
1.5
1.0
0.5
0.0
*
Control
GRmesKO
B
Fibin
mRNA level ratio to Rps29
1.5
1.0
0.5
0.0
*
Control
GRmesKO
C
Penk
mRNA level ratio to Rps29
1.5
1.0
0.5
0.0
*
Control
GRmesKO
D
Smoc2
mRNA level ratio to Rps29
1.5
1.0
0.5
0.0
**
Control
GRmesKO
E
AdamtsL2
mRNA level ratio to Rps29
1.5
1.0
0.5
0.0
**
Control
GRmesKO
F
AdamtsL4
mRNA level ratio to Rps29
1.5
1.0
0.5
0.0
ns
Control
GRmesKO
G
Ecm1
mRNA level ratio to Rps29
1.5
1.0
0.5
0.0
ns
Control
GRmesKO
H
Igfbp3
mRNA level ratio to Rps29
1.5
1.0
0.5
0.0
ns
Control
GRmesKO
I
Col15a1
mRNA level ratio to Rps29
2.0
1.5
1.0
0.5
0.0
*
Control
GRmesKO

Figure 3.5: mRNA levels of ECM-associated target genes in the GRmesKO fetal lung at E18.5. mRNA levels (mean $\pm$ SEM) of 8 ECM-associated genes in GRmesKO lung at E18.5 analysed by qPCR (*n*=4/group), (A) *Eln*, (B) *Fibin*, (C) *Penk*, (D) *Smoc2*, (E) *Adamtsl2*, (F) *Adamtsl4*, (G) *Ecm1* and (H) *Igfbp3*. The mRNA levels in all groups are expressed relative to mRNA levels of the housekeeping gene *Rps29*. Significant differences were analysed by unpaired student's t-test. Significant differences indicated by * $p \leq 0.05$, ** $p \leq 0.01$, ns= not significant.

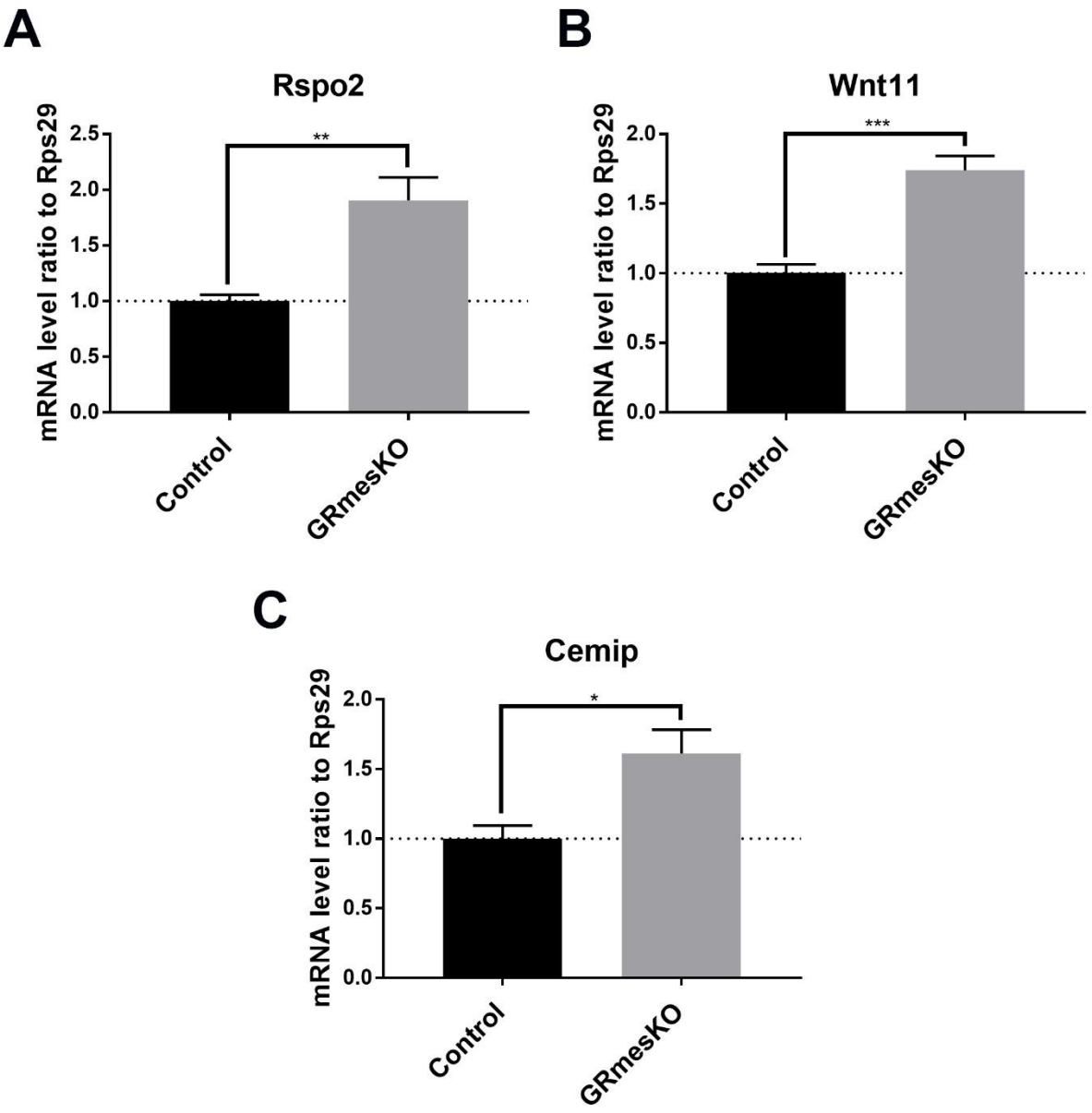

Figure 3.6: mRNA levels for Wnt signalling associated target genes in the GRmesKO fetal lung at E18.5. mRNA levels (mean ± SEM) of 4 Wnt associated genes in GRmesKO lung at E18.5 were measured by qPCR (*n*=4/group), (A) *Rspo2*, (B) *Wnt11* and (C) *Cemip* The mRNA levels in all groups are expressed relative to mRNA levels of the housekeeping gene *Rps29*. Significant differences were analysed by unpaired student's t-test. Significant differences indicated by * $p \leq 0.05$, ** $p \leq 0.01$, *** $p < 0.001$m, ns= not significant

3.4 Discussion

GC signalling via the GR during late gestation promotes rapid remodelling of the lung tissue architecture to decrease the blood-air barrier reducing the diffusion distance required for normal gas exchange at birth. Previous studies have determined that mesenchymal localised GR is the most critical for contributing to the regulation of this process (Bird et al. 2014; Bird et al. 2007). In this chapter I have used isolated and FACS enriched fetal mesenchymal cells to identify potential mesenchymal GR gene targets by performing whole cell NGS RNA seq on mesenchymal cells isolated from fetal GRmesKO mouse lung at E18.5. E18.5 was chosen for the transcriptome analysis because this time point is after the rapid remodelling of the mesenchyme tissue required for gases exchange at birth, that occurs during the transition of the canalicular to the saccular stage of lung development. Furthermore, GRmesKO mouse lungs prior to E16.5 appear normal then develop progressive hypercellularity due to unrestricted cell proliferation (Bird et al. 2007). We show that GR loss in lung mesenchymal cells results in 290 differentially expressed genes with more genes significantly decreased in expression than increased relative to control mesenchymal cells. This was not unexpected as GC treatment of rat primary fetal fibroblasts favoured transactivation over transrepression of GC-target genes (Seow et al. 2019). Furthermore, I show that expression of known GC-regulated genes with identified GREs were significantly decreased including *Sgk1*, *Fkbp5*, *Tgm2* and *Crispld2* (Seow et al. 2019; So, et al. 2007), indicating that we had successfully isolated enriched mesenchymal cells deficient in the GR.

Gene ontology analysis of the 290 genes identified, showed an enrichment of differentially expressed genes associated with the ECM. 42 ECM target genes were downregulated including both *Crispld2* and *Tgm2* which have been previously identified as GC target genes in the developing lung mesenchyme (Seow et al. 2019). It has been shown that gene expression of both *Tgm2* and *Crispld2* dramatically increases in rat primary lung fibroblasts treated with

GCs, both endogenous corticosterone and with the synthetic GC betamethasone (Seow et al. 2019). TGM2 is involved in both the formation of covalent bonds that help stabilise the ECM and cell apoptosis, both important processes during lung maturation (Hu, et al. 2011; Jung, et al. 2012). CRISPLD2 is involved in ECM deposition and heterozygous *Crispld2*$^{+/-}$ mice have immature lung morphology with increased mesenchymal content (Grabski, et al. 2003; Lan, et al. 2009). We also show that other target genes that contribute to the structural integrity of the ECM were downregulated and included Spondin 1, (*Spon1*), *Col15a1*, *Eln*, *ECM1*, Collagen, type VII, alpha 1 (*Col7a1*), Matrilin 2 (*Matn2*) and Reelin (*Reln*). These gene targets need further analysis to determine if these are directly regulated by the GR via closely located GREs. This could be achieved by performing Chip sequencing on primary fetal lung mesenchymal cells treated with betamethasone or dexamethasone utilising a GR antibody.

Furthermore, we show that two members of the ADAMTS protease family *Adamtsl2* and *Adamtsl4* were downregulated in lung mesenchymal cells deficient in GR. In Chapter 2 we identified that the ADAMTS protein family were important in the remodelling of the lung ECM prior to birth. We also demonstrated that GCs could induce the expression of one of the ADAMTS family members, ADAMTS12 in the mouse lung at E18.5. We did detect *Adamts12* mRNA expression across the samples but interestingly it was not differentially expressed. ADAMTS proteases are involved in the proteolytic breakdown of the ECM in several developing fetal tissues. The rapid clearance and remodelling of the ECM in response to elevated GC hormones is essential during late lung development, to increase alveolar surface areas and to decrease the diffusion distance for gaseous exchange at birth. However, unlike the "true" ADAMTS family members the ADAMTS-like proteins lack a protease domain and therefore are not considered proteases (Apte 2009). Interestingly, mice lacking *Adamtsl2* are cyanotic at birth and rapidly develop respiratory distress leading to death (Hubmacher et al. 2015). These mice have severe bronchial dysplasia consistent with the human recessive

condition geleophysic dysplasia (GD) (Hubmacher et al. 2015). The ADAMTSl2 protein is secreted by bronchial smooth muscle cells which are a subset of mesenchymal cells (Hubmacher et al. 2015). However, due to the prominent lung epithelial phenotype of *Adamtsl2* null mice it is unlikely that the decrease in *Adamtsl2* gene expression is responsible for the lung mesenchymal hyperplasia observed in GRnull and GRmesKO mice. Furthermore, mice deficient in epithelial GR (GRepiKO) survive into adulthood and have no overt lung developmental phenotype (Bird et al. 2014). The decreased expression level of *Adamtsl2* in mesenchymal cells lacking GR, and the potential effect on epithelial development requires further investigation but highlights the complexity of crosstalk between the lung tissue compartments.

Unfortunately, it was not possible to validate the NGS RNA seq data by qPCR with the same original RNA due to the difficulties in isolating large enough quantities of RNA from FACS sorted cells that would be required for both the NGS RNA seq analysis and follow up qPCR analysis. Therefore, to further explore and validate some of the ECM-associated differentially expressed genes identified in the RNA-sequencing dataset we performed qPCR on RNA from whole GRmesKO fetal lung at E18.5. Of the gene targets tested so far, *Eln*, *Fibin*, *Penk*, *Smoc2* and *Adamtsl2* were all decreased as expected in the GRmesKO lung RNA relative to control lung at E18.5. *Adamtsl4*, *ECM1* and *Igfbp3* showed a downward trend but didn't reach statistical significance. Interestingly, one target, *Col15a1*, had increased mRNA levels in GRmesKO lungs compared to decreased levels in isolated GRmesKO enriched mesenchymal cells. While mesenchymal cells types including fibroblasts, smooth muscle cells and endothelial cells are the main sites of COL15A1 protein production, it has been shown that epithelial cells can also secrete COL15A1 protein (Muona, et al. 2002). The epithelial cells of GRmesKO mouse lung may compensate for the loss of mesenchymal derived COL15A1 protein. This may explain why overall *Col15a1* mRNA levels were increased in total lung

isolated from GRmesKO mice but decreased in the isolated mesenchymal cells. *Col15a1* has also been shown to be developmentally regulated in the fetal lung with higher expression prior to birth. After birth *Col15a1* dramatically decreases in expression and is restricted to a few capillaries in the lung (Muona et al. 2002).

Interestingly, a small number of ECM-Wnt signalling associated genes were upregulated in GR deficient mesenchymal cells, including *Rspo2*, *Wnt11* and *Cemip*. In line with these results *Rspo2*, *Wnt11* and *Cemip* were also significantly upregulated in whole GRmesKO fetal lung mRNA at E18.5. RSPO2 is a Wnt signalling activator that is required for normal morphogenesis of the respiratory system and limbs (Nam, et al. 2007). RSPO2 expression can be detected in the early lung bud at E9.5 and is increased during mid gestation (E12.5 -E15.5), and at E17.5 RSPO2 can still be detected but at lower levels (Nam et al. 2007). Mice lacking *Rspo2* develop lung hypoplasia due to reduced branching morphogenesis and decreased overall growth of the lung (Bell, et al. 2008) highlighting the importance of RSPO2 to activate canonical Wnt signalling in lung development.

CEMIP promotes cell proliferation, migration and epithelial-to-mesenchymal transitions. Therefore, overexpression of CEMIP is commonly associated with poor patient prognosis in many cancers including brain, ovarian, breast, colorectal, pancreatic and lung cancer (Li, et al. 2017). CEMIP interacts with the canonical Wnt signalling pathway by stimulating the formation and movement of the DSH-Wnt complex into the cell nucleus (Li et al. 2017). Unlike RSPO2 which activates the canonical Wnt signalling pathway and CEMIP that interacts with the canonical Wnt signalling pathway to promote cell proliferation, WNT11 is a non-canonical Wnt/Ca^{2+} signalling activator that is expressed in both the lung epithelium and lung mesenchyme cells from E12.5 through E16.5 (Weidenfeld, et al. 2002). However, the role of WNT11 during lung development is unclear and further investigation is required to establish its function in the developing lung mesenchyme.

Normal Wnt-β-Catenin signalling is essential for normal lung mesenchyme development. Mice lacking mesenchymal β-Catenin have small compact lungs at E18.5 and mice die at birth due to respiratory failure (Yin et al. 2008). Morphologically the lungs of these mice have decreased epithelial branching, decreased distal mesenchyme areas and dysregulation of the distal lung tissue areas with poorly formed air sacs (Yin et al. 2008). The smaller lung size and decreased mesenchymal and epithelial content is due to a decrease in cell proliferation (Yin et al. 2008). In comparison, the hypercellular lung phenotype observed in GRmesKO mice is a result of an increase in cell proliferation rather than a decrease in cell apoptosis (Bird et al. 2014). Therefore, we suggest that GCs acting through the GR may decrease the expression of Wnt-associated genes to promote a reduction in cell proliferation rates in late lung development that will promote interstitial thinning of an expanding airway network. However, further investigation is required to establish the relationship between GCs, Wnt signalling and late gestational lung development. This hypothesis could be explored using lung explants isolated from GRmesKO mice. These lung explants could be treated with Wnt inhibitors to try rescue the hypercellular lung phenotype. In summary, GCs acting through the GR in the mesenchymal compartment may regulate the expression of key ECM-associated genes that include the Wnt signalling associated genes *Rspo2*, *Wnt11* and *Cemip* to coordinate the remodelling of the mesenchyme during late gestational lung development to provide a well organised lung structure that can efficiently inflate at birth.

Supplementary Table 3.1: All Differentially Expressed Genes. Genes in clusters green, aqua, red and dark blue were all downregulated while genes in clusters pink and purple were upregulated in fetal mouse lung mesenchymal cells deficient in GR relative to controls. FDR = false discovery rate.

GeneID	Gene symbol	Gene name	Cluster	Fold change	FDR
ENSMUSG00000058740	Kcnt1	potassium channel, subfamily member 1	green	-4.5	1.67E-13
ENSMUSG00000038663	Fsd2	fibronectin type III and SPRY domain containing 2	green	-4.5	7.50E-12
ENSMUSG00000086040	Wipf3	WAS/WASL interacting protein family, member 3	green	-3.4	7.53E-13
ENSMUSG00000054342	Kcnn4	potassium intermediate/small conductance calcium-activated channel, subfamily N, member 4	green	-3.2	2.80E-10
ENSMUSG00000020774	Aspa	aspartoacylase	green	-3.0	1.40E-06
ENSMUSG00000031543	Ank1	ankyrin 1, erythroid	green	3.0	6.13E-09
ENSMUSG00000113737	AC160765.1	-	green	-3.0	1.88E-05
ENSMUSG00000026841	Fibcd1	fibrinogen C domain containing 1	green	-2.9	1.62E-05
ENSMUSG00000044352	Sowaha	sosondowah ankyrin repeat domain family member A	green	-2.9	4.41E-07
ENSMUSG00000024302	Dtna	dystrobrevin alpha	green	-2.9	4.56E-21
ENSMUSG00000021061	Sptb	spectrin beta, erythrocytic	green	-2.9	2.36E-11
ENSMUSG00000032028	Nxpe2	neurexophilin and PC-esterase domain family, member 2	green	-2.9	8.12E-07
ENSMUSG00000053846	Lipg	lipase, endothelial	green	-2.9	2.95E-11
ENSMUSG00000028717	Tal1	T cell acute lymphocytic leukemia 1	green	-2.7	5.17E-07
ENSMUSG00000030237	Slco1a4	solute carrier organic anion transporter family, member 1a4	green	-2.7	9.87E-05
ENSMUSG00000023216	Epb42	erythrocyte membrane protein band 4.2	green	-2.7	1.79E-09
ENSMUSG00000024039	Cbs	cystathionine beta-synthase	green	-2.7	8.19E-10
ENSMUSG00000030268	Bcat1	branched chain aminotransferase 1, cytosolic	green	-2.7	0.00015
ENSMUSG00000037709	Fam13a	family with sequence similarity 13, member A	green	-2.7	7.43E-12
ENSMUSG00000066170	E230001N04Rik	RIKEN cDNA E230001N04 gene	green	-2.6	0.00011
ENSMUSG00000024011	Pi16	peptidase inhibitor 16	green	-2.6	0.00014

ENSMUSG00000020591	Ntsr2	neurotensin receptor 2	green	-2.6	0.0002
ENSMUSG00000037124	Trim58	tripartite motif-containing 58	green	-2.6	0.00015
ENSMUSG00000032649	Colgalt2	collagen beta(1-O) galactosyltransferase 2	green	-2.5	1.76E-06
ENSMUSG00000042476	Abcb4	ATP-binding cassette, sub-family B (MDR/TAP), member 4	green	-2.5	0.00012
ENSMUSG00000056222	Spock1	sparc/osteonectin, cwcv and kazal-like domains proteoglycan 1	green	-2.5	0.00046
ENSMUSG00000004552	Ctse	cathepsin E	green	-2.5	1.66E-05
ENSMUSG00000002831	Plin4	perilipin 4	green	-2.5	0.00057
ENSMUSG00000085272	Sbk3	SH3 domain binding kinase family, member 3	green	-2.5	2.07E-06
ENSMUSG00000015134	Aldh1a3	aldehyde dehydrogenase family 1, subfamily A3	green	-2.5	5.48E-05
ENSMUSG00000033688	1300017J02Rik	RIKEN cDNA 1300017J02 gene	green	-2.4	0.0006
ENSMUSG00000027488	Snta1	syntrophin, acidic 1	green	-2.4	7.85E-12
ENSMUSG00000038725	Pkhd1l1	polycystic kidney and hepatic disease 1-like 1	green	-2.4	0.00051
ENSMUSG00000022419	Deptor	DEP domain containing MTOR-interacting protein	green	-2.4	9.74E-07
ENSMUSG00000032420	Nt5e	5' nucleotidase, ecto	green	-2.4	3.86E-05
ENSMUSG00000096351	Samd11	sterile alpha motif domain containing 11	green	-2.4	7.07E-07
ENSMUSG00000026614	Slc30a10	solute carrier family 30, member 10	green	-2.4	0.00114
ENSMUSG00000032204	Aqp9	aquaporin 9	green	-2.3	0.00057
ENSMUSG00000022099	Dmtn	dematin actin binding protein	green	-2.3	6.37E-05
ENSMUSG00000104214	Gm36638	predicted gene, 36638	green	-2.3	0.00182
ENSMUSG00000019970	Sgk1	serum/glucocorticoid regulated kinase 1	green	-2.3	1.07E-10
ENSMUSG00000020490	Btnl10	butyrophilin-like 10	green	-2.3	0.00207
ENSMUSG00000022340	Sybu	syntabulin (syntaxin-interacting)	green	-2.3	5.94E-08
ENSMUSG00000035109	Shc4	SHC (Src homology 2 domain containing, family%2C member 4	green	-2.3	6.99E-05
ENSMUSG00000041193	Pla2g5	phospholipase A2, group V	green	-2.3	0.00231
ENSMUSG00000028108	Ecm1	extracellular matrix protein 1	green	-2.3	3.30E-14
ENSMUSG00000034248	Slc25a37	solute carrier family 25, member 37	green	-2.3	2.11E-10
ENSMUSG00000007379	Dennd2c	DENN/MADD domain containing 2C	green	-2.3	7.96E-07
ENSMUSG00000021281	Tnfaip2	tumor necrosis factor, alpha-induced protein 2	green	-2.3	0.00099

ENSMUSG00000055567	Unc80	unc-80, NALCN activator	green	-2.3	3.50E-06
ENSMUSG00000063681	Crb1	crumbs family member 1, photoreceptor morphogenesis associated	green	-2.3	0.00265
ENSMUSG00000063796	Slc22a8	solute carrier family 22 (organic anion transporter), member 8	green	-2.3	0.00255
ENSMUSG00000008843	Cldn13	claudin 13	green	-2.3	8.26E-05
ENSMUSG00000060131	Atp8b4	ATPase, class I, type 8B, member 4	green	-2.3	0.00156
ENSMUSG00000032625	Thsd7a	thrombospondin, type I, domain containing 7A	green	-2.3	0.00245
ENSMUSG00000025650	Col7a1	collagen, type VII,C alpha 1	green	-2.3	1.12E-07
ENSMUSG00000066361	Serpina3c	serine (or cysteine) peptidase inhibitor, clade A, member 3C	green	-2.3	0.0011
ENSMUSG00000021055	Esr2	estrogen receptor 2 (beta)	green	-2.2	0.002
ENSMUSG00000066867	Oas1e	2'-5' oligoadenylate synthetase 1E	green	-2.2	0.0037
ENSMUSG00000041548	Hspb8	heat shock protein 8	green	-2.2	8.51E-12
ENSMUSG00000038843	Gcnt1	glucosaminyl (N-acetyl) transferase 1, core 2	green	-2.2	0.00013
ENSMUSG00000032548	Slco2a1	solute carrier organic anion transporter family, member 2a1	green	-2.2	0.00025
ENSMUSG00000099907	Gm10421	predicted gene 10421	green	-2.2	0.00321
ENSMUSG00000031698	Mylk3	myosin light chain kinase 3	green	-2.2	0.00021
ENSMUSG00000031162	Gata1	GATA binding protein 1	green	-2.2	0.0005
ENSMUSG00000040740	Slc25a34	solute carrier family 25, member 34	green	-2.2	0.0046
ENSMUSG00000031605	Klhl2	kelch-like 2, Mayven	green	-2.2	4.40E-06
ENSMUSG00000036863	Syde2	synapse defective 1, Rho GTPase, homolog 2 (C. elegans)	green	-2.2	1.81E-05
ENSMUSG00000020303	Stc2	stanniocalcin 2	green	-2.2	0.0002
ENSMUSG00000074971	Fibin	fin bud initiation factor homolog (zebrafish)	green	-2.2	4.29E-09
ENSMUSG00000032528	Vipr1	vasoactive intestinal peptide receptor 1	green	-2.2	0.00257
ENSMUSG00000022548	Apod	apolipoprotein D	green	-2.2	0.00576
ENSMUSG00000020524	Gria1	glutamate receptor, ionotropic, AMPA1 (alpha 1)	green	-2.1	0.0018
ENSMUSG00000024164	C3	complement component 3	green	-2.1	2.96E-05
ENSMUSG00000026237	Nmur1	neuromedin U receptor 1	green	-2.1	0.00321
ENSMUSG00000089703	Gm15833	predicted gene 15833	green	-2.1	0.00079
ENSMUSG00000039943	Plcb4	phospholipase C, beta 4	green	-2.1	8.49E-11

ENSMUSG00000023960	Enpp5	ectonucleotide pyrophosphatase/phosphodiesterase 5	green	-2.1	1.20E-06
ENSMUSG00000015468	Notch4	notch 4	green	-2.1	5.45E-07
ENSMUSG00000027556	Car1	carbonic anhydrase 1	green	-2.1	0.00641
ENSMUSG00000035948	Acss3	acyl-CoA synthetase short-chain family member 3	green	-2.1	8.91E-05
ENSMUSG00000069814	Ccdc92b	coiled-coil domain containing 92B	green	-2.1	0.00114
ENSMUSG00000005640	Insrr	insulin receptor-related receptor	green	-2.1	0.00877
ENSMUSG00000032271	Nnmt	nicotinamide N-methyltransferase	green	-2.1	0.00253
ENSMUSG00000028906	Epb41	erythrocyte membrane protein band 4.1	green	-2.1	2.09E-11
ENSMUSG00000044792	Isca1	iron-sulfur cluster assembly 1	green	-2.1	6.17E-09
ENSMUSG00000009216	Fam163b	family with sequence similarity 163, member B	green	-2.1	0.00278
ENSMUSG00000021091	Serpina3n	serine (or cysteine) peptidase inhibitor, clade A, member 3N	green	-2.1	0.0068
ENSMUSG00000001763	Tspan33	tetraspanin 33	green	-2.1	0.00093
ENSMUSG00000026069	Il1rl1	interleukin 1 receptor-like 1	green	-2.1	0.0105
ENSMUSG00000064225	Paqr9	progestin and adipoQ receptor family member IX	green	-2.1	0.00715
ENSMUSG00000087107	AI662270	expressed sequence AI662270	green	-2.1	0.00086
ENSMUSG00000067203	H2-K2	histocompatibility 2, K region locus 2	green	-2.1	0.01149
ENSMUSG00000027869	Hsd3b6	hydroxy-delta-5-steroid dehydrogenase, 3 beta- and steroid delta-isomerase 6	green	-2.1	0.01123
ENSMUSG00000020140	Lgr5	leucine rich repeat containing G protein coupled receptor 5	green	-2.1	0.01257
ENSMUSG00000019905	Gprc6a	G protein-coupled receptor, family C. group 6, member A	green	-2.1	0.00122
ENSMUSG00000029659	Medag	mesenteric estrogen dependent adipogenesis	green	-2.1	0.00633
ENSMUSG00000027330	Cdc25b	cell division cycle 25B	green	-2.1	6.42E-11
ENSMUSG00000067206	Lrrc66	leucine rich repeat containing 66	green	-2.0	0.00766
ENSMUSG00000035877	Zhx3	zinc fingers and homeoboxes 3	green	-2.0	2.45E-05
ENSMUSG00000032698	Lmo2	LIM domain only 2	green	-2.0	1.81E-05
ENSMUSG00000017679	Ttpal	tocopherol (alpha) transfer protein-like	green	-2.0	3.74E-12
ENSMUSG00000078566	Bnip3	BCL2/adenovirus E1B interacting protein 3	green	-2.0	2.45E-11
ENSMUSG00000087684	1200007C13Rik	RIKEN cDNA 1200007C13 gene	green	-2.0	0.00363

ENSMUSG00000026697	Myoc	myocilin	green	-2.0	0.01523
ENSMUSG00000042453	Reln	reelin	green	-2.0	0.00502
ENSMUSG00000032661	Oas3	2'-5' oligoadenylate synthetase 3	green	-2.0	0.01726
ENSMUSG00000023067	Cdkn1a	cyclin-dependent kinase inhibitor 1A (P21)	green	-2.0	0.00047
ENSMUSG00000025064	Col17a1	collagen, type XVII, alpha 1	green	-2.0	4.41E-07
ENSMUSG00000039648	Kyat1	kynurenine aminotransferase 1	green	-2.0	2.94E-05
ENSMUSG00000024014	Pim1	proviral integration site 1	green	-2.0	2.35E-05
ENSMUSG00000020681	Ace	angiotensin I converting enzyme (peptidyl-dipeptidase A) 1	green	-2.0	0.0005
ENSMUSG00000027510	Rbm38	RNA binding motif protein 38	green	-2.0	4.49E-06
ENSMUSG00000029843	Slc13a4	solute carrier family 13 (sodium/sulfate symporters), member 4	aqua	-6.4	1.64E-19
ENSMUSG00000039903	Eva1c	eva-1 homolog C (C. elegans)	aqua	-5.8	2.35E-16
ENSMUSG00000024678	Ms4a4d	membrane-spanning 4-domains, subfamily A, member 4D	aqua	-3.8	4.76E-13
ENSMUSG00000036832	Lpar3	lysophosphatidic acid receptor 3	aqua	-3.7	8.54E-12
ENSMUSG00000023886	Smoc2	SPARC related modular calcium binding 2	aqua	-3.7	2.05E-18
ENSMUSG00000047330	Kcne4	potassium voltage-gated channel, Isk-related subfamily, gene 4	aqua	-3.4	3.63E-24
ENSMUSG00000026473	Glul	glutamate-ammonia ligase (glutamine synthetase)	aqua	-3.2	7.12E-24
ENSMUSG00000086765	Gm11827	predicted gene 11827	aqua	-3.2	5.59E-08
ENSMUSG00000025911	Adhfe1	alcohol dehydrogenase, iron containing, 1	aqua	-3.2	3.38E-10
ENSMUSG00000112246	AC121871.1	-	aqua	-3.1	5.89E-06
ENSMUSG00000041992	Rapgef5	Rap guanine nucleotide exchange factor (GEF) 5	aqua	-3.1	9.52E-14
ENSMUSG00000048218	Amigo2	adhesion molecule with Ig like domain 2	aqua	-3.1	5.62E-27
ENSMUSG00000006574	Slc4a1	solute carrier family 4 (anion exchanger), member 1	aqua	-3.0	3.56E-21
ENSMUSG00000038156	Spon1	spondin, (f-spondin) extracellular matrix protein	aqua	-3.0	1.06E-14
ENSMUSG00000045658	Pid1	phosphotyrosine interaction domain containing 1	aqua	-3.0	1.57E-16
ENSMUSG00000036040	Adamtsl2	ADAMTS-like 2	aqua	-2.9	6.23E-22
ENSMUSG00000031613	Hpgd	hydroxyprostaglandin dehydrogenase 15 (NAD)	aqua	-2.9	3.45E-10
ENSMUSG00000093954	Gm16867	predicted gene, 16867	aqua	-2.9	2.01E-07
ENSMUSG00000098708	Gm27252	predicted gene 27252	aqua	-2.9	6.98E-07

ENSMUSG00000042622	Maff	v-maf musculoaponeurotic fibrosarcoma oncogene family, protein F (avian)	aqua	-2.9	1.50E-35
ENSMUSG00000045573	Penk	preproenkephalin	aqua	-2.8	2.27E-19
ENSMUSG00000050860	Phospho1	phosphatase orphan 1	aqua	-2.8	1.01E-08
ENSMUSG00000015850	Adamtsl4	ADAMTS-like 4	aqua	-2.8	4.37E-14
ENSMUSG00000030087	Klf15	Kruppel-like factor 15	aqua	-2.8	4.20E-16
ENSMUSG00000058794	Nfe2	nuclear factor, erythroid derived 2	aqua	-2.8	9.39E-08
ENSMUSG00000030711	Sult1a1	sulfotransferase family 1A, phenol-preferring, member 1	aqua	-2.7	2.38E-23
ENSMUSG00000051839	Gypa	glycophorin A	aqua	-2.7	2.52E-09
ENSMUSG00000025573	6030468B19Rik	RIKEN cDNA 6030468B19 gene	aqua	-2.7	0.00014
ENSMUSG00000040170	Fmo2	flavin containing monooxygenase 2 [	aqua	-2.6	2.70E-16
ENSMUSG00000029866	Kel	Kell blood group	aqua	-2.6	3.81E-06
ENSMUSG00000039004	Bmp6	bone morphogenetic protein 6	aqua	-2.6	3.82E-10
ENSMUSG00000028825	Rhd	Rh blood group, D antigen	aqua	-2.5	2.56E-05
ENSMUSG00000025270	Alas2	aminolevulinic acid synthase 2, erythroid	aqua	-2.5	6.75E-09
ENSMUSG00000025889	Snca	synuclein, alpha	aqua	-2.5	1.00E-10
ENSMUSG00000019838	Slc16a10	solute carrier family 16 (monocarboxylic acid transporters), member 10	aqua	-2.5	5.97E-09
ENSMUSG00000073400	Trim10	tripartite motif-containing 10	aqua	-2.5	6.12E-07
ENSMUSG00000001918	Slc1a5	solute carrier family 1 (neutral amino acid transporter), member 5	aqua	-2.5	4.19E-07
ENSMUSG00000020641	Rsad2	radical S-adenosyl methionine domain containing 2	aqua	-2.5	1.03E-11
ENSMUSG00000027078	Ube2l6	ubiquitin-conjugating enzyme E2L 6	aqua	-2.5	4.75E-10
ENSMUSG00000073940	Hbb-bt	hemoglobin, beta adult t chain	aqua	-2.5	5.84E-07
ENSMUSG00000031431	Tsc22d3	TSC22 domain family, member 3	aqua	-2.4	1.15E-19
ENSMUSG00000061878	Sphk1	sphingosine kinase 1	aqua	-2.4	2.52E-06
ENSMUSG00000030088	Aldh1l1	aldehyde dehydrogenase 1 family, member L1	aqua	-2.4	6.91E-05
ENSMUSG00000071637	Cebpd	CCAAT/enhancer binding protein (C/EBP), delta	aqua	-2.4	1.66E-08
ENSMUSG00000083012	Fam220a	family with sequence similarity 220, member A	aqua	-2.3	2.08E-09
ENSMUSG00000047139	Cd24a	CD24a antigen	aqua	-2.3	5.89E-06
ENSMUSG00000107451	Gm44421	predicted gene, 44421	aqua	-2.3	0.00132

ENSMUSG00000018659	Pnpo	pyridoxine 5'-phosphate oxidase	aqua	-2.3	1.95E-06
ENSMUSG00000039236	Isg20	interferon-stimulated protein	aqua	-2.3	4.13E-07
ENSMUSG00000029675	Eln	elastin	aqua	-2.3	6.27E-17
ENSMUSG00000024588	Fech	ferrochelatase	aqua	-2.3	3.55E-12
ENSMUSG00000030790	Adm	adrenomedullin	aqua	-2.3	3.10E-05
ENSMUSG00000038393	Txnip	thioredoxin interacting protein	aqua	-2.3	2.05E-17
ENSMUSG00000030747	Dgat2	diacylglycerol O-acyltransferase 2	aqua	-2.3	6.95E-08
ENSMUSG00000014361	Mertk	c-mer proto-oncogene tyrosine kinase	aqua	-2.3	1.57E-16
ENSMUSG00000000739	Sult5a1	sulfotransferase family 5A, member 1	aqua	-2.3	1.14E-08
ENSMUSG00000038871	Bpgm	2, 3-bisphosphoglycerate mutase	aqua	-2.3	1.85E-06
ENSMUSG00000052305	Hbb-bs	hemoglobin, beta adult s chain	aqua	-2.3	4.20E-05
ENSMUSG00000044468	Fam46c	family with sequence similarity 46, member C	aqua	-2.2	6.95E-07
ENSMUSG00000022324	Matn2	matrilin 2	aqua	-2.2	6.83E-19
ENSMUSG00000046828	Mettl21e	methyltransferase like 21E	aqua	-2.2	8.15E-06
ENSMUSG00000021265	Slc25a29	solute carrier family 25 (mitochondrial carrier, palmitoylcarnitine transporter), member 29	aqua	-2.2	0.00014
ENSMUSG00000029922	Mkrn1	makorin, ring finger protein, 1	aqua	-2.2	9.23E-06
ENSMUSG00000042066	Tmcc2	transmembrane and coiled-coil domains 2	aqua	-2.2	5.29E-07
ENSMUSG00000031750	Il34	interleukin 34	aqua	-2.2	9.63E-05
ENSMUSG00000052217	Hbb-bh1	hemoglobin Z, beta-like embryonic chain	aqua	-2.1	0.0052
ENSMUSG00000049436	Upk1b	uroplakin 1B	aqua	-2.1	2.54E-06
ENSMUSG00000030878	Cdr2	cerebellar degeneration-related 2	aqua	-2.1	6.77E-06
ENSMUSG00000069919	Hba-a1	hemoglobin alpha, adult chain 1	aqua	-2.1	0.00023
ENSMUSG00000040435	Ppp1r15a	protein phosphatase 1, regulatory (inhibitor) subunit 15A	aqua	-2.1	6.64E-18
ENSMUSG00000079557	Tspan33	tetraspanin 33	aqua	-2.1	1.52E-05
ENSMUSG00000035692	Isg15	ISG15 ubiquitin-like modifier	aqua	-2.0	9.50E-05
ENSMUSG00000025936	Gm4956	predicted gene 4956	red	-3.8	3.36E-10
ENSMUSG00000018339	Gpx3	glutathione peroxidase 3	red	-3.7	1.07E-10

ENSMUSG00000028072	Ntrk1	neurotrophic tyrosine kinase, receptor, type 1	red	-3.2	3.38E-10
ENSMUSG00000039956	Mrap	melanocortin 2 receptor accessory protein	red	-3.2	1.63E-08
ENSMUSG00000073063	Hbq1b	hemoglobin, theta 1B	red	-2.7	2.90E-05
ENSMUSG00000052187	Hbb-y	hemoglobin Y, beta-like embryonic chain	red	-2.2	0.00146
ENSMUSG00000050164	Mchr1	melanin-concentrating hormone receptor 1	dark blue	-6.8	2.39E-34
ENSMUSG00000024222	Fkbp5	FK506 binding protein 5	dark blue	-5.8	8.68E-54
ENSMUSG00000020427	Igfbp3	insulin-like growth factor binding protein 3	dark blue	-5.5	1.64E-19
ENSMUSG00000028862	Map3k6	mitogen-activated protein kinase kinase kinase 6	dark blue	-5.4	3.23E-66
ENSMUSG00000037686	Aspg	asparaginase	dark blue	-5.3	3.63E-38
ENSMUSG00000024066	Xdh	xanthine dehydrogenase	dark blue	-5.2	1.46E-42
ENSMUSG00000037820	Tgm2	transglutaminase 2, C polypeptide	dark blue	-4.7	1.11E-38
ENSMUSG00000019577	Pdk4	pyruvate dehydrogenase kinase, isoenzyme 4	dark blue	-4.2	3.50E-14
ENSMUSG00000027875	Hmgcs2	3-hydroxy-3-methylglutaryl-Coenzyme A synthase 2	dark blue	-3.9	3.48E-13
ENSMUSG00000028332	Hemgn	hemogen	dark blue	-3.8	4.97E-09
ENSMUSG00000028644	Ermap	erythroblast membrane-associated protein	dark blue	-3.6	3.42E-11
ENSMUSG00000034796	Cpne7	copine VII	dark blue	-3.5	1.73E-10
ENSMUSG00000045392	Olfr1033	olfactory receptor 1033	dark blue	-3.1	4.56E-10
ENSMUSG00000023926	Rhag	Rhesus blood group-associated A glycoprotein	dark blue	-2.9	2.44E-06
ENSMUSG00000028339	Col15a1	collagen, type XV, alpha 1	dark blue	-2.8	3.98E-07
ENSMUSG00000021990	Spata13	spermatogenesis associated 13	dark blue	-2.8	7.65E-08
ENSMUSG00000050505	Pcdh20	protocadherin 20	dark blue	-2.8	2.38E-05
ENSMUSG00000027947	Il6ra	interleukin 6 receptor, alpha	dark blue	-2.7	2.12E-11
ENSMUSG00000031825	Crispld2	cysteine-rich secretory protein LCCL domain containing 2	dark blue	-2.6	9.39E-06
ENSMUSG00000002266	Zim1	zinc finger, imprinted 1	dark blue	-2.5	9.14E-05
ENSMUSG00000026840	Lamc3	laminin gamma 3	dark blue	-2.4	0.00096
ENSMUSG00000056069	Fam105a	family with sequence similarity 105, member A	dark blue	-2.4	3.81E-05
ENSMUSG00000002265	Peg3	paternally expressed 3	dark blue	-2.2	9.10E-05
ENSMUSG00000068122	Agtr2	angiotensin II receptor, type 2	dark blue	-2.1	0.0008

ENSMUSG00000033863	Klf9	Kruppel-like factor 9	dark blue	-2.1	0.00971
ENSMUSG00000022512	Cldn1	claudin 1	dark blue	-2.1	0.00254
ENSMUSG00000054555	Adam12	a disintegrin and metallopeptidase domain 12 (meltrin alpha)	Pink	2.0	6.29E-05
ENSMUSG00000069171	Nr2f1	nuclear receptor subfamily 2, group F, member 1	Pink	2.0	2.20E-05
ENSMUSG00000015957	Wnt11	wingless-type MMTV integration site family, member 11	Pink	2.2	9.76E-08
ENSMUSG00000045871	Slitrk6	SLIT and NTRK-like family, member 6	Pink	2.2	0.00107
ENSMUSG00000015709	Arnt2	aryl hydrocarbon receptor nuclear translocator 2	Pink	2.6	2.17E-09
ENSMUSG00000022057	Adamdec1	ADAM-like, decysin 1	Pink	3.2	3.55E-12
ENSMUSG00000030854	Ptpn5	protein tyrosine phosphatase, non-receptor type 5	Pink	4.6	2.43E-38
ENSMUSG00000050010	Shisa3	shisa family member 3	Pink	6.2	4.30E-52
ENSMUSG00000032128	Robo3	roundabout guidance receptor 3	Pink	7.4	9.41E-40
ENSMUSG00000097789	Gm2115	predicted gene 2115	Pink	11.8	4.49E-84
ENSMUSG00000113216	AL590503.1	-	purple	2.0	0.01807
ENSMUSG00000037362	Nov	nephroblastoma overexpressed gene	purple	2.0	0.00066
ENSMUSG00000110631	Gm45836	predicted gene 45836	purple	2.0	4.31E-05
ENSMUSG00000085828	Gm15612	predicted gene 15612	purple	2.0	0.00013
ENSMUSG00000021485	Mxd3	Max dimerization protein 3	purple	2.0	4.75E-05
ENSMUSG00000051920	Rspo2	R-spondin 2	purple	2.0	0.00153
ENSMUSG00000032017	Grik4	glutamate receptor, ionotropic, kainate 4	purple	2.0	0.00281
ENSMUSG00000071551	Akr1c19	aldo-keto reductase family 1, member C19	purple	2.1	0.0099
ENSMUSG00000068744	Psrc1	proline/serine-rich coiled-coil 1	purple	2.1	7.67E-07
ENSMUSG00000007682	Dio2	deiodinase, iodothyronine, type II	purple	2.1	0.00948
ENSMUSG00000068794	Col28a1	collagen, type XXVIII, alpha 1	purple	2.1	3.10E-06
ENSMUSG00000112481	AC155710.1	-	purple	2.1	0.01043
ENSMUSG00000026955	Sapcd2	suppressor APC domain containing 2	purple	2.1	2.40E-05
ENSMUSG00000024301	Kifc5b	kinesin family member C5B	purple	2.1	7.91E-05
ENSMUSG00000025420	Katnal2	katanin p60 subunit A-like 2	purple	2.1	0.00526
ENSMUSG00000006930	Hap1	huntingtin-associated protein 1	purple	2.1	0.00105

ENSMUSG00000062393	Dgkk	diacylglycerol kinase kappa	purple	2.1	0.0105
ENSMUSG00000047986	Palm3	paralemmin 3	purple	2.1	0.00104
ENSMUSG00000050503	Fbxl22	F-box and leucine-rich repeat protein 22	purple	2.1	0.00014
ENSMUSG00000085601	Gm4969	predicted gene 4969	purple	2.1	0.00234
ENSMUSG00000035385	Ccl2	chemokine (C-C motif) ligand 2	purple	2.1	0.00238
ENSMUSG00000109130	Gm45187	predicted gene 45187	purple	2.1	0.00843
ENSMUSG00000028678	Kif2c	kinesin family member 2C	purple	2.1	6.90E-05
ENSMUSG00000087150	BC064078	cDNA sequence BC064078	purple	2.1	0.00111
ENSMUSG00000028020	Glrb	glycine receptor, beta subunit	purple	2.1	0.00014
ENSMUSG00000022887	Masp1	mannan-binding lectin serine peptidase 1	purple	2.1	0.00431
ENSMUSG00000113057	AC171004.1	-	purple	2.1	0.00173
ENSMUSG00000022322	Shcbp1	Shc SH2-domain binding protein 1	purple	2.2	1.04E-06
ENSMUSG00000079598	Clec2l	C-type lectin domain family 2, member L	purple	2.2	0.00498
ENSMUSG00000040649	Rimklb	ribosomal modification protein rimK-like family member B	purple	2.2	1.81E-05
ENSMUSG00000036452	Arhgap26	Rho GTPase activating protein 26	purple	2.2	2.45E-10
ENSMUSG00000062184	Hs6st2	heparan sulfate 6-O-sulfotransferase 2	purple	2.2	1.81E-05
ENSMUSG00000042846	Lrrtm3	leucine rich repeat transmembrane neuronal 3	purple	2.2	0.00316
ENSMUSG00000022180	Slc7a8	solute carrier family 7 (cationic amino acid transporter, y+ system), member 8	purple	2.2	2.03E-05
ENSMUSG00000032783	Troap	trophinin associated protein	purple	2.2	2.96E-06
ENSMUSG00000062372	Otof	otoferlin	purple	2.2	0.00108
ENSMUSG00000042116	Vwa1	von Willebrand factor A domain containing 1	purple	2.3	1.05E-06
ENSMUSG00000041476	Smpx	small muscle protein, X-linked	purple	2.3	2.52E-09
ENSMUSG00000040138	Ndp	Norrie disease (pseudoglioma) (human)	purple	2.3	0.00254
ENSMUSG00000046961	Gpr156	G protein-coupled receptor 156	purple	2.3	7.58E-05
ENSMUSG00000020808	Fam64a	family with sequence similarity 64, member A	purple	2.3	4.71E-11
ENSMUSG00000058153	Sez6l	seizure related 6 homolog like	purple	2.4	0.00032
ENSMUSG00000022332	Khdrbs3	KH domain containing, RNA binding, signal transduction associated 3	purple	2.4	1.52E-10

ENSMUSG00000098090	2700099C18Rik	RIKEN cDNA 2700099C18 gene	purple	2.4	2.98E-05
ENSMUSG00000056648	Hoxb8	homeobox B8	purple	2.4	1.15E-10
ENSMUSG00000036192	Rorb	RAR-related orphan receptor beta	purple	2.4	0.00092
ENSMUSG00000052353	Cemip	cell migration inducing protein%2C hyaluronan binding	purple	2.4	9.03E-09
ENSMUSG00000004360	9330159F19Rik	RIKEN cDNA 9330159F19 gene	purple	2.4	0.00089
ENSMUSG00000031891	Hsd11b2	hydroxysteroid 11-beta dehydrogenase 2	purple	2.4	6.69E-05
ENSMUSG00000022311	Csmd3	CUB and Sushi multiple domains 3	purple	2.4	0.00088
ENSMUSG00000026712	Mrc1	mannose receptor C type 1	purple	2.4	2.96E-05
ENSMUSG00000017724	Etv4	ets variant 4	purple	2.4	9.34E-11
ENSMUSG00000055022	Cntn1	contactin 1	purple	2.5	0.00015
ENSMUSG00000037653	Kctd8	potassium channel tetramerisation domain containing 8	purple	2.5	0.00025
ENSMUSG00000078773	Rad54b	RAD54 homolog B (S. cerevisiae) [	purple	2.6	3.81E-06
ENSMUSG00000056972	Magel2	melanoma antigen%2C family L%2C 2	purple	2.6	1.93E-05
ENSMUSG00000036030	Prtg	protogenin	purple	2.7	7.72E-05
ENSMUSG00000030223	Ptpro	protein tyrosine phosphatase, receptor type, O	purple	2.8	4.43E-05
ENSMUSG00000005089	Slc1a2	solute carrier family 1 (glial high affinity glutamate transporter), member 2	purple	2.8	2.35E-13
ENSMUSG00000030518	Fam189a1	family with sequence similarity 189, member A1	purple	2.8	1.20E-05
ENSMUSG00000030226	Lmo3	LIM domain only 3	purple	3.0	8.37E-06
ENSMUSG00000031285	Dcx	doublecortin	purple	4.2	1.19E-11
ENSMUSG00000085289	Gm15337	predicted gene 15337	purple	4.2	1.53E-17

Chapter 4: Glucocorticoid Receptor Ontogeny in the Fetal Mouse Kidney and Identification of Glucocorticoid-Regulated Target Genes by Transcriptome Analysis

Glucocorticoid receptor ontogeny in the fetal mouse kidney and identification of glucocorticoid-regulated target genes by transcriptome analysis

K. L. Short[1], Rachel Lam[2], Julie L.M. Moreau[2], Judy Ng[1], Alexander N. Combes[2] and Timothy J. Cole[1,3]

[1] Department of Biochemistry and Molecular Biology, Monash University, Melbourne, Vic, 3800, Australia

[2] Department of Anatomy and Developmental Biology, Monash University, Melbourne, Vic, 3800, Australia

[3] Corresponding author: Associate Professor Timothy J. Cole, Department of Biochemistry and Molecular Biology, Monash University, Clayton, Victoria, 3800, Australia

Phone: 61-3-9902-9118, Fax: 61-3-9902 9500

Email: tim.cole@monash.edu

Abbreviated Title: Glucocorticoid receptor targets in kidney development

Word count:

Number of figures and tables: 8 figures and 2 tables

Disclosure statement: The authors have nothing to disclose

Abstract

Glucocorticoid (GC) hormones have well characterised roles in the development of several fetal organs, however, the specific developmental role of GCs in the kidney are relatively unknown. This study explores both the expression and localisation of the glucocorticoid receptor (GR) within developing kidney structures during organogenesis and the effect of eliminating GR expression within different compartments of the kidney. We show that the GR is localised to specific kidney cell types and regions from E13.5 to E18.5 including nephron progenitor, pretubular aggregate, ureteric epithelium, stroma and immune cells. We also show that total loss of GR expression by Cre-recombinase gene targeted ablation has the most profound effect on the renal transcriptome compared to conditional ablation of GR in the renal collecting duct epithelium or the kidney mesenchyme. 454 genes were differentially expressed in GRnull mouse kidney with more genes being significantly downregulated (305) than upregulated (99) relative to control animals including the primary cilia associated gene Centrosomal protein 290 (*Cep290*) with a fold change of -3.6. Two renal tubule markers, Kidney androgen regulated protein (*Kap)* (proximal tubule marker) and S100 calcium binding protein G, (*S100g)* (distal tubule marker) were also downregulated with fold changes of -8.61 and -2.5 respectively. These results indicate that the GR is required for normal mouse kidney development.

Key words: Kidney development, Glucocorticoids, Glucocorticoid Receptor

4.1 Introduction

GC steroid hormones play an essential role in the functional maturation and growth of many fetal tissues and organs including the lung, heart and central nervous system (Fowden and Forhead 2015; Whirledge and DeFranco 2018). However, the kidney-specific developmental actions of GC/GR signalling are not well characterised. GCs exert their actions in cells by binding and activating the intracellular GR. Once activated the GR translocates to the nucleus and acts as a transcription factor via binding to glucocorticoid response elements (GRE) in the genome to either increase or decrease gene expression of specific target genes (Quax, et al. 2013). GCs, however, can activate both the GR and the related mineralocorticoid receptor (MR) that is localised to epithelial cells of distal convoluted tubules and collecting ducts in the kidney. In these cells the MR is protected from GC activation by the enzyme 11β-hydroxysteroid dehydrogenase type 2 (11βHSD2) which converts active GCs to an inactivate metabolite. This allows the MR to be activated and regulated by another adrenal steroid, aldosterone, to regulate sodium and water reabsorption along the renal tubule (Ackermann, et al. 2010). In the developing mouse kidney GR gene expression occurs in a specific temporal pattern. mRNA levels in the fetal mouse kidney increase from E9.5 to ~E14.5 (Speirs, et al. 2004), and correlates with the start of GC biosynthesis in the fetal mouse adrenal at ~ E14.5 (Speirs et al. 2004). This is followed by a reduction in GR mRNA levels until ~E17, after which GR levels increase until birth (Speirs et al. 2004), coinciding with a surge of maternal GCs prior to birth (Venihaki, et al. 2000). This pattern of GR expression indicates that GC/GR signalling plays important roles in kidney development. The exact localisation of GR expression and activity in different regions and structures in the developing fetal kidney is not known.

Gene-targeted mice lacking GR expression die shortly after birth due to respiratory failure (Cole, et al. 1995; Daniel Bird, et al. 2015). With the use of conditional mouse gene knockouts of the GR it has been demonstrated that GR activity is specifically required within the mesenchymal compartment of the lung for normal lung development (Bird, et al. 2014). Mice lacking the GR in the mesenchymal compartment of the lung (GRmesKO) have a similar fate and phenotype to complete GRnull mice of

perinatal lethality due to respiratory failure (Bird et al. 2014). Histologically both GRnull and GRmesKO mouse lungs have a hypercellular interstitial mesenchymal compartment (Bird et al. 2014; Bird, et al. 2007). The perinatal lethality of GRnull mice make, studying GC signalling postnatally in other tissues and organs such as the kidney difficult. A small number of studies have used mouse models of conditional GR deletion in kidney epithelium. Deletion of GR in the distal nephron using a *Kspcre* driver resulted in a mild increase in blood pressure in adult mice with normal renal histology (Goodwin, et al. 2010). A more extensive renal tubular deletion of GR in mice using an inducible *Pax8* cre driver altered the expression of several epithelial sodium transporters including the thiazide-sensitive Na^+/Cl^- cotransporter (*Ncc*), Sodium transport, sodium and hydrogen exchanger 3 (*Nhe3*) and the Na-K-Cl cotransporter-2 (*Nkcc2*) (Canonica, et al. 2019). Furthermore, adult mice heterozygous for a GR null allele developed salt sensitive hypertension and reduced mRNA levels of *Ncc* when on a high salt diet (Ivy, et al. 2018).

Synthetic GCs such as betamethasone and dexamethasone are routinely administered in situations of preterm birth to decrease the morbidity and mortality of infants at risk of respiratory distress syndrome (RDS). However, the long-term side-effects of GC treatments on kidney function are relatively unknown and currently under investigation. Antenatal dexamethasone treatment in rats alters 431 renal genes including key developmental genes for example; *Gfra1* that encodes glial cell line-derived neurotrophic factor (GDNF) which is essential for ureteric bud outgrowth (Sheen, et al. 2015). It has been demonstrated experimentally in animal models that exposure to powerful synthetic GC such as betamethasone or dexamethasone antenatally reduces birth weight and increases the risk of high blood pressure in adulthood (Seckl 2004). Additionally, dexamethasone has been shown to reduce nephron number in the rat kidney if exposure occurs at either fetal day 15 and 16 or 17 and 18 (Ortiz, et al. 2001). Interestingly, a study by Habib et al. demonstrated that inhibiting maternal GCs in a mouse model of low protein diet ameliorated the associated increase in blood pressure postnatally (Habib, et al. 2011). However, the link between GCs and salt sensitive blood pressure regulation is complex. It has been shown that both GC excess and GC deficiency can lead to salt-sensitive

hypertension (Bailey, et al. 2009; Ivy et al. 2018). The gestational timing of GC exposure and dosage concentration may explain some of the differences in responses observed. With the increasing evidence supporting the developmental origins of health and disease (DOHad) theory (Barker 2007; Barker, et al. 1993), it is essential to understand the cell-type specific actions of GR signalling during fetal development in the kidney, to avoid the consequences of excessive and poorly timed exposure to inappropriate GCs. In this study we use single-cell sequencing of fetal kidney cells and immunohistochemistry to localise the specific cells in the fetal kidney expressing the GR, and combine this with genetic mouse models of conditional GR deficiency in different cell types of the kidney to investigate the localisation of the GR during kidney organogenesis and the target genes and pathways activated at E18.5, just prior to birth. We show for the first time that the GR is present in all major cell types from E13.5. Additionally, we show that at E18.5 GR is more highly expressed in proximal tubule, distal tubule and stroma cells. Lastly, we identify novel GC target genes in the developing kidney and show that complete GR deficiency has a more profound effect on the renal transcriptome than mesenchymal or collecting duct specific deletion.

4.2 Materials and Methods

Animals

The use of all mice (Mus musculus) was approved by the Monash Animal Research Platform-1 Animal Ethics Committee at Monash University. Global GRnull, GRmesKO and collecting duct specific GR-null (GRcdKO) mice were all of an isogenic C57BL/6 genetic background. GRnull mice were generated by gene targeting as previously described (Cole et al. 1995). GRmesKO and GRcd7KO mice were generated using the Cre/Loxp gene recombination system as described previously (Bird et al. 2014). Briefly, mice expressing Cre under the control of either the dermo1 (mesenchymal specific) (mice provided by Prof. Brandon Wainwright, University of Queensland, Brisbane, Australia) or the Hoxb7 (collecting duct specific) (mice provided by Prof. Ian Smyth, Monash University, Melbourne Australia) promoter were bred with $GR^{loxp/loxp}$ mice to generate $GR^{loxp/+,}$, $Dermo1^{cre/+}$ or $GR^{loxp/+}$, $Hoxb7^{cre/+}$ mice. These mice were then time-mated with $GR^{loxp/loxp}$ to generate $GR^{loxp/loxp}$, $Dermo1^{cre/+}$ or $GR^{loxp/loxp}$, $Hoxb7^{cre/+}$ mice. Pregnant mice were sacrificed according to approved guidelines of the Animal Ethics Committee at Monash University at gestation E18.5 and pups sacrificed by decapitation. The kidneys of fetal pups (at least n=3 for each genotype collected from 2-3 litters) were isolated and either snap frozen in liquid N_2 or fixed in 4% paraformaldehyde for further analysis. Tail snips from pups were collected for genotyping by qPCR and analysis by gel electrophoresis. Primer sequences for hoxb7 Cre were from Jackson Laboratories (Protocol 22392: Standard PCR Assay-generic Cre), Dermo1 and loxp/loxp primer sequences used for genotyping are available on request.

Fetal Kidney Single Cell Data Analysis

The E18.5 data was generated and processed as previously described (Combes, et al. 2019) and is available at GEO (GSE108291). E13.0 and E15.5 embryonic kidneys were dissociated in 500µl Accutase (Stemcell technologies) at 37°C for 6-8 min. Samples were gently agitated by pipetting every 2 min then washed with cold PBS 0.05% BS, pelleted by centrifugation (400g, 5 min), and

stored on ice. Samples were filitered with Flowmi Cell Strainers (70µm, Bel-Art Products) and stained with DAPI before removal of dead cells by FACS (100µm nozzle). Cell concentration was determined using a hemocytometer and adjusted prior to the generation of signal cell libraries using 10x Chromium v3 kits. Sequencing data was processed using Cell Ranger (v1.3.1, 10x Genomics) and aligned to mm10 with STAR (v2.5.1b) (Dobin, et al. 2013). Subsequent analysis was performed in the R statistical programming language using Seurat (v3.1.4) (Butler, et al. 2018; Stuart, et al. 2019). Quality control for the E13.0 and E15.5 datasets involved removing cells with <1000 genes, >20% mitochondrial gene content (E13.0); <1500 genes, >8% mitochondrial gene content (E15.5). Doublets were identified and filtered out using Scrublet (Wolock, et al. 2019) or with the *HTODemux* function in Seurat. Cell cycle phase was predicted using either Cyclone (Scialdone, et al. 2015) or Seurat's *CellCycleScoring* function. Cell cycle effects were regressed out and gene expression data normalised using *SCTransform* with default parameters. Following all quality control steps, the E13.0 dataset consisted of 19252 genes and 4176 cells and the E15.5 dataset of 18549 genes and 3294 cells. The E13.0 and E15.5 datasets are available on request. Principle component analysis on highly variable genes informed selection of clustering resolution (0.8). Cluster identity was determined by referencing top cluster marker genes (*FindAllMarkers*) to Combes et al previous analysis (Combes et al. 2019). Clusters in each dataset were manually curated to generate 13 broad clusters that were comparable between the three developmental timepoints. Clusters representing cell cycle effects or non-renal cell types such as neural progenitors (E13.0) were not displayed. Seurat's *DotPlot* and *FeaturePlot* functions were used for plotting and visualisation.

PAS, Immunohistochemistry and Immunofluorescence Staining

Fetal mouse kidneys were fixed in 4% paraformaldehyde (diluted in PBS) before they were processed and embedded in paraffin. Paraffin blocks were cut and 4µm sections mounted on slides and used for Periodic acid-Schiff (PAS), immunohistochemistry or immunofluorescence staining. Sections were incubated with primary antibodies at either room temperature for 2 h or overnight at 4°C. Primary antibodies used were GR (1:200; cell signalling, D6H2L), Biotinylated Dolichos Biflorus Agglutinin

(DBA) (1:250; Vector Laboratories, B-1035), Biotinylated Lotus Tertragonolobus lectin (LTL) (1:250; Vector Laboratories, B-1325), Ki67 (1:500; Abcam, ab15580) or Pan-Cytokeratin (1:100, Abcam, ab115959). Sections were then washed and incubated with either secondary antibodies or streptavidin. Secondary antibodies used for immunofluorescence were Alexa Fluor® donkey anti-rabbit IgG (H+L) 555 or 488, Alexa Fluor® donkey anti-mouse IgG (H + L) 555 or 647 or streptavidin, Alexa Fluor® 647 or 488. Hoechst (life technologies) was used as a counterstain and added to the secondary antibody mix. Sections were imaged with either Leica SP5 5-Channel Confocal Microscope or scanned with a Lecica DMi8 microscope. The secondary antibody used for immunohistochemistry was goat anti-rabbit IgG (H+L) Biotin (1:1000; Life technologies, B2770). This was followed by washing and incubation with Streptavidin-Horseradish Peroxidase (HRP) conjugate (1:1000) and finally development with a DAB substrate (Dako, K3468). PAS staining was performed on Leica ST5010 Autostainer and CV5030 coverslipper. Sections from PAS staining or immunohistochemistry were either scanned by Monash Histology Platform with Aperio Scanscope AT turbo or imaged using Eclipse E400, Nikon microscope

Western Blot Analysis

Proteins were isolated from mouse kidney tissue in Radioimmunoprecipitation (RIPA) buffer. One tablet of Complete mini protease inhibitor corktail (Roche) was added per 10 ml of RIPA buffer. Briefly, 250 µl of RIPA buffer was added to each kidney sample and the samples were homogenised and incubated on ice for 15 min. Kidney homogenates were then sonicated for 10 sec followed by a 30 min incubation on ice. The samples were centrifuged at 14000 g-force for 20 min at 4°C, the supernatant was collected, and protein concentration was determined using a DC assay (Biorad, USA). 15 µg of protein lysates was separated by electrophoresis on a TGX sain-free 10% fastcast SDS-PAGE polyacrylamide gel (Biorad, USA). Following a standard protocol, the protein was transferred onto a 0.44 µm Immobilion-P membrane (Sigma-Aldrich). The membranes were blocked using 5% skim milk powder diluted in Tris-buffered saline containing 0.1% Tween (TBST) (block buffer) for 1 h at room temperature. The membranes were then incubated with a GR antibody (1:2000;

cell signalling, D6H2L) diluted in block buffer overnight at 4°C , followed by 5 x 5 min washes in TBST and a 1 h room temperature incubation with anti-rabbit IgG HRP-linked secondary antibody (1:10000; cell signalling; 7074). Before X-ray imaging membranes were washed 5 x 5 min in TBST and incubated with enhanced chemiluminescence (ECL) (Biorad, USA) for 5 min. After X-ray imaging, the membranes were stripped with 0.5 M NaOH, washed 5 x 5 min with TBST and incubated with Beta actin antibody (1:1000000; Sigma-Aldrich; A5316) for 1 h at room temperature. Followed by 5 x 5 min TBST washes and incubation with Anti-mouse-HRP-linked secondary antibody (1:10000; Dako; P0447) for 1 h at room temperature. The membranes were washed 5 x 5 min with TBST and imaged by X-ray to control for protein loading. Developed X-ray films were scanned, and images produced using image J software.

Total RNA Isolation and NGS Transcriptome Sequencing

Total RNA was extracted from embryonic kidneys using TRIzol^{TM} reagent (Invitrogen, USA) according to the manufacturer's instructions. Purified total RNA was analysed using a Bioanalyzer 2100 (Agilent Technologies, USA) and Next generation RNA sequencing (NGS RNA-seq) was performed by Genewiz Biotechnology, Suzhou, China. RNA Sequencing (20 million reads) was performed on the Illumina Hiseq platform, in a 2 x 150bp paired-end format. The Raw sequencing data was interpreted by Genwiz's bioinformatics team which included quality control, alignment to the reference mouse genome (ENSEMBL, version GRm38.97), assembly and gene expression analysis (Bioconductor package edgeR (V3.4.6)) including clustering, GO enrichment and pathway enrichment. Additional, enrichment terms were identified by DAVID and Enrichr (Ma'ayan Laboratory).

cDNA Synthesis and Quantitative PCR

cDNA was synthesised with a QuantiTect RT kit (Qiagen) following the manufacturer's instructions from the same fetal kidney RNA samples used for RNA sequencing. To measure mRNA levels of Hemoglobin alpha, adult chain 1 (*Hba1-a1*), Interferon activated gene 203, 2'-5' (*ifi203*),

Oligoadenylate synthetase 2 (*Oas2*), Centrosomal protein 290 (*Cep290*), 2'-5' Oligoadenylate synthetase-like 2 (*Oasl2*), Myeloid nuclear differentiation antigen like (*Mndal*), Guanylate binding protein 7 (*Gbp7*), Kidney androgen regulated protein (*Kap*), Cysteine-rich secretory protein 1 (*Crisp1*), Interferon-induced protein with tetratricopeptide repeats 1 (*Ifit1*) and S100 calcium binding protein G (*S100g*) qPCR was performed using QuantiNova® SYBR® green master mix (Qiagen) on a CFX384 Touch Real-Time PCR Detection System (Biorad), following normal protocols. The relative mRNA level of each gene was normalised to the housekeeping gene Ribosomal protein 29 *(Rps29*) using the ΔΔCt method and expressed relative to the mRNA levels of control animals. PCR products for each primer set were verified for a single PCR product by a PCR melt-curve analysis, visualisation of a single product on an agarose gel and finally the PCR product verified by DNA sequencing. Primer sequences are available in supplementary Table 4.1.

Statistical Analysis

For qPCR and western blot analysis, GraphPad Prism statistical analysis software was used, with statistical significance set at $P<0.05$. Two groups were compared using an unpaired t-test, and multiple groups were compared by a 1-way ANOVA with a Tukey's post hoc test.

4.3 Results

4.3.1 Expression and Localisation of the GR in the Developing Kidney During Embryogenesis

To investigate the expression of the GR in specific cell types of the fetal kidney we first utilised single cell RNA-seq datasets from the fetal mouse kidney. Combes et al. recently performed single cell RNA sequencing on E13.5 (unpublished), E15.5 (unpublished) and E18.5 (Combes et al. 2019) fetal mouse kidneys to explore the gene-expression profiles and developmental programming of different cell types within the kidney. Data collected for the *Nr3c1/GR* gene show that the GR is expressed at E13.5 within nephron progenitor, pretubular aggregate, ureteric epithelium, stroma and immune cells within the kidney. The highest expression of GR at E13.5 was within stroma cluster 3 which is distinguished by the expression of Collagen type III alpha 1 (*Cola1*), Decorin (*Dcn*), Delta like non-canonical Notch ligand 1 (*Dlk1*) and Periostin osteoblast specific factor (*Postn*) cell markers, followed by expression within stroma cluster 4 which is a miscellaneous cluster of stromal cells that do not have a strong distinctive set of marker genes. At E15.5 GR expression in stroma cell populations becomes more wide-spread, and expression is now detected in tubular structures such as the proximal tubules and distal tubule/loop of Henle. Other expression sites appear in immune cells and the vasculature. At E18.5 GR maintains a wider expression pattern across these locations and cell types with high expression in stroma compartments, the distal tubule and proximal tubule cell clusters (Figure 4.1A).

To compare localisation of GR at the protein level in the fetal kidney we performed immunofluorescence using a GR antibody and two kidney cell markers LTL, a lectin, and DBA, an agglutinin, which mark the proximal tubules and collecting ducts of the kidney respectively. At E14.5 GR was strongly localised to the developing collecting ducts and detected in the stroma tissue (Figure 4.1E), consistent with the single cell data from E13.5 to 15.5. At E14.5 GR appeared to show a gradient of expression with more abundance in the renal medulla compared to the renal cortex (Figure 4.1B). Proximal tubules are not developed until after E14.5 and therefore we did not perform LTL staining at this time point (Davidson 2009; Short and Smyth 2016). At E16.5 GR is widely localised

in the kidney with positive staining in the collecting ducts, proximal tubules and mesenchyme. Similarly, at E18.5 GR was also seen in collecting ducts, proximal tubules and mesenchyme also consistent with the single cell RNA_seq data (Figure 4.1).

4.3.2 Ablation of GR Expression in the Fetal Kidney by Cre Recombinase-Mediated Gene Targeting

To study the role of GR in the developing fetal kidney we utilised three different GR knockout mouse models; total GR deletion in mice (GRnull), mesenchymal-selective GR deletion (GRmesKO) and kidney collecting duct GR specific deletion (GRcdKO). The effective ablation of GR expression was demonstrated by immunohistochemistry at E18.5 with antibodies to the GR, and co-staining with LTL, for proximal tubules and DBA for collecting ducts (Figure 4.2A). Wild type (control) mice showed abundant GR expression across the E18.5 fetal kidney, while GRnull mice had a complete loss of detectable GR expression (Figure 4.2A). In GRmesKO fetal mice GR immunostaining was detected in the epithelial cells of the proximal tubules and collecting ducts but there was a dramatic reduction in expression in stromal areas (Figure 4.2A). To further demonstrate the loss of GR protein in the mesenchyme of the GRmesKO mouse kidney at E18.5, a GR western blot analysis was performed from whole fetal kidneys and showed a significant reduction of ~40% in GR protein levels (Figure 4.2B & C). Finally, GRcdKO fetal mice had detectable GR expression in most areas of the kidney, primarily the mesenchyme, but had a complete loss of GR expression in nearly all DBA positively stained collecting duct epithelial cells (Figure 4.2A). To examine if there were any major abnormalities in renal structures, histology sections of fetal kidneys at E18.5 from wild type, GRnull, GRmesKO and GRcdKO mice were stained with periodic acid Schiff (PAS) and compared (Figure 4.3). All three GR deficient mouse models displayed normal renal histology at E18.5 compared to wild type control mice and indicated that GR-mediated signalling was not required for the normal structural development of the mouse kidney (Figure 4.3). In the fetal mouse lung of GRnull and GRmesKO mice there is a significant two-to three-fold increase in the number of proliferating mesenchymal cells at E18.5 that leads to a thickened interstitial mesenchyme at birth and eventual

respiratory failure. We therefore examined the numbers of proliferating renal mesenchymal cells in GRnull and GRmesKO fetal mice using the cell proliferation marker Ki67. E18.5 fetal kidney sections were analysed by immunofluorescent staining for Ki67 and the epithelial cell marker Pan-Cytokeratin (Figure 4.4). We detected no significant differences in numbers of Ki67 positive cells in the Pan-cytokeratin-minus mesenchymal compartment in kidney sections from E18.5 fetal GRnull and GRmesKO mice compared to wild type controls, indicating that in contrast to lung mesenchyme at the same stage of development there were normal rates of mesenchymal cell proliferation (Figure 4.4).

4.3.3 GRnull and GRmesKO Mice have an Altered Renal Transcriptome

The GR is a steroid ligand-activated transcriptional regulator. We therefore analysed the effect of the loss of GR expression on whole fetal kidney gene expression at E18.5 in GRnull and GRmesoKO mice using transcriptome sequencing. Total RNA was extracted from wild type control (n=4), GRnull (n=3) and GRmesKO (n=3) mouse kidneys at E18.5 and analysed by NGS transcriptome sequencing. Global changes in mRNA levels are shown as a heatmap for genes with a fold change greater than 2 and a false discovery rate (FDR) of less than 0.05 (Figure 4.5). Hierarchical clustering was used to group both the samples and gene clusters with similar expression patterns. As predicted the samples group into the three genotypes of wild type control, GRnull, and GRmesKO. The genes clustered into three main groups colour coded on the heatmap (dark blue, aqua and green). The differentially expressed genes in the dark blue cluster (157 gene) were down regulated in GRnull kidney relative to both control and GRmesKO kidney. The differentially expressed genes in the aqua cluster (310 genes) are downregulated in both GRnull and GRmesKO kidney relative to control and the green cluster (204 genes) is composed of differentially expressed genes that are upregulated in both GRnull and GRmesKO kidney relative to control kidney. Individual volcano plots comparing control to GRnull (figure 4.6A), control to GRmesKO (figure 4.6B) and GRnull to GRmesKO (Figure 4.6C) showed that more genes were in fact significantly decreased than increased in the two GR-ablated lines. Total loss of GR, in GRnull mice, had the most profound effect on the fetal kidney transcriptome

at E 18.5 with a total of 454 genes with altered mRNA levels compared to controls, with a fold change greater than 2 and an FDR less than 0.05 (Figure 4.6A). While mesenchymal loss of GR resulted in 285 genes with altered RNA levels using the same parameters (Figure 4.6B), with 85 gene in common between the two groups (figure 4.6D). Table 4.1 lists the most differently expressed protein coding genes that overlap and have a fold change greater than 2 and an FDR less than 0.05 including the norepinephrine transporter, Solute carrier family 6 (neurotransmitter transporter, noradrenalin), member 2 (*Slc6a2*), the kidney proximal tubule marker, *Kap*, the distal tubule marker *S100g* which is involved in calcium ion transport, α-2-HS-glycoprotein (Ahsg) that is involved in system development and the extracellular matrix stabilisation gene, Aggrecan (Acan).

4.4.4 Analysis of the mRNA Levels for Differentially Expressed Genes in E18.5 Fetal Kidney by qPCR

To validate and confirm the gene expression changes detected by the NGS transcriptome sequencing, we performed real-time qPCR to quantify mRNA levels of 12 selected differently expressed protein coding genes. The genes were selected based on fold change and quantity of reads. There was a significant decrease in GRnull fetal kidney mRNA levels at E18.5 in all selected down regulated genes compared to controls, *Ifi203* ($p \leq 0.0001$, 5.6-fold), *Kap* ($p \leq 0.0001$, 9.2-fold), *S100g* ($p \leq 0.001$, 2.7-fold), *Cep290* ($p \leq 0.05$, 2.9-fold), *Crisp1* ($p \leq 0.001$, 9.6-fold), *Gbp7* ($p \leq 0.05$, 3.7-fold), *Ifit1* ($p \leq 0.05$, 8.6-fold), *Mndal* ($p \leq 0.001$, 3.8-fold), *Oas2* ($p \leq 0.05$, 2.6-fold), *Oasl2* ($p \leq 0.01$, 4.6-fold) and *Igf2* ($p \leq$,-fold) (Figure 4.7B-L). There was a significance decrease in GRmesKO kidney mRNA levels at E18.5 only for *Kap* ($p \leq 0.001$, 2.8-fold) and *S100g* ($P \leq 0.05$, 1.5-fold) (Figure 4.7C-D). *Hba-a1* was significantly increased in both GRnull ($p \leq 0.01$, 3.3-fold) and GRmesKO ($p \leq 0.05$, 1.6-fold) kidney RNA at E18.5 (Figure 4.7A). Interestingly, in contrast to GR-null mice, *Gbp7* was significantly increased in GRmesKO mouse kidney mRNA at E18.5 ($p \leq 0.05$, 1.6-fold) (Figure 4.7G).

4.4.5 Localisation of Differentially Expressed Gene Targets in the Fetal Mouse Kidney at E18.5 using Whole Fetal Kidney Single Cell Datasets

To explore where in the kidney the 12 differentially expressed genes validated by qPCR were localised we utilised the E18.5 single cell dataset produced by Combes et al. (Combes et al. 2019). We found *Hba-a1* had high expression across all the kidney clusters at E18.5 (Figure 4.8A). *Igf2* was also expressed and localised across several kidney cell clusters including the S-Shaped body, vasculature and mesenchymal stroma cells (Figure 4.8B). As expected *Cep290* was predominately expressed in kidney tubule cells where primary cilia are found on epithelial cells (Figure 4.8B). *Gbp7*, *Ifit1*, *Mndal*, *Ifit1*, *Oas2* and *Oasl2* were all expressed in the vasculature and immune cells also as expected and *Kap* was expressed in renal proximal tubule cells while *S100g* was expressed in distal tubule cells (Figure 4.8B).

4.4.6 Loss of GR in Collecting Duct Epithelial Cells does not Dramatically Alter Gene Expression Profiles in the Fetal Kidney at E18.5

NGS RNA sequencing was used to determine if loss of GR in renal collecting duct cells alters renal gene expression profiles. Total RNA was extracted from control (n=4) and GRcdKO (n=4) fetal mouse kidneys at E18.5 and analysed and compared by transcriptome sequencing. The two groups of samples had a very high correlation shown in the Pearson correlation heatmap where a value of 1 indicates a linear relationship (Figure 4.9A). Due to the high correlation between the samples there were no genes with significant differences in mRNA levels using the comparison filter criteria of a fold change greater than 2 and FDR less than 0.05 (Figure 4.9B) indicating that a loss of GR in fetal kidney collecting duct cells at E18.5 does not appreciably affect the renal transcriptome, and indicates that in these cells GR-mediated signalling is either not activated or somehow blocked downstream in the genomic pathway. Furthermore, principal component analysis (Figure 4.9C) showed that control samples and GRcdKO samples grouped together in this comparative analysis. After altering our filter criteria, we did detect 11 genes that had small differences in expression, with a fold change equal or greater to 1.2-fold and a p-value of less than 0.05 (Figure 4.9B). These genes can be seen in the

volcano plot (Figure 4.9D) and are listed in supplementary Table 4.2 and could be investigated further for localisation in the kidney and any functional link to known glucocorticoid actions.

4.4 Discussion

This study has investigated the expression of the GR in the fetal kidney and the potential role for GC/GR signalling in the fetal kidney prior to birth. We first showed that GR is expressed at detectable levels and with a moderately restricted profile at E13.5 within the nephron progenitor, peritubular, uretic epithelium, mesenchymal stroma and in immune cells in the mouse kidney. We also demonstrated that by E15.5 and also at E18.5 the GR is expressed in almost all cell types within the fetal mouse kidney where it has the capacity to respond to rising levels of corticosterone prior to birth. To explore the role of GC signalling in the developing mouse kidney prior to birth we utilised mice with varying degrees of deficiency in the GR. Our results indicated that total loss of GR in all kidney cells has the most profound effect on the renal transcriptome, with 484 genes differently expressed more than 2-fold. In comparison loss of mesenchymal-expressed GR resulted in an alteration to the mRNA levels of 285 genes. Furthermore, despite the high expression of the GR within the renal collecting ducts we observed no strong alterations in the renal transcriptome of GRcdKO mice at E18.5. However, surprisingly unlike the lung, mesenchymal GC signalling is unlikely to be the most critical despite high expression of the GR in stroma cells at E13.5, E15.5 and E18.5. Further investigation is required to determine the key cell types important in GC signalling in the fetal kidney at E18.5.

We analysed and validated a number of putative GR-regulated gene targets, identified by the transcriptome analysis, using qPCR. Most of these genes demonstrated changes in mRNA level in a pattern similar with the NGS RNA sequencing dataset. This indicates that the NGS RNA seq is representative of gene expression in total and mesenchymal GR deficient mouse kidney at E18.5. We showed that more genes were significantly decreased than increased including the kidney tubule markers *Kap* and *S100g*. *Kap* is one of the most abundant specific genes expressed in the kidney proximal tubule cells and is regulated by androgens. The role and function of *Kap* in proximal tubule cells is unknown. One study by de Quixano et al. showed that overexpression of *Kap* protected mice from metabolic syndrome induced by a high fat diet including associated hypertension (de Quixano,

et al. 2017). They also showed that the KAP protein is excreted into the extracellular matrix (ECM) and speculated that KAP may exert effects in other tissues (de Quixano et al. 2017). Another GC/GR-regulated gene target, *S100g*, is a calcium-binding protein and in the kidney, it is localised to the distal tubule at E18.5. The decreased expression of *S100g* may indicate that GC signalling is involved in calcium transport within the kidney. However, *S100g* knockout mice are indistinguishable from control mice (Kutuzova, et al. 2006; Lee, et al. 2007). This may be a result of compensation from other calcium transporter genes. Additionally, both *Kap* and *S100g* expression was not altered in GRcdKO mice at E18.5 indicating normal tubule development.

Cep290 was also significantly decreased in the mouse kidney of GRnull fetal mice at E18.5. The CEP290 protein is localised to the centrosome and cilia where it is essential for assembly of microtubules and for primary cilia formation. *Cep290* genetic mutations are found in a number of human diseases collectively known as ciliopathies and include Joubert syndrome, characterised by brain abnormalities, but is also associated with kidney diseases, Meckel syndrome which is characterised by cystic dysplastic kidneys, brain malformations, hepatic fibrosis and proliferation of the bile ducts, Nephronophthisis, that commonly leads to end-stage renal disease by the age of 30 and is characterised by cystic kidneys, and finally Senior-Loken syndrome characterised by kidney cysts, inflammation and scarring leading to end stage kidney disease (Baala, et al. 2007; Helou, et al. 2007; Hildebrandt, et al. 2011; Valente, et al. 2006). Furthermore, mice deficient in *Cep290* develop symptoms consistent with ciliopathies including reduced numbers of primary cilia on renal epithelial cells and the development of kidney cysts (Rachel, et al. 2015). Development of kidney cysts in *Cep290* knockout mice is progressive and cysts become more prominent at 2 weeks of age (Rachel et al. 2015). Unfortunately, due to the early lethality of GRnull mice we are unable to determine if GRnull mice develop kidney cysts. More investigation is required to establish primary cilia formation and morphology in GRnull mice. This could be achieved by staining kidney sections with primary cilia markers including Kinesin family member 3A (KIF3A) and acetylated tubulin. Further study would require the development of a postnatal renal knockout mouse for the GR. Furthermore, the

development of a conditional primary cilia GR deficient mouse would also lead to more insight into the role of GC signalling in primary cilia formation and function.

Interestingly, we also demonstrated that *Hba-1* encoding the haemoglobin A protein is upregulated in both GRnull and GRmesKO mouse kidneys at E18.5. We also show that *Hba-a1* is expressed in all cell types of the kidney. Other studies have also shown that haemoglobins are expressed in tissues other than erythrocytes (Fordel, et al. 2006; Vinogradov and Moens 2008). A recent study has also demonstrated a connection between GC deficiency and haemoglobins (Meimaridou, et al. 2018). The study used a mutant C57BL/6 mouse strain that contained an inactivating mutation of the nicotinamide nucleotide transhydrogenase (NNT) gene resulting in these mice having GC deficiency (Meimaridou et al. 2018). They performed NGS RNA seq on the adrenals from these mice and showed that several haemoglobin genes were significantly increased including *Hba-1*, *Hba-a2*, *Hbb-b1* and *Hbb-b2* (Meimaridou et al. 2018). This is evidence that haemoglobins may have roles in other cellular functions unrelated to red blood cell oxygen transport. However, the GC regulation of haemoglobin gene expression requires further investigation.

Igf2, encoding insulin-like growth factor 2, was significantly increased in the GRmesKO fetal kidney at E18.5. IGF2 is a growth factor that promotes cell proliferation, differentiation and cell survival. Both IGF1 and IGF2 are essential for normal metanephric kidney development (Bach and Hale 2015; Rogers, et al. 1991). At birth Igf2 levels rapidly decrease in several tissues including the kidney (Lui, et al. 2008). *Igf2* levels have also been found to be elevated in several cancers. Here we show that *Igf2* was expressed across the majority of cell types within the fetal kidney. Additionally, overexpression of *Igf2* in mice results in enlarged kidneys (Wolf, et al. 1994). We were interested to explore the proliferation rate of cells within the kidney mesenchyme of GRmesKO, as in the fetal lung GRmesKO animals have a hyperproliferative phenotype that results in more interstitial tissue and a thickened blood-air barrier causing respiratory failure at birth (Bird et al. 2014). An increase in *Igf2* would be consistent with driving increased cell proliferation in the mesenchyme of the kidney, yet analysis of cell proliferation using the proliferative marker Ki67 showed no major difference in

cell proliferation in stromal areas of the kidney in both GR-null and GRmesKO mice. Therefore GC-regulation of Igf2 in the fetal kidney may have another purpose yet to be discovered.

In conclusion we show 1. From E13.5 to E18.5 there is an increase in GR expression in almost all structures of the fetal kidney. 2. A complete loss of GR expression across the kidney had a more profound effect on the kidney transcriptome compared to conditional loss of GR in the mesenchymal/stromal compartment. 3. At E18.5 mice with ablated expression of the GR in the fetal kidney collecting duct had only very minor changes in the whole kidney transcriptome. This may indicate that GC/GR signalling is not required before the renal tubule is fully functional in trans-epithelial transport one week after birth. We have also identified novel GC target genes whose functions are not well understood within the fetal kidney. Further investigation on the regulation of these gene targets by GR-mediated signalling within the fetal kidney will be required to establish their specific roles in kidney development and the role GR plays in regulating their expression.

Figure legends

Figure 4.1: Localisation of GR in the fetal kidney during kidney development

(A) Expression of the GR at the RNA level within the kidney in cell type clusters at E13.5, E15.5 and E18.5. Scale represents average expression. (B-D) To localise GR protein immunohistochemistry was performed with a GR antibody on the fetal kidney at E14.5, E16.5 and E18.5, and slides were scanned at either 100x (B) or 200x (C&D) magnification to show one kidney per time-point, scale bar B= 100µm, C =200µm and D = 400µm. Immunofluorescence was also performed on wild type kidneys at E14.5, E16.5 and E18.5 with a GR antibody, Lotus Tetragonolobus lectin (LTL) which marks proximal tubules and Dolichos Biflorus Agglutinin (DBA) which marks collecting ducts (E-G). Sections were imaged at 400x magnification. All images are representative of three animals per age group. PT = proximal tubule and CD= collecting duct. Scale bar: 100µm.

Figure 4.2: Ablation of GR signalling in kidney cells by Cre recombinase-mediated gene-targeting

Immunofluorescence was performed on control, GRnull, GRmesKO and Hoxb7KO mouse kidneys at E18.5 to demonstrate ablation of GR expression with a GR antibody, LTL which marks proximal tubules and BDA which marks collecting ducts (A) sections were imaged at 400x magnification. All images are representative of three animals per group. Western blot analysis (mean $\pm$ SEM) (B & C) for protein levels of GR at E18.5 in the fetal kidney of GRmesKO and control mice. Total protein levels were determined relative to β-ACTIN levels. Significance was analysed by an unpaired t-test, $*P \geq 0.05$ (n=3). PT= proximal tubule and CD= collecting duct.

Figure 4.3: Renal histology of GRcdKO, GRmesKO and GRnull fetal mouse kidney at E18.5

PAS staining of E18.5 Control, GRHoxb7KO, GRmesKO and GRnull fetal mouse kidneys. Left panel: whole kidney brightfield scans at 200x magnification, middle panel: Region of the renal cortex

at 400x magnification. Boxed regions are magnified in the right panel and show a glomerulus within the Bowman capsule.

Figure 4.4: Cell proliferation within GRnull and GRmesKO Fetal mouse kidney at E18.5

Immunofluorescence was performed on control, GRmesKO and GRnull kidneys at E18.5 with a Ki67 antibody and Pan-Cytokeratin antibody. Sections were imaged at 400x magnification. All images are representative of three animals per age group. Pk= Pan-Cytokeratin. Scale bar=100µm

Figure 4.5: Hierarchical cluster analysis of differentially expressed genes

NGS RNA seq was performed on total RNA isolated from control (n=4), GRmesKO (n=3) and GRnull (n=3) mouse kidneys at E18.5. Heatmap with cluster analysis of differently expressed genes with a fold change greater than 2 and an FDR less than 0.05. Log10(FPKM + 1) values were used for hierarchical clustering and generation of dendrogram. The colours on the left represent different gene clusters. N=GRnull, C=control and D=GRmesKO.

Figure 4.6: Transcriptome analysis of E18.5 fetal kidney RNA from GRnull and GRmesKO mice

NGS RNA seq was performed on total RNA isolated from control (n=4), GRmesKO (n=3) and GRnull (n=3) mouse kidneys at E18.5. (A-C) Individual volcano plots; red dots represent genes that are significantly up regulated and blue dots represent genes that are down regulated. (D) A Venn diagram showing the number of genes uniquely expressed in each group and the number of genes differently expressed in multiple groups with a fold change greater than 2 and an FDR less than 0.05. genes; control vs GRmesKO (purple), Control vs GRnull (yellow), GRmesKO vs GRnull (green). DEG= Differentially expressed genes.

Figure 4.7: Analysis of the mRNA levels for differentially expressed Genes in E18.5 fetal kidney by qPCR

mRNA levels (mean ± SEM) of 12 target genes identified from NGS RNA seq. (A) *Hba-a1*, (B) *Ifi203*, (C) *Kap*, (D) *S100g*, (E) *Cep290*, (F) *Crisp1*, (G) *Gbp7*, (H) *Ifit1*, (I) *Mndal*, (J) *Oas2*, (K) *Oasl2* and (L) *Igf2* mRNA levels in fetal mouse kidney at E18.5. The mRNA levels in all groups are expressed relative to mRNA levels of the housekeeping gene Rps29. Significant differences were analysed by 1-way ANOVA with Tukey's post hoc test. Significant differences indicated by * $p \leq 0.05$, ** $p \leq 0.01$, *** $p \leq 0.001$, ns= not significant.

Figure 4.8: Localisation of target gene expression in the Fetal mouse kidney at E18

(A) Feature plots showing the expression of target genes across the cell clusters. (B) Expression of target genes within different cell types of the kidney. Scale represents average expression.

Figure 4.9: Transcriptome analysis of E18.5 fetal kidney RNA from GRcdKO GRcdKO mice

NGS RNA seq was performed on total RNA extracted from control and GRcdKO kidneys at E18.5 (n=4). (A) Pearson correlation heatmap ($R^{\wedge}2$); the greater the value the stronger the linear relationship (between 0 and 1). (B) Table showing the different parameters used to identify differently expressed genes. (C) Principal component analysis (PCA) plot using two principal components. (D) Volcano plot red dots represent the 5 up-regulated genes and the blue dots represent the 6 down regulated genes with a fold change greater than 1.2 and a p-value less than 0.05. C=control, K=GRcdKO, FC=fold change.

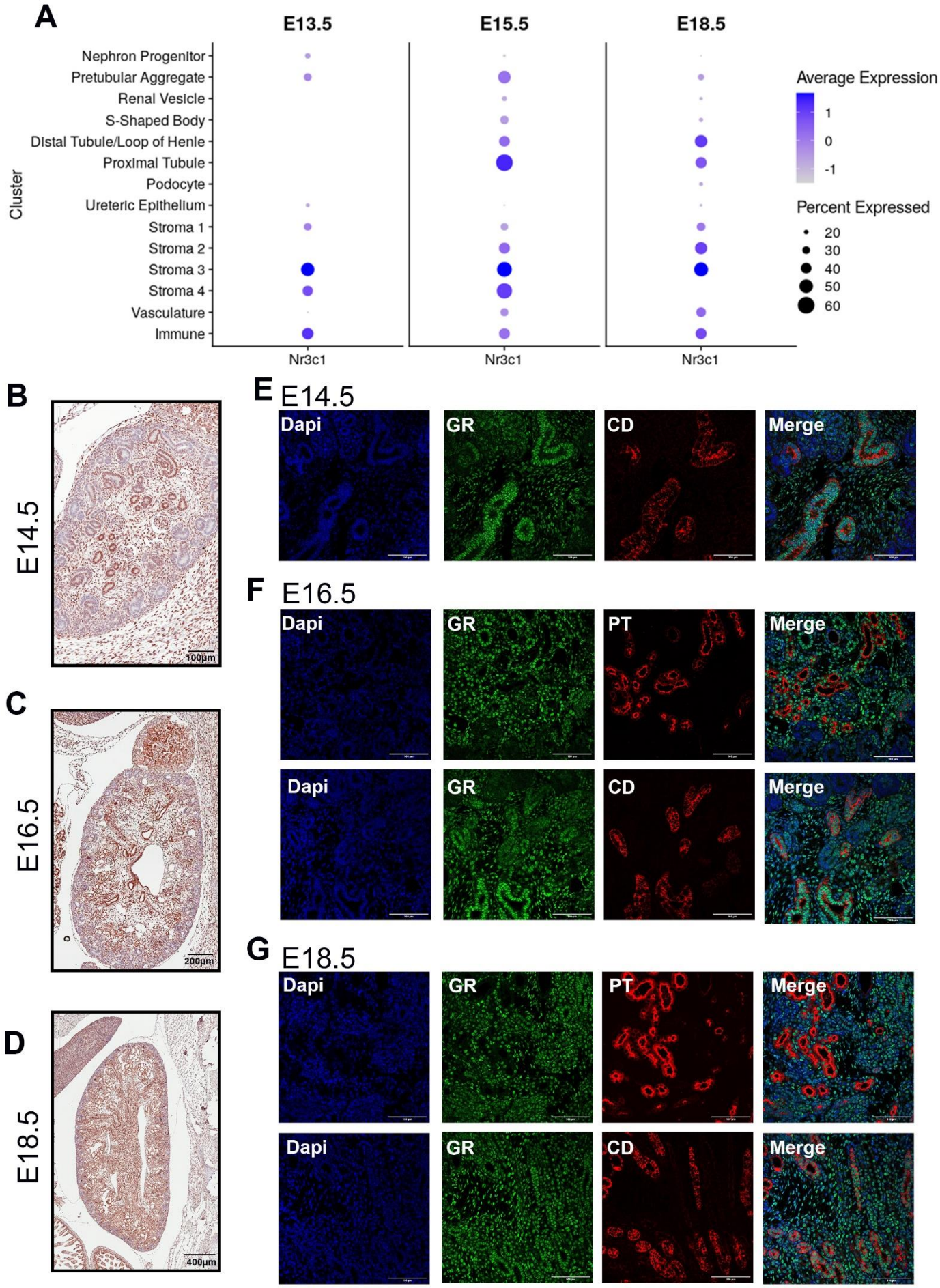
A
E13.5
E15.5
E18.5
Nephron Progenitor
Pretubular Aggregate
Renal Vesicle
S-Shaped Body
Distal Tubule/Loop of Henle
Proximal Tubule
Podocyte
Ureteric Epithelium
Stroma 1
Stroma 2
Stroma 3
Stroma 4
Vasculature
Immune
Cluster
Nr3c1
Average Expression
1
0
-1
Percent Expressed
20
30
40
50
60
B
E14.5
100µm
C
E16.5
200µm
D
E18.5
400µm
E
E14.5
Dapi
GR
CD
Merge
F
E16.5
Dapi
GR
PT
Merge
Dapi
GR
CD
Merge
G
E18.5
Dapi
GR
PT
Merge
Dapi
GR
CD
Merge

Figure 4.1

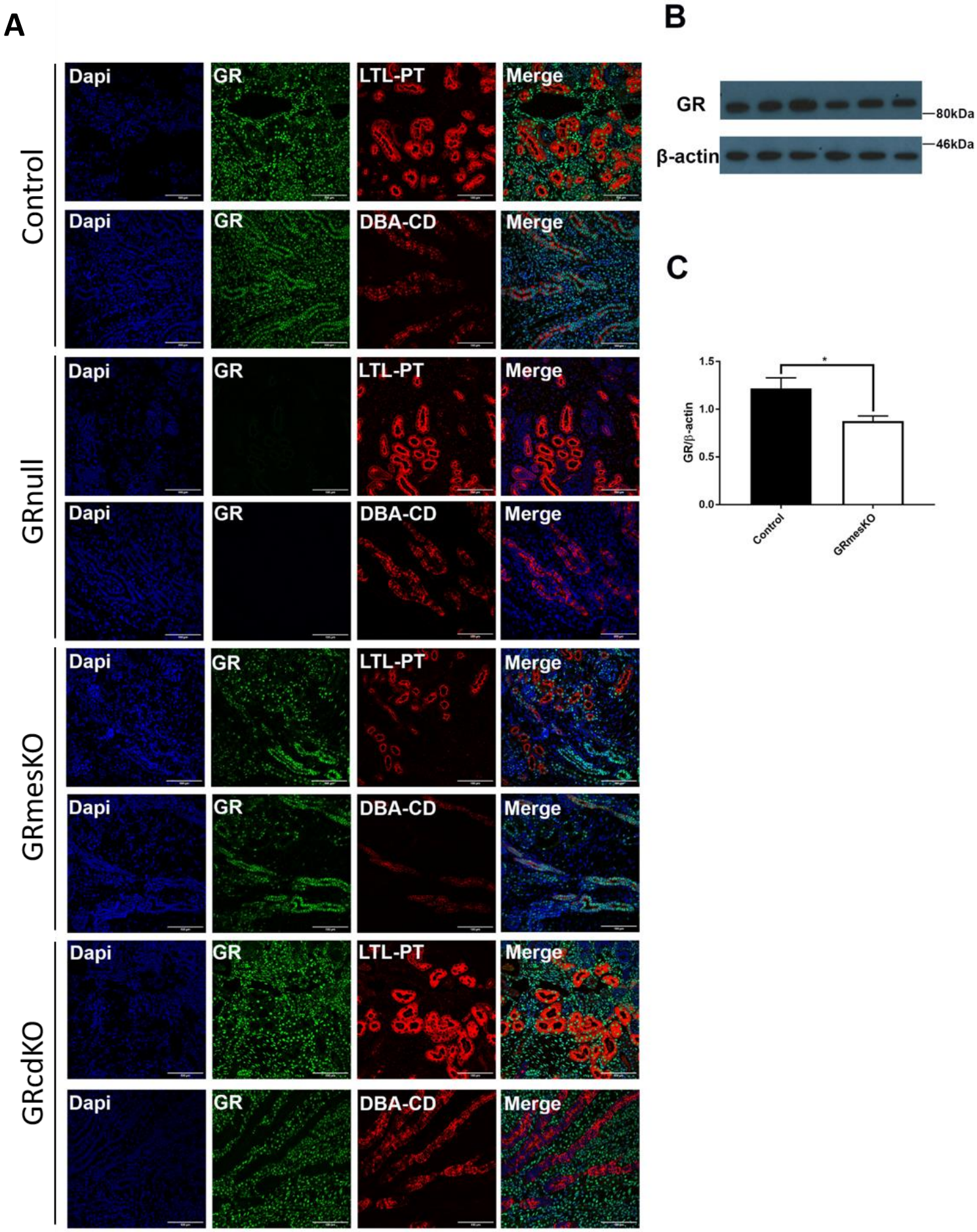
A
Control
GRnull
GRmesKO
GRcdKO
Dapi
GR
LTL-PT
DBA-CD
Merge
B
GR
β-actin
80kDa
46kDa
C
GR/β-actin
1.5
1.0
0.5
0.0
*
Control
GRmesKO

Figure 4.2

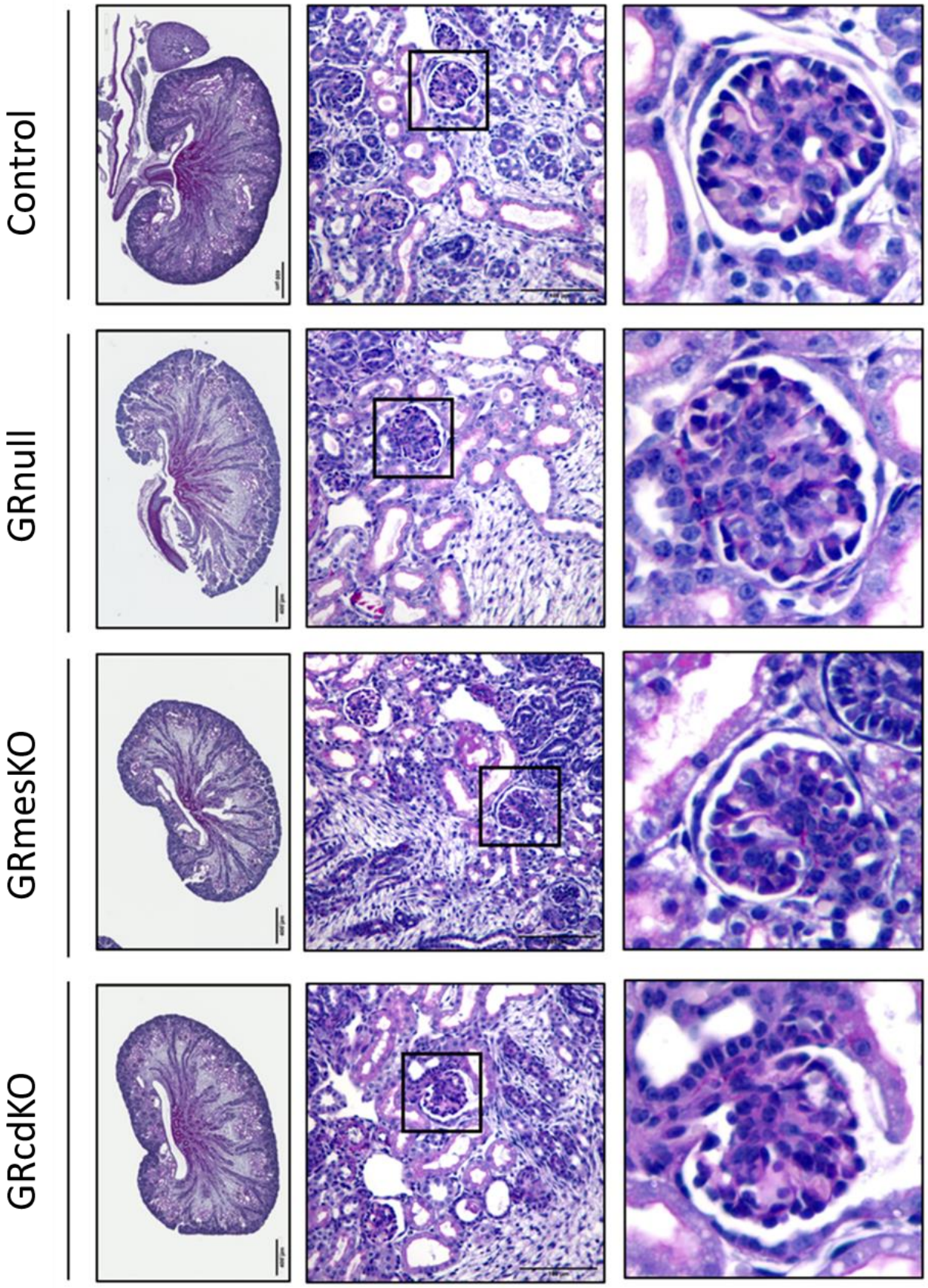

Figure 4.3

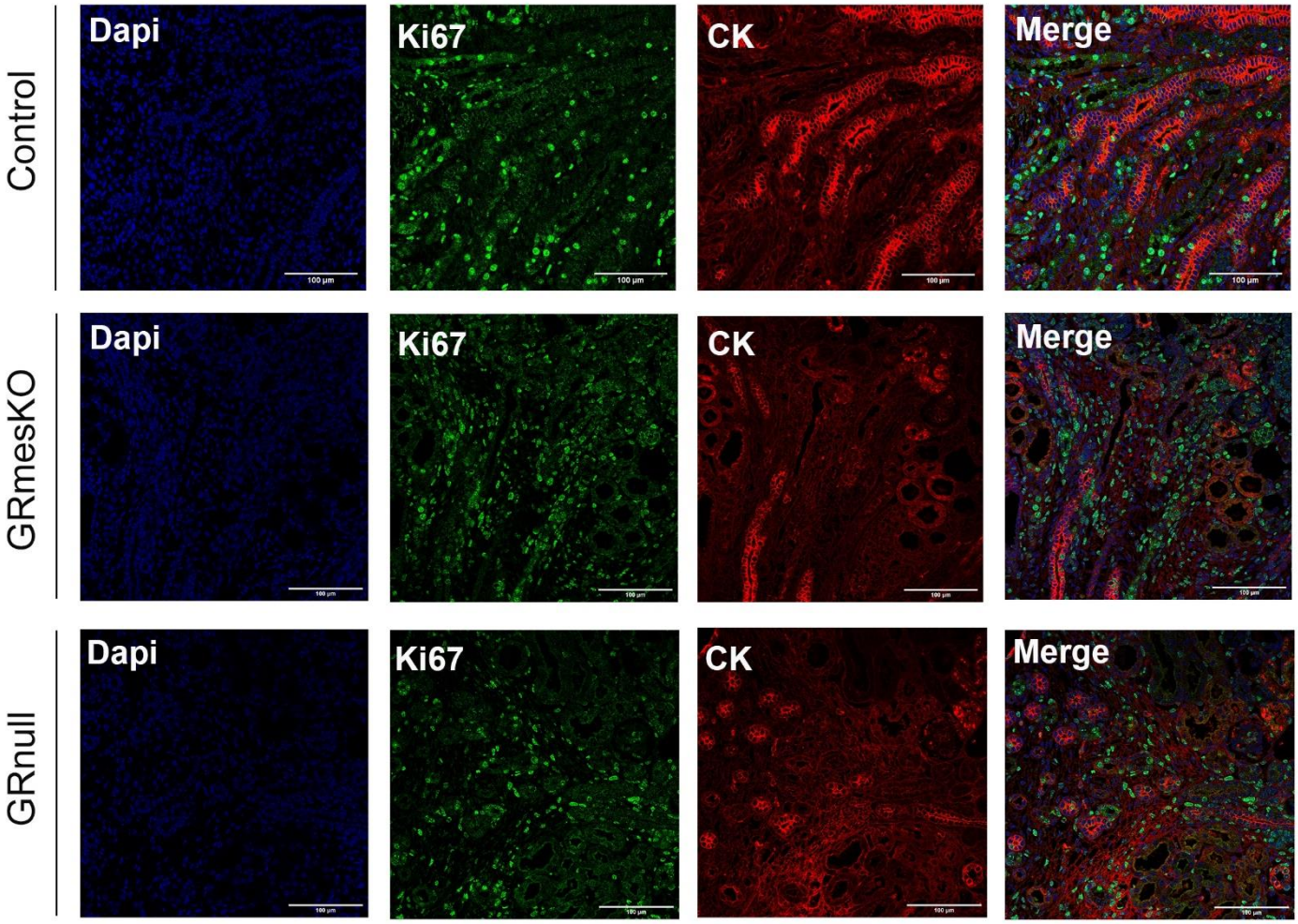

Figure 4.4

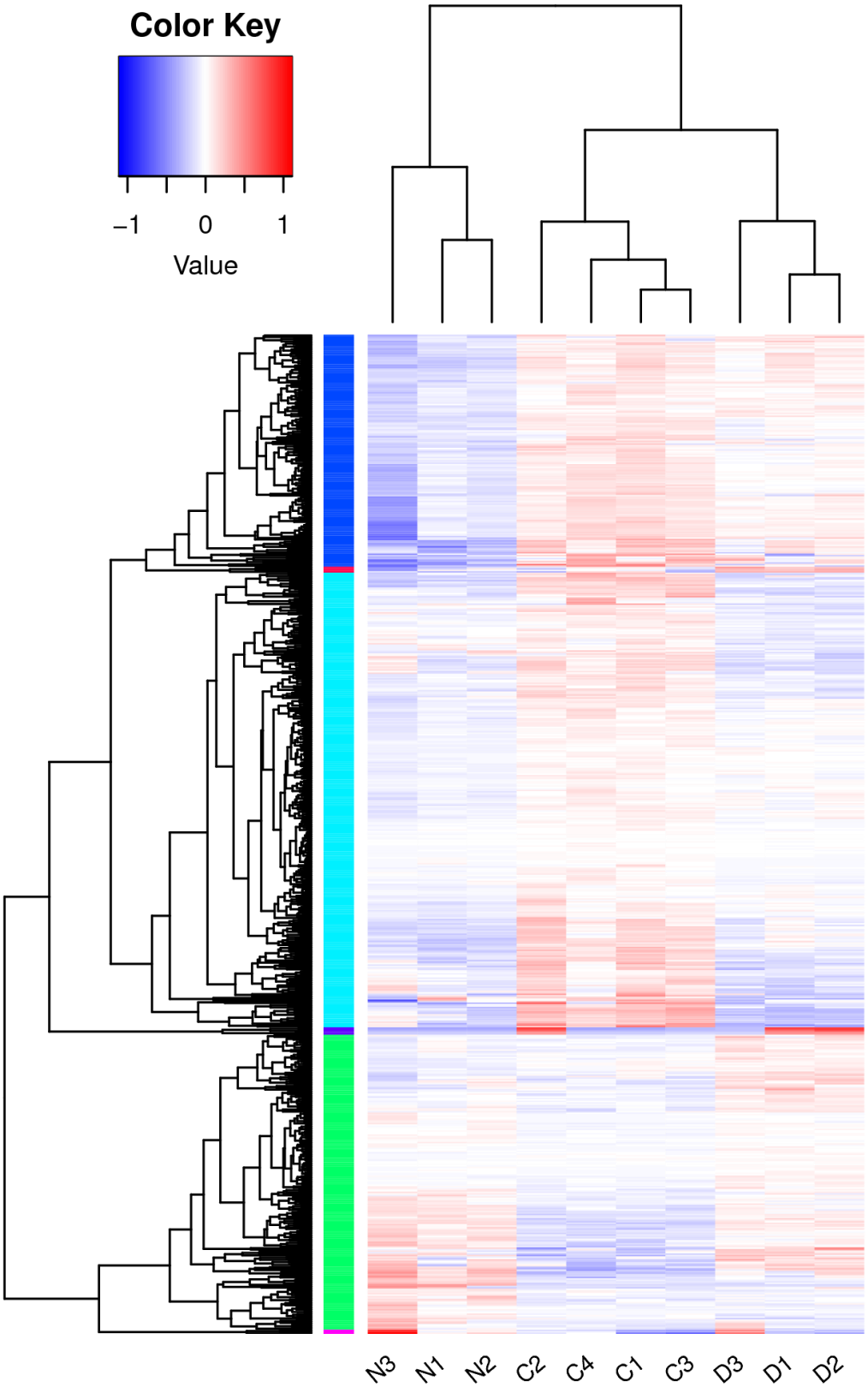

Figure 4.5

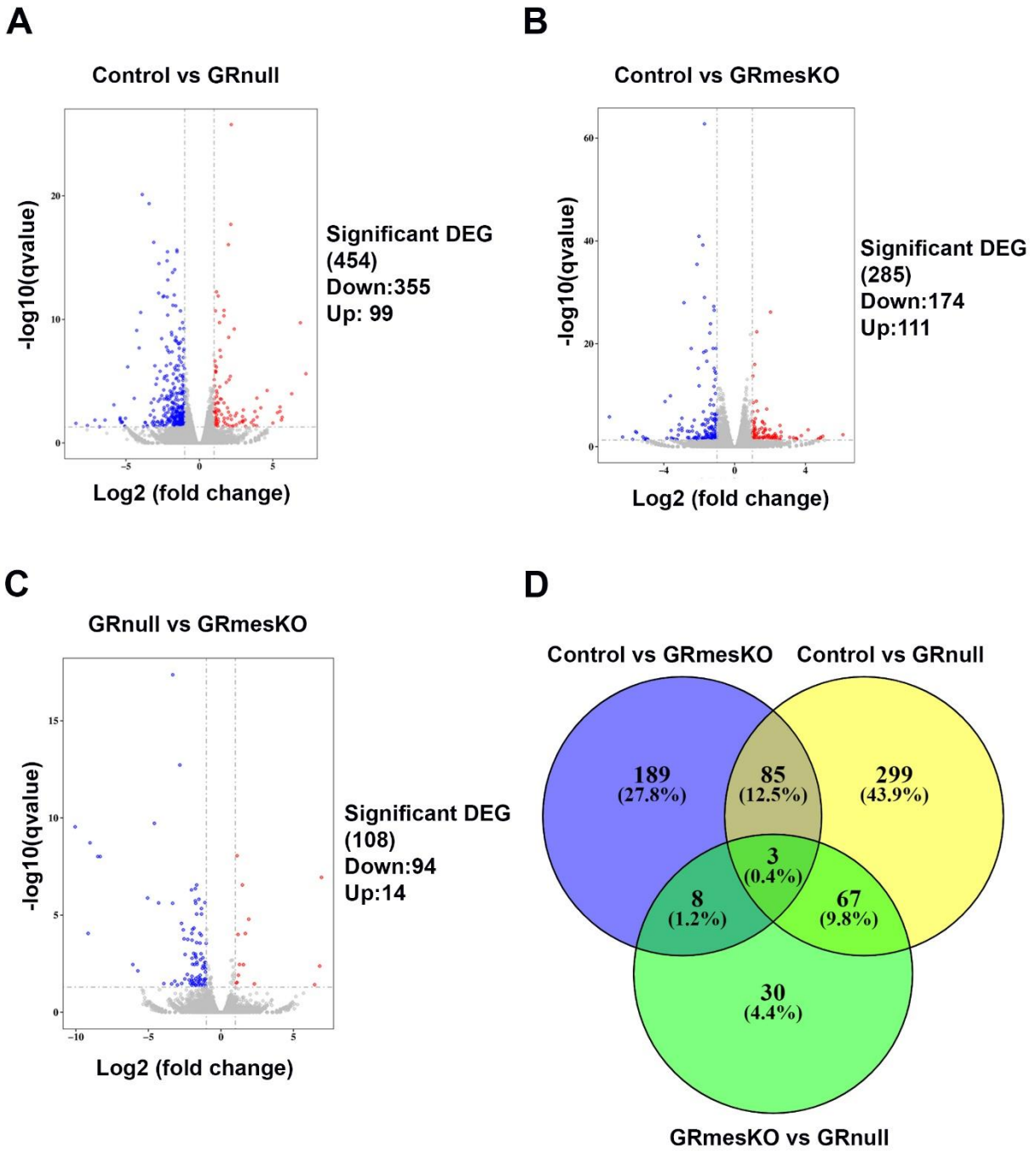
A
Control vs GRnull
-log10(qvalue)
Log2 (fold change)
Significant DEG
(454)
Down:355
Up: 99
B
Control vs GRmesKO
-log10(qvalue)
Log2 (fold change)
Significant DEG
(285)
Down:174
Up:111
C
GRnull vs GRmesKO
-log10(qvalue)
Log2 (fold change)
Significant DEG
(108)
Down:94
Up:14
D
Control vs GRmesKO
Control vs GRnull
GRmesKO vs GRnull
189
(27.8%)
85
(12.5%)
299
(43.9%)
3
(0.4%)
8
(1.2%)
67
(9.8%)
30
(4.4%)

Figure 4.6

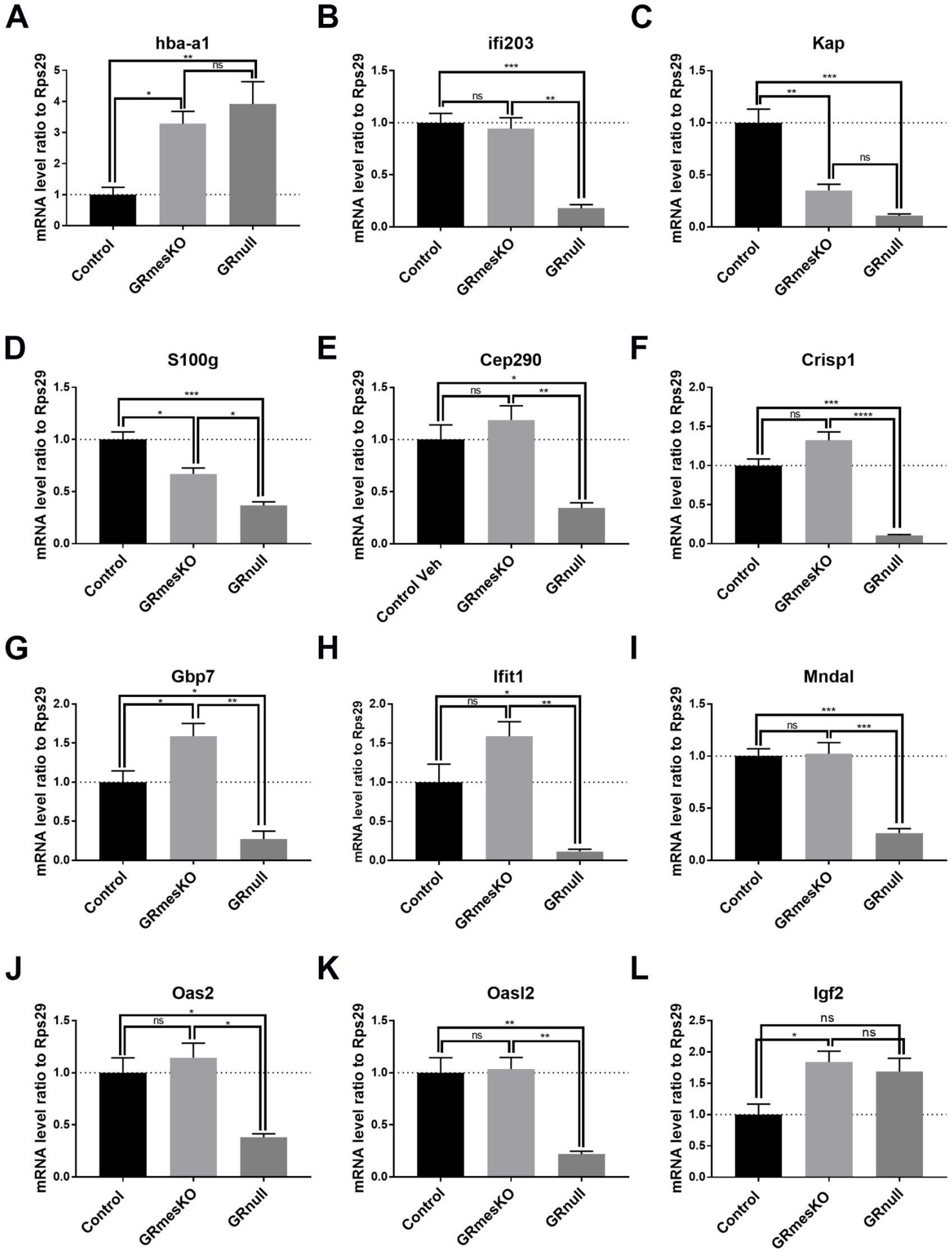
A
hba-a1
mRNA level ratio to Rps29
Control
GRmesKO
GRnull
B
ifi203
C
Kap
D
S100g
E
Cep290
Control Veh
F
Crisp1
G
Gbp7
H
Ifit1
I
Mndal
J
Oas2
K
Oasl2
L
Igf2

Figure 4.7

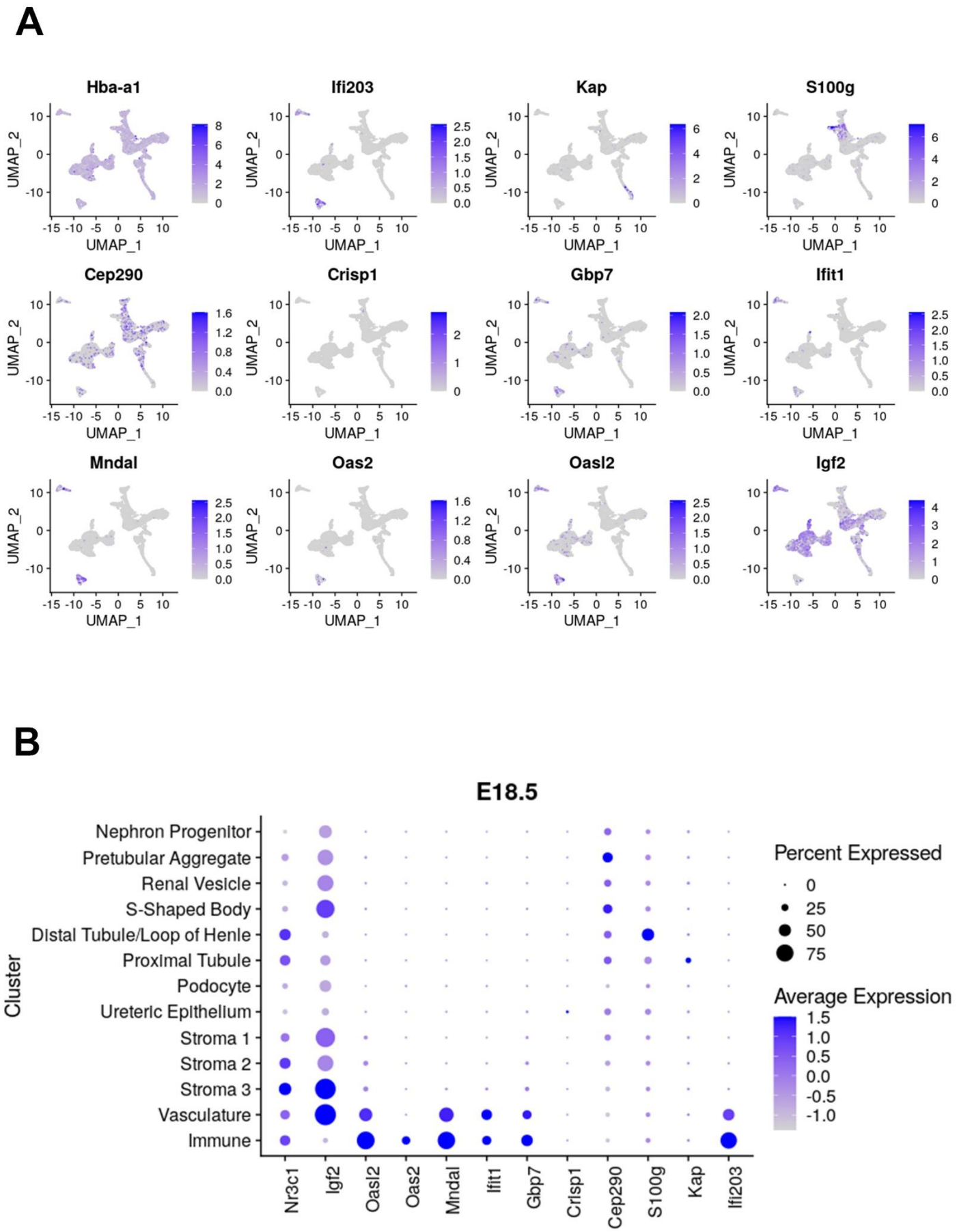
A
Hba-a1
Ifi203
Kap
S100g
Cep290
Crisp1
Gbp7
Ifit1
Mndal
Oas2
Oasl2
Igf2
UMAP_1
UMAP_2
B
E18.5
Cluster
Nephron Progenitor
Pretubular Aggregate
Renal Vesicle
S-Shaped Body
Distal Tubule/Loop of Henle
Proximal Tubule
Podocyte
Ureteric Epithelium
Stroma 1
Stroma 2
Stroma 3
Vasculature
Immune
Nr3c1
Igf2
Oasl2
Oas2
Mndal
Ifit1
Gbp7
Crisp1
Cep290
S100g
Kap
Ifi203
Percent Expressed
0
25
50
75
Average Expression
1.5
1.0
0.5
0.0
-0.5
-1.0

Figure 4.8

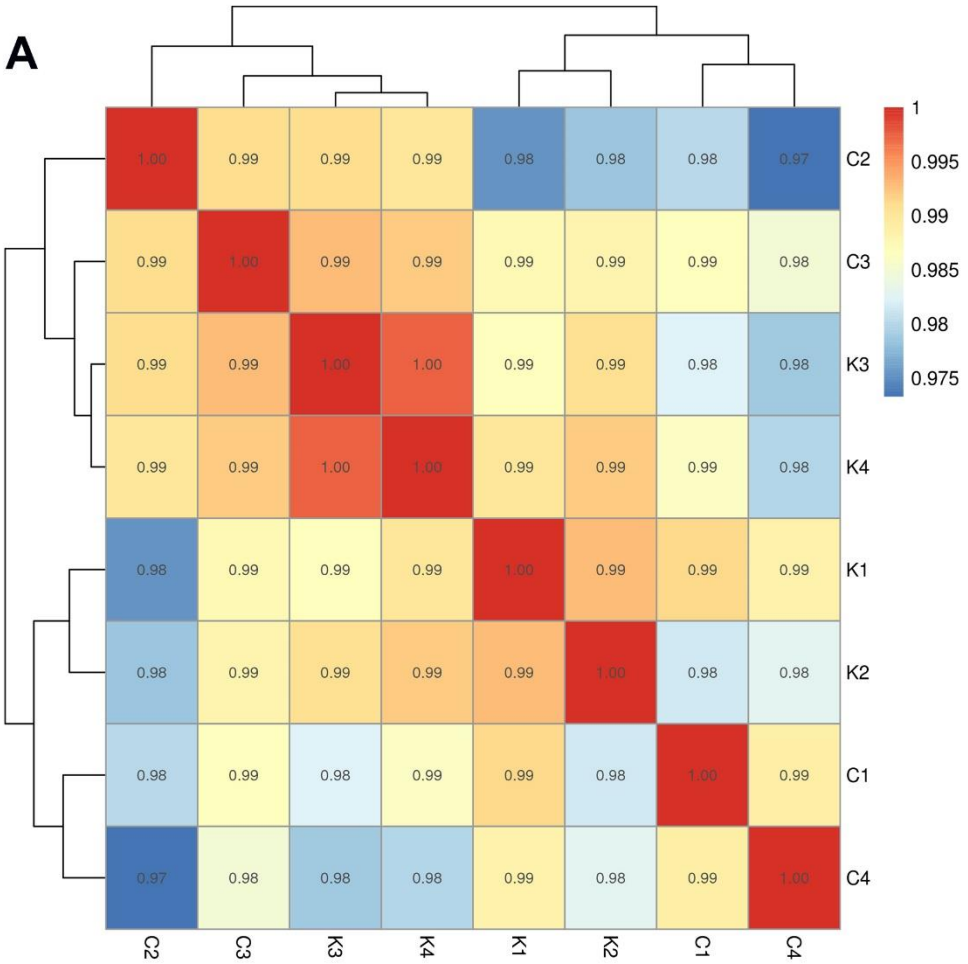

B

Condition	Up	Down
FC>=2FDR<+0.05	0	0
FC>=2Pvalue<=0.05	0	0
FC>=1.5FDR<=0.05	0	0
FC>=1.5Pvalue<+0.05	0	0
FC>=1.2FDR<=0.05	2	1
FC>=1.2Pvalue<=0.05	5	6

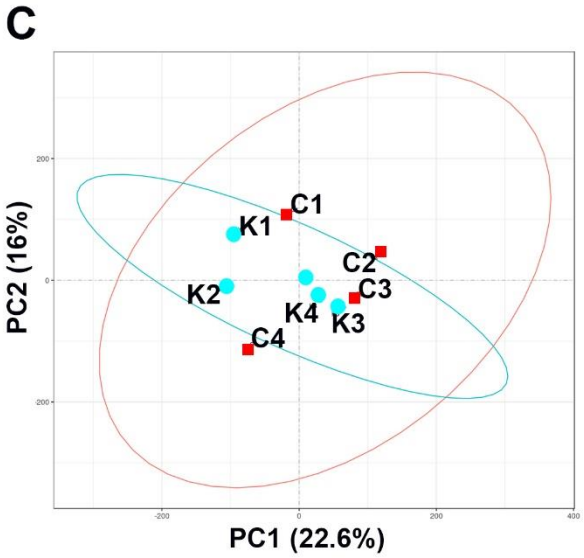

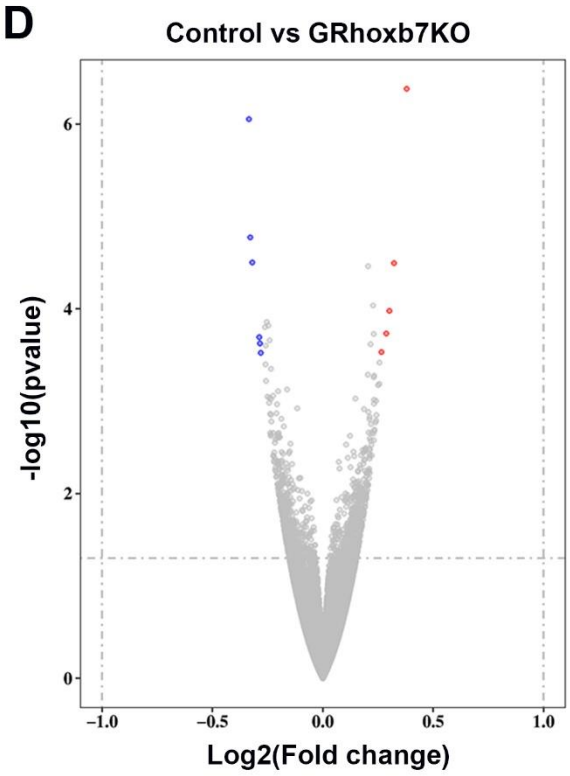

Figure 4.9

Table 4.1: Overlapping protein coding differentially expressed genes in GRnull and GRmeskO mouse kidney at E18.5 with a fold change greater than 2 and an FDR less than 0.05.

Gene ID	Gene name	Fold change Control vs GRnull	FDR Control vs GRnull	Fold change Control vs dermo1	FDR Control vs GRmesKO	Function/Ontology
ENSMUSG00000022868	α-2-HS-glycoprotein (Ahsg)	15.07	2.34E-04	5.79	4.6E-02	System Development
ENSMUSG00000006522	Inter-α trypsin inhibitor, heavy chain 3 (Itih3)	7.65	7.18E-03	5.02	1.6E-02	Extracellular matrix stabilisation
ENSMUSG00000024173	Tryptase α/β 1 (Tpsab1)	4.90	4.09E-02	5.04	6.5E-03	Serine protease
ENSMUSG00000069919	Hemoglobin α, adult chain 1 (Hba-a1)	4.40	2.04E-18	2.35	1.4E-09	Oxygen binding
ENSMUSG00000030607	Aggrecan (Acan)	3.77	1.42E-03	3.10	1.5E-03	Extracellular matrix proteoglycan
ENSMUSG00000025270	Aminolevulinic acid synthase 2, erythroid (Alas2)	3.18	5.12E-11	2.03	1.6E-07	Heme biosynthesis
ENSMUSG00000043903	Zin finger protein 469 (Zfp469)	2.44	5.83E-04	2.09	3.2E-04	Nucleic acid binding
ENSMUSG00000048583	Insulin-like growth factor 2 (Igf2)	2.43	1.28E-12	2.20	1.0E-16	Growth factor activity
ENSMUSG00000035459	Stabilin 2 (Stab2)	2.22	1.66E-02	2.07	1.5E-03	Mediates endocytosis
ENSMUSG00000050700	Elastin microfibril interfacer 3 (Emilin3)	2.04	2.38E-05	2.05	1.8E-14	Extracellular matrix glycoprotein
ENSMUSG00000038717	ATP synthase, H+ transporting, mitochondrial F0 complex, subuint G (Atp5l)	-2.14	4.02E-09	-2.22	3.0E-27	ATP synthesis
ENSMUSG00000079480	Peptidyl-prolyl cis-trans isomerase NIMA-interacting 4 (Pin4)	-2.23	1.63E-02	-2.00	7.3E-03	Ribosomal RNA processing

ENSMUSG00000040808	S100 calcium binding protein G (S100g)	-2.51	5.59E-10	-2.23	1.9E-12	Calcium ion binding
ENSMUSG00000049152	UDP glycosyltransferases 3 family, polypeptide A2 (Ugt3a2)	-2.58	9.12E-09	-2.17	2.8E-06	Elimination of toxic endogenous compounds
ENSMUSG00000032103	Pseudouridine synthase 3 (Pus3)	-2.60	3.78E-02	-2.25	3.4E-02	RNA binding
ENSMUSG00000050069	Gremlin 2, DAN family BMP antagonist (Grem2)	-2.71	1.25E-06	-2.22	8.0E-06	Negative regulation of BMP signalling
ENSMUSG00000026986	Histamine N-methyltransferase (Hnmt)	-2.87	8.06E-04	-2.33	3.2E-04	Degradation of histamine
ENSMUSG00000024552	Solute carrier family 14 (urea transporter), member 2 (Slc14a2)	-2.89	5.37E-06	-2.13	5.8E-03	Urea transport in the collecting duct
ENSMUSG00000034591	Solute carrier family 41, member 2 (Slc41a2)	-3.10	3.24E-04	-2.06	4.0E-03	Plasma-membrane magnesium transporter
ENSMUSG00000047586	Non-specific cytotoxic cell receptor protein 1 homolog (zebrafish) (Nccrp1)	-3.16	5.03E-09	-2.04	1.5E-05	Cell population proliferation
ENSMUSG00000025758	Polo like kinase 4 (Plk4)	-3.20	8.31E-07	-4.04	1.5E-12	System Development
ENSMUSG00000034402	Potassium voltage-gated channel, subfamily H (eag-related), member 5 (Kcnh5)	-3.48	3.37E-02	-2.57	4.2E-02	Potassium ion transport
ENSMUSG00000071562	Stefin A1 (Stfa1)	-3.63	5.06E-04	-2.11	9.0E-03	Intracellular thiol proteinase inhibitor
ENSMUSG00000091649	PHD finger protein11B (Phf11b)	-3.68	1.30E-03	-2.00	4.5E-02	Metal ion binding
ENSMUSG00000054072	Interferon inducible GTPase 1 (Iigp1)	-4.53	3.36E-16	-2.06	6.1E-06	Immune system process
ENSMUSG00000048424	RAN binding protein 3-like (Ranbp3l)	-4.69	1.71E-08	-2.04	5.1E-05	Regulation of mesenchymal stem cell differentiation
ENSMUSG00000028268	Guanylate binding protein 3 (Gbp3)	-6.77	3.04E-15	-2.01	1.3E-02	Guanine nucleotide binding (GMP, GDP and GTP)

ENSMUSG00000079017	Interferon, alpha-inducible protein 27 like 2A (Ifi27l2a)	-6.96	4.19E-04	-5.21	8.8E-04	Transcription regulation
ENSMUSG00000068246	Apolipoprotein L 9b (Apol9b)	-8.17	4.13E-02	-5.86	4.5E-02	Lipid binding
ENSMUSG00000032758	Kidney androgen regulated protein (Kap)	-8.63	5.79E-17	-3.16	6.4E-05	Unkown, expressed in kidney proximal tubule cells
ENSMUSG00000000214	Tyrosine hydroxylase (Th)	-32.67	9.99E-03	-9.45	4.1E-02	Catecholamine biosynthesis
ENSMUSG00000055368	Solute carrier family 6 (neurotransmitter transporter, noradrenalin), member (Slc6a2)	-85.63	1.40E-02	-10.56	3.4E-02	Norepinephrine transporter

Supplementary Table 4.1: DNA Sequence of Primer Pairs used for qPCR Analysis

Gene	Forward	Reverse
Hba-a1	5’-AAGCCCTGGAAAGGATGTTT-3’	5’-CTCAGGAGCTTGAAGTTGAC-3’
Igf2	5’-TCTCATCTCTTTGGCCTTCG-3’	5’-CAAACTGAAGCGTGTCAACA-3’
S100g	5’-GAGCTGGATAAGAATGGCGA-3’	5’-TTCAGGATTGGAGAGCGTG-3’
Kap	5’-TTAAGCACTGACTCTGAGCA-3’	5’-ACTGTGATGTCTGTGTTCTCA-3’
Ifi203	5’-CAGTGGTGGTTTATGGACGA-3’	5’-CTCAGGAGGCACACATCTTT-3’
Oas2	5’-AGTCTACTCCGCCTGATCAA-3’	5’-TGTCAAAGTCATCTGTGCCA-3’
Cep290	5’-AATGAAGATGAAAGCCCAGGA-3’	5’-TGCTTCTCAAGTTGGCGAAT-3’
Oasl2	5’-GATTAAGGTGGTGAAGGGAGG-3’	5’-CCTGCTCTTCGAAACTGGAA-3’
Mndal	5’-TCGTCAAGATCAAGGTCACC-3’	5’-ACGTGATAGTCTGGCATCTC-3’
Gbp7	5’-CAGCTGCACTATGTCACAG-3’	5’-CACGTCCCTCTAACTTCAGC-3’
Crisp1	5’-TGGTCTTCTGCAATCCAAGG-3’	5’-TGAGTTCCAAACAACCTGAGT-3’
Ifit1	5’-GCTGTCCGGTTAAATCCAGA-3’	5’-AAGTAGCCAGAGGAAGGTGA-3’
Rps29	5’-GGACATAGGCTTCATTAAGTTGG-3’	5’-TCAGTCGAATCCATTCAAGGT-3’

Supplementary table 4.2: Protein coding differently expressed genes in GRcdKO at E18.5 with a p value less than 0.05 and a fold change greater than 1.2

Gene ID	Gene name	Log2FC	Pvalue	Function/Ontology
ENSMUSG00000043719	Collagen, type VI, α6 (Col6α6)	0.379906	4.17E-07	Cell adhesion
ENSMUSG00000025758	Polo like kinase 4 (Plk4)	-0.33466	8.87E-07	System Development
ENSMUSG00000025431	Cysteine-rich secretory protein 1 (Crisp1)	-0.32873	1.69E-05	Spermatozoa maturation
ENSMUSG00000049152	UDP glycosyltransferases 3 family polypeptide A2 (Ugt3a2)	-0.31947	3.16E-05	Elimination of toxic endogenous compounds
ENSMUSG00000091021	Gm17300	0.322608	3.21E-05	IncRNA, no protein
ENSMUSG00000030787	Lymphatic vessel endothelial hyaluronan receptor 1 (Lyve1)	0.30145	0.000105	Ligand-specific transport/hyaluronic acid binding
ENSMUSG00000052854	Nik related kinase (Nrk)	0.287422	0.000185	Protein kinase activity
ENSMUSG00000062480	Acetyl-Coenzyme A acetyltransferase (Acat3)	-0.28789	0.000203	Fatty acid beta-oxidation
ENSMUSG00000032690	2’-5’ Oligoadenylate synthetase 2 (Oasl11)	-0.28488	0.000237	dsRNA-activated antiviral enzyme
ENSMUSG0000005413	Heme oxygenase 1 (Hmox1)	0.265582	0.000294	Heme oxygenase (decydizing) activity
ENSMUSG00000033634	N-acetyltransferase 8 (GCN5-related) family member 2 (Nat8f2)	-0.28096	0.0003	N-acetyltransferase activity

4.5 References

Ackermann D, Gresko N, Carrel M, Loffing-Cueni D, Habermehl D, Gomez-Sanchez C, Rossier BC & Loffing J 2010 In vivo nuclear translocation of mineralocorticoid and glucocorticoid receptors in rat kidney: differential effect of corticosteroids along the distal tubule. *Am J Physiol Renal Physiol* **299** F1473-1485.

Baala L, Audollent S, Martinovic J, Ozilou C, Babron MC, Sivanandamoorthy S, Saunier S, Salomon R, Gonzales M, Rattenberry E, et al. 2007 Pleiotropic effects of CEP290 (NPHP6) mutations extend to Meckel syndrome. *Am J Hum Genet* **81** 170-179.

Bach LA & Hale LJ 2015 Insulin-like growth factors and kidney disease. *Am J Kidney Dis* **65** 327-336.

Bailey MA, Mullins JJ & Kenyon CJ 2009 Mineralocorticoid and glucocorticoid receptors stimulate epithelial sodium channel activity in a mouse model of Cushing syndrome. *Hypertension* **54** 890-896.

Barker DJ 2007 The origins of the developmental origins theory. *J Intern Med* **261** 412-417.

Barker DJ, Gluckman PD, Godfrey KM, Harding JE, Owens JA & Robinson JS 1993 Fetal nutrition and cardiovascular disease in adult life. *Lancet* **341** 938-941.

Bird AD, Choo YL, Hooper SB, McDougall AR & Cole TJ 2014 Mesenchymal glucocorticoid receptor regulates the development of multiple cell layers of the mouse lung. *American Journal of Respiratory Cell and Molecular Biology* **50** 419-428.

Bird AD, Tan KH, Olsson PF, Zieba M, Flecknoe SJ, Liddicoat DR, Mollard R, Hooper SB & Cole TJ 2007 Identification of glucocorticoid-regulated genes that control cell proliferation during murine respiratory development. *J Physiol* **585** 187-201.

Butler A, Hoffman P, Smibert P, Papalexi E & Satija R 2018 Integrating single-cell transcriptomic data across different conditions, technologies, and species. *Nat Biotechnol* **36** 411-420.

Canonica J, Frateschi S, Boscardin E, Ebering A, Sergi C, Jager Y, Peyrollaz T, Merillat AM, Maillard M, Klusonova P, et al. 2019 Lack of Renal Tubular Glucocorticoid Receptor Decreases the Thiazide-Sensitive Na(+)/Cl(-) Cotransporter NCC and Transiently Affects Sodium Handling. *Front Physiol* **10** 989.

Cole TJ, Blendy JA, Monaghan AP, Krieglstein K, Schmid W, Aguzzi A, Fantuzzi G, Hummler E, Unsicker K & Schutz G 1995 Targeted disruption of the glucocorticoid receptor gene blocks adrenergic chromaffin cell development and severely retards lung maturation. *Genes Dev* **9** 1608-1621.

Combes AN, Phipson B, Lawlor KT, Dorison A, Patrick R, Zappia L, Harvey RP, Oshlack A & Little MH 2019 Correction: Single cell analysis of the developing mouse kidney provides deeper insight into marker gene expression and ligand-receptor crosstalk (doi:10.1242/dev.178673). *Development* **146**.

Daniel Bird A, McDougall AR, Seow B, Hooper SB & Cole TJ 2015 Minireview: Glucocorticoid regulation of lung development: Lessons learned from conditional GR knockout mice. *Molecular Endocrinology* **29** 158-171.

Davidson A 2009 Mouse kidney development. Cambridge (MA): Harvard Stem Cell Institute

de Quixano BB, Villena JA, Aranda M, Brils G, Cuevas A, Hespel T, Lekuona H, Suarez C, Tornavaca O & Meseguer A 2017 Kidney Androgen-Regulated Protein (KAP) Transgenic Mice Are Protected Against High-Fat Diet Induced Metabolic Syndrome. *Sci Rep* **7** 16102.

Dobin A, Davis CA, Schlesinger F, Drenkow J, Zaleski C, Jha S, Batut P, Chaisson M & Gingeras TR 2013 STAR: ultrafast universal RNA-seq aligner. *Bioinformatics* **29** 15-21.

Fordel E, Thijs L, Martinet W, Lenjou M, Laufs T, Van Bockstaele D, Moens L & Dewilde S 2006 Neuroglobin and cytoglobin overexpression protects human SH-SY5Y neuroblastoma cells against oxidative stress-induced cell death. *Neurosci Lett* **410** 146-151.

Fowden AL & Forhead AJ 2015 Glucocorticoids as regulatory signals during intrauterine development. *Exp Physiol* **100** 1477-1487.

Goodwin JE, Zhang J, Velazquez H & Geller DS 2010 The glucocorticoid receptor in the distal nephron is not necessary for the development or maintenance of dexamethasone-induced hypertension. *Biochem Biophys Res Commun* **394** 266-271.

Habib S, Gattineni J, Twombley K & Baum M 2011 Evidence that prenatal programming of hypertension by dietary protein deprivation is mediated by fetal glucocorticoid exposure. *Am J Hypertens* **24** 96-101.

Helou J, Otto EA, Attanasio M, Allen SJ, Parisi MA, Glass I, Utsch B, Hashmi S, Fazzi E, Omran H, et al. 2007 Mutation analysis of NPHP6/CEP290 in patients with Joubert syndrome and Senior-Loken syndrome. *J Med Genet* **44** 657-663.

Hildebrandt F, Benzing T & Katsanis N 2011 Ciliopathies. *N Engl J Med* **364** 1533-1543.

Ivy JR, Evans LC, Moorhouse R, Richardson RV, Al-Dujaili EAS, Flatman PW, Kenyon CJ, Chapman KE & Bailey MA 2018 Renal and Blood Pressure Response to a High-Salt Diet in Mice With Reduced Global Expression of the Glucocorticoid Receptor. *Front Physiol* **9** 848.

Kutuzova GD, Akhter S, Christakos S, Vanhooke J, Kimmel-Jehan C & Deluca HF 2006 Calbindin D(9k) knockout mice are indistinguishable from wild-type mice in phenotype and serum calcium level. *Proc Natl Acad Sci U S A* **103** 12377-12381.

Lee GS, Lee KY, Choi KC, Ryu YH, Paik SG, Oh GT & Jeung EB 2007 Phenotype of a calbindin-D9k gene knockout is compensated for by the induction of other calcium transporter genes in a mouse model. *J Bone Miner Res* **22** 1968-1978.

Lui JC, Finkielstain GP, Barnes KM & Baron J 2008 An imprinted gene network that controls mammalian somatic growth is down-regulated during postnatal growth deceleration in multiple organs. *Am J Physiol Regul Integr Comp Physiol* **295** R189-196.

Meimaridou E, Goldsworthy M, Chortis V, Fragouli E, Foster PA, Arlt W, Cox R & Metherell LA 2018 NNT is a key regulator of adrenal redox homeostasis and steroidogenesis in male mice. *J Endocrinol* **236** 13-28.

Ortiz LA, Quan A, Weinberg A & Baum M 2001 Effect of prenatal dexamethasone on rat renal development. *Kidney Int* **59** 1663-1669.

Quax RA, Manenschijn L, Koper JW, Hazes JM, Lamberts SWJ, van Rossum EFC & Feelders RA 2013 Glucocorticoid sensitivity in health and disease. *Nat Rev Endocrinol* **9** 670-686.

Rachel RA, Yamamoto EA, Dewanjee MK, May-Simera HL, Sergeev YV, Hackett AN, Pohida K, Munasinghe J, Gotoh N, Wickstead B, et al. 2015 CEP290 alleles in mice disrupt tissue-specific cilia biogenesis and recapitulate features of syndromic ciliopathies. *Hum Mol Genet* **24** 3775-3791.

Rogers SA, Ryan G & Hammerman MR 1991 Insulin-like growth factors I and II are produced in the metanephros and are required for growth and development in vitro. *J Cell Biol* **113** 1447-1453.

Scialdone A, Natarajan KN, Saraiva LR, Proserpio V, Teichmann SA, Stegle O, Marioni JC & Buettner F 2015 Computational assignment of cell-cycle stage from single-cell transcriptome data. *Methods* **85** 54-61.

Seckl JR 2004 Prenatal glucocorticoids and long-term programming. *Eur J Endocrinol* **151 Suppl 3** U49-62.

Sheen JM, Yu HR, Tiao MM, Chen CC, Huang LT, Chang HY & Tain YL 2015 Prenatal dexamethasone-induced programmed hypertension and renal programming. *Life Sci* **132** 41-48.

Short KM & Smyth IM 2016 The contribution of branching morphogenesis to kidney development and disease. *Nat Rev Nephrol* **12** 754-767.

Speirs HJ, Seckl JR & Brown RW 2004 Ontogeny of glucocorticoid receptor and 11beta-hydroxysteroid dehydrogenase type-1 gene expression identifies potential critical periods of glucocorticoid susceptibility during development. *J Endocrinol* **181** 105-116.

Stuart T, Butler A, Hoffman P, Hafemeister C, Papalexi E, Mauck WM, 3rd, Hao Y, Stoeckius M, Smibert P & Satija R 2019 Comprehensive Integration of Single-Cell Data. *Cell* **177** 1888-1902.e1821.

Valente EM, Silhavy JL, Brancati F, Barrano G, Krishnaswami SR, Castori M, Lancaster MA, Boltshauser E, Boccone L, Al-Gazali L, et al. 2006 Mutations in CEP290, which encodes a centrosomal protein, cause pleiotropic forms of Joubert syndrome. *Nat Genet* **38** 623-625.

Venihaki M, Carrigan A, Dikkes P & Majzoub JA 2000 Circadian rise in maternal glucocorticoid prevents pulmonary dysplasia in fetal mice with adrenal insufficiency. *Proc Natl Acad Sci U S A* **97** 7336-7341.

Vinogradov SN & Moens L 2008 Diversity of globin function: enzymatic, transport, storage, and sensing. *J Biol Chem* **283** 8773-8777.

Whirledge S & DeFranco DB 2018 Glucocorticoid Signaling in Health and Disease: Insights From Tissue-Specific GR Knockout Mice. *Endocrinology* **159** 46-64.

Wolf E, Kramer R, Blum WF, Foll J & Brem G 1994 Consequences of postnatally elevated insulin-like growth factor-II in transgenic mice: endocrine changes and effects on body and organ growth. *Endocrinology* **135** 1877-1886.

Wolock SL, Lopez R & Klein AM 2019 Scrublet: Computational Identification of Cell Doublets in Single-Cell Transcriptomic Data. *Cell Syst* **8** 281-291.e289.

Acknowledgements

We would like to thank Professor Ian Smyth and Dr Denny Cottle for providing Hoxb7 cre mice and kidney markers. We would also like to acknowledge the facilities and the scientific and technical assistance of Monash Histology platform, Department of Anatomy and Developmental Biology, Monash University, the Monash Animal Research Platform for their technical expertise and Monash Micro Imaging, Monash University for their facilities and technical assistance.

Chapter 5: General Discussion

Chapter 5: General Discussion

It is now well established that GC hormones such as cortisol play an important and essential role in the functional maturation of many fetal tissues and organs prior to birth, and in particular the fetal respiratory system (Liggins 1994). GCs exert their actions by binding to the intracellular GR. Once activated by GCs the GR complex translocates to the nucleus and acts as a transcription factor that can bind to GREs in the genome to either increase or decrease gene expression of a specific subset of target genes that can vary between different cell types. The critical importance of GC signalling via the GR in lung development was first demonstrated in gene-targeted GRnull mice that die at birth due to respiratory failure (Cole et al. 1995), and for nearly 50 years it has been routine in neonatology wards to use synthetic GCs such as betamethasone to treat preterm birth. Synthetic GCs accelerate lung maturation and improve both the morbidity and survival of these infants who are at risk of RDS (Liggins and Howie 1972). The development of conditional mouse lung knockout models of the GR has established that GR activity in the lung mesenchyme is essential for normal lung development prior to birth (Bird et al. 2014). Mice lacking the GR in the mesenchymal compartment of the lung have a similar fate and phenotype to GRnull mice in that they die shortly after birth due to respiratory failure (Bird et al. 2014). However, despite the well-known importance of GCs in the functional maturation of the lung the underlying molecular mechanisms and gene networks regulated by GC signalling in different lung cells and compartments remain elusive. Even less is known about the actions of GCs and the GR in the developing kidney. This is concerning as the GR is uniformly expressed in nearly all tissues and therefore strong acting synthetic GCs such as betamethasone or dexamethasone will act on all body systems including the kidney. This thesis investigated the molecular actions and gene targets of GC hormone signalling in the developing fetal lung and kidney. In Chapter 2 I explored the role of the ECM proteoglycan VCAN that was identified as strongly overexpressed in GRmesKO mouse lung

at E18.5. I showed that GC signalling drives rapid clearance of VCAN prior to birth in the lung mesenchyme. In Chapter 3 I identified potential lung mesenchymal GC target genes that were associated with cell proliferation and ECM remodelling. Lastly, in Chapter 4 I explored the localisation of the GR and the role of GC signalling in the developing fetal mouse kidney.

In Chapter 2 I have shown that *Vcan* mRNA levels decrease rapidly during late gestational lung development from E14.5 to P0.5. This initial age range was selected to observe the effect of rising GC levels on *Vcan* gene expression. I also demonstrated that the V1 isoform of VCAN was localised to all lung mesenchymal compartments at E16.5 but was restricted to only the smooth muscle layer surrounding the large proximal airways at E18.5. This coincides with the naturally occurring late gestation cortisol surge that induces rapid remodelling of the lung ECM, including the thinning of the lung mesenchyme to allow sufficient gas exchange at birth. Furthermore, we showed that loss of the GR in the lung mesenchyme leads to the overexpression of the VCAN-V1 isoform in the distal lung at E18.5 contributing to the hypercellular lung phenotype observed in GRmesKO mice.

The hypercellular lung phenotype observed in GRmesKO mice is the result of an increased cell proliferation rate rather than a decrease in cell apoptosis (Bird et al. 2014; Bird et al. 2007). VCAN is able to interact with many binding partners to rapidly promote cell proliferation. One interaction that may be essential in lung development is with Midkine (MK). MK is a growth factor excreted from epithelial cells that has known roles in cell survival, differentiation and migration. In chapter 2 I postulated that GC/GR signalling repress *Vcan* gene expression in late lung development preventing formation of MK/VCAN complexes promoting cell proliferation. It has been shown that MK can restore the development of the mesenchyme in a model of reduced heparin binding growth factors including MK. In this study mouse embryonic lung explants were treated with heparitinase to reduce the endogenous levels of heparin-binding growth factors. Without heparin-binding growth factors the lung explants had decreased

branching and thinner mesenchymal tissue. Interestingly, the reduction in mesenchymal tissue could be restored in heparitinase treated explants by MK indicating that MK can promote the deposition of mesenchymal tissue (Toriyama, et al. 1997). The explants cultured in this study were isolated at E12 when the mesenchyme is thicker and producing many factors essential for branching morphogenesis. Later in lung development after the pseudoglandular stage the mesenchymal tissue dramatically thins over a short period to reduce the diffusion distance for gaseous exchange at birth. This correlates with the well documented preparturition cortisol surge. This fits with the hypothesis that GC signalling reduces MK cell proliferation through the clearance of VCAN. Furthermore, it has been demonstrated that postnatal dexamethasone treatment decreases MK expression in newborn rats (Zhang, et al. 2009).

VCAN is a known strong promoter of cell proliferation and therefore VCAN expression and degradation is tightly regulated (Wight 2002). VCAN is degraded by a family of proteases known as ADAMTS and in Chapter 2 I demonstrated that loss of mesenchymal GC signalling dramatically reduces the mRNA expression of *Adamts12* (Kelwick et al. 2015). Lastly, I showed that corticosterone and betamethasone can induce the mRNA expression of *Adamts12* in primary rat lung fibroblasts and that dexamethasone can also increase ADAMTS12 protein expression in distal mouse lung mesenchyme. We predict that GC signalling late in lung development represses VCAN by inducing the expression of ADAMTS12, leading to an overall reduction in mesenchymal cell proliferation. Further functional studies are required to determine if GCs induce ADAMTS12 through direct genomic signalling or via an indirect mechanism. This could be achieved by using siRNA or CRISPR-Cas9 technologies to delete *Adamts12* in primary fetal lung fibroblasts followed by treatment with GCs. At both E16.5 and E18.5 VCAN protein persisted in the bronchial smooth muscle, which suggests that VCAN has an important function in this mesenchymal cell subset. It would be interesting to conditionally

delete VCAN specifically in smooth muscle cells of the lung to investigate a loss of function phenotype in these mice.

In Chapter 3 I isolated enriched fetal lung mesenchymal cells from the GRmesKO mouse lung and performed NGS RNA seq to identify potential GC-signalling gene targets. 290 genes were differently expressed at the mRNA level with more genes being significantly decreased in level due to the loss of GR than were increased. Gene ontology analysis revealed enrichment of differentially expressed gene targets that were associated with the ECM, including a small subset of genes that were associated with Wnt signalling. Wnt signalling is a well-known and studied pathway that is involved in body axis patterning, cell differentiation, cell migration and cell proliferation and growth (Eisenmann 2005). I showed that three Wnt signalling associated genes Rspo2, Wnt11 and Cemip were increased in expression in the absence of the GR. Future studies are required to determine how GC-GR signalling may regulate these genes, such as the presence of nearby GREs in the genome or other indirect mechanisms that utilise GC regulation.

Similarly, to Chapter 2 we also observed the reduction in expression of two ADAMTS family members, ADAMTS-Like 2 and ADAMTS-like 4 in the GR-deficient mesenchymal fetal lung cells. However, only ADAMTS-like 2 mRNA levels were also significantly reduced in the GRmesKO mouse lung at E18.5. ADAMTS-like 2 is produced and secreted from bronchial smooth muscle cells, a subset of mesenchymal cells (Hubmacher et al. 2015). Adamts-like 2 null mice develop bronchial dysplasia and die shortly after birth due to respiratory failure (Hubmacher et al. 2015). This phenotype highlights the communication between the epithelial and mesenchyme in the developing lung. Future studies could involve conditional deletion of the GR from the smooth muscle layer of the lung in mice to establish the importance of GC stimulated proteins released from this subtype of mesenchymal cells in the fetal lung. Furthermore, single cell sequencing technologies could also be used to establish the GR-

mediated response of sub-populations of lung mesenchymal cells to GC stimulation. In the past this has been difficult due to the lack of specific mesenchymal sub-population cell markers.

In Chapter 4 I utilised single cell sequencing data sets produced by Combes et al. from E13.5 (unpublished), E15.5 (unpublished) and E18.5 (Combes et al 2019) fetal mouse kidneys to determine the timing, expression and localisation of GR within the developing fetal kidney. We showed that GR was expressed in all major cell clusters present at E13.5 including nephron progenitor, pretubular aggregate, ureteric epithelium, mesenchyme and immune cells. At E15.5 GR is more widely expressed across the kidney cell clusters with higher expression in the proximal tubule and mesenchymal stromal cells. At E18.5 GR is still widely expressed with higher expression in stroma, distal tubule and proximal tubule cells. Tubular epithelial cells of the kidney are protected from stimulation of GCs by the enzyme 11β-HSD2 which inactivates cortisol (or corticosterone in rodents) to inactive cortisone (Chapman et al. 2013). However, synthetic GCs including betamethasone and dexamethasone which are commonly used in situations of preterm birth to accelerate lung development are not readily metabolised by 11β-HSD2 allowing active GCs to enter the kidney, where the GR is expressed in most cell types during fetal development (Brown, et al. 1996; Weinstock 2008). The effects of synthetic GCs on the kidney are relatively unknown. A small number of animal studies have shown synthetic GCs can alter the renal transcriptome, impair renal cell proliferation and depending on the timing of exposure reduce nephron numbers (Ortiz et al. 2001; Sheen et al. 2015; Slotkin et al. 1991). More long-term studies are required to establish the true impact of synthetic GC exposure on renal function.

To explore the role of endogenous GC signalling in the developing fetal kidney we performed NGS RNA seq on GRnull, GRmeskO and GRcdKO kidneys at E18.5. Total loss of the GR had the most profound effect on the renal transcriptome with 454 genes detected with significantly altered mRNA levels including *Cep290*. *Cep290* mRNA was significantly decreased in GRnull

fetal mouse kidney at E18.5. Mutations in *Cep290* are associated with polycystic kidney disease and ciliopathies including Joubert, Meckel and Senior-Loken syndromes (Baala et al. 2007; Helou et al. 2007; Hildebrandt et al. 2011; Valente et al. 2006). Interestingly, most ciliopathies have associated lung phenotypes including bronchiectasis (Driscoll, et al. 2008). Furthermore, primary cilia have known roles in communication between mesenchymal cells and the ECM of the developing lung and can influence cell proliferation, differentiation and migration (Christensen, et al. 2007). Future studies could explore the expression and the morphology and function of primary cilia in GRnull kidney and lung to establish if both organs have a similar primary cilia phenotype.

Consistent with NGS RNA seq results performed on lung mesenchymal cells deficient in GR we observed that most affected genes were decreased in mRNA levels, than were increased, including two renal tubule markers *Kap* (proximal tubule) and *S100g* (distal tubule). This finding is interesting because at E18.5 GR was more highly expressed in proximal and distal tubule cells compared to other renal cell types. Together these findings indicate that the GR may have a functional role in epithelial tubule maturation in the developing kidney. However, due to the early lethality of both GRnull and GRmesKO mice it is difficult to establish the impact of GR loss on trans-epithelial transport. Additionally, the kidney is not functional as a filtration unit until approximately one week after birth and it is possible the epithelial cells in the kidney may not be primed to respond to GCs before birth. A similar response is seen with the cardiovascular steroid aldosterone in the mouse kidney. MR-null mice develop normally until birth but die 1-2 weeks postnatally due to renal salt wasting and hyperkalaemia (Berger, et al. 1998; Cole and Young 2017). In comparison the lung is primed to respond to GCs before birth from approximately E16.5. This is evident by the lung phenotype observed in GRnull and GRmesKO mice. The lungs of GRnull and GRmesKO mice develop normally until approximately E15.5 but from E16.5 develop a progressive hypercellular phenotype (Bird et

al. 2014; Cole et al. 1995). The difference in response to GCs between the lung and kidney could be explained by the presence of either an activator in the lung or a GR chaperone or repressor in the kidney that keeps GRs from dimerising or forming active complexes in the nucleus. To determine the presence of an activator, chaperone or repressor factor future studies could include single cell sequencing on both kidney and lung at E18.5 and perhaps postnatally to compare cell-type specific gene expression profiles. Despite the GR being strongly expressed in the collecting duct we observed no obvious kidney phenotype in GRcdKO mice. The next step would be to investigate the adult phenotype of these mice and potentially see how they react to a challenge such as, a high sodium diet. Furthermore, the stronger effect on the transcriptome caused by total GR deletion in comparison to mesenchymal or collecting duct deletion in the fetal kidney indicates that GC signalling may be important in another specialised cell type. More studies are required to dissect the role of GC signalling in other cell types including the proximal and distal tubules.

In summary this thesis has explored the gene targets and networks associated with GC hormone signalling in specific cells of the developing mouse lung and kidney. My studies show that GCs regulated the expression of lung mesenchymal genes associated with ECM remodelling and Wnt signalling including *Vcan*, *Adamts12*, *Rspo2*, *Wnt11* and *Cemip*. Additionally, I have shown for the first time that the GR is localised to many cell types present within the developing kidney from E13.5. I have also demonstrated that at E18.5 GR is more highly expressed in the renal proximal tubule, distal tubule and stromal mesenchymal cells compared to other cell types within the kidney. Lastly, this thesis explores the role of GC signalling in the developing kidney by performing NGS RNA seq on the fetal kidney deficient in GR. Complete deletion of the GR has the most profound effect on the renal transcriptome with 454 genes differently expressed compared to 285 differentially expressed renal genes in GRmesKO mouse kidney. In both the lung and kidney GR deficiency leads to more differently expressed genes being downregulated

than upregulated indicating that GC signalling favours transactivation of gene targets over transrepression in both organs. Understanding the complex and tissue specific actions of GC signalling in cells during fetal development and programming is essential for the development of new approaches to treat the complications of preterm birth and avoid the consequences caused by the use of synthetic GCs to treat preterm birth.

References

Acconcia F & Marino M 2016 Steroid Hormones: Synthesis, Secretion, and Transport. In *Principles of Endocrinology and Hormone Action*, pp 1-31. Eds A Belfiore & D LeRoith. Cham: Springer International Publishing.

Ackermann D, Gresko N, Carrel M, Loffing-Cueni D, Habermehl D, Gomez-Sanchez C, Rossier BC & Loffing J 2010 In vivo nuclear translocation of mineralocorticoid and glucocorticoid receptors in rat kidney: differential effect of corticosteroids along the distal tubule. *Am J Physiol Renal Physiol* **299** F1473-1485.

Adhya D, Annuario E, Lancaster MA, Price J, Baron-Cohen S & Srivastava DP 2018 Understanding the role of steroids in typical and atypical brain development: Advantages of using a "brain in a dish" approach. *J Neuroendocrinol* **30**.

Agnew EJ, Ivy JR, Stock SJ & Chapman KE 2018 Glucocorticoids, antenatal corticosteroid therapy and fetal heart maturation. *Journal of molecular endocrinology* **61** R61-R73.

Allen J, Zwerdling R, Ehrenkranz R, Gaultier C, Geggel R, Greenough A, Kleinman R, Klijanowicz A, Martinez F, Ozdemir A, et al. 2003 Statement on the care of the child with chronic lung disease of infancy and childhood. *Am J Respir Crit Care Med* **168** 356-396.

Almlof T, Wallberg AE, Gustafsson JA & Wright AP 1998 Role of important hydrophobic amino acids in the interaction between the glucocorticoid receptor tau 1-core activation domain and target factors. *Biochemistry* **37** 9586-9594.

Amy RW, Bowes D, Burri PH, Haines J & Thurlbeck WM 1977 Postnatal growth of the mouse lung. *Journal of anatomy* **124** 131-151.

Apte SS 2009 A disintegrin-like and metalloprotease (reprolysin-type) with thrombospondin type 1 motif (ADAMTS) superfamily: functions and mechanisms. *J Biol Chem* **284** 31493-31497.

Arnold JD, Bonacruz G, Leslie GI, Veldhuis JD, Milmlow D & Silink M 1998 Antenatal glucocorticoids modulate the amplitude of pulsatile cortisol secretion in premature neonates. *Pediatr Res* **44** 876-881.

Baala L, Audollent S, Martinovic J, Ozilou C, Babron MC, Sivanandamoorthy S, Saunier S, Salomon R, Gonzales M, Rattenberry E, et al. 2007 Pleiotropic effects of CEP290 (NPHP6) mutations extend to Meckel syndrome. *Am J Hum Genet* **81** 170-179.

Bach LA & Hale LJ 2015 Insulin-like growth factors and kidney disease. *Am J Kidney Dis* **65** 327-336.

Bailey MA, Mullins JJ & Kenyon CJ 2009 Mineralocorticoid and glucocorticoid receptors stimulate epithelial sodium channel activity in a mouse model of Cushing syndrome. *Hypertension* **54** 890-896.

Ballard PL, Granberg P & Ballard RA 1975 Glucocorticoid levels in maternal and cord serum after prenatal betamethasone therapy to prevent respiratory distress syndrome. *J Clin Invest* **56** 1548-1554.

Ballard PL & Liggins GC 1982 Glucocorticoid activity in cord serum: comparison of hydrocortisone and betamethasone regimens. *J Pediatr* **101** 468-470.

Ballard PL, Ning Y, Polk D, Ikegami M & Jobe AH 1997 Glucocorticoid regulation of surfactant components in immature lambs. *Am J Physiol* **273** L1048-1057.

Bamberger CM, Bamberger AM, de Castro M & Chrousos GP 1995 Glucocorticoid receptor beta, a potential endogenous inhibitor of glucocorticoid action in humans. *J Clin Invest* **95** 2435-2441.

Barar J, Campbell L, Hollins AJ, Thomas NP, Smith MW, Morris CJ & Gumbleton M 2007 Cell selective glucocorticoid induction of caveolin-1 and caveolae in differentiating pulmonary alveolar epithelial cell cultures. *Biochem Biophys Res Commun* **359** 360-366.

Barker DJ 2007 The origins of the developmental origins theory. *J Intern Med* **261** 412-417.

Barker DJ, Gluckman PD, Godfrey KM, Harding JE, Owens JA & Robinson JS 1993 Fetal nutrition and cardiovascular disease in adult life. *Lancet* **341** 938-941.

Barker PM, Nguyen MS, Gatzy JT, Grubb B, Norman H, Hummler E, Rossier B, Boucher RC & Koller B 1998 Role of gammaENaC subunit in lung liquid clearance and electrolyte balance in newborn mice. Insights into perinatal adaptation and pseudohypoaldosteronism. *J Clin Invest* **102** 1634-1640.

Barker PM & Olver RE 2002 Invited review: Clearance of lung liquid during the perinatal period. *J Appl Physiol* **93** 1542-1548.

Barnes PJ 2011 Glucocorticosteroids: current and future directions. *British Journal of Pharmacology* **163** 29-43.

Bateman ED, Turner-Warwick M & Adelmann-Grill BC 1981 Immunohistochemical study of collagen types in human foetal lung and fibrotic lung disease. *Thorax* **36** 645-653.

Beauchemin KJ, Wells JM, Kho AT, Philip VM, Kamir D, Kohane IS, Graber JH & Bult CJ 2016 Temporal dynamics of the developing lung transcriptome in three common inbred strains of laboratory mice reveals multiple stages of postnatal alveolar development. *PeerJ* **4** e2318.

Bell SM, Schreiner CM, Wert SE, Mucenski ML, Scott WJ & Whitsett JA 2008 R-spondin 2 is required for normal laryngeal-tracheal, lung and limb morphogenesis. *Development* **135** 1049-1058.

Ben Y, Chen J, Zhu R, Gao L & Bai C 2008 Upregulation of AQP3 and AQP5 induced by dexamethasone and ambroxol in A549 cells. *Respir Physiol Neurobiol* **161** 111-118.

Beneke S & Rooney SA 2001 Glucocorticoids regulate expression of the fatty acid synthase gene in fetal rat type II cells. *Biochim Biophys Acta* **1534** 56-63.

Berger S, Bleich M, Schmid W, Cole TJ, Peters J, Watanabe H, Kriz W, Warth R, Greger R & Schutz G 1998 Mineralocorticoid receptor knockout mice: pathophysiology of Na+ metabolism. *Proc Natl Acad Sci U S A* **95** 9424-9429.

Bird AD, Choo YL, Hooper SB, McDougall AR & Cole TJ 2014 Mesenchymal glucocorticoid receptor regulates the development of multiple cell layers of the mouse lung. *American Journal of Respiratory Cell and Molecular Biology* **50** 419-428.

Bird AD, Tan KH, Olsson PF, Zieba M, Flecknoe SJ, Liddicoat DR, Mollard R, Hooper SB & Cole TJ 2007 Identification of glucocorticoid-regulated genes that control cell proliferation during murine respiratory development. *J Physiol* **585** 187-201.

Bledsoe RK, Montana VG, Stanley TB, Delves CJ, Apolito CJ, McKee DD, Consler TG, Parks DJ, Stewart EL, Willson TM, et al. 2002 Crystal structure of the glucocorticoid receptor ligand binding domain reveals a novel mode of receptor dimerization and coactivator recognition. *Cell* **110** 93-105.

Blencowe H, Cousens S, Chou D, Oestergaard M, Say L, Moller A-B, Kinney M, Lawn J & Born Too Soon Preterm Birth Action G 2013 Born too soon: the global epidemiology of 15 million preterm births. *Reproductive health* **10 Suppl 1** S2-S2.

Blencowe H, Cousens S, Oestergaard MZ, Chou D, Moller AB, Narwal R, Adler A, Vera Garcia C, Rohde S, Say L, et al. 2012 National, regional, and worldwide estimates of preterm birth rates in the year 2010 with time trends since 1990 for selected countries: a systematic analysis and implications. *Lancet* **379** 2162-2172.

Boerboom D, Lafond JF, Zheng X, Lapointe E, Mittaz L, Boyer A, Pritchard MA, DeMayo FJ, Mort JS, Drolet R, et al. 2011 Partially redundant functions of Adamts1 and Adamts4 in the perinatal development of the renal medulla. *Dev Dyn* **240** 1806-1814.

Bolt RJ, van Weissenbruch MM, Lafeber HN & Delemarre-van de Waal HA 2001 Glucocorticoids and lung development in the fetus and preterm infant. *Pediatric Pulmonology* **32** 76-91.

Botas C, Poulain F, Akiyama J, Brown C, Allen L, Goerke J, Clements J, Carlson E, Gillespie AM, Epstein C, et al. 1998 Altered surfactant homeostasis and alveolar type II cell morphology in mice lacking surfactant protein D. *Proc Natl Acad Sci U S A* **95** 11869-11874.

Bouchard M 2004 Transcriptional control of kidney development. *Differentiation* **72** 295-306.

Bouchard M, Pfeffer P & Busslinger M 2000 Functional equivalence of the transcription factors Pax2 and Pax5 in mouse development. *Development* **127** 3703-3713.

Bouchard M, Souabni A, Mandler M, Neubuser A & Busslinger M 2002 Nephric lineage specification by Pax2 and Pax8. *Genes Dev* **16** 2958-2970.

Boyden EA 1927 Experimental Obstruction of the Mesonephric Ducts. *Proceedings of the Society for Experimental Biology and Medicine* **24** 572-576.

Braun T, Husar A, Challis JR, Dudenhausen JW, Henrich W, Plagemann A & Sloboda DM 2013 Growth restricting effects of a single course of antenatal betamethasone treatment and the role of human placental lactogen. *Placenta* **34** 407-415.

Braun T, Meng W, Shang H, Li S, Sloboda DM, Ehrlich L, Lange K, Xu H, Henrich W, Dudenhausen JW, et al. 2015 Early dexamethasone treatment induces placental apoptosis in sheep. *Reprod Sci* **22** 47-59.

Bremner HR, Freywald T, O'Brodovich HM & Otulakowski G 2002 Promoter analysis of the gene encoding the beta-subunit of the rat amiloride-sensitive epithelial sodium channel. *Am J Physiol Lung Cell Mol Physiol* **282** L124-134.

Brown MS, Kovanen PT & Goldstein JL 1979 Receptor-mediated uptake of lipoprotein-cholesterol and its utilization for steroid synthesis in the adrenal cortex. *Recent Prog Horm Res* **35** 215-257.

Brown RW, Diaz R, Robson AC, Kotelevtsev YV, Mullins JJ, Kaufman MH & Seckl JR 1996 The ontogeny of 11 beta-hydroxysteroid dehydrogenase type 2 and mineralocorticoid receptor gene expression reveal intricate control of glucocorticoid action in development. *Endocrinology* **137** 794-797.

Brownfoot FC, Gagliardi DI, Bain E, Middleton P & Crowther CA 2013 Different corticosteroids and regimens for accelerating fetal lung maturation for women at risk of preterm birth. *The Cochrane database of systematic reviews* Cd006764.

Brunskill EW, Aronow BJ, Georgas K, Rumballe B, Valerius MT, Aronow J, Kaimal V, Jegga AG, Yu J, Grimmond S, et al. 2008 Atlas of gene expression in the developing kidney at microanatomic resolution. *Dev Cell* **15** 781-791.

Buckingham JC 2006 Glucocorticoids: Exemplars of multi-tasking. *British Journal of Pharmacology* **147** S258-S268.

Bunton TE & Plopper CG 1984 Triamcinolone-induced structural alterations in the development of the lung of the fetal rhesus macaque. *Am J Obstet Gynecol* **148** 203-215.

Burri PH 1974 The postnatal growth of the rat lung. 3. Morphology. *Anat Rec* **180** 77-98.

Burri PH 1984 Fetal and postnatal development of the lung. *Annu Rev Physiol* **46** 617-628.

Butler A, Hoffman P, Smibert P, Papalexi E & Satija R 2018 Integrating single-cell transcriptomic data across different conditions, technologies, and species. *Nat Biotechnol* **36** 411-420.

Caduff JH, Fischer LC & Burri PH 1986 Scanning electron microscope study of the developing microvasculature in the postnatal rat lung. *Anat Rec* **216** 154-164.

Canonica J, Frateschi S, Boscardin E, Ebering A, Sergi C, Jager Y, Peyrollaz T, Merillat AM, Maillard M, Klusonova P, et al. 2019 Lack of Renal Tubular Glucocorticoid Receptor Decreases the Thiazide-Sensitive Na(+)/Cl(-) Cotransporter NCC and Transiently Affects Sodium Handling. *Front Physiol* **10** 989.

Cardoso WV & Lu J 2006 Regulation of early lung morphogenesis: questions, facts and controversies. *Development* **133** 1611-1624.

Carlo WA, McDonald SA, Fanaroff AA, Vohr BR, Stoll BJ, Ehrenkranz RA, Andrews WW, Wallace D, Das A, Bell EF, et al. 2011 Association of antenatal corticosteroids with mortality and neurodevelopmental outcomes among infants born at 22 to 25 weeks' gestation. *Jama* **306** 2348-2358.

Carroll TJ, Park JS, Hayashi S, Majumdar A & McMahon AP 2005 Wnt9b plays a central role in the regulation of mesenchymal to epithelial transitions underlying organogenesis of the mammalian urogenital system. *Dev Cell* **9** 283-292.

Celsi G, Nishi A, Akusjarvi G & Aperia A 1991 Abundance of Na(+)-K(+)-ATPase mRNA is regulated by glucocorticoid hormones in infant rat kidneys. *Am J Physiol* **260** F192-197.

Cerqueira JJ, Taipa R, Uylings HB, Almeida OF & Sousa N 2007 Specific configuration of dendritic degeneration in pyramidal neurons of the medial prefrontal cortex induced by differing corticosteroid regimens. *Cereb Cortex* **17** 1998-2006.

Chanda D, Kurundkar A, Rangarajan S, Locy M, Bernard K, Sharma NS, Logsdon NJ, Liu H, Crossman DK, Horowitz JC, et al. 2016 Developmental Reprogramming in Mesenchymal Stromal Cells of Human Subjects with Idiopathic Pulmonary Fibrosis. *Sci Rep* **6** 37445.

Chapman K, Holmes M & Seckl J 2013 11β-hydroxysteroid dehydrogenases: intracellular gate-keepers of tissue glucocorticoid action. *Physiological reviews* **93** 1139-1206.

Chehade H, Simeoni U, Guignard JP & Boubred F 2018 Preterm Birth: Long Term Cardiovascular and Renal Consequences. *Curr Pediatr Rev* **14** 219-226.

Chen X, Hyatt BA, Mucenski ML, Mason RJ & Shannon JM 2006 Identification and characterization of a lysophosphatidylcholine acyltransferase in alveolar type II cells. *Proc Natl Acad Sci U S A* **103** 11724-11729.

Chen YZ, Hua SY, Wang CA, Wu LG, Gu Q & Xing BR 1991 An electrophysiological study on the membrane receptor-mediated action of glucocorticoids in mammalian neurons. *Neuroendocrinology* **53 Suppl 1** 25-30.

Chida D, Sato T, Sato Y, Kubo M, Yoda T, Suzuki H & Iwakura Y 2009 Characterization of mice deficient in melanocortin 2 receptor on a B6/Balbc mix background. *Molecular and cellular endocrinology* **300** 32-36.

Chow YH, Wang Y, Plumb J, O'Brodovich H & Hu J 1999 Hormonal regulation and genomic organization of the human amiloride-sensitive epithelial sodium channel alpha subunit gene. *Pediatr Res* **46** 208-214.

Christensen ST, Pedersen LB, Schneider L & Satir P 2007 Sensory cilia and integration of signal transduction in human health and disease. *Traffic* **8** 97-109.

Chrousos GP & Kino T 2005 Intracellular glucocorticoid signaling: a formerly simple system turns stochastic. *Sci STKE* **2005** pe48.

Chung S, Son GH & Kim K 2011 Circadian rhythm of adrenal glucocorticoid: Its regulation and clinical implications. *Biochimica et Biophysica Acta* **1812** 581-591.

Cole TJ, Blendy JA, Monaghan AP, Krieglstein K, Schmid W, Aguzzi A, Fantuzzi G, Hummler E, Unsicker K & Schutz G 1995 Targeted disruption of the glucocorticoid receptor gene blocks adrenergic chromaffin cell development and severely retards lung maturation. *Genes Dev* **9** 1608-1621.

Cole TJ, Short KL & Hooper SB 2019 The science of steroids. *Semin Fetal Neonatal Med* **24** 170-175.

Cole TJ, Solomon NM, Van Driel R, Monk JA, Bird D, Richardson SJ, Dilley RJ & Hooper SB 2004 Altered epithelial cell proportions in the fetal lung of glucocorticoid receptor null mice. *Am J Respir Cell Mol Biol* **30** 613-619.

Cole TJ & Young MJ 2017 30 YEARS OF THE MINERALOCORTICOID RECEPTOR: Mineralocorticoid receptor null mice: informing cell-type-specific roles. *J Endocrinol* **234** T83-t92.

Combes AN, Phipson B, Lawlor KT, Dorison A, Patrick R, Zappia L, Harvey RP, Oshlack A & Little MH 2019 Correction: Single cell analysis of the developing mouse kidney provides deeper insight into marker gene expression and ligand-receptor crosstalk (doi:10.1242/dev.178673). *Development* **146**.

Costantini F & Shakya R 2006 GDNF/Ret signaling and the development of the kidney. *Bioessays* **28** 117-127.

Cottrell EC & Seckl JR 2009 Prenatal stress, glucocorticoids and the programming of adult disease. *Front Behav Neurosci* **3** 19.

Crowther CA, McKinlay CJ, Middleton P & Harding JE 2015 Repeat doses of prenatal corticosteroids for women at risk of preterm birth for improving neonatal health outcomes. *The Cochrane database of systematic reviews* Cd003935.

Dalziel SR, Walker NK, Parag V, Mantell C, Rea HH, Rodgers A & Harding JE 2005 Cardiovascular risk factors after antenatal exposure to betamethasone: 30-year follow-up of a randomised controlled trial. *Lancet* **365** 1856-1862.

Daniel Bird A, McDougall AR, Seow B, Hooper SB & Cole TJ 2015 Minireview: Glucocorticoid regulation of lung development: Lessons learned from conditional GR knockout mice. *Molecular Endocrinology* **29** 158-171.

Davidson A 2009 Mouse kidney development. Cambridge (MA): Harvard Stem Cell Institute

Davidson LM & Berkelhamer SK 2017 Bronchopulmonary Dysplasia: Chronic Lung Disease of Infancy and Long-Term Pulmonary Outcomes. *Journal of clinical medicine* **6** 4.

Davis EP, Sandman CA, Buss C, Wing DA & Head K 2013 Fetal glucocorticoid exposure is associated with preadolescent brain development. *Biol Psychiatry* **74** 647-655.

Davis EP, Townsend EL, Gunnar MR, Georgieff MK, Guiang SF, Ciffuentes RF & Lussky RC 2004 Effects of prenatal betamethasone exposure on regulation of stress physiology in healthy premature infants. *Psychoneuroendocrinology* **29** 1028-1036.

de Quixano BB, Villena JA, Aranda M, Brils G, Cuevas A, Hespel T, Lekuona H, Suarez C, Tornavaca O & Meseguer A 2017 Kidney Androgen-Regulated Protein (KAP) Transgenic Mice Are Protected Against High-Fat Diet Induced Metabolic Syndrome. *Sci Rep* **7** 16102.

de Vries A, Holmes MC, Heijnis A, Seier JV, Heerden J, Louw J, Wolfe-Coote S, Meaney MJ, Levitt NS & Seckl JR 2007 Prenatal dexamethasone exposure induces changes in nonhuman primate offspring cardiometabolic and hypothalamic-pituitary-adrenal axis function. *J Clin Invest* **117** 1058-1067.

Dean F, Yu C, Lingas RI & Matthews SG 2001 Prenatal glucocorticoid modifies hypothalamo-pituitary-adrenal regulation in prepubertal guinea pigs. *Neuroendocrinology* **73** 194-202.

DeFelice M, Silberschmidt D, DiLauro R, Xu Y, Wert SE, Weaver TE, Bachurski CJ, Clark JC & Whitsett JA 2003 TTF-1 phosphorylation is required for peripheral lung morphogenesis, perinatal survival, and tissue-specific gene expression. *J Biol Chem* **278** 35574-35583.

Deng Q, Riquelme D, Trinh L, Low MJ, Tomić M, Stojilkovic S & Aguilera G 2015 Rapid Glucocorticoid Feedback Inhibition of ACTH Secretion Involves Ligand-Dependent Membrane Association of Glucocorticoid Receptors. *Endocrinology* **156** 3215-3227.

Dobin A, Davis CA, Schlesinger F, Drenkow J, Zaleski C, Jha S, Batut P, Chaisson M & Gingeras TR 2013 STAR: ultrafast universal RNA-seq aligner. *Bioinformatics* **29** 15-21.

Dours-Zimmermann MT & Zimmermann DR 1994 A novel glycosaminoglycan attachment domain identified in two alternative splice variants of human versican. *J Biol Chem* **269** 32992-32998.

Dreyfuss D & Saumon G 1998 Ventilator-induced lung injury: lessons from experimental studies. *Am J Respir Crit Care Med* **157** 294-323.

Driscoll JA, Bhalla S, Liapis H, Ibricevic A & Brody SL 2008 Autosomal dominant polycystic kidney disease is associated with an increased prevalence of radiographic bronchiectasis. *Chest* **133** 1181-1188.

Du Y, Guo M, Whitsett JA & Xu Y 2015 'LungGENS': a web-based tool for mapping single-cell gene expression in the developing lung. *Thorax* **70** 1092-1094.

Du Y, Kitzmiller JA, Sridharan A, Perl AK, Bridges JP, Misra RS, Pryhuber GS, Mariani TJ, Bhattacharya S, Guo M, et al. 2017 Lung Gene Expression Analysis (LGEA): an integrative web portal for comprehensive gene expression data analysis in lung development. *Thorax* **72** 481-484.

Dubail J & Apte SS 2015 Insights on ADAMTS proteases and ADAMTS-like proteins from mammalian genetics. *Matrix Biol* **44-46** 24-37.

Eisenmann DM 2005 Wnt signaling. *WormBook* 1-17.

Ervin MG, Berry LM, Ikegami M, Jobe AH, Padbury JF & Polk DH 1996 Single dose fetal betamethasone administration stabilizes postnatal glomerular filtration rate and alters endocrine function in premature lambs. *Pediatr Res* **40** 645-651.

Ervin MG, Seidner SR, Leland MM, Ikegami M & Jobe AH 1998 Direct fetal glucocorticoid treatment alters postnatal adaptation in premature newborn baboons. *Am J Physiol* **274** R1169-1176.

Fan YS, Eddy RL, Byers MG, Haley LL, Henry WM, Nowak NJ & Shows TB 1989 The human mineralocorticoid receptor gene (MLR) is located on chromosome 4 at q31.2. *Cytogenet Cell Genet* **52** 83-84.

Flecknoe S, Harding R, Maritz G & Hooper SB 2000 Increased lung expansion alters the proportions of type I and type II alveolar epithelial cells in fetal sheep. *Am J Physiol Lung Cell Mol Physiol* **278** L1180-1185.

Flecknoe SJ, Wallace MJ, Harding R & Hooper SB 2002 Determination of alveolar epithelial cell phenotypes in fetal sheep: evidence for the involvement of basal lung expansion. *J Physiol* **542** 245-253.

Fordel E, Thijs L, Martinet W, Lenjou M, Laufs T, Van Bockstaele D, Moens L & Dewilde S 2006 Neuroglobin and cytoglobin overexpression protects human SH-SY5Y neuroblastoma cells against oxidative stress-induced cell death. *Neurosci Lett* **410** 146-151.

Fowden AL & Forhead AJ 2004 Endocrine mechanisms of intrauterine programming. *Reproduction* **127** 515-526.

Fowden AL & Forhead AJ 2015 Glucocorticoids as regulatory signals during intrauterine development. *Exp Physiol* **100** 1477-1487.

Fowden AL, Valenzuela OA, Vaughan OR, Jellyman JK & Forhead AJ 2016 Glucocorticoid programming of intrauterine development. *Domest Anim Endocrinol* **56 Suppl** S121-132.

French NP, Hagan R, Evans SF, Mullan A & Newnham JP 2004 Repeated antenatal corticosteroids: effects on cerebral palsy and childhood behavior. *Am J Obstet Gynecol* **190** 588-595.

Garbrecht MR, Klein JM, Schmidt TJ & Snyder JM 2006 Glucocorticoid metabolism in the human fetal lung: implications for lung development and the pulmonary surfactant system. *Biol Neonate* **89** 109-119.

Glasson SS, Askew R, Sheppard B, Carito B, Blanchet T, Ma HL, Flannery CR, Peluso D, Kanki K, Yang Z, et al. 2005 Deletion of active ADAMTS5 prevents cartilage degradation in a murine model of osteoarthritis. *Nature* **434** 644-648.

Glasson SS, Askew R, Sheppard B, Carito BA, Blanchet T, Ma HL, Flannery CR, Kanki K, Wang E, Peluso D, et al. 2004 Characterization of and osteoarthritis susceptibility in ADAMTS-4-knockout mice. *Arthritis Rheum* **50** 2547-2558.

Goldenberg RL, Culhane JF, Iams JD & Romero R 2008 Epidemiology and causes of preterm birth. *Lancet* **371** 75-84.

Goodwin JE, Zhang J, Velazquez H & Geller DS 2010 The glucocorticoid receptor in the distal nephron is not necessary for the development or maintenance of dexamethasone-induced hypertension. *Biochem Biophys Res Commun* **394** 266-271.

Grabski R, Szul T, Sasaki T, Timpl R, Mayne R, Hicks B & Sztul E 2003 Mutations in COCH that result in non-syndromic autosomal dominant deafness (DFNA9) affect matrix deposition of cochlin. *Hum Genet* **113** 406-416.

Grad I & Picard D 2007 The glucocorticoid responses are shaped by molecular chaperones. *Mol Cell Endocrinol* **275** 2-12.

Grote D, Souabni A, Busslinger M & Bouchard M 2006 Pax 2/8-regulated Gata 3 expression is necessary for morphogenesis and guidance of the nephric duct in the developing kidney. *Development* **133** 53-61.

Guettari N, Dufour ME & Marin L 1990 Effects of the antiglucocorticoid RU 486 on the initiation of ultrastructural type-II cell differentiation in fetal rat lung. *Biol Neonate* **58** 173-180.

Habermehl D, Parkitna JR, Kaden S, Brügger B, Wieland F, Gröne HJ & Schütz G 2011 Glucocorticoid activity during lung maturation is essential in mesenchymal and less in alveolar epithelial cells. *Molecular Endocrinology* **25** 1280-1288.

Habib S, Gattineni J, Twombley K & Baum M 2011 Evidence that prenatal programming of hypertension by dietary protein deprivation is mediated by fetal glucocorticoid exposure. *Am J Hypertens* **24** 96-101.

Hao H, Rhodes R, Ingbar DH & Wendt CH 2003 Dexamethasone responsive element in the rat Na, K-ATPase beta1 gene coding region. *Biochim Biophys Acta* **1630** 55-63.

Harding R, Pinkerton K & Plopper C Eds 2003 *The Lung: Development, Aging and the Environment*: Academic Press.

Helou J, Otto EA, Attanasio M, Allen SJ, Parisi MA, Glass I, Utsch B, Hashmi S, Fazzi E, Omran H, et al. 2007 Mutation analysis of NPHP6/CEP290 in patients with Joubert syndrome and Senior-Loken syndrome. *J Med Genet* **44** 657-663.

Herriges M & Morrisey EE 2014 Lung development: orchestrating the generation and regeneration of a complex organ. *Development* **141** 502-513.

Hildebrandt F, Benzing T & Katsanis N 2011 Ciliopathies. *N Engl J Med* **364** 1533-1543.

Hill KJ, Lumbers ER & Elbourne I 1988 The actions of cortisol on fetal renal function. *J Dev Physiol* **10** 85-96.

Hind M & Maden M 2004 Retinoic acid induces alveolar regeneration in the adult mouse lung. *Eur Respir J* **23** 20-27.

Hintz SR, Van Meurs KP, Perritt R, Poole WK, Das A, Stevenson DK, Ehrenkranz RA, Lemons JA, Vohr BR, Heyne R, et al. 2007 Neurodevelopmental outcomes of premature infants with severe respiratory failure enrolled in a randomized controlled trial of inhaled nitric oxide. *J Pediatr* **151** 16-22, 22.e11-13.

Hoffman DJ, Reynolds RM & Hardy DB 2017 Developmental origins of health and disease: current knowledge and potential mechanisms. *Nutr Rev* **75** 951-970.

Howard KJ, Holley SJ, Yamamoto KR & Distelhorst CW 1990 Mapping the HSP90 binding region of the glucocorticoid receptor. *J Biol Chem* **265** 11928-11935.

Hu X, Zhao M, Sun W, Zhao G & Ren J 2011 Effects of microfluidization treatment and transglutaminase cross-linking on physicochemical, functional, and conformational properties of peanut protein isolate. *J Agric Food Chem* **59** 8886-8894.

Hua SY & Chen YZ 1989 Membrane receptor-mediated electrophysiological effects of glucocorticoid on mammalian neurons. *Endocrinology* **124** 687-691.

Huang C, Li Z, Wang M & Martorell R 2010 Early life exposure to the 1959-1961 Chinese famine has long-term health consequences. *J Nutr* **140** 1874-1878.

Huang CC, Shih MC, Hsu NC, Chien Y & Chung BC 2012 Fetal glucocorticoid synthesis is required for development of fetal adrenal medulla and hypothalamus feedback suppression. *Endocrinology* **153** 4749-4756.

Hubmacher D, Wang LW, Mecham RP, Reinhardt DP & Apte SS 2015 Adamtsl2 deletion results in bronchial fibrillin microfibril accumulation and bronchial epithelial dysplasia--a novel mouse model providing insights into geleophysic dysplasia. *Dis Model Mech* **8** 487-499.

Hummler E, Barker P, Gatzy J, Beermann F, Verdumo C, Schmidt A, Boucher R & Rossier BC 1996 Early death due to defective neonatal lung liquid clearance in alpha-ENaC-deficient mice. *Nat Genet* **12** 325-328.

Hundertmark S, Dill A, Ebert A, Zimmermann B, Kotelevtsev YV, Mullins JJ & Seckl JR 2002 Foetal lung maturation in 11beta-hydroxysteroid dehydrogenase type 1 knockout mice. *Horm Metab Res* **34** 545-549.

Ingbar DH, Duvick S, Savick SK, Schellhase DE, Detterding R, Jamieson JD & Shannon JM 1997 Developmental changes of fetal rat lung Na-K-ATPase after maternal treatment with dexamethasone. *Am J Physiol* **272** L665-672.

Iozzo RV, Naso MF, Cannizzaro LA, Wasmuth JJ & McPherson JD 1992 Mapping of the versican proteoglycan gene (CSPG2) to the long arm of human chromosome 5 (5q12-5q14). *Genomics* **14** 845-851.

Ivy JR, Evans LC, Moorhouse R, Richardson RV, Al-Dujaili EAS, Flatman PW, Kenyon CJ, Chapman KE & Bailey MA 2018 Renal and Blood Pressure Response to a High-Salt Diet in Mice With Reduced Global Expression of the Glucocorticoid Receptor. *Front Physiol* **9** 848.

Jahnukainen T, Chen M, Berg U & Celsi G 2001 Antenatal glucocorticoids and renal function after birth. *Semin Neonatol* **6** 351-355.

Jung HJ, Chen Z, Wang M, Fayad L, Romaguera J, Kwak LW & McCarty N 2012 Calcium blockers decrease the bortezomib resistance in mantle cell lymphoma via manipulation of tissue transglutaminase activities. *Blood* **119** 2568-2578.

Kadzik RS, Cohen ED, Morley MP, Stewart KM, Lu MM & Morrisey EE 2014 Wnt ligand/Frizzled 2 receptor signaling regulates tube shape and branch-point formation in the lung through control of epithelial cell shape. *Proc Natl Acad Sci U S A* **111** 12444-12449.

Kajantie E, Raivio T, Janne OA, Hovi P, Dunkel L & Andersson S 2004 Circulating glucocorticoid bioactivity in the preterm newborn after antenatal betamethasone treatment. *J Clin Endocrinol Metab* **89** 3999-4003.

Kaplan F, Comber J, Sladek R, Hudson TJ, Muglia LJ, Macrae T, Gagnon S, Asada M, Brewer JA & Sweezey NB 2003 The growth factor midkine is modulated by both glucocorticoid and retinoid in fetal lung development. *Am J Respir Cell Mol Biol* **28** 33-41.

Kauffman SL 1977 Acceleration of canalicular development in lungs of fetal mice exposed transplacentally to dexamethasone. *Lab Invest* **36** 395-401.

Kelwick R, Desanlis I, Wheeler GN & Edwards DR 2015 The ADAMTS (A Disintegrin and Metalloproteinase with Thrombospondin motifs) family. *Genome Biol* **16** 113.

Kemp MW, Jobe AH, Usuda H, Nathanielsz PW, Li C, Kuo A, Huber HF, Clarke GD, Saito M, Newnham JP, et al. 2018 Efficacy and safety of antenatal steroids. *Am J Physiol Regul Integr Comp Physiol* **315** R825-r839.

Kimura S, Hara Y, Pineau T, Fernandez-Salguero P, Fox CH, Ward JM & Gonzalez FJ 1996 The T/ebp null mouse: thyroid-specific enhancer-binding protein is essential for the organogenesis of the thyroid, lung, ventral forebrain, and pituitary. *Genes Dev* **10** 60-69.

Kino T 2000 Glucocorticoid Receptor. In *Endotext*. Ed AB Feingold KR, Boyce A, et al. South Dartmouth (MA): MDText.com.

Kischel P, Waltregny D, Dumont B, Turtoi A, Greffe Y, Kirsch S, De Pauw E & Castronovo V 2010 Versican overexpression in human breast cancer lesions: known and new isoforms for stromal tumor targeting. *Int J Cancer* **126** 640-650.

Kitamura K, Miura H, Miyagawa-Tomita S, Yanazawa M, Katoh-Fukui Y, Suzuki R, Ohuchi H, Suehiro A, Motegi Y, Nakahara Y, et al. 1999 Mouse Pitx2 deficiency leads to anomalies of the ventral body wall, heart, extra- and periocular mesoderm and right pulmonary isomerism. *Development* **126** 5749-5758.

Kobayashi A, Kwan KM, Carroll TJ, McMahon AP, Mendelsohn CL & Behringer RR 2005 Distinct and sequential tissue-specific activities of the LIM-class homeobox gene Lim1 for tubular morphogenesis during kidney development. *Development* **132** 2809-2823.

Korfhagen TR, Bruno MD, Ross GF, Huelsman KM, Ikegami M, Jobe AH, Wert SE, Stripp BR, Morris RE, Glasser SW, et al. 1996 Altered surfactant function and structure in SP-A gene targeted mice. *Proc Natl Acad Sci U S A* **93** 9594-9599.

Kotelevtsev Y, Holmes MC, Burchell A, Houston PM, Schmoll D, Jamieson P, Best R, Brown R, Edwards CR, Seckl JR, et al. 1997 11beta-hydroxysteroid dehydrogenase type 1 knockout mice show attenuated glucocorticoid-inducible responses and resist hyperglycemia on obesity or stress. *Proc Natl Acad Sci U S A* **94** 14924-14929.

Kreidberg JA, Sariola H, Loring JM, Maeda M, Pelletier J, Housman D & Jaenisch R 1993 WT-1 is required for early kidney development. *Cell* **74** 679-691.

Kutuzova GD, Akhter S, Christakos S, Vanhooke J, Kimmel-Jehan C & Deluca HF 2006 Calbindin D(9k) knockout mice are indistinguishable from wild-type mice in phenotype and serum calcium level. *Proc Natl Acad Sci U S A* **103** 12377-12381.

Lan J, Ribeiro L, Mandeville I, Nadeau K, Bao T, Cornejo S, Sweezey NB & Kaplan F 2009 Inflammatory cytokines, goblet cell hyperplasia and altered lung mechanics in Lgl1+/- mice. *Respir Res* **10** 83.

Leavitt MG, Aberdeen GW, Burch MG, Albrecht ED & Pepe GJ 1997 Inhibition of fetal adrenal adrenocorticotropin receptor messenger ribonucleic acid expression by betamethasone administration to the baboon fetus in late gestation. *Endocrinology* **138** 2705-2712.

Lee GS, Lee KY, Choi KC, Ryu YH, Paik SG, Oh GT & Jeung EB 2007 Phenotype of a calbindin-D9k gene knockout is compensated for by the induction of other calcium transporter genes in a mouse model. *J Bone Miner Res* **22** 1968-1978.

Lee NV, Rodriguez-Manzaneque JC, Thai SN, Twal WO, Luque A, Lyons KM, Argraves WS & Iruela-Arispe ML 2005 Fibulin-1 acts as a cofactor for the matrix metalloprotease ADAMTS-1. *J Biol Chem* **280** 34796-34804.

LeVine AM, Bruno MD, Huelsman KM, Ross GF, Whitsett JA & Korfhagen TR 1997 Surfactant protein A-deficient mice are susceptible to group B streptococcal infection. *J Immunol* **158** 4336-4340.

Levitt NS, Lindsay RS, Holmes MC & Seckl JR 1996 Dexamethasone in the last week of pregnancy attenuates hippocampal glucocorticoid receptor gene expression and elevates blood pressure in the adult offspring in the rat. *Neuroendocrinology* **64** 412-418.

Li A, Hardy R, Stoner S, Tuckermann J, Seibel M & Zhou H 2013 Deletion of mesenchymal glucocorticoid receptor attenuates embryonic lung development and abdominal wall closure. *PLoS One* **8** e63578.

Li L, Yan LH, Manoj S, Li Y & Lu L 2017 Central Role of CEMIP in Tumorigenesis and Its Potential as Therapeutic Target. *J Cancer* **8** 2238-2246.

Liggins GC 1994 The role of cortisol in preparing the fetus for birth. *Reprod Fertil Dev* **6** 141-150.

Liggins GC & Howie RN 1972 A controlled trial of antepartum glucocorticoid treatment for prevention of the respiratory distress syndrome in premature infants. *Pediatrics* **50** 515-525.

Lin HY, Muller YA & Hammond GL 2010 Molecular and structural basis of steroid hormone binding and release from corticosteroid-binding globulin. *Mol Cell Endocrinol* **316** 3-12.

Lindahl P, Karlsson L, Hellstrom M, Gebre-Medhin S, Willetts K, Heath JK & Betsholtz C 1997 Alveogenesis failure in PDGF-A-deficient mice is coupled to lack of distal spreading of

alveolar smooth muscle cell progenitors during lung development. *Development* **124** 3943-3953.

Lindsay RS, Lindsay RM, Edwards CR & Seckl JR 1996 Inhibition of 11-beta-hydroxysteroid dehydrogenase in pregnant rats and the programming of blood pressure in the offspring. *Hypertension* **27** 1200-1204.

Liu L, Oza S, Hogan D, Perin J, Rudan I, Lawn JE, Cousens S, Mathers C & Black RE 2015 Global, regional, and national causes of child mortality in 2000-13, with projections to inform post-2015 priorities: an updated systematic analysis. *Lancet* **385** 430-440.

Livak KJ & Schmittgen TD 2001 Analysis of relative gene expression data using real-time quantitative PCR and the 2(-Delta Delta C(T)) Method. *Methods* **25** 402-408.

Llamazares M, Obaya AJ, Moncada-Pazos A, Heljasvaara R, Espada J, Lopez-Otin C & Cal S 2007 The ADAMTS12 metalloproteinase exhibits anti-tumorigenic properties through modulation of the Ras-dependent ERK signalling pathway. *J Cell Sci* **120** 3544-3552.

Love MI, Huber W & Anders S 2014 Moderated estimation of fold change and dispersion for RNA-seq data with DESeq2. *Genome Biol* **15** 550.

Lu NZ & Cidlowski JA 2005 Translational regulatory mechanisms generate N-terminal glucocorticoid receptor isoforms with unique transcriptional target genes. *Mol Cell* **18** 331-342.

Lu NZ & Cidlowski JA 2006 Glucocorticoid receptor isoforms generate transcription specificity. *Trends Cell Biol* **16** 301-307.

Lui JC, Finkielstain GP, Barnes KM & Baron J 2008 An imprinted gene network that controls mammalian somatic growth is down-regulated during postnatal growth deceleration in multiple organs. *Am J Physiol Regul Integr Comp Physiol* **295** R189-196.

Lupien SJ, McEwen BS, Gunnar MR & Heim C 2009 Effects of stress throughout the lifespan on the brain, behaviour and cognition. *Nat Rev Neurosci* **10** 434-445.

Mansouri A, Chowdhury K & Gruss P 1998 Follicular cells of the thyroid gland require Pax8 gene function. *Nat Genet* **19** 87-90.

Martis PC, Whitsett JA, Xu Y, Perl AK, Wan H & Ikegami M 2006 C/EBPalpha is required for lung maturation at birth. *Development* **133** 1155-1164.

Massaro GD & Massaro D 1992 Formation of alveoli in rats: postnatal effect of prenatal dexamethasone. *Am J Physiol* **263** L37-41.

Massaro GD & Massaro D 2000 Retinoic acid treatment partially rescues failed septation in rats and in mice. *Am J Physiol Lung Cell Mol Physiol* **278** L955-960.

Mastorakos G & Ilias I 2003 Maternal and fetal hypothalamic-pituitary-adrenal axes during pregnancy and postpartum. *Ann N Y Acad Sci* **997** 136-149.

McCabe L, Marash D, Li A & Matthews SG 2001 Repeated antenatal glucocorticoid treatment decreases hypothalamic corticotropin releasing hormone mRNA but not corticosteroid receptor mRNA expression in the fetal guinea-pig brain. *J Neuroendocrinol* **13** 425-431.

McCulley D, Wienhold M & Sun X 2015 The pulmonary mesenchyme directs lung development. *Current opinion in genetics & development* **32** 98-105.

McDonald FJ, Yang B, Hrstka RF, Drummond HA, Tarr DE, McCray PB, Jr., Stokes JB, Welsh MJ & Williamson RA 1999 Disruption of the beta subunit of the epithelial Na+ channel in mice: hyperkalemia and neonatal death associated with a pseudohypoaldosteronism phenotype. *Proc Natl Acad Sci U S A* **96** 1727-1731.

Meimaridou E, Goldsworthy M, Chortis V, Fragouli E, Foster PA, Arlt W, Cox R & Metherell LA 2018 NNT is a key regulator of adrenal redox homeostasis and steroidogenesis in male mice. *J Endocrinol* **236** 13-28.

Meno C, Shimono A, Saijoh Y, Yashiro K, Mochida K, Ohishi S, Noji S, Kondoh H & Hamada H 1998 lefty-1 is required for left-right determination as a regulator of lefty-2 and nodal. *Cell* **94** 287-297.

Merkus PJ, ten Have-Opbroek AA & Quanjer PH 1996 Human lung growth: a review. *Pediatr Pulmonol* **21** 383-397.

Metzger RJ, Klein OD, Martin GR & Krasnow MA 2008 The branching programme of mouse lung development. *Nature* **453** 745-750.

Meyer JS 1983 Early adrenalectomy stimulates subsequent growth and development of the rat brain. *Exp Neurol* **82** 432-446.

Michelsohn AM & Anderson DJ 1992 Changes in competence determine the timing of two sequential glucocorticoid effects on sympathoadrenal progenitors. *Neuron* **8** 589-604.

Minoo P, Su G, Drum H, Bringas P & Kimura S 1999 Defects in tracheoesophageal and lung morphogenesis in Nkx2.1(-/-) mouse embryos. *Dev Biol* **209** 60-71.

Mjaatvedt CH, Yamamura H, Capehart AA, Turner D & Markwald RR 1998 The Cspg2 gene, disrupted in the hdf mutant, is required for right cardiac chamber and endocardial cushion formation. *Dev Biol* **202** 56-66.

Moisiadis VG & Matthews SG 2014 Glucocorticoids and fetal programming part 1: Outcomes. *Nat Rev Endocrinol* **10** 391-402.

Morgan DJ, Poolman TM, Williamson AJ, Wang Z, Clark NR, Ma'ayan A, Whetton AD, Brass A, Matthews LC & Ray DW 2016 Glucocorticoid receptor isoforms direct distinct mitochondrial programs to regulate ATP production. *Sci Rep* **6** 26419.

Moss TJ 2006 Respiratory consequences of preterm birth. *Clin Exp Pharmacol Physiol* **33** 280-284.

Moss TJ, Nitsos I, Harding R & Newnham JP 2003 Differential effects of maternal and fetal betamethasone injections in late-gestation fetal sheep. *J Soc Gynecol Investig* **10** 474-479.

Motto DG, Chauhan AK, Zhu G, Homeister J, Lamb CB, Desch KC, Zhang W, Tsai HM, Wagner DD & Ginsburg D 2005 Shigatoxin triggers thrombotic thrombocytopenic purpura in genetically susceptible ADAMTS13-deficient mice. *J Clin Invest* **115** 2752-2761.

Muglia L, Jacobson L, Dikkes P & Majzoub JA 1995 Corticotropin-releasing hormone deficiency reveals major fetal but not adult glucocorticoid need. *Nature* **373** 427-432.

Muller OG, Parnova RG, Centeno G, Rossier BC, Firsov D & Horisberger JD 2003 Mineralocorticoid effects in the kidney: correlation between alphaENaC, GILZ, and Sgk-1 mRNA expression and urinary excretion of Na+ and K+. *J Am Soc Nephrol* **14** 1107-1115.

Muona A, Eklund L, Väisänen T & Pihlajaniemi T 2002 Developmentally regulated expression of type XV collagen correlates with abnormalities in Col15a1(-/-) mice. *Matrix Biol* **21** 89-102.

Murphy VE, Smith R, Giles WB & Clifton VL 2006 Endocrine regulation of human fetal growth: the role of the mother, placenta, and fetus. *Endocr Rev* **27** 141-169.

Mustafa SB, DiGeronimo RJ, Petershack JA, Alcorn JL & Seidner SR 2004 Postnatal glucocorticoids induce alpha-ENaC formation and regulate glucocorticoid receptors in the preterm rabbit lung. *Am J Physiol Lung Cell Mol Physiol* **286** L73-80.

Nam JS, Turcotte TJ & Yoon JK 2007 Dynamic expression of R-spondin family genes in mouse development. *Gene Expr Patterns* **7** 306-312.

Nandadasa S, Foulcer S & Apte SS 2014 The multiple, complex roles of versican and its proteolytic turnover by ADAMTS proteases during embryogenesis. *Matrix Biol* **35** 34-41.

Nardo L, Hooper SB & Harding R 1998 Stimulation of lung growth by tracheal obstruction in fetal sheep: relation to luminal pressure and lung liquid volume. *Pediatr Res* **43** 184-190.

Nguyen NM, Kelley DG, Schlueter JA, Meyer MJ, Senior RM & Miner JH 2005 Epithelial laminin alpha5 is necessary for distal epithelial cell maturation, VEGF production, and alveolization in the developing murine lung. *Dev Biol* **282** 111-125.

Noorlander CW, De Graan PN, Middeldorp J, Van Beers JJ & Visser GH 2006 Ontogeny of hippocampal corticosteroid receptors: effects of antenatal glucocorticoids in human and mouse. *J Comp Neurol* **499** 924-932.

Northway WH, Jr., Rosan RC & Porter DY 1967 Pulmonary disease following respirator therapy of hyaline-membrane disease. Bronchopulmonary dysplasia. *N Engl J Med* **276** 357-368.

Oakley RH & Cidlowski JA 2013 The biology of the glucocorticoid receptor: new signaling mechanisms in health and disease. *The Journal of allergy and clinical immunology* **132** 1033-1044.

Oakley RH, Ramamoorthy S, Foley JF, Busada JT, Lu NZ & Cidlowski JA 2018 Glucocorticoid receptor isoform-specific regulation of development, circadian rhythm, and inflammation in mice. *Faseb j* **32** 5258-5271.

Ohashi T, Takada S, Motoike T, Tsuneishi S, Matsuo M, Sano K & Nakamura H 1991 Effect of dexamethasone on pulmonary surfactant metabolism in hyperoxia-treated rat lungs. *Pediatr Res* **29** 173-177.

Olver RE, Walters DV & S MW 2004 Developmental regulation of lung liquid transport. *Annu Rev Physiol* **66** 77-101.

Ortiz LA, Quan A, Weinberg A & Baum M 2001 Effect of prenatal dexamethasone on rat renal development. *Kidney Int* **59** 1663-1669.

Osathanondh V & Potter EL 1963 DEVELOPMENT OF HUMAN KIDNEY AS SHOWN BY MICRODISSECTION. III. FORMATION AND INTERRELATIONSHIP OF COLLECTING TUBULES AND NEPHRONS. *Arch Pathol* **76** 290-302.

Oshika E, Liu S, Singh G, Michalopoulos GK, Shinozuka H & Katyal SL 1998a Antagonistic effects of dexamethasone and retinoic acid on rat lung morphogenesis. *Pediatr Res* **43** 315-324.

Oshika E, Liu S, Ung LP, Singh G, Shinozuka H, Michalopoulos GK & Katyal SL 1998b Glucocorticoid-induced effects on pattern formation and epithelial cell differentiation in early embryonic rat lungs. *Pediatr Res* **43** 305-314.

Ozmen A, Unek G & Korgun ET 2017 Effect of glucocorticoids on mechanisms of placental angiogenesis. *Placenta* **52** 41-48.

Pan J, Copland I, Post M, Yeger H & Cutz E 2006 Mechanical stretch-induced serotonin release from pulmonary neuroendocrine cells: implications for lung development. *Am J Physiol Lung Cell Mol Physiol* **290** L185-193.

Paulissen G, El Hour M, Rocks N, Guéders MM, Bureau F, Foidart JM, Lopez-Otin C, Noel A & Cataldo DD 2012 Control of allergen-induced inflammation and hyperresponsiveness by the metalloproteinase ADAMTS-12. *J Immunol* **189** 4135-4143.

Perl AK, Hokuto I, Impagnatiello MA, Christofori G & Whitsett JA 2003 Temporal effects of Sprouty on lung morphogenesis. *Dev Biol* **258** 154-168.

Petershack JA, Nagaraja SC & Guillery EN 1999 Role of glucocorticoids in the maturation of renal cortical Na+-K+-ATPase during fetal life in sheep. *Am J Physiol* **276** R1825-1832.

Pooley JR, Rivers CA, Kilcooley MT, Paul SN, Cavga AD, Kershaw YM, Muratcioglu S, Gursoy A, Keskin O & Lightman SL 2020 Beyond the heterodimer model for mineralocorticoid and glucocorticoid receptor interactions in nuclei and at DNA. *PLoS One* **15** e0227520.

Post M & Copland I 2002 Overview of lung development. *Acta Pharmacol Sin* **23 Supplement** 4-7.

Pozarska A, Rodriguez-Castillo JA, Surate Solaligue DE, Ntokou A, Rath P, Mizikova I, Madurga A, Mayer K, Vadasz I, Herold S, et al. 2017 Stereological monitoring of mouse lung alveolarization from the early postnatal period to adulthood. *Am J Physiol Lung Cell Mol Physiol* **312** L882-l895.

Purisch SE & Gyamfi-Bannerman C 2017 Epidemiology of preterm birth. *Semin Perinatol* **41** 387-391.

Quax RA, Manenschijn L, Koper JW, Hazes JM, Lamberts SWJ, van Rossum EFC & Feelders RA 2013 Glucocorticoid sensitivity in health and disease. *Nat Rev Endocrinol* **9** 670-686.

Rachel RA, Yamamoto EA, Dewanjee MK, May-Simera HL, Sergeev YV, Hackett AN, Pohida K, Munasinghe J, Gotoh N, Wickstead B, et al. 2015 CEP290 alleles in mice disrupt tissue-specific cilia biogenesis and recapitulate features of syndromic ciliopathies. *Hum Mol Genet* **24** 3775-3791.

Rakers F, Frauendorf V, Rupprecht S, Schiffner R, Bischoff SJ, Kiehntopf M, Reinhold P, Witte OW, Schubert H & Schwab M 2013 Effects of early- and late-gestational maternal stress and synthetic glucocorticoid on development of the fetal hypothalamus-pituitary-adrenal axis in sheep. *Stress* **16** 122-129.

Ravelli AC, van der Meulen JH, Michels RP, Osmond C, Barker DJ, Hales CN & Bleker OP 1998 Glucose tolerance in adults after prenatal exposure to famine. *Lancet* **351** 173-177.

Reynolds EO, Roberton NR & Wigglesworth JS 1968 Hyaline membrane disease, respiratory distress, and surfactant deficiency. *Pediatrics* **42** 758-768.

Reynolds RM 2013 Glucocorticoid excess and the developmental origins of disease: two decades of testing the hypothesis--2012 Curt Richter Award Winner. *Psychoneuroendocrinology* **38** 1-11.

Ricciardelli C, Sakko AJ, Ween MP, Russell DL & Horsfall DJ 2009 The biological role and regulation of versican levels in cancer. *Cancer metastasis reviews* **28** 233-245.

Rice WR, Sarin VK, Fox JL, Baatz J, Wert S & Whitsett JA 1989 Surfactant peptides stimulate uptake of phosphatidylcholine by isolated cells. *Biochim Biophys Acta* **1006** 237-245.

Rivier C & Vale W 1983 Modulation of stress-induced ACTH release by corticotropin-releasing factor, catecholamines and vasopressin. *Nature* **305** 325-327.

Roberts D, Brown J, Medley N & Dalziel SR 2017 Antenatal corticosteroids for accelerating fetal lung maturation for women at risk of preterm birth. *The Cochrane database of systematic reviews* **3** CD004454-CD004454.

Roberts D & Dalziel S 2006 Antenatal corticosteroids for accelerating fetal lung maturation for women at risk of preterm birth. *The Cochrane database of systematic reviews* Cd004454.

Robinson-Rechavi M, Escriva Garcia H & Laudet V 2003 The nuclear receptor superfamily. *J Cell Sci* **116** 585-586.

Rogers SA, Ryan G & Hammerman MR 1991 Insulin-like growth factors I and II are produced in the metanephros and are required for growth and development in vitro. *J Cell Biol* **113** 1447-1453.

Russell DL, Doyle KM, Ochsner SA, Sandy JD & Richards JS 2003 Processing and localization of ADAMTS-1 and proteolytic cleavage of versican during cumulus matrix expansion and ovulation. *J Biol Chem* **278** 42330-42339.

Rutledge EA, Parvez RK, Short KM, Smyth IM & McMahon AP 2019 Morphogenesis of the kidney and lung requires branch-tip directed activity of the Adamts18 metalloprotease. *Dev Biol* **454** 156-169.

Ryu J, Vicencio AG, Yeager ME, Kashgarian M, Haddad GG & Eickelberg O 2005 Differential expression of matrix metalloproteinases and their inhibitors in human and mouse lung development. *Thromb Haemost* **94** 175-183.

Sainio K, Hellstedt P, Kreidberg JA, Saxen L & Sariola H 1997 Differential regulation of two sets of mesonephric tubules by WT-1. *Development* **124** 1293-1299.

Sandy JD, Westling J, Kenagy RD, Iruela-Arispe ML, Verscharen C, Rodriguez-Mazaneque JC, Zimmermann DR, Lemire JM, Fischer JW, Wight TN, et al. 2001 Versican V1 proteolysis in human aorta in vivo occurs at the Glu441-Ala442 bond, a site that is cleaved by recombinant ADAMTS-1 and ADAMTS-4. *J Biol Chem* **276** 13372-13378.

Saxen L & Sariola H 1987 Early organogenesis of the kidney. *Pediatr Nephrol* **1** 385-392.

Schaaf MJM & Cidlowski JA 2003 Molecular mechanisms of glucocorticoid action and resistance. *Journal of Steroid Biochemistry & Molecular Biology* **83** 37-48.

Schaffer L, Luzi F, Burkhardt T, Rauh M & Beinder E 2009 Antenatal betamethasone administration alters stress physiology in healthy neonates. *Obstet Gynecol* **113** 1082-1088.

Schittny JC 2017 Development of the lung. *Cell Tissue Res* **367** 427-444.

Schittny JC, Miserocchi G & Sparrow MP 2000 Spontaneous peristaltic airway contractions propel lung liquid through the bronchial tree of intact and fetal lung explants. *Am J Respir Cell Mol Biol* **23** 11-18.

Schittny JC, Paulsson M, Vallan C, Burri PH, Kedei N & Aeschlimann D 1997 Protein cross-linking mediated by tissue transglutaminase correlates with the maturation of extracellular matrices during lung development. *Am J Respir Cell Mol Biol* **17** 334-343.

Scialdone A, Natarajan KN, Saraiva LR, Proserpio V, Teichmann SA, Stegle O, Marioni JC & Buettner F 2015 Computational assignment of cell-cycle stage from single-cell transcriptome data. *Methods* **85** 54-61.

Seckl JR 2004 Prenatal glucocorticoids and long-term programming. *Eur J Endocrinol* **151 Suppl 3** U49-62.

Sekine K, Ohuchi H, Fujiwara M, Yamasaki M, Yoshizawa T, Sato T, Yagishita N, Matsui D, Koga Y, Itoh N, et al. 1999 Fgf10 is essential for limb and lung formation. *Nat Genet* **21** 138-141.

Self M, Lagutin OV, Bowling B, Hendrix J, Cai Y, Dressler GR & Oliver G 2006 Six2 is required for suppression of nephrogenesis and progenitor renewal in the developing kidney. *Embo j* **25** 5214-5228.

Seow BKL, McDougall ARA, Short KL, Wallace MJ, Hooper SB & Cole TJ 2019 Identification of Betamethasone-Regulated Target Genes and Cell Pathways in Fetal Rat Lung Mesenchymal Fibroblasts. *Endocrinology* **160** 1868-1884.

Shannon JM, Nielsen LD, Gebb SA & Randell SH 1998 Mesenchyme specifies epithelial differentiation in reciprocal recombinants of embryonic lung and trachea. *Dev Dyn* **212** 482-494.

Sharma A, Gonzales LW & Ballard PL 1993 Hormonal regulation of cholinephosphate cytidylyltransferase in human fetal lung. *Biochim Biophys Acta* **1170** 237-244.

Shawlot W & Behringer RR 1995 Requirement for Lim1 in head-organizer function. *Nature* **374** 425-430.

Sheen JM, Yu HR, Tiao MM, Chen CC, Huang LT, Chang HY & Tain YL 2015 Prenatal dexamethasone-induced programmed hypertension and renal programming. *Life Sci* **132** 41-48.

Shoener JA, Baig R & Page KC 2006 Prenatal exposure to dexamethasone alters hippocampal drive on hypothalamic-pituitary-adrenal axis activity in adult male rats. *Am J Physiol Regul Integr Comp Physiol* **290** R1366-1373.

Short KM, Combes AN, Lefevre J, Ju AL, Georgas KM, Lamberton T, Cairncross O, Rumballe BA, McMahon AP, Hamilton NA, et al. 2014 Global quantification of tissue dynamics in the developing mouse kidney. *Dev Cell* **29** 188-202.

Short KM & Smyth IM 2016 The contribution of branching morphogenesis to kidney development and disease. *Nat Rev Nephrol* **12** 754-767.

Slattery MM & Morrison JJ 2002 Preterm delivery. *Lancet* **360** 1489-1497.

Slotkin TA, Seidler FJ, Kavlock RJ & Bartolome JV 1991 Fetal dexamethasone exposure impairs cellular development in neonatal rat heart and kidney: effects on DNA and protein in whole tissues. *Teratology* **43** 301-306.

Smith C & Mackay S 1991 Morphological development and fate of the mouse mesonephros. *Journal of anatomy* **174** 171-184.

Smith GW, Aubry JM, Dellu F, Contarino A, Bilezikjian LM, Gold LH, Chen R, Marchuk Y, Hauser C, Bentley CA, et al. 1998 Corticotropin releasing factor receptor 1-deficient mice display decreased anxiety, impaired stress response, and aberrant neuroendocrine development. *Neuron* **20** 1093-1102.

Smith SM & Vale WW 2006 The role of the hypothalamic-pituitary-adrenal axis in neuroendocrine responses to stress. *Dialogues Clin Neurosci* **8** 383-395.

Snyder JM, Rodgers HF, O'Brien JA, Mahli N, Magliato SA & Durham PL 1992 Glucocorticoid effects on rabbit fetal lung maturation in vivo: an ultrastructural morphometric study. *Anat Rec* **232** 133-140.

Snyder JM, Washington IM, Birkland T, Chang MY & Frevert CW 2015 Correlation of Versican Expression, Accumulation, and Degradation During Embryonic Development by Quantitative Immunohistochemistry. *J Histochem Cytochem*.

So AY, Chaivorapol C, Bolton EC, Li H & Yamamoto KR 2007 Determinants of cell- and gene-specific transcriptional regulation by the glucocorticoid receptor. *PLoS Genet* **3** e94.

Sorokin LM, Pausch F, Frieser M, Kroger S, Ohage E & Deutzmann R 1997 Developmental regulation of the laminin alpha5 chain suggests a role in epithelial and endothelial cell maturation. *Dev Biol* **189** 285-300.

Speirs HJ, Seckl JR & Brown RW 2004 Ontogeny of glucocorticoid receptor and 11beta-hydroxysteroid dehydrogenase type-1 gene expression identifies potential critical periods of glucocorticoid susceptibility during development. *J Endocrinol* **181** 105-116.

Stankunas K, Hang CT, Tsun ZY, Chen H, Lee NV, Wu JI, Shang C, Bayle JH, Shou W, Iruela-Arispe ML, et al. 2008 Endocardial Brg1 represses ADAMTS1 to maintain the microenvironment for myocardial morphogenesis. *Dev Cell* **14** 298-311.

Stanton H, Rogerson FM, East CJ, Golub SB, Lawlor KE, Meeker CT, Little CB, Last K, Farmer PJ, Campbell IK, et al. 2005 ADAMTS5 is the major aggrecanase in mouse cartilage in vivo and in vitro. *Nature* **434** 648-652.

Stein AD, Zybert PA, van der Pal-de Bruin K & Lumey LH 2006 Exposure to famine during gestation, size at birth, and blood pressure at age 59 y: evidence from the Dutch Famine. *Eur J Epidemiol* **21** 759-765.

Stonestreet BS, Hansen NB, Laptook AR & Oh W 1983 Glucocorticoid accelerates renal functional maturation in fetal lambs. *Early Hum Dev* **8** 331-341.

Strehl C & Buttgereit F 2014 Unraveling the functions of the membrane-bound glucocorticoid receptors: first clues on origin and functional activity. *Ann N Y Acad Sci* **1318** 1-6.

Stuart T, Butler A, Hoffman P, Hafemeister C, Papalexi E, Mauck WM, 3rd, Hao Y, Stoeckius M, Smibert P & Satija R 2019 Comprehensive Integration of Single-Cell Data. *Cell* **177** 1888-1902.e1821.

Suff N, Story L & Shennan A 2019 The prediction of preterm delivery: What is new? *Semin Fetal Neonatal Med* **24** 27-32.

Tham MS & Smyth IM 2019 Cellular and molecular determinants of normal and abnormal kidney development. *Wiley Interdiscip Rev Dev Biol* **8** e338.

Thomas CP, Auerbach SD, Zhang C & Stokes JB 1999 The structure of the rat amiloride-sensitive epithelial sodium channel gamma subunit gene and functional analysis of its promoter. *Gene* **228** 111-122.

Timmermans S, Souffriau J & Libert C 2019 A General Introduction to Glucocorticoid Biology. *Frontiers in Immunology* **10**.

Tokieda K, Whitsett JA, Clark JC, Weaver TE, Ikeda K, McConnell KB, Jobe AH, Ikegami M & Iwamoto HS 1997 Pulmonary dysfunction in neonatal SP-B-deficient mice. *Am J Physiol* **273** L875-882.

Toriyama K, Muramatsu H, Hoshino T, Torii S & Muramatsu T 1997 Evaluation of heparin-binding growth factors in rescuing morphogenesis of heparitinase-treated mouse embryonic lung explants. *Differentiation* **61** 161-167.

Torres M, Gomez-Pardo E, Dressler GR & Gruss P 1995 Pax-2 controls multiple steps of urogenital development. *Development* **121** 4057-4065.

Uno H, Eisele S, Sakai A, Shelton S, Baker E, DeJesus O & Holden J 1994 Neurotoxicity of glucocorticoids in the primate brain. *Horm Behav* **28** 336-348.

Vale W, Spiess J, Rivier C & Rivier J 1981 Characterization of a 41-residue ovine hypothalamic peptide that stimulates secretion of corticotropin and beta-endorphin. *Science* **213** 1394-1397.

Valente EM, Silhavy JL, Brancati F, Barrano G, Krishnaswami SR, Castori M, Lancaster MA, Boltshauser E, Boccone L, Al-Gazali L, et al. 2006 Mutations in CEP290, which encodes a centrosomal protein, cause pleiotropic forms of Joubert syndrome. *Nat Genet* **38** 623-625.

Vaughan OR, Sferruzzi-Perri AN, Coan PM & Fowden AL 2011 Environmental regulation of placental phenotype: implications for fetal growth. *Reprod Fertil Dev* **24** 80-96.

Venihaki M, Carrigan A, Dikkes P & Majzoub JA 2000 Circadian rise in maternal glucocorticoid prevents pulmonary dysplasia in fetal mice with adrenal insufficiency. *Proc Natl Acad Sci U S A* **97** 7336-7341.

Venkatesh VC, Iannuzzi DM, Ertsey R & Ballard PL 1993 Differential glucocorticoid regulation of the pulmonary hydrophobic surfactant proteins SP-B and SP-C. *Am J Respir Cell Mol Biol* **8** 222-228.

Vernocchi S, Battello N, Schmitz S, Revets D, Billing AM, Turner JD & Muller CP 2013 Membrane glucocorticoid receptor activation induces proteomic changes aligning with classical glucocorticoid effects. *Mol Cell Proteomics* **12** 1764-1779.

Vetter MR & Gibley CW, Jr. 1966 Morphogenesis and histochemistry of the developing mouse kidney. *J Morphol* **120** 135-155.

Vinogradov SN & Moens L 2008 Diversity of globin function: enzymatic, transport, storage, and sensing. *J Biol Chem* **283** 8773-8777.

Waddington CH 1938 The Morphogenetic Function of a Vestigial Organ in the Chick. *Journal of Experimental Biology* **15** 371.

Wan H, Xu Y, Ikegami M, Stahlman MT, Kaestner KH, Ang SL & Whitsett JA 2004 Foxa2 is required for transition to air breathing at birth. *Proc Natl Acad Sci U S A* **101** 14449-14454.

Wang J, Li Y, Han X, Liu B, Hu H, Wang F, Li X, Yang K, Yuan J, Yao P, et al. 2016 Exposure to the Chinese Famine in Childhood Increases Type 2 Diabetes Risk in Adults. *J Nutr* **146** 2289-2295.

Weidenfeld J, Shu W, Zhang L, Millar SE & Morrisey EE 2002 The WNT7b promoter is regulated by TTF-1, GATA6, and Foxa2 in lung epithelium. *J Biol Chem* **277** 21061-21070.

Weinstock M 2008 The long-term behavioural consequences of prenatal stress. *Neurosci Biobehav Rev* **32** 1073-1086.

Westling J, Gottschall PE, Thompson VP, Cockburn A, Perides G, Zimmermann DR & Sandy JD 2004 ADAMTS4 (aggrecanase-1) cleaves human brain versican V2 at Glu 405-Gln406 to generate glial hyaluronate binding protein. *Biochemical Journal* **377** 787-795.

Whirledge S & DeFranco DB 2018 Glucocorticoid Signaling in Health and Disease: Insights From Tissue-Specific GR Knockout Mice. *Endocrinology* **159** 46-64.

Wight TN 2002 Versican: a versatile extracellular matrix proteoglycan in cell biology. *Current opinion in cell biology* **14** 617-623.

Wolf E, Kramer R, Blum WF, Foll J & Brem G 1994 Consequences of postnatally elevated insulin-like growth factor-II in transgenic mice: endocrine changes and effects on body and organ growth. *Endocrinology* **135** 1877-1886.

Wolock SL, Lopez R & Klein AM 2019 Scrublet: Computational Identification of Cell Doublets in Single-Cell Transcriptomic Data. *Cell Syst* **8** 281-291.e289.

Yang H, Lu MM, Zhang L, Whitsett JA & Morrisey EE 2002 GATA6 regulates differentiation of distal lung epithelium. *Development* **129** 2233-2246.

Yin Y, Wang F & Ornitz DM 2011 Mesothelial- and epithelial-derived FGF9 have distinct functions in the regulation of lung development. *Development* **138** 3169-3177.

Yin Y, White AC, Huh SH, Hilton MJ, Kanazawa H, Long F & Ornitz DM 2008 An FGF-WNT gene regulatory network controls lung mesenchyme development. *Dev Biol* **319** 426-436.

Zako M, Shinomura T, Ujita M, Ito K & Kimata K 1995 Expression of PG-M(V3), an alternatively spliced form of PG-M without a chondroitin sulfate attachment in region in mouse and human tissues. *J Biol Chem* **270** 3914-3918.

Zhang H, Garber SJ, Cui Z, Foley JP, Mohan GS, Jobanputra M, Kaplan F, Sweezey NB, Gonzales LW & Savani RC 2009 The angiogenic factor midkine is regulated by

dexamethasone and retinoic acid during alveolarization and in alveolar epithelial cells. *Respir Res* **10** 77.

Zhou J & Cidlowski JA 2005 The human glucocorticoid receptor: one gene, multiple proteins and diverse responses. *Steroids* **70** 407-417.

Zhou Y, Horowitz JC, Naba A, Ambalavanan N, Atabai K, Balestrini J, Bitterman PB, Corley RA, Ding B-S, Engler AJ, et al. 2018 Extracellular matrix in lung development, homeostasis and disease. *Matrix Biol* **73** 77-104.

Zimmermann DR & Ruoslahti E 1989 Multiple domains of the large fibroblast proteoglycan, versican. *EMBO Journal* **8** 2975-2981.

Appendix A: Identification of Betamethasone-Regulated Target Genes and Cell Pathways in Fetal Rat Lung Mesenchymal Fibroblasts

Identification of Betamethasone-Regulated Target Genes and Cell Pathways in Fetal Rat Lung Mesenchymal Fibroblasts

Bennet K. L. Seow,[1,2] Annie R. A. McDougall,[2,3] Kelly L. Short,[1] Megan J. Wallace,[2,3] Stuart B. Hooper,[2,3] and Timothy J. Cole[1,4]

[1]Department of Biochemistry and Molecular Biology, Monash University, Melbourne, Victoria 3800, Australia; [2]The Ritchie Centre, Hudson Institute of Medical Research, Clayton, Victoria 3168, Australia; [3]Department of Obstetrics and Gynaecology, Monash University, Clayton, Victoria 3168, Australia; and [4]Division of Endocrinology and Metabolism, Hudson Institute of Medical Research, Clayton, Victoria 3168, Australia

ORCiD numbers: 0000-0001-5725-5010 (T. J. Cole).

Preterm birth is characterized by severe lung immaturity that is frequently treated antenatally or postnatally with the synthetic steroid betamethasone. The underlying cellular targets and pathways stimulated by betamethasone in the fetal lung are poorly defined. In this study, betamethasone was compared with corticosterone in steroid-treated primary cultures of fetal rat lung fibroblasts stimulated for 6 hours and analyzed by whole-cell transcriptome sequencing and glucocorticoid (GC) receptor (GR) chromatin immunoprecipitation sequencing (ChIP-Seq) analysis. Strikingly, betamethasone stimulated a much stronger transcriptional response compared with corticosterone for both induced and repressed genes. A total of 483 genes were significantly stimulated by betamethasone or corticosterone, with 476 stimulated by both steroids, indicating a strong overlap in regulation. Changes in mRNA levels were confirmed by quantitative PCR for eight induced and repressed target genes. Pathway analysis identified cell proliferation and cytoskeletal/cell matrix remodeling pathways as key processes regulated by both steroids. One target, transglutaminase 2 (Tgm2), was localized to fetal lung mesenchymal cells. Tgm2 mRNA and protein levels were strongly increased in fibroblasts by both steroids. Whole-genome GR ChIP-Seq analysis with betamethasone identified GC response element–binding sites close to the previously characterized GR target genes Per1, Dusp1, Fkbp5, and Sgk1 and near the genes identified by transcriptome sequencing encoding Crispld2, Tgm2, Hif3α, and Kdr, defining direct genomic induction of expression in fetal lung fibroblasts via the GR. These results demonstrate that betamethasone stimulates specific genes and cellular pathways controlling cell proliferation and extracellular matrix remodeling in lung mesenchymal fibroblasts, providing a basis for betamethasone's treatment efficacy in preterm birth. **(*Endocrinology* 160: 1868–1884, 2019)**

ISSN Online 1945-7170

Received 17 December 2018. Accepted 14 May 2019.
First Published Online 20 May 2019

Abbreviations: / , null or deficient; *Aspa*, aspartoacylase; BAM, Binary Alignment/Map; ChIP-Seq, chromatin immunoprecipitation sequencing; *Cntfr*, ciliary neurotrophic factor receptor; *Crispld2*, cysteine-rich secretory protein Limulus factor C, Coch-5b2, and Lgl1 domain containing 2; *Dusp1*, dual-specificity phosphatase 1; E, embryonic day; ECM, extracellular matrix; *Edn1*, endothelin 1; FDR, false discovery rate; *Fkbp5*, FK506 binding protein 5; *Foxc2*, forkhead box C2; GC, glucocorticoid; GDNF, glial cell line–derived neurotrophic factor; GR, glucocorticoid receptor; GRE, glucocorticoid response element; HA, hyaluronan; *Has2*, hyaluronan synthase 2; *Hif3α*, hypoxia-inducible factor 3α; IPA, Ingenuity® Pathway Analysis; *Kdr*, kinase insert domain receptor; LCCL, Limulus factor C, Coch-5b2, and Lgl1; NGS, next-generation sequencing; *Nov*, nephroblastoma overexpressed; *Pde1a*, phosphodiesterase 1A, calmodulin dependent; *Per1*, period circadian clock 1; PKA, protein kinase A; *Plk2*, Polo-like kinase 2; q, quantitative; Rap1, Ras-related protein 1; RNA-Seq, RNA-sequencing; *Rps29*, ribosomal protein 29; RTK, receptor tyrosine kinase; *Rxfp1*, relaxin/insulin-like family peptide receptor 1; S-1P, sphingosine-1-phosphate; *Sgk1*, serum- and glucocorticoid-regulated kinase 1; *Spry1*, sprouty receptor tyrosine kinase signaling antagonist 1; *Srgap3*, SLIT-ROBO Rho GTPase-activating protein 3; TBST, Tris-buffered saline–Tween 20, 0.1%; Tgm2, transglutaminase 2; *Timp3*, tissue inhibitor of metalloproteinase 3; TSS, transcriptional start site; VEGFR, vascular endothelial growth factor receptor.

Glucocorticoids (GCs) are important steroid hormones that facilitate the final stage of fetal lung development (1). The primary role of GCs is to induce rapid lung remodeling by thinning the pulmonary interstitial tissue to facilitate efficient gas exchange at birth (1–3). Other reported benefits of GCs during lung development include increased lung liquid reabsorption (4), differentiation of type II alveolar epithelial cells, and increased lung surfactant synthesis (5). Many preterm babies (<37 weeks gestation age) are born before the endogenous fetal GC surge and have a structurally immature lung that is characterized by reduced pulmonary surfactant, a thickened mesenchymal layer, and immature terminal alveolar development. A single course of synthetic GCs, such as betamethasone, administered antenatally to pregnant women at risk for preterm delivery, reduces the incidence of respiratory distress syndrome in the infant by ~35% to 50% (6, 7). Although GCs are used globally as a routine therapy for driving accelerated fetal lung maturation, the molecular mechanisms underlying their effects on the lung remain poorly understood. Previous studies also suggest that there could be additional adverse side effects of synthetic GC treatment in other developing organs, such as decreased formation of brain white matter, reduced total brain tissue volume (8), altered systemic endocrine functions (9, 10), decreased fetal growth (11), and reduced placental weight (12, 13).

The classic genomic pathway of GC signaling begins with GCs diffusing into the cell and binding to the intracellular GC receptor (GR). This induces a conformational change that activates the GR to become a ligand-dependent transcription factor that dimerizes, translocates to the nucleus, and binds to specific GC-response elements (GREs) near genomic target genes. Upon binding, the GR regulates gene expression through transactivation or transrepression of target genes (14). We have previously shown, using conditional GR-deficient (GR /) mice, that GC-induced lung maturation is primarily mediated via actions in lung mesenchymal cells (15, 16). To investigate further the molecular mechanisms of GC signaling in lung mesenchymal cells during lung development, we have used a whole genome-wide next-generation sequencing (NGS)–RNA-sequencing (RNA-Seq) and GR chromatin immunoprecipitation sequencing (ChIP-Seq) approach to identify the subset of genes specifically regulated by the GR in fetal rat lung fibroblast cells, comparing regulation by the endogenous GC corticosterone and the clinically relevant and more potent synthetic GC betamethasone. We show that betamethasone and corticosterone regulate a similar discrete subset of ~480 target genes in primary fetal rat lung fibroblasts. Strikingly, however, betamethasone drives a much higher level of induction in nearly all gene targets tested to illicit a stronger GC response compared with corticosterone. Two specific GC-regulated targets, transglutaminase 2 (*Tgm2*) and cysteine-rich secretory protein Limulus factor C, Coch-5b2, and Lgl1 (LCCL) domain containing 2 (*Crispld2*), were shown to be strongly induced early response genes associated with normal lung development and were directly induced by GCs via the GR.

Materials and Methods

Animals and isolation of fetal rat lung fibroblast cells

All experimental procedures involving the use of animals were approved by the Monash University Animal Ethics Committee. At embryonic day 20 (E20; term ~E22), pregnant Sprague-Dawley rats were humanely euthanized by CO_2 inhalation. Fetal lungs were harvested, and primary fetal rat lung fibroblasts were isolated by differential attachment, as previously described (17, 18). All cells isolated from a single litter were pooled together, and each litter was considered as an n = 1 biological replicate. Cells were seeded onto six-well tissue-culture plates at a density of 3.31×10^5 cells/cm^2 in Waymouth MB 752/1 medium [containing 10% charcoal/dextran fetal bovine serum (Thermo Fisher Scientific, Waltham, MA), 50 U/mL penicillin, and 50 μg/mL streptomycin] and incubated overnight at 37°C in 5% CO_2.

GC treatment of fibroblast cells

After overnight culture, fetal rat lung fibroblasts were treated with the following: (i) 1 μM to 10 nM betamethasone (Celestone Chronodose; Schering-Plough, Kenilworth, NJ), (ii) 1 μM corticosterone (Sigma-Aldrich, St. Louis, MO), or (iii) vehicle control (0.01% EtOH), in Waymouth MB 752/1 medium (containing 10% charcoal/dextran fetal bovine serum, 50 U/mL penicillin, and 50 μg/mL streptomycin). After 6 hours at 37°C in 5% CO_2, total RNA was collected for sequencing or real-time quantitative (q)PCR. Additional experiments included fetal rat lung fibroblast cells treated with the following: (iv) 1 μM betamethasone + 10 μM RU486 (Sigma-Aldrich), (v) 1 μM corticosterone + 10 μM RU486, or (vi) vehicle control (0.01% EtOH) + 10 μM RU486 for 6 hours, followed by total RNA collection for 24 hours, followed by protein extraction. To examine the dose response to betamethasone, the human WI-38 fetal lung fibroblast cell line was incubated with 1 μM to 10 nM betamethasone for 6 hours and changes in mRNA levels of three target genes assessed by real-time qPCR. Experiments were performed using technical triplicate or quadruplicate wells and were repeated using three to four individual biological experiments for each type of analysis.

$GR^{-}/^{-}$ mice and tissue collection

$GR^{-}/^{-}$ mice were generated as previously described (19). At E18.5 (term E20), pregnant mice were humanely euthanized, and fetal mice were removed from the uterus and euthanized by decapitation. The fetal lung was immersion fixed with 4% paraformaldehyde and then embedded in paraffin for histological examination or snap frozen in liquid N_2 for molecular analysis.

NGS–RNA-Seq and GR ChIP-Seq analysis

Total RNA was isolated from fetal rat lung fibroblast cells using the RNeasy Mini RNA extraction kit (Qiagen, Redwood City, CA), according to the manufacturer's instructions. NGS–RNA-Seq was performed by the Monash Health Translation Precinct Medical Genomics Facility, using Illumina 100-base sequencing chemistry in a paired read format performer on the HiSeq 1500 sequencing system (Illumina, San Diego, CA). The raw FASTQ files were processed using the RNAsik pipeline (Monash Bioinformatics Platform, Australia). In brief, FASTQ files were aligned to rat genome [Rnor_6.0 (Ensembl release 89)] using the STAR program (Cold Spring Harbor Laboratory, Huntington, NY), after which, the featureCounts function (Walter+Eliza Hall Institute of Medical Research, Australia) was used to count the reads to annotated features in the rat genome. The final RNA-Seq differential gene-expression data were presented in Degust (formerly DGE-Vis; Monash Bioinformatics Platform) for analysis. For whole-genome GR ChIP-Seq analysis, steroid-treated fibroblast cell samples were fixed and lysed and chromatin sheared using the True MicroChIP kit (Diagenode, Liege, Belgium) and GR ChIP DNA fragments isolated using the MicroChIP DiaPure columns (Diagenode), per the manufacturer's instructions, with the following modifications: all reagents were provided in the kit with exception of the ChIP-grade mouse anti-rat human GR monoclonal antibody (20) (1 μg/μL; Diagenode; c15200010), Hanks balance salt solution, 100% EtOH, and 37% formaldehyde. ChIP DNA fragments were cloned in DNA libraries and sequenced with 75 bp single end reads on the NextSeq 550 sequencing system (Illumina). Adaptors were trimmed from the raw FASTQ files using Trimmomatic v0.35 (Rheinisch-Westfälische Technische Hochschule Aachen University, Aachen, Germany). Sequences were mapped to the rat genome [Rnor_6.0 (Ensembl release 89)] using Bowtie2 v2.2.5 (Johns Hopkins University, Baltimore, MD). The resulting Sequence Alignment/Map files were converted to Binary Alignment/Map (BAM) files using Samtools, version 1.4.1 (Genome Research Limited, Hinxton, UK). The BAM files were filtered to remove unmapped and low-quality reads and then sorted using Samtools. Duplicate reads were marked using Picard, version 2.9.0 (Broad Institute, Boston, MA). As each input and immunoprecipitation sample had four sample replicates, these were merged together into one BAM file for each individual treatment group using Samtools. The final data were visualized using Integrative Genomics Viewer (Broad Institute).

RNA isolation, cDNA synthesis, and real-time qPCR

Total RNA and cDNA were prepared from fetal lung fibroblast cells, WI-38 cells, or $GR^{-/-}$ mouse lungs using TRIzol reagent (Invitrogen, Carlsbad, CA) and Moloney murine leukemia virus RT (Promega, Madison, WI), respectively, per the manufacturer's instructions. Relative mRNA levels of *Tgm2*, nephroblastoma overexpressed (*Nov*), *Crispld2*, hypoxia-inducible factor 3α (*Hif3α*), aspartoacylase (*Aspa*), SLIT-ROBO Rho GTPase-activating protein 3 (*Srgap3*), tissue inhibitor of metalloproteinase 3 (*Timp3*), kinase insert domain receptor (*Kdr*), hyaluronan (HA) synthase 2 (*Has2*), endothelin 1 (*Edn1*), Polo-like kinase 2 (*Plk2*), relaxin/insulin-like family peptide receptor 1 (*Rxfp1*), phosphodiesterase 1A, calmodulin dependent (*Pde1a*), sprouty receptor tyrosine kinase (RTK) signaling antagonist 1 (*Spry1*), forkhead box C2 (*Foxc2*), and ciliary neurotrophic factor receptor (*Cntfr*) were measured by real-time qPCR (7900HT Fast Real-Time PCR system), as previously described (17). The sequence of qPCR primers were the following (all forward/reverse): *Tgm2* rat GGAGAAGAGCGAAGGAACAT/GGAGAAGAGCGAAGGAACAT, mouse CAGCCGATGATGTGTACCTA/CAGCCGATGATGTGTACCTA, human CGTGACCAACTACAACTCGG/CATCCACGACTCCACCCAG; *Crispld2* rat GCTTGGAGTCCCTGAGTAAA/GCTTGGAGTCCCTGAGTAAA, mouse GCACCCACTACACACAGATG/GCACCCACTACACACAGATG, human GCCCAAGGTCACTCTCTTAGA/GTTGTGCAGCATGAGGATCTC; ribosomal protein 29 (*Rps29*) rat GACATAGGCTTCATTAAGTTG/GACATAGGCTTCATTAAGTTG, mouse GCAAATACGGGCTGAACA/GCAAATACGGGCTGAACA, human GTGCCAAGGAAGACAGCTCA/GGTTCTCGCTCTTGTCGTGT; *Nov* rat ATGGTTCCAGAGGGAGACA/ATGGTTCCAGAGGGAGACA, mouse CGCAGACCCCAACAACCAGA/CGCAGACCCCAACAACCAGA; *Hif3α* rat AGGACCCTGACACTCTGGA/AGGACCCTGACACTCTGGA, mouse GAGGGTTTCGTCATGGTACTC/GAGGGTTTCGTCATGGTACTC; *Aspa* rat GCAGGATCAAGACTGGAAAC/GCAGGATCAAGACTGGAAAC, mouse AATCTTAGCAAAGAGATGTCTGAAG/AATCTTAGCAAAGAGATGTCTGAAG; *Srgap3* rat TTGAGAACGAAGAGGTTAGGAAA/TTGAGAACGAAGAGGTTAGGAAA, mouse ACCTGGGCTTGTACTGCTCC/ACCTGGGCTTGTACTGCTCC; *Timp3* rat AGACCTGTCCCACCTCACCT/AGACCTGTCCCACCTCACCT, mouse TGGTGCCAAGCCAGAAAGAA/TGGTGCCAAGCCAGAAAGAA; *Kdr* rat TTCCCTCCATCCACCCAAGC/TTCCCTCCATCCACCCAAGC, mouse ATTGTTGGCGATGAACTCAC/ATTGTTGGCGATGAACTCAC; *Has2* rat GCTGAACAAGCATTGTGAGAG/GCTGAACAAGCATTGTGAGAG, mouse TCTCCTTCCTCAGCAGCGTG/TCTCCTTCCTCAGCAGCGTG; *Edn1* rat CCCAAAGTACCATGCAGAAA/CCCAAAGTACCATGCAGAAA, mouse ACGCACAACCGAGCACATTG/ACGCACAACCGAGCACATTG; *Plk2* rat CTCCAGCCTCCTCCAACTAC/CTCCAGCCTCCTCCAACTAC, mouse TTGACAGAGCCAGAAGTCCG/TTGACAGAGCCAGAAGTCCG, human CTACGCCGCAAAAATTATTCCTC/TCTTTGTCCTCGAAGTAGTGG; *Rxfp1* rat ACATCAGTAAGTGCCTGCCT/ACATCAGTAAGTGCCTGCCT, mouse TCCAGTGGCTTCGCTCTAAG/TCCAGTGGCTTCGCTCTAAG; *Pde1a* rat ATGACTGGAGGGATCTTCGGA/ATGACTGGAGGGATCTTCGGA, mouse CAGACTGACTCCGTCCCATC/CAGACTGACTCCGTCCCATC; *Spry1* rat GCTTGGACACGGTAGTTGAC/GCTTGGACACGGTAGTTGAC, mouse TACCCTGCTTGCTCTGCTAC/TACCCTGCTTGCTCTGCTAC; *Foxc2* rat GCGGATTTGTAACCAGGCGA/GCGGATTTGTAACCAGGCGA, mouse GGATGTGCCCAAGGACAAGG/GGATGTGCCCAAGGACAAGG; *Cntfr* rat CGGCATCTCACCACTGAAGC/CGGCATCTCACCACTGAAGC, mouse GGGACATGGAGTGACTGGAG/GGGACATGGAGTGACTGGAG. The mRNA level of each gene was normalized to the appropriate species (rat, mouse, or human) *Rps29* RNA levels using the $\Delta\Delta$Ct method and expressed as a fold change relative to the mRNA levels of the control group.

Protein isolation and Western blot analysis

Protein was extracted from fibroblast cells, as previously described (18). Protein samples (40 μg), together with Precision Plus Protein™ Unstained Standards (Bio-Rad), were separated by SDS-PAGE at 200 V for 40 minutes on 1.5 mm polyacrylamide gels made from TGX Stain-Free FastCast

Acrylamide (Bio-Rad). Proteins were then transferred to Protran nitrocellulose membranes (0.45 mm; Schleicher and Schuell, Germany) at 4°C at 100 V for 50 minutes. Membranes were blocked with 5% skim milk in Tris-buffered saline–Tween 20 (0.1%; TBST) for 1 hour at room temperature with agitation. Membranes were then incubated with a rabbit monoclonal IgG primary antibody against TGM2 (1:200; Cell Signaling Technology, Danvers, MA; no. 3557) (21) or rabbit polyclonal IgG primary antibody against CRISPLD22 (1:100; Abcam, Cambridge, UK; catalog no. ab105656) (22), diluted in blocking buffer 5% skim milk in TBST overnight at 4°C. Membranes were washed in TBST (5 × 5 minutes) and then incubated with goat anti-rabbit IgG (1:1000; Cell Signaling Technology; no. 7074), along with Precision Protein StrepTactin–Horseradish Peroxidase Conjugate (1:10,000; Bio-Rad) for 1 hour at room temperature. Membranes were washed in TBST 5 × 5 minutes and then incubated in chemiluminescence reagent Clarity Western ECL Substrate (Bio-Rad) for 5 minutes. Membranes were imaged digitally using the ChemiDoc Touch Imaging System (Bio-Rad). Analysis was performed as previously described (18).

Histology and immunostaining

To determine the cell-specific localization of TGM2 and CRISPLD2 in the normally developing lung, sections of lung from wild-type mice were colabeled with either antibodies against TGM2 or CRISPLD2 simultaneously with antibodies against the epithelial marker pan-cytokeratin, as previously described (23). In brief, wild-type fetal mouse lung sections (5 μm, n = 3, one section/animal) were de-waxed and dehydrated. Antigen retrieval was performed by microwaving slides in 10 mM sodium citrate for a total of 27 minutes (7 minutes for boiling and another 20 minutes for antigen retrieval). Sections were blocked with 5% normal goat/donkey serum for 30 minutes at room temperature to prevent nonspecific binding. Sections were incubated in either rabbit anti-TGM2 (1:100; Cell Signaling Technology) (21) or rabbit anti-CRISPLD2 (1:100; Abcam) (22) in combination with mouse anti-pan-cytokeratin (1:200; Cell Signaling Technology) (24) overnight at 4°C and then in secondary antibody (anti-rabbit IgG, Alexa Fluor 488 conjugate, 1:1000; and anti-mouse IgG1, Alexa Fluor 555 conjugate, 1:1000; Thermo Fisher Scientific). Specificity of the antibodies was determined by individually omitting each of the primary antibodies. Immunofluorescent labeling of lung sections was visualized, and digital images were captured by use of a Nikon C1 confocal laser-scanning microscope. Fluorophores were excited specifically with 488 and 555 nm lasers and detected with 515/30 and 605/75 filters. High-power and digital images were captured for Z-stack analysis, which was performed using Autoaligner (Bitplane) and Fiji software. Sections were qualitatively assessed for colocalization between the epithelial marker pan-cytokeratin and the proteins TGM2 and CRISPLD2.

Pathway analysis

Online pathway analysis software data were analyzed through the use of Ingenuity® Pathway Analysis (IPA; Qiagen).

Statistical analysis

For all tissue-culture experiments, technical replicates were pooled and the data presented as means ± SEM of the biological replicates. All values from *in vivo* experiments are presented as means ±SEM of individual mice from different litters. The data were tested for normal distribution using Shapiro-Wilk before analysis, and $P \leq 0.05$ was considered significant. When only two groups were being compared, a nonpaired Student *t* test was used. When more than two groups were being compared, a one-way ANOVA was used. When significant differences were identified, a least-significant difference Tukey *post hoc* test was performed to determine which groups were significantly different. Statistical tests were performed using the software GraphPad Prism (version 6.04; GraphPad, San Diego, CA) and SigmaPlot (version 13).

Results

Treatment of rat fetal lung fibroblasts with GCs and transcriptome analysis

NGS transcriptome RNA-Seq was used to determine the subset of genes regulated by GCs in fetal rat lung fibroblast cells treated with either the endogenous GC corticosterone or the synthetic GC betamethasone. Primary cells were treated with steroids in charcoal-stripped fetal bovine serum medium for 6 hours and total RNA prepared for NGS analysis. Global changes in mRNA levels are shown with a heat map analysis, depicted in Fig. 1A, which shows a similar pattern of altered gene expression between betamethasone- and corticosterone-treated cells compared with control, with betamethasone primarily modulating the same groups of genes as corticosterone but in most cases, to a stronger degree. Individual Bland–Altman plots of betamethasone- (Fig. 1B) and corticosterone-treated (Fig. 1C) samples show that the majority of genes is significantly increased in expression following GC treatment, as opposed to the relatively small proportion that was decreased in mRNA level. In total, 483 genes, with a fold change ≥2 and false discovery rate (FDR) ≥0.05, were regulated by GCs (Fig. 1D), with the mRNA level of 358 genes increased by both betamethasone and corticosterone and 118 genes decreased by both betamethasone and corticosterone using these parameters. There was high overlap between genes regulated by betamethasone and corticosterone. Curiously, the mRNA levels of seven genes were increased by betamethasone yet were decreased by corticosterone treatment (Fig. 1D).

Pathway analysis

IPA software identified 292 pathways that involved one or more of the genes identified by the RNA-Seq analysis described above. The top eight important pathways were involved in regulation of cell proliferation and extracellular matrix (ECM) remodeling and are described in Table 1. These included the following: Gαq signaling, ERK/MAPK signaling, sphingosine-1 phosphate (S-1P) signaling, relaxin signaling, GC receptor signaling, Gαi signaling, protein kinase A (PKA)

signaling, and D-myo-inositol (1,4,5)-trisphosphate biosynthesis.

Analysis of gene targets upregulated by GC signaling

To confirm the validity of the NGS–RNA-Seq data, we performed real-time qPCR to quantify eight selected GC-induced genes (Table 2). In primary fetal lung fibroblast cells treated with betamethasone, there was a significant increase in the mRNA levels in all of the selected upregulated genes (Table 2), *Tgm2* ($P \leq 0.0001$, 17.1-fold), *Nov* ($P \leq 0.01$, 4.7-fold), *Crispld2* ($P \leq 0.001$, 12.9-fold), *Hif3α* ($P \leq 0.01$, fivefold), *Aspa* ($P \leq 0.05$, 2.5-fold), *Srgap3* ($P \leq 0.05$, 2.8-fold), *Timp3* ($P \leq 0.05$, 2.4-fold), and *Kdr* ($P \leq 0.05$, 29.7-fold), compared with controls (Fig. 2A–2D and 2I–2L). In primary fetal lung fibroblast cells treated with corticosterone, there was a significant increase in the mRNA levels of the following genes: *Tgm2* ($P \leq 0.05$, 8.81-fold), *Crispld2* ($P \leq 0.01$, 8.61-fold), and *Hif3α* ($P \leq 0.01$, 4.3-fold), compared with control-treated cell cultures (Fig. 2A, 2C, and 2D). There was no difference in the mRNA levels of *Nov*, *Aspa*, *Srgap3*, *Timp3*, and *Kdr* between cells treated with corticosterone and vehicle control (Fig. 2B and 2I–2L).

To determine if these target genes were directly regulated via the GR, fetal lung fibroblast cells were pre-incubated with the GR antagonist RU486, 1 hour before steroid treatment. Pretreatment with 10 μM RU486 completely blocked induction of *Tgm2* ($P \leq 0.0001$), *Nov* ($P \leq 0.001$), *Crispld2* ($P \leq 0.001$), *Hif3α* ($P \leq 0.01$), *Aspa* ($P \leq 0.01$), *Srgap3* ($P \leq 0.01$), and *Kdr* ($P \leq 0.05$) by betamethasone (Fig. 2A–2D, 2I, 2J, and 2L). There was no difference in the mRNA levels of *Timp3* between cells pretreated with 10 μM RU486 before treatment with betamethasone (Fig. 2K). The mRNA levels for *Tgm2* ($P \leq 0.05$), *Crispld2* ($P \leq 0.001$), and *Hif3α* ($P < 0.05$) were significantly lower in fibroblasts

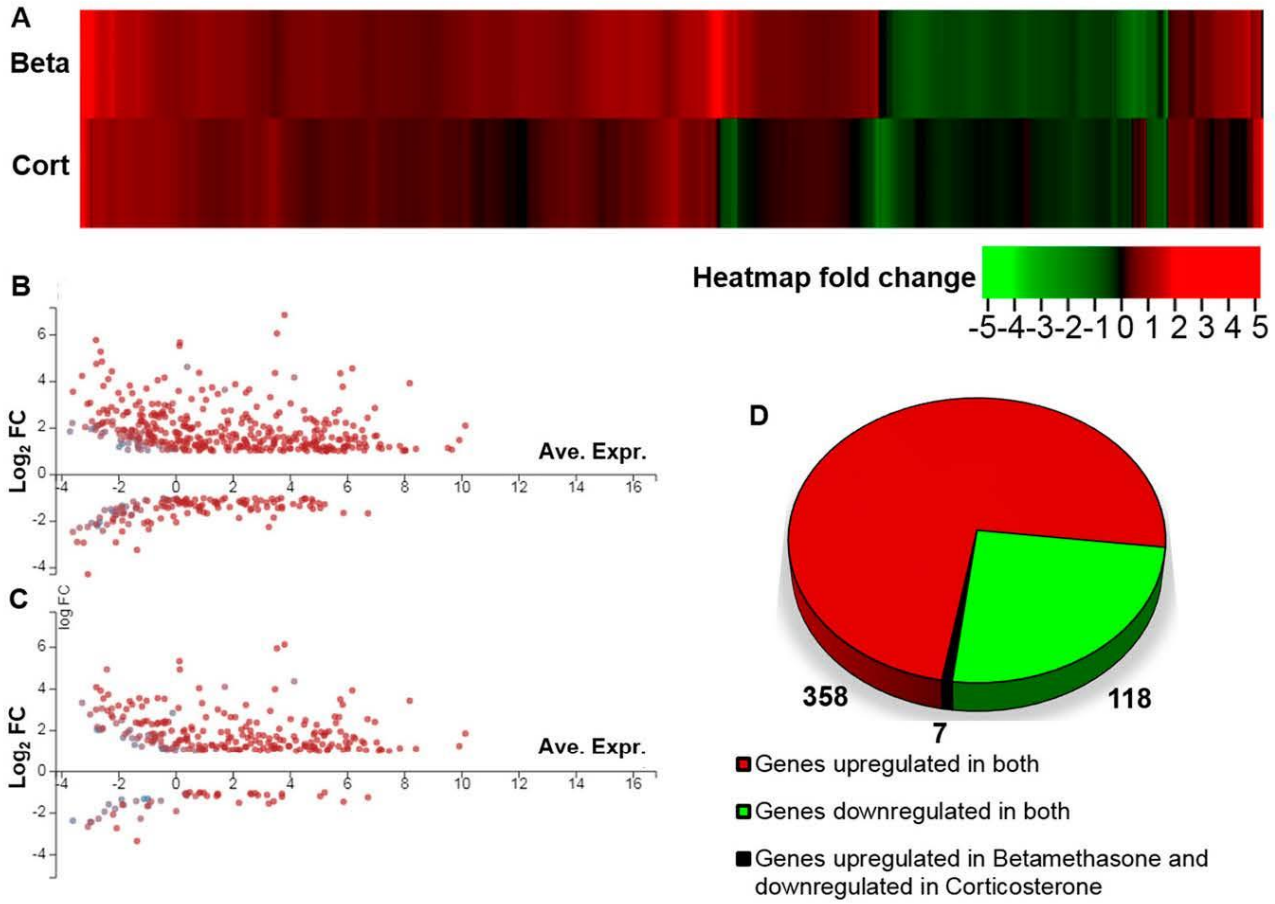

Figure 1. Genome-wide NGS–RNA-Seq of GC-treated primary fetal rat lung fibroblast cells (n = 4 per group). The RNA expression profile for corticosterone and betamethasone treatment groups was normalized to a vehicle-treated (solvent ethanol) control group [at a false discovery rate (FDR) = 0.05 and a minimum fold change (FC) of 2]. (A) A side-by-side heat map for the fold changes of induced and repressed genes in fibroblast cells treated with betamethasone (Beta) and corticosterone (Cort). Fold changes are represented as a $\log_2$ of the expression ratio for (B) betamethasone and (C) corticosterone against the average expression (Ave. Expr.) level of the vehicle control group within the same study. (D) Pie chart of identified GC-regulated genes between betamethasone and corticosterone against the vehicle treatment control group. A total of 510 genes were identified as significantly regulated by 6 h of GC treatment in rat lung fetal fibroblast cells.

Table 1. IPA-Generated Pathway Analysis From NGS–RNA-Seq Data

Biological Pathway	GC-Regulated Genes Identified With Pathway	Description[a]	*P* Value	*z* Score
Gαq signaling	*Hrh1, Plcb4, Nfkbia, Prkcb, Pld6, Rhof, Adra1d, Rgs7, Rhoj, Rgs4, Nfatc1*	Gαq is one of the four families of G-protein signaling molecules, which can promote Rho activation. Rho-associated protein kinase acts downstream of Rho to regulate cytoskeletal rearrangements.	0.0004	1.897
ERK/MAPK signaling	*Pparg, Ppp1r14c, Prkcb, Dusp1, Hspb7, Rapgef4, Itga3, Pak3, Pxn, Nfatc1*	The ERK/MAPK pathway transduces cellular information on meiosis/mitosis, growth, and differentiation within a cell. Activation of membrane-bound RTK leads to a cascade of events that ends up activating ERK (a MAPK) in the cytoplasm, which can phosphorylate cytoskeleton proteins, ion channels/receptors, and translation regulators.	0.0069	0.632
Sphingosine-1 phosphate signaling	*Plcb4, Plce1, Rhof, Rhoj, Adcy5, Sphk1, Adcy8*	Sphingolipids are a group of lipids that are signal transducers. Sphingolipids are linked to fatty acids to create ceramide. The addition of a phosphocholine substituent or sugar to ceramide gives rise to sphingolipid sphingomyelin. The bioactive sphingosine-1-phosphate (S-1P), a sphingolipid metabolite, has been linked to cell growth, survival, and motility, which are prominent. S-1P is a ligand for a family of G-protein-coupled receptors, which upon stimulation, result in either activation or inhibition of Rho and Rac (subfamily of small GTP-binding proteins). Activated Rho induces the formation of stress fibers, whereas activated Rac induces formation of the cortical actin network.	0.0089	1.890
Relaxin signaling	*Nfkbia, Gucy1b3, Adcy5, Pde7b, Gucy1a3, Pde2a, Rxfp1, Adcy8*	Relaxin is a polypeptide hormone best known for its connective tissue remodeling effects on the female reproductive system. It can relax cells by inducing changes in cell shape and the actin cytoskeleton. It also has a role in regulation of pituitary hormone release, renal vasculature, and lung and skin remodeling.	0.0112	0.00
GR signaling	*Il1r2, Bcl2l1, Dusp1, Sgk1, Nr3c2, Fkbp5, Nfkbia, Dpf1, Pgr, Il1b, Ptgs2, Nfatc1*	GCs are a class of steroid hormones that are released from the adrenal cortex under the control of the hypothalamic-pituitary-adrenal axis. GCs exert their effects by activation of the intracellular GR to modulate directly or indirectly the expression of target genes that contains the conserved GRE.	0.0141	NaN
Gαi signaling	*Gpr17, Htr1b, Rgs7, Lpar1, Adcy5, Adcy8, Rgs4*	Gαi/o is one of four families belonging to the heterotrimeric G-proteins, which are signaling molecules that transduce signals from a number of types of ligands, such as hormones. The Gαi protein is a downregulator of Rap1 signaling by inducing GTP hydrolytic activity. Rap1 belongs to the Ras subfamily of small GTP-binding proteins, which is known to control cell growth, differentiation, and survival.	0.0162	1.134
Heparan-sulfate biosynthesis (late stages)	*Hs3st3b1, Hs3st1, Chst3, Chst1*	This pathway initiates the formation of the tetrasaccharide linkage region on the core protein to make heparan-sulfate, which binds to various protein ligands (known as heparin-binding proteins). This regulates developmental processes, cell adhesion and motility, angiogenesis, blood coagulation, and tumor metastasis.	0.0004	NaN
Protein kinase A signaling	*Ppp1r14c, Plcb4, Pxn, Pde7b, Adcy5, Dusp1, Plce1, Nfkbia, Cnga4, Prkcb, Ptgs2, Adcy8, Pde2a, Ptprc, Nfatc1*	Protein kinase A (PKA) regulates processes as diverse as growth, development, memory, and metabolism.	0.0069	0.00

Abbreviations: NaN, not a number; Rap1, Ras-related protein 1.

[a]The descriptions were generated through the use of Ingenuity Target Explorer (Ingenuity® Systems).

Table 2. Upregulated Target Genes From Genome-Wide NGS–RNA-Seq

Gene ID	Description	Biological Function[a]	Mean Fold Change in Betamethasone vs Ethanol	Mean Fold Change in Corticosterone vs Ethanol	FDR
Tgm2	Transglutaminase 2	A calcium-dependent enzyme that stabilizes ECM proteins	20.39	11.39	7.76e-13
Nov	Nephroblastoma overexpressed	A member of the cysteine-rich angiogenic protein 61, connective tissue growth factor, Nov protein family that associates with the ECM and plays an important role in cardiovascular development and fibrosis	14.72	6.28	9.06e-9
Crispld2	Cysteine-rich secretory protein LCCL domain containing 2	A GC-inducible gene that regulates lung development by driving mesenchymal-epithelial interactions	15.24	10.85	1.64e-13
Hif3α	Hypoxia-inducible factor 3, alpha subunit	Part of the α/β-subunit heterodimeric transcription factor that regulates a cellular response to hypoxia	46.2	40.5	1.13e-6
Aspa	Aspartoacylase	An enzyme that catalyzes the conversion of *N*-acetyl-L-aspartic acid to aspartate and acetate to help maintain white matter in the brain	13.45	2.44	2.25e-8
Srgap3	SLIT-ROBO Rho GTPase-activating protein 3	GTPase-activating protein for Rac1, which is involved in actin cytoskeleton remodeling and cell alignment in fetal epithelial cells	5.8	3.0	1.25e-5
Timp3	Tissue inhibitor of metalloproteinase 3	Inhibits matrix metalloproteinases to prevent the degradation of the ECM	3.16	1.89	1.38e-11
Kdr	Kinase insert domain receptor	A VEGFR responsible for endothelial proliferation, survival, migration, tubular morphogenesis, and sprouting	11.08	8.11	5.20e-8

Abbreviation: VEGFR, vascular endothelial growth factor receptor.

[a]The descriptions were generated through the use of Ingenuity Target Explorer (Ingenuity® Systems).

pretreated with 10 μM RU486 before treatment with corticosterone (Fig. 2A, 2C, and 2D). There was no difference in the mRNA levels of *Nov*, *Aspa*, *Srgap3*, *Timp3*, and *Kdr* between cells pretreated with 10 μM RU486 before treatment with corticosterone (Fig. 2B and 2I–2L).

The requirement of the GR for induction of these target genes *in vivo* in the lung was also examined with whole mouse fetal lung RNA from GR $^{/}$ mice and littermate controls. In E18.5 GR $^{/}$ mouse lung, there was a significant decrease in the mRNA levels for *Tgm2* ($P \leq 0.01$, 3.5-fold), *Crispld2* ($P \leq 0.001$, 6.6-fold), *Hif3α* ($P \leq 0.01$, 3.8-fold), *Aspa* ($P \leq 0.01$, 4.5-fold), *Timp3* ($P \leq 0.01$, 3.3-fold), and *Kdr* ($P \leq 0.05$, 1.7-fold) compared with the wild-type control lung (Fig. 2E, 2G, 2H, 2M, 2O, and 2P). The mRNA levels of *Nov* and *Srgap3* were not different between E18.5 wild-type control and GR $^{/}$ mouse lung (Fig. 2F and 2N).

Analysis of genes downregulated by GC signaling

To confirm the gene-expression changes of the NGS–RNA-Seq data, we performed real-time qPCR to quantify eight selected GC-repressed genes (Table 3). In primary fetal lung fibroblast cells treated with betamethasone, the mRNA levels for *Has2* ($P \leq 0.01$, 3.3-fold) and *Plk2* ($P \leq 0.0001$, 2.5-fold) were significantly lower compared with control-treated cultures (Fig. 3A and 3C). There was no difference in the mRNA levels for *Edn1*, *Rxfp1*, *Pde1a*, *Spry1*, *Foxc2*, and *Cntfr* between controls and fibroblasts treated with betamethasone (Fig. 3B, 3D, and 3I–3L). In fetal lung fibroblast cells treated with corticosterone, the mRNA levels of *Has2* ($P \leq 0.05$, 2.4-fold) and *Plk2* ($P \leq 0.0001$, 2.4-fold) were significantly lower compared with control-treated cells (Fig. 3A and 3C). There was no significant difference with the mRNA levels for *Edn1*, *Rxfp1*, *Pde1a*, *Spry1*, *Foxc2*, and *Cntfr* between control cells and fibroblasts treated

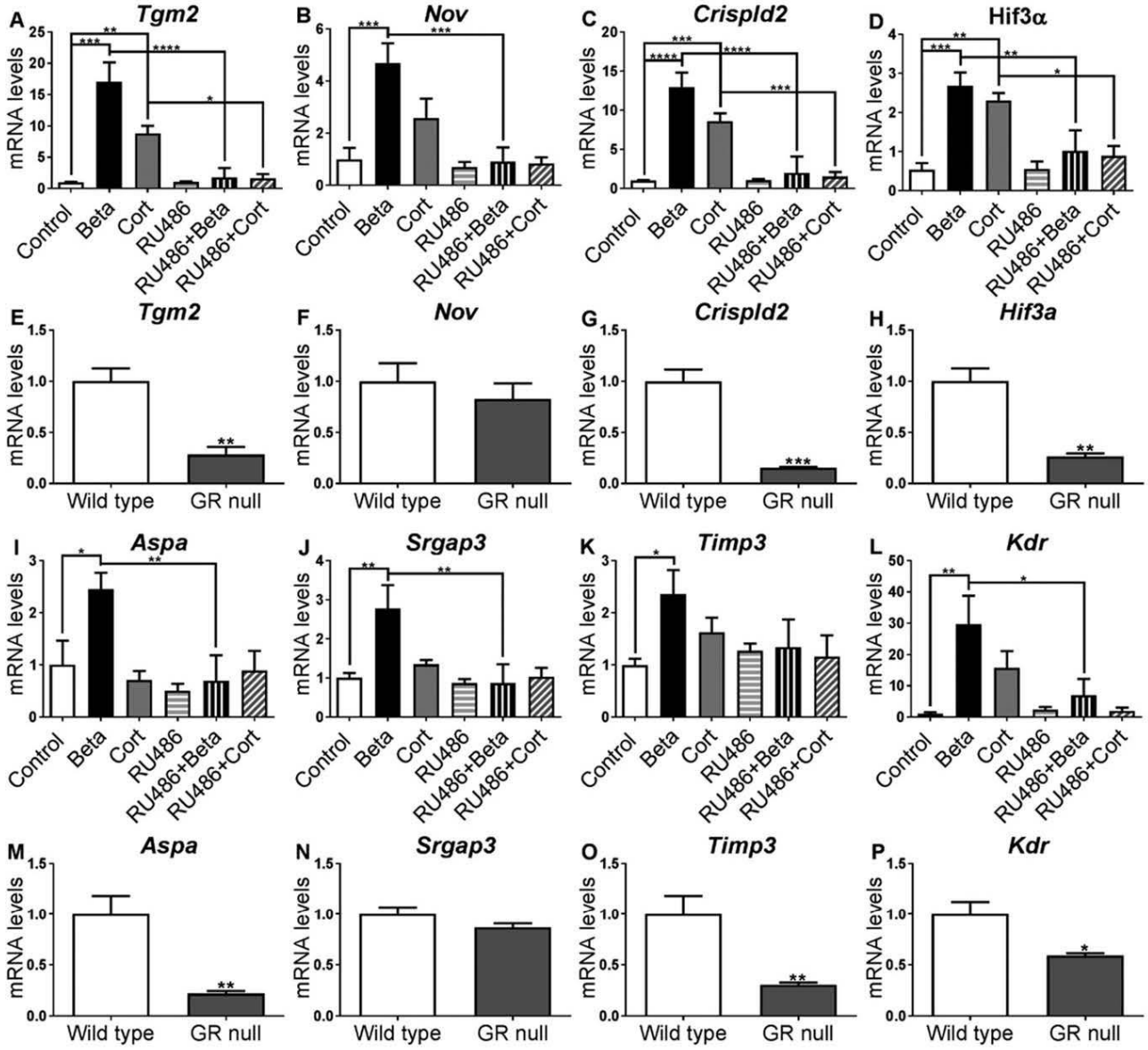

Figure 2. mRNA levels of eight induced GC-target genes (means ± SEM). (A) *Tgm2*, (B) *Nov*, (C) *Crispld2*, (D) *Hif3α*, (I) *Aspa*, (J) *Srgap3*, (K) *Timp3*, and (L) *Kdr* levels in fetal rat lung fibroblast cells (n = 4), treated for 6 h with vehicle (Control; white bars), betamethasone (Beta; black bars), corticosterone (Cort; dark gray bars), RU486 (horizontally striped bars), RU486 and betamethasone (vertically striped bars), and RU486 and corticosterone (diagonally striped bars). mRNA levels (means ± SEM) of (E) *Tgm2*, (F) *Nov*, (G) *Crispld2*, (H) *Hif3a*, (M) *Aspa*, (N) *Srgap3*, (O) *Timp3*, and (P) *Kdr* in lung tissue from wild-type control mice (n = 5) and total $GR^{-}/^{-}$ mice (n = 5) at E18.5. The mRNA levels in all groups are expressed relative to levels of *Rps29* mRNA and as a fold change relative to control group. Significant differences are indicated by $*P \leq 0.05$, $**P \leq 0.01$, $***P \leq 0.001$, and $****P < 0.0001$.

with corticosterone (Fig. 3B, 3D, and 3I–3L). These downregulated genes were also analyzed for direct regulation by the GR in fetal lung fibroblasts by pretreating fibroblast cell cultures (as described above) with the GR antagonist RU486. There was no significant differences in the mRNA levels of any of the GC-repressed genes between fibroblast cells treated with betamethasone alone and fibroblasts treated with betamethasone plus pretreatment with RU486. The mRNA levels for *Has2* ($P < 0.01$, 2.6-fold), *Plk2* ($P < 0.01$, 2.5-fold), and *Cntfr* ($P < 0.01$, 2.6-fold) were significantly higher in fibroblast cells treated with corticosterone plus RU486 compared with fibroblasts treated with corticosterone alone (Fig. 3A, 3C, and 3L). There was no significant difference in the mRNA levels for *Edn1*, *Rxfp1*, *Pde1a*, *Spry1*, and *Foxc2* (Fig. 3B, 3D, and 3I–3K) between control cells and fibroblasts treated with corticosterone. The requirement of the GR for repression of these target genes *in vivo* was also examined with whole mouse fetal lung total RNA from GR $^{/}$ mice. The mRNA level of *Spry1* ($P \leq 0.01$, 1.5-fold; Fig. 3N) was significantly increased in GR $^{/}$ mice

Table 3. Downregulated Target Genes From Genome-Wide NGS–RNA-Seq

Gene	Description	Biological Function[a]	Mean Fold Change in Betamethasone vs Ethanol	Mean Fold Change in Corticosterone vs Ethanol	FDR
Has2	HA synthase 2	Involved in the synthesis of HA, a component in ECM formation, which functions as a matrix to facilitate cell migration, such as the in-growth of blood vessels and fibroblasts during wound healing	4.7	2.9	3.42e-9
Edn1	Endothelin 1	A member of the endothelin family of peptides that positively regulates cell proliferation and endothelial cell migration	2.4	2.0	4.26e-9
Plk2	Polo-like kinase 2	A member of the polo family of serine/threonine protein kinases that facilitates cells undergoing rapid cell division	3.1	2.7	2.78e-10
Rxfp1	Relaxin/insulin-like family peptide receptor 1	A G protein-coupled 7-transmembrane receptor for relaxin, which reduces matrix synthesis and increases ECM degradation	5.1	3.1	0.01
Pde1a	Phosphodiesterase 1A, calmodulin dependent	Regulates intracellular cyclic nucleotide concentrations through hydrolysis of cAMP and/or cyclic GMP, which regulates myofibroblast formation	4.1	3.8	1.43e-3
Spry1	Sprouty RTK signaling antagonist 1	Functions in conjunction with Spry2 to promote normal lung airway tube development by negative regulating of ERK1/2 signaling	2.7	2.3	5.36e-10
Foxc2	Forkhead box C2	May play a role in the development of mesenchymal tissue	2.4	2.0	1.05e-4
Cntfr	Ciliary neurotrophic factor receptor	Plays a critical role in neuronal cell survival, differentiation, and gene expression	2.7	6.6	2.55e-3

[a]The descriptions were generated through the use of Ingenuity Target Explorer (Ingenuity® Systems).

compared with wild-type controls, whereas *Pde1a* mRNA levels ($P \leq 0.05$, 1.3-fold; Fig. 3M) were significantly lower in GR $^{/}$ mouse lung compared with wild-type controls. The mRNA levels for *Has2*, *Edn1*, *Plk2*, *Rxfp1*, *Foxc2*, and *Cntfr* were not different between wild-type controls and the GR $^{/}$ mouse lung (Fig. 3E–3H, 3K, and 3L). Finally, the sensitivity for the GC-mediated response was assessed for three target genes (*Crispld2*, *Tgm2*, and *Plk2*) at a dose of betamethasone from 1 μM to 10 nM in a human fetal lung fibroblast cell line (WI-38; Fig. 4A–4C) and demonstrated regulation of all three targets down to 10^{-8} M of betamethasone.

GC regulation of CRISPLD2 and TGM2 protein levels in the fetal lung

Protein levels for CRISPLD2 and TGM2 were analyzed in rat fetal fibroblast cells by Western blot analysis, following 24 hour stimulation with both corticosterone and betamethasone. CRISPLD2 protein levels were not significantly different between fibroblast cells treated with corticosterone, betamethasone, or vehicle control (Fig. 4D and 4E). TGM2 protein levels, however, were significantly higher in fibroblast cells treated for 24 hours with betamethasone ($P \leq 0.05$, 4.1-fold) and corticosterone ($P \leq 0.05$, fivefold) compared with control cells (Fig. 4F and 4G). CRISPLD2 protein levels were undetectable in the media of fibroblast cells treated at 24 hours in all groups tested (data not shown).

Cell localization of CRISPLD2 and TGM2 protein in the fetal lung

CRISPLD2 was localized primarily to the cytoplasm of both pan-cytokeratin-positive epithelial cells in the parenchyma and airways, as well as pan-cytokeratin-negative cells, most likely mesenchymal cells at E18.5 (Fig. 5A and 5B) and E16.5 (data not shown). At E16.5, TGM2 was colocalized to pan-cytokeratin-positive epithelial cells in the developing airways, as well as to the pan-cytokeratin-negative mesenchymal cell layer of the

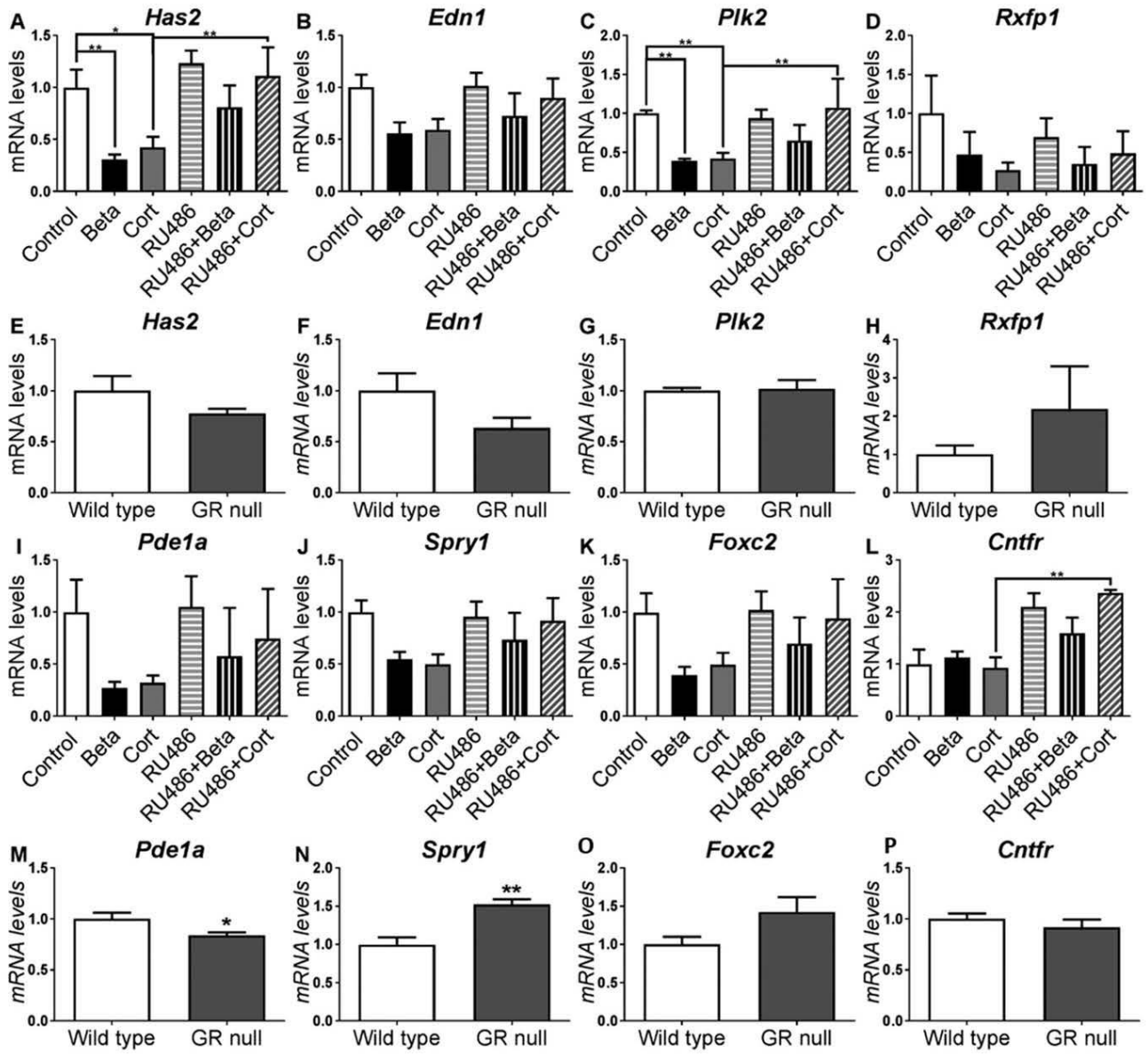

Figure 3. Steady-state mRNA levels of eight repressed GC-target genes (means ± SEM). (A) *Has2*, (B) *Edn1*, (C) *Plk2*, (D) *Rxfp1*, (I) *Pde1a*, (J) *Spry1*, (K) *Foxc2*, and (L) *Cntfr* in fetal rat lung fibroblast cells (n = 4) treated for 6 h with vehicle (Control; white bars), betamethasone (Beta; black bars), corticosterone (Cort; gray bars), RU486 (horizontal striped bars), RU486 and betamethasone (vertical striped bars), and RU486 and corticosterone (diagonal striped bars). mRNA levels (means ± SEM) of (E) *Has2*, (F) *Edn1*, (G) *Plk2*, (H) *Rxfp1*, (M) *Pde1a*, (N) *Spry1*, (O) *Foxc2*, and (P) *Cntfr* in lung tissue from wild-type control mice (n = 5) and total $GR^{-}/^{-}$ mice (n = 5) at E18.5. The mRNA levels in all groups are expressed relative to levels of *Rps29* mRNA and as fold change relative to control group. Significant differences are indicated by $*P < 0.05$, $**P < 0.01$, and $***P < 0.001$.

lung (data not shown). At E18.5, TGM2 was localized exclusively to pan-cytokeratin-negative cells. These appeared primarily to be cells in the mesenchymal layer of the lung, as well as to endothelial cells in blood vessels (Fig. 5C and 5D).

Identification of GRE-binding sites near GC-responsive target genes in primary fetal fibroblasts by GR ChIP-Seq analysis

To define further the direct induction of GC-responsive target genes with respect to the binding of the GR to specific sites within the genome in the nucleus, we performed whole-genome GR ChIP-Seq analysis with primary fetal rat lung fibroblast cells following treatment with betamethasone. Whole-cell GR ChIP DNA was sequenced and analyzed for identity and location in the rat genome sequence with Integrative Genomics Viewer software (Broad Institute), with Beta-ChIP peaks assigned across the rat genome. We detected the presence of ~168 prominent GR/betamethasone peaks (data not shown) that included many previously characterized GREs for regulated target genes, such as period circadian

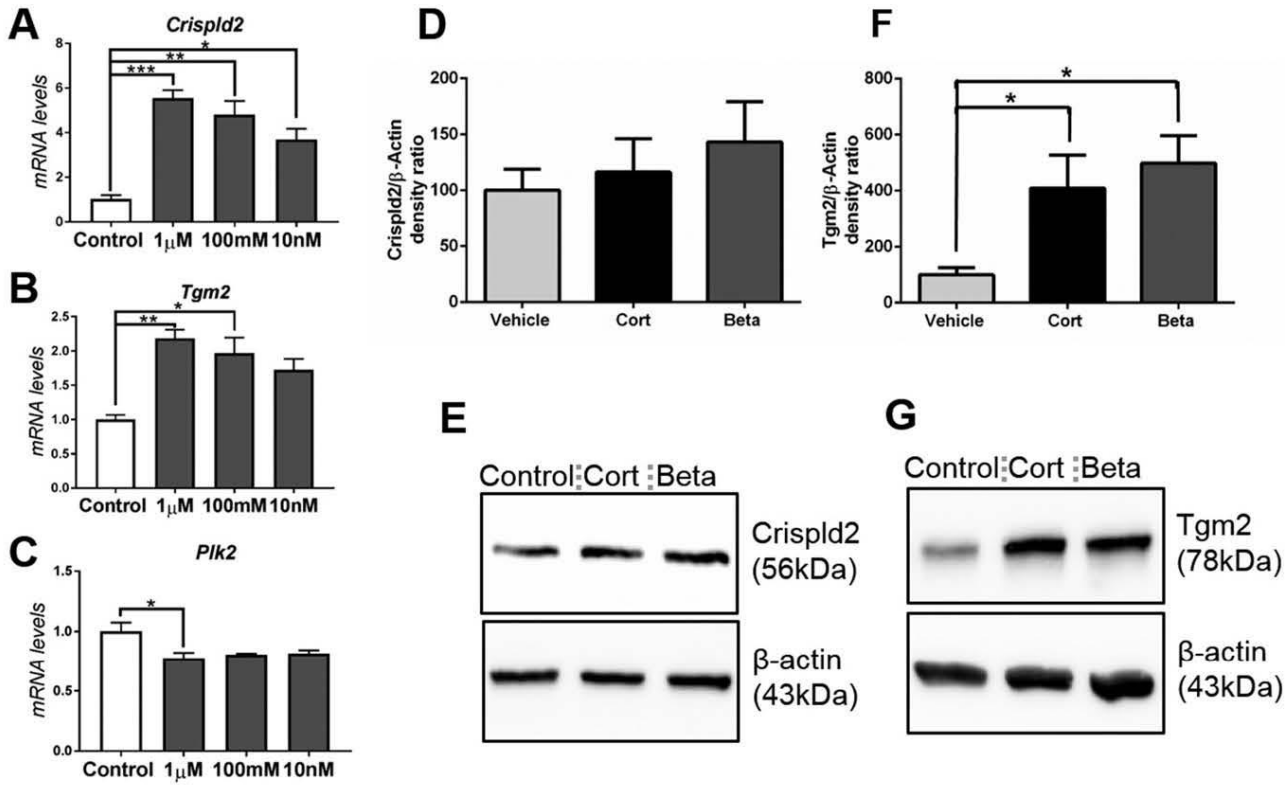

Figure 4. (A–C) Dose response for the three GC-target genes *Crispld2*, *Tgm2*, and *Plk2* from 1 μM to 10 nM betamethasone in the human fetal lung fibroblast cell line WI-38, and Western blot analysis of protein levels for (D and E) CRISPLD2 and (F and G) TGM2 in primary fetal lung fibroblast cells treated with vehicle (Control; white and light gray bars), corticosterone (Cort; black bars), or betamethasone (Beta; dark gray bars) for 24 h. Significant differences are indicated by $*P < 0.05$, $**P < 0.01$, and $***P < 0.001$. Data are presented as means ± SEM of three separate biological replicates. Total protein levels were corrected for the β-ACTIN loading control. Representative Western blot images are shown for (E) CRISPLD2 and (G) TGM2.

clock 1 (*Per1*), dual-specificity phosphatase 1 (*Dusp1*), FK506 binding protein 5 (*Fkbp5*), and serum- and glucocorticoid-regulated kinase 1 (*Sgk1*) (Fig. 6A–6D). These identified GR ChIP regions covered ~100 to 150 bp and contained a previously characterized canonical GRE sequence almost identical to an AGAACANNNTGTTCT consensus (shown in Table 4). These corresponded, for example, to the same GREs previously identified for *Fkbp5* (25) and *Per1* and *Sgk1* (26). We next assessed the four GC-induced genes, *Crispld2*, *Tgm2*, *Hif3a*, and *Kdr*, and were also able to identify similar Beta-ChIP peaks within the proximity of these genes in the rat genome that also contained a similar consensus GRE motif (Fig. 6E–6H and Table 4). These results define these four genes in fetal lung fibroblast as putative direct genomic targets for GC/GR-mediated induction by betamethasone.

Discussion

The action of GCs is critical for the normal development of a functional human lung at birth. We and others (15) have previously shown that during development, GCs contribute to this by important cellular signaling to the lung mesenchymal fibroblasts to direct changes in cell-proliferation rates and to coordinate remodeling of the ECM. GC regulation of lung airway epithelial cell functions seems less critical, as loss of the GR in epithelial cells does not severely compromise the developing lung or dramatically reduce surfactant production or secretion from alveolar epithelial cells (15, 27). The current study aimed to identify the specific changes in global gene expression in primary fetal rat lung fibroblasts that are induced by endogenous GCs compared with the synthetic GC betamethasone. Our results show that betamethasone and corticosterone regulate a very similar discrete subset of target genes in fetal lung fibroblasts but that betamethasone induces a much stronger response for many specific target genes, and we propose that this is the underlying reason for their clinical potency and efficacy for acceleration of lung remodeling and maturation and thereby, improvement of survival rates with preterm human infants.

Pathway analysis has identified specific cell-signaling pathways regulating control of cell proliferation, cytoskeletal dynamics, and ECM remodeling. These included Ras-Raf-MAPK kinase-ERK/MAPK signaling, Gαq signaling, PKA signaling, and S-1P signaling, each

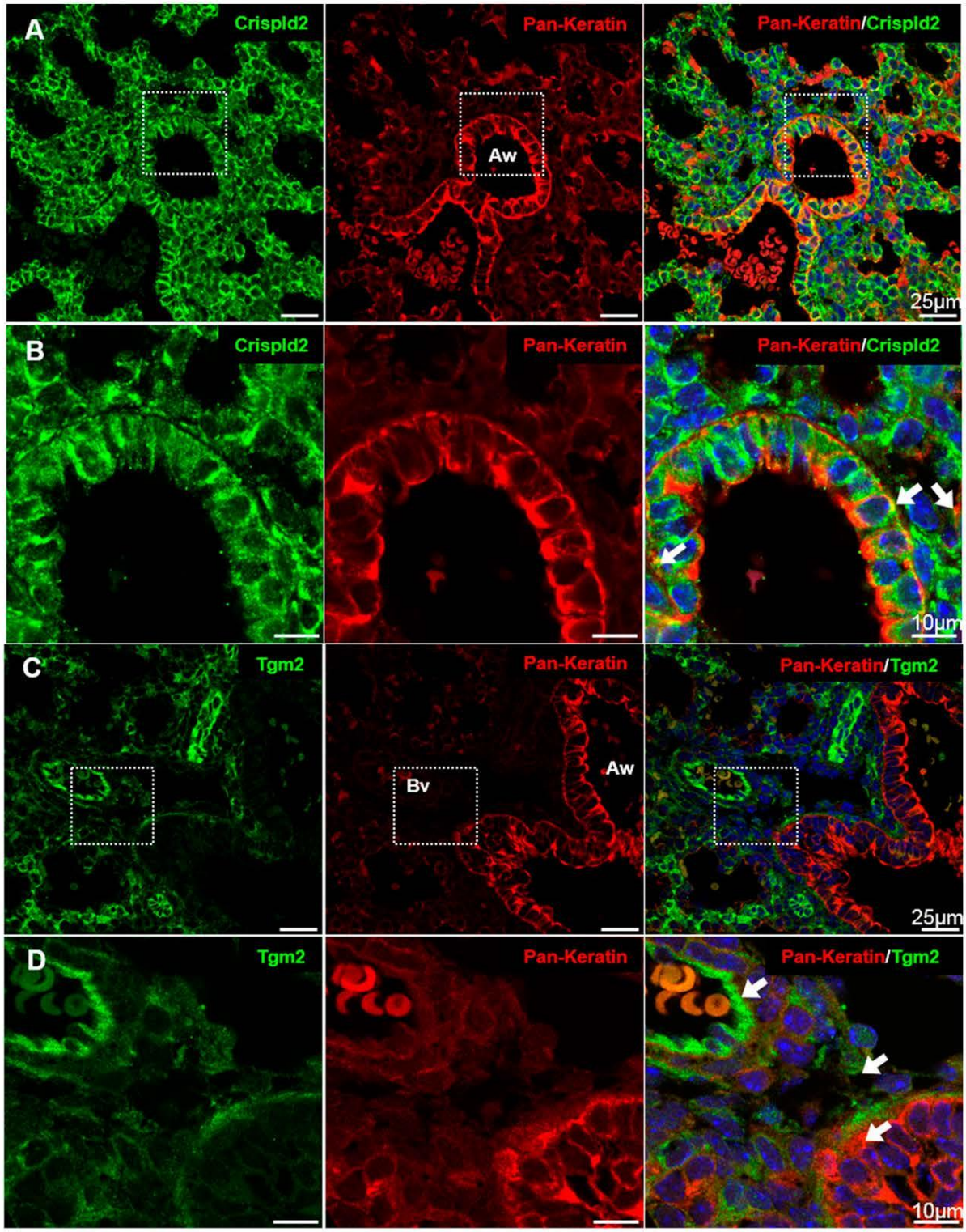

Figure 5. Representative images showing colocalization by double-immunofluorescence labeling for (A and B) CRISPLD2 and (C and D) TGM2 proteins with pan-cytokeratin in fetal mouse lungs at E18.5 (n = 3). (A and B) Left is section labeled with CRISPLD2 (green), middle is section labeled with pan-cytokeratin (red), and right is colocalization of CRISPLD2 and pan-cytokeratin (overlay of left and middle images). All sections were counterstained with the nuclear stain 4′,6-diamidino-2-phenylindole (blue). (A) Original images, 60× objective; (B) ×3 zoom of area indicated by white boxes in (A). Arrows indicate colocalization in epithelial cells. (C and D) Left is section labeled with TGM2, middle is section with pan-cytokeratin, and right is colocalization of TGM2 and pan-cytokeratin (overlay of left and middle images). (C) Original images at 60× objective; (D) ×3 zoom of area indicated by white boxes in (C). Arrows in high-powered images indicate colocalization in epithelial cells. Original scale bars,10 and 25 μm. Aw, airway; Bv, blood vessel.

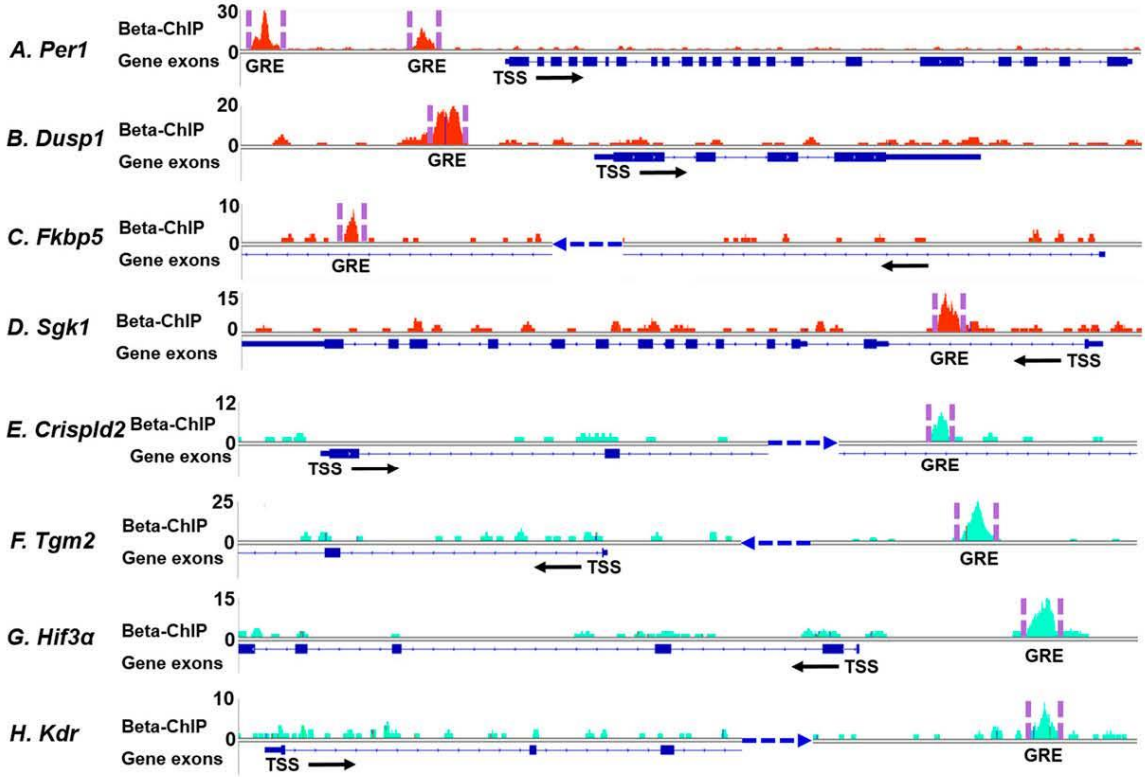

Figure 6. Whole-genome GR ChIP-Seq analysis for GRE-binding sites close to eight genes in rat fetal lung fibroblasts following 6 h stimulation with 1 μM betamethasone. (A) Two Beta-GR ChIP peaks were identified in close proximity (1.2 and 3.5 kb) upstream to the transcriptional start site (TSS) of the *Per1* gene. (B) A strong single Beta-GR ChIP peak was identified 1.2 kb upstream of the TSS of the *Dusp1* gene. (C) A strong single Beta-GR ChIP peak was identified in an intron D of the *Fkbp5* gene. (D) A strong single Beta-GR ChIP peak was identified in intron A of the *Sgk1* gene. (E) A single Beta-GR ChIP peak was identified 30.7 kb far downstream to the TSS of the *Crispld2* gene. (F) A single Beta-GR ChIP peak was identified 50.6 kb far upstream of the TSS of the *Tgm2* gene. (G) A single Beta-GR ChIP peak was identified in close proximity (1.6 kb) upstream of the TSS of the *Hif3α* gene. (H) A single Beta-GR ChIP peak was identified 85.4 kb far downstream of the TSS of the *Kdr* gene. The direction of transcription is shown by the horizontal arrow under each gene. Sequence read number at each nucleotide is denoted on the *y*-axis. The GRE-binding sites directly underlying the betamethasone-GR ChIP peak region of 100 to 200 bp were very similar or identical to the 15-bp GRE canonical consensus AGAACANNNTGTTCT and are shown in Table 4.

able to influence fibroblast cell dynamics. For example, Gαq signaling promotes Rho/Rho-associated protein kinase activation, which is important for myofibroblast differentiation and apoptosis (28). Normal fibroblast mitogenesis involves nuclear translocation of ERK/MAPK (29). Gαi triggers Src/Ras-related protein 1 (Rap1) activation to sequester Ras activity to inhibit fibroblast cell growth (30, 31). This suggests that a primary function of GCs, particularly betamethasone, is to promote rapid mesenchymal thinning by activation of various regulatory molecules involved in Ras-Raf-MAPK kinase-ERK/MAPK signaling to regulate fibroblast cell proliferation negatively and possibly promote their differentiation into myofibroblasts, a critical cellular step in alveolar formation late in fetal lung development. Future experiments will target these pathways in fetal lung fibroblasts for their specific role in the determination of fibroblast cell fate and differentiation status.

Target genes, such as *Has2* and *Plk2*, were repressed in betamethasone- and corticosterone-treated primary fibroblast cells. These genes mediate fibroblast cell differentiation and proliferation most likely to assist in the thinning of the mesenchymal layer. For example, *Has2* is responsible for the biosynthesis of the matrix polysaccharide HA. In fibroblast cells, the main source of HA is synthesized by *Has2* (32) and is responsible for TGF-β1-mediated myofibroblast differentiation (33) and proliferation (34). Overexpression of TGF-β1 induces transdifferentiating of rat alveolar epithelial cells to a mesenchymal phenotype (35) and suppresses alveolar formation in newborn rat lung (36). *Plk2* has been shown to be important during embryonic development and cell-cycle progression, with cultured *Plk2* $^{/}$ embryonic fibroblast cells proliferating slower than the *Plk2*-positive cell, with evidence of delayed entry from G_1- to S-phase (37).

We also identified two genes important for the regulation of cell growth, called *Spry1* and *Foxc2*, whose expression was repressed by both betamethasone and corticosterone treatment in cultured primary fibroblast

Table 4. Locations and Sequence of Betamethasone-GR ChIP GREs for GC-Regulated Genes Identified by Transcriptome Sequencing and GR ChIP-Seq Analysis

Gene ID	Chromosome Location Rat	Location of GRE	Distance to TSS, bp	ChIP Peak: 15 bp GRE Sequence	Beta FC	Cort FC	FDR
Hif3a	Chr 1 (−)	Upstream	−1585	AGGACATTCCGTCCT	46.3	40.5	1.1E-06
Tgm2	Chr 3 (−)	Upstream	−50,551	CGGACAGTTTGTCCT	20.4	11.4	7.8E-13
Kdr	Chr 14 (+)	Downstream	85,437	AGTACTCTCTGTTCT	11.0	8.1	5.2E-08
Crispld2	Chr 19 (−)	Intron	30,720	AGAACAGACTGTCCT	15.2	10.8	1.6E-13
Sgk1	Chr 1 (−)	Intron	110,207	AGAACATTCTGTCCT	5.4	5.9	8.8E-13
Dusp1	Chr 10 (+)	Upstream	−1222	GGTACAGTTTGTTCC	3.3	2.7	6.0E-11
Per1	Chr 10 (+)	Upstream	−3509	GGAACATCGTGTTCT	4.8	5.2	2.2E-11
Per1	Chr 10 (+)	Upstream	−1216	GGAACATCCTGTTCC			
Fkbp5	Chr 20	Intron	19,929	AGAACAGGGTGTTCT	4.3	3.3	2.5E-12

Betamethasone/GR ChIP-Seq peaks were assigned to the nearest GC-responsive gene target identified from previous RNA-Seq of betamethasone-stimulated primary fetal lung fibroblasts. GREs were identified by MEME in 100 to 150 bp of the rat genomic DNA sequence underlying the betamethasone/GR ChIP peak region and were very similar or identical to the 15-p GRE canonical consensus AGAACANNNTGTTCT. The distance of the GRE from the TSS is shown in base pairs either upstream (−) or downstream (+) of the TSS. The fold change (FC) in mRNA levels is shown following 6 h of stimulation with betamethasone and corticosterone, together with the FDR.

cells. Foxc2 is an important inducer for epithelial-mesenchymal transition, where parent epithelial cells change into a mesenchymal or fibroblast-like cell (38). During embryonic development, Foxc2 is widely expressed and is important for the promotion of angiogenesis, myogenesis, and organogenesis (39). GCs might repress this target gene to assist in mesenchymal thinning. Spry1 negatively regulates the glial cell line–derived neurotrophic factor (GDNF)/c-Ret/Wnt11 signaling pathway (40). In the fetal lung, GDNF is suspected to be an important chemoattractant for peripheral neuron development (41). GDNF mRNA is expressed in the mesenchymal smooth muscle cells and might play a role in the attraction of nerve fibers and migration of neural crest–derived cells (42). Therefore, GCs may play a role in the promotion of GDNF-mediated neuron development in the lung via the repression of Spry1.

We examined eight target genes upregulated by GCs in fetal lung fibroblast cells, with most showing a stronger response to the synthetic steroid betamethasone. Pretreatment of primary fibroblast cultures with the GR antagonist RU486 blocked GC induction of all eight genes, indicating a direct requirement of the GR for induction. This was further confirmed using GR ChIP-Seq to identify the GR-binding sites in the genome of fetal rat lung fibroblasts. We identified previously characterized GR-binding sites or GREs that regulate the *Per1*, *Dusp1*, *Fkbp5*, and *Sgk1* genes (25, 26). We also identified GREs in the proximity of four GC/GR-induced genes, *Crispld2*, *Tgm2*, *Hif3α*, and *Kdr*.

KDR is the primary cell-surface receptor for vascular endothelial growth factor (VEGF), an important inducer of angiogenesis in fetal lung vasculature (43). In *Kdr* / mice, there is a failure to develop mature endothelial cells, leading to disorganized blood-vessel formation (44). KDR is also important for intracellular crosstalk between epithelial and endothelial cells influencing branching morphogenesis (45). *Hif3α* is an isoform of the oxygen-sensitive HIFα proteins. Transgenic mice with an induced *Hif3α* gene develop altered branching morphogenesis with reduced numbers of alveoli and changes in alveolar type I and type II cell differentiation (46). Both *Kdr* and *Hif3α* mRNA levels were markedly reduced in the fetal lung of GR / mice, and the GC-induced increase in their levels was largely abolished by pretreatment with the GR antagonist RU486. There results suggest that *Kdr* and *Hif3α* are important direct GC-regulated gene targets in the fetal lung.

Two of the most strongly upregulated target genes were *Tgm2* and *Crispld2*, and these two GC-regulated targets were characterized in further detail. Analysis by qPCR showed that both were strongly increased in expression in fibroblasts by both betamethasone and corticosterone, with a stronger response induced by betamethasone, and this was abolished by pretreatment of fibroblasts with RU486. There was also greatly reduced expression of *Tgm2* and *Crispld2* in the fetal lung from fetal GR / mice, and finally, functional GREs were identified in close proximity to these genes in the rat fetal fibroblast genome. TGM2 is a calcium-dependent protease, which catalyzes the formation of covalent bonds among glutamine, lysine, or other primary amines, forming γ-glutamyl-ϵ-lysine peptide chain bridges, which are highly resistant to proteolytic degradation (47–49). Extracellularly, TGM2 stabilizes ECM proteins by forming crosslinks (50) or by influencing cell adhesion via association with fibronectin (51). Important ECM proteins crosslinked by TGM2 include fibronectin and collagen (52, 53). The induction of *Tgm2* in fibroblast cells has been demonstrated to activate nuclear factor κB,

which increases the expression and activation of TGF-β1, subsequently increasing collagen I, III, and IV and fibronectin synthesis and deposition to the ECM (54). In addition, TGM2 is involved in other cellular processes, which include apoptosis (55), angiogenesis (56), and cell differentiation (57). We have shown that the TGM2 protein is localized to the cytoplasm of mesenchymal cells and to endothelial cells of blood vessels in the fetal lung. Previous studies have demonstrated that *Tgm2* is important for increasing the numbers of endothelial cells by extracellularly mediating cell adhesion and intracellularly promoting cell proliferation and apoptosis (58). TGM2 forms complexes with VEGF receptor 2 (VEGFR2)/KDR on the surface and in the cytoplasm of endothelial cells (59). VEGFR2/KDR is an important receptor involved in angiogenesis (60), and the complex translocates into the nucleus to modulate VEGFR2 intracellular signaling involved in proliferation, survival, and migration of endothelial cells (61). Overall, we have demonstrated that *Tgm2* is a strongly inducible GC target gene in the developing lung, which plays an important role in the remodeling of the ECM and lung maturation before birth.

Crispld2 mRNA levels were also very strongly induced in fetal rat fibroblasts by both betamethasone and corticosterone, with again a stronger response by betamethasone. During normal mouse lung development, *Crispld2* mRNA levels are highest late in gestation at the start of alveologenesis (62). Our data suggest that GC signaling drives induction of *Crispld2* gene expression at the later stages of fetal gestation. CRISPLD2 is a member of the cysteine-rich secretory proteins, antigen 5, and pathogenesis-related 1 superfamily of proteins. The LCCL domain in CRISPLD2 has been implicated in various cellular processes, including cell migration and differentiation (63, 64), ECM deposition (63, 65), and cell adhesion (66). It is a secreted mesenchymal glycoprotein (67) that may signal to distal fetal lung epithelial cells in the latter stage of lung development, promoting epithelial cell migration (68). Human fetal lung fibroblast cells with reduced levels of *Crispld2* displayed a substantial reduction in cell proliferation, impaired MAPK activity, increased apoptosis, reduced cell migration, and altered expression of ECM genes (68). We have localized CRISPLD2 to both fibroblast and epithelial cells in the developing mouse lung. CRISPLD2 is involved in branching morphogenesis, by assisting in mesenchymal-epithelial interactions (69). Reduced *Crispld2* in fetal rat lung explant cultures produced a 47% decrease in terminal airway bud number (69). During the alveolar stage of lung development in the rats, CRISPLD2 is secreted from the myofibroblasts adjacent to the epithelium, where it is concentrated at the tips of budding secondary alveolar septa (67). Although Crispld2 / mice are embryonic lethal, heterozygous Crispld2$^{+/}$ mice displayed disorganized elastin fibers from E16.5 to postnatal day 1, and immature morphology with thickened respiratory interstitium and the appearance of delayed secondary septation, characteristics similar to bronchopulmonary dysplasia (70).

In conclusion, this study has identified the key subset of target genes specifically induced by GCs in fetal rat lung mesenchymal fibroblasts by both the endogenous GC corticosterone and the clinically relevant and potent synthetic GC betamethasone. We have shown that betamethasone and corticosterone regulate a very similar subset of ~490 target genes in fetal lung fibroblasts with betamethasone inducing a much higher and stronger response in many gene targets identified and that this explains, in part, the clinical efficacy of betamethasone in the treatment of very preterm human birth. Further analysis of these GC targets, their associated pathways, and downstream physiological responses will lead to the development of better lung-focused treatments for the respiratory complications of preterm birth.

Acknowledgments

We thank Judy Ng for technical assistance.

Financial Support: This study was funded by a program grant (384100) from the National Health and Medical Research Council (NHMRC, Australia; to T.J.C.). Scholarship support was from the School of Biomedical Science, Monash University (to B.K.L.S.), and also from a Rebecca Cooper Foundation (Australia) Grant-in-Aid. We also acknowledge support by the Victorian Government's Operational Infrastructure Support Program.

Correspondence: Timothy J. Cole, PhD, Department of Biochemistry and Molecular Biology, Monash University, Clayton, Victoria 3800, Australia. E-mail: tim.cole@monash.edu.

Disclosure Summary: The authors have nothing to disclose.

References and Notes

1. Wallace MJ, Hooper SB, Harding R. Effects of elevated fetal cortisol concentrations on the volume, secretion, and reabsorption of lung liquid. *Am J Physiol.* 1995;**269**(4 Pt 2):R881–R887.
2. Warburton D, Parton L, Buckley S, Cosico L, Enns G, Saluna T. Combined effects of corticosteroid, thyroid hormones, and beta-agonist on surfactant, pulmonary mechanics, and beta-receptor binding in fetal lamb lung. *Pediatr Res.* 1988;**24**(2):166–170.
3. Kendall JZ, Lakritz J, Plopper CG, Richards GE, Randall GC, Nagamani M, Weir AJ. The effects of hydrocortisone on lung structure in fetal lambs. *J Dev Physiol.* 1990;**13**(3):165–172.
4. Wallace MJ, Hooper SB, Harding R. Role of the adrenal glands in the maturation of lung liquid secretory mechanisms in fetal sheep. *Am J Physiol.* 1996;**270**(1 Pt 2):R33–R40.
5. Boland R, Joyce BJ, Wallace MJ, Stanton H, Fosang AJ, Pierce RA, Harding R, Hooper SB. Cortisol enhances structural maturation of the hypoplastic fetal lung in sheep. *J Physiol.* 2004;**554**(2):505–517.

6. Gilstrap LC, Christensen R, Clewell WH, D'Alton ME, Davidson EC Jr, Escobedo MB, Gjerdingen DK, Goddard-Finegold J, Goldenberg RL, Grimes DA, Hansen TN, Kauffman RE, Keeler EB, Oh W, Susman EJ, Vogel MG, Avery ME, Ballard PL, Ballard RA, Crowley P, Garite T, Hankins GDV, Jobe AH, Koppe JG, Maher JE, Merkatz IR, Shankaran S, Simpson KN, Sinclair JC, Slotkin TA, Taeusch HW Jr, Wright LL, Alexander D, Berberich MA, Bracken M, Cooper L, Culpepper L, Elliott JM, Ferguson JH, Frigoletto F, Gail DB, Hall WH, Jones D Jr, Medoff-Cooper B, Merenstein GB, Whalen JM Lenfant C, Hinshaw AS. NIH Consensus Development Panel on the Effect of Corticosteroids for Fetal Maturation on Perinatal Outcomes. Effect of corticosteroids for fetal maturation on perinatal outcomes. *JAMA*. 1995;**273**(5):413–418.
7. Roberts D, Dalziel S. Antenatal corticosteroids for accelerating fetal lung maturation for women at risk of preterm birth. *Cochrane Database Syst Rev*. 2006; (3):CD004454.
8. Cheong JL, Burnett AC, Lee KJ, Roberts G, Thompson DK, Wood SJ, Connelly A, Anderson PJ, Doyle LW; Victorian Infant Collaborative Study Group. Association between postnatal dexamethasone for treatment of bronchopulmonary dysplasia and brain volumes at adolescence in infants born very preterm. *J Pediatr*. 2014;**164**(4):737–743.e**1**.
9. Jellyman JK, Valenzuela OA, Fowden AL. Horse Species Symposium: glucocorticoid programming of hypothalamic-pituitary-adrenal axis and metabolic function: animal studies from mouse to horse. *J Anim Sci*. 2015;**93**(7):3245–3260.
10. Fowden AL, Forhead AJ. Hormones as epigenetic signals in developmental programming. *Exp Physiol*. 2009;**94**(6):607–625.
11. Fowden AL, Li J, Forhead AJ. Glucocorticoids and the preparation for life after birth: are there long-term consequences of the life insurance? *Proc Nutr Soc*. 1998;**57**(1):113–122.
12. O'Connell BA, Moritz KM, Walker DW, Dickinson H. Synthetic glucocorticoid dexamethasone inhibits branching morphogenesis in the spiny mouse placenta. *Biol Reprod*. 2013;**88**(1):26.
13. Vaughan OR, Fisher HM, Dionelis KN, Jeffreys EC, Higgins JS, Musial B, Sferruzzi-Perri AN, Fowden AL. Corticosterone alters materno-fetal glucose partitioning and insulin signalling in pregnant mice. *J Physiol*. 2015;**593**(5):1307–1321.
14. Zhou J, Cidlowski JA. The human glucocorticoid receptor: one gene, multiple proteins and diverse responses. *Steroids*. 2005;**70**(5-7):407–417.
15. Bird AD, Choo YL, Hooper SB, McDougall AR, Cole TJ. Mesenchymal glucocorticoid receptor regulates the development of multiple cell layers of the mouse lung. *Am J Respir Cell Mol Biol*. 2014;**50**(2):419–428.
16. Habermehl D, Parkitna JR, Kaden S, Brügger B, Wieland F, Gröne HJ, Schütz G. Glucocorticoid activity during lung maturation is essential in mesenchymal and less in alveolar epithelial cells. *Mol Endocrinol*. 2011;**25**(8):1280–1288.
17. McDougall AR, Hooper SB, Zahra VA, Sozo F, Lo CY, Cole TJ, Doran T, Wallace MJ. The oncogene Trop2 regulates fetal lung cell proliferation. *Am J Physiol Lung Cell Mol Physiol*. 2011;**301**(4): L478–L489.
18. McDougall AR, Hooper SB, Zahra VA, Cole TJ, Lo CY, Doran T, Wallace MJ. Trop2 regulates motility and lamellipodia formation in cultured fetal lung fibroblasts. *Am J Physiol Lung Cell Mol Physiol*. 2013;**305**(7):L508–L521.
19. Cole TJ, Blendy JA, Monaghan AP, Krieglstein K, Schmid W, Aguzzi A, Fantuzzi G, Hummler E, Unsicker K, Schütz G. Targeted disruption of the glucocorticoid receptor gene blocks adrenergic chromaffin cell development and severely retards lung maturation. *Genes Dev*. 1995;**9**(13):1608–1621.
20. RRID:AB_2801409, https://scicrunch.org/resolver/AB_2801409.
21. RRID:AB_2202883, https://scicrunch.org/resolver/AB_2202883.
22. RRID:AB_10858135, https://scicrunch.org/resolver/AB_10858135.
23. Bird AD, Flecknoe SJ, Tan KH, Olsson PF, Antony N, Mantamadiotis T, Mollard R, Hooper SB, Cole TJ. cAMP response element binding protein is required for differentiation of respiratory epithelium during murine development [published correction appears in *PLoS One*. 2012;**7**(1). doi:10.1371/annotation/ec04ad74-63cc-4fbe-9ad8-074a1d62fdf4]. *PLoS One*. 2011; **6**(3):e17843.
24. RRID:AB_490860, https://scicrunch.org/resolver/AB_490860.
25. Hubler TR, Scammell JG. Intronic hormone response elements mediate regulation of FKBP5 by progestins and glucocorticoids. *Cell Stress Chaperones*. 2004;**9**(3):243–252.
26. So AY, Chaivorapol C, Bolton EC, Li H, Yamamoto KR. Determinants of cell- and gene-specific transcriptional regulation by the glucocorticoid receptor. *PLoS Genet*. 2007;**3**(6):e94.
27. Cole TJ, Solomon NM, Van Driel R, Monk JA, Bird D, Richardson SJ, Dilley RJ, Hooper SB. Altered epithelial cell proportions in the fetal lung of glucocorticoid receptor null mice. *Am J Respir Cell Mol Biol*. 2004;**30**(5):613–619.
28. Shimizu Y, Dobashi K, Iizuka K, Horie T, Suzuki K, Tukagoshi H, Nakazawa T, Nakazato Y, Mori M. Contribution of small GTPase Rho and its target protein rock in a murine model of lung fibrosis. *Am J Respir Crit Care Med*. 2001;**163**(1):210–217.
29. Brunet A, Roux D, Lenormand P, Dowd S, Keyse S, Pouysségur J. Nuclear translocation of p42/p44 mitogen-activated protein kinase is required for growth factor-induced gene expression and cell cycle entry. *EMBO J*. 1999;**18**(3):664–674.
30. Bunda S, Heir P, Srikumar T, Cook JD, Burrell K, Kano Y, Lee JE, Zadeh G, Raught B, Ohh M. Src promotes GTPase activity of Ras via tyrosine 32 phosphorylation. *Proc Natl Acad Sci USA*. 2014; **111**(36):E3785–E3794.
31. Schmitt JM, Stork PJ. PKA phosphorylation of Src mediates cAMP's inhibition of cell growth via Rap1. *Mol Cell*. 2002;**9**(1): 85–94.
32. Simpson RM, Meran S, Thomas D, Stephens P, Bowen T, Steadman R, Phillips A. Age-related changes in pericellular hyaluronan organization leads to impaired dermal fibroblast to myofibroblast differentiation. *Am J Pathol*. 2009;**175**(5):1915–1928.
33. Midgley AC, Rogers M, Hallett MB, Clayton A, Bowen T, Phillips AO, Steadman R. Transforming growth factor-β1 (TGF-β1)-stimulated fibroblast to myofibroblast differentiation is mediated by hyaluronan (HA)-facilitated epidermal growth factor receptor (EGFR) and CD44 co-localization in lipid rafts. *J Biol Chem*. 2013; **288**(21):14824–14838.
34. Meran S, Luo DD, Simpson R, Martin J, Wells A, Steadman R, Phillips AO. Hyaluronan facilitates transforming growth factor-β1-dependent proliferation via CD44 and epidermal growth factor receptor interaction. *J Biol Chem*. 2011;**286**(20):17618–17630.
35. Gauldie J, Galt T, Bonniaud P, Robbins C, Kelly M, Warburton D. Transfer of the active form of transforming growth factor-beta 1 gene to newborn rat lung induces changes consistent with bronchopulmonary dysplasia. *Am J Pathol*. 2003;**163**(6):2575–2584.
36. Ambalavanan N, Nicola T, Hagood J, Bulger A, Serra R, Murphy-Ullrich J, Oparil S, Chen YF. Transforming growth factor-beta signaling mediates hypoxia-induced pulmonary arterial remodeling and inhibition of alveolar development in newborn mouse lung. *Am J Physiol Lung Cell Mol Physiol*. 2008;**295**(1):L86–L95.
37. Ma S, Charron J, Erikson RL. Role of Plk2 (Snk) in mouse development and cell proliferation. *Mol Cell Biol*. 2003;**23**(19): 6936–6943.
38. Hader C, Marlier A, Cantley L. Mesenchymal-epithelial transition in epithelial response to injury: the role of Foxc2. *Oncogene*. 2010; **29**(7):1031–1040.
39. Hayashi H, Kume T. Forkhead transcription factors regulate expression of the chemokine receptor CXCR4 in endothelial cells and CXCL12-induced cell migration. *Biochem Biophys Res Commun*. 2008;**367**(3):584–589.
40. Basson MA, Akbulut S, Watson-Johnson J, Simon R, Carroll TJ, Shakya R, Gross I, Martin GR, Lufkin T, McMahon AP, Wilson

PD, Costantini FD, Mason IJ, Licht JD. Sprouty1 is a critical regulator of GDNF/RET-mediated kidney induction. *Dev Cell.* 2005;8(2):229–239.
41. Tollet J, Everett AW, Sparrow MP. Development of neural tissue and airway smooth muscle in fetal mouse lung explants: a role for glial-derived neurotrophic factor in lung innervation. *Am J Respir Cell Mol Biol.* 2002;26(4):420–429.
42. Towers PR, Woolf AS, Hardman P. Glial cell line-derived neurotrophic factor stimulates ureteric bud outgrowth and enhances survival of ureteric bud cells in vitro. *Exp Nephrol.* 1998;6(4): 337–351.
43. Raoul W, Chailley-Heu B, Barlier-Mur AM, Delacourt C, Maître B, Bourbon JR. Effects of vascular endothelial growth factor on isolated fetal alveolar type II cells. *Am J Physiol Lung Cell Mol Physiol.* 2004;286(6):L1293–L1301.
44. Fong GH, Rossant J, Gertsenstein M, Breitman ML. Role of the Flt-1 receptor tyrosine kinase in regulating the assembly of vascular endothelium. *Nature.* 1995;376(6535):66–70.
45. Ahlbrecht K, Schmitz J, Seay U, Schwarz C, Mittnacht-Kraus R, Gaumann A, Haberberger RV, Herold S, Breier G, Grimminger F, Seeger W, Voswinckel R. Spatiotemporal expression of flk-1 in pulmonary epithelial cells during lung development. *Am J Respir Cell Mol Biol.* 2008;39(2):163–170.
46. Huang Y, Kapere Ochieng J, Kempen MB, Munck AB, Swagemakers S, van Ijcken W, Grosveld F, Tibboel D, Rottier RJ. Hypoxia inducible factor 3α plays a critical role in alveolarization and distal epithelial cell differentiation during mouse lung development [published correction appears in *PLoS One.* 2015;10(3): e0119359]. *PLoS One.* 2013;8(2):e57695.
47. Hu X, Zhao M, Sun W, Zhao G, Ren J. Effects of microfluidization treatment and transglutaminase cross-linking on physicochemical, functional, and conformational properties of peanut protein isolate. *J Agric Food Chem.* 2011;59(16):8886–8894.
48. Jung HJ, Chen Z, Wang M, Fayad L, Romaguera J, Kwak LW, McCarty N. Calcium blockers decrease the bortezomib resistance in mantle cell lymphoma via manipulation of tissue transglutaminase activities. *Blood.* 2012;119(11):2568–2578.
49. Li H, Zhang L, Cui Y, Luo X, Xue C, Wang S. Expression of soluble recombinant transglutaminase from Zea mays in Pichia pastoris. *World J Microbiol Biotechnol.* 2013;29(5):939–947.
50. Jones RA, Nicholas B, Mian S, Davies PJ, Griffin M. Reduced expression of tissue transglutaminase in a human endothelial cell line leads to changes in cell spreading, cell adhesion and reduced polymerisation of fibronectin. *J Cell Sci.* 1997;110(Pt 19):2461–2472.
51. Gaudry CA, Verderio E, Aeschlimann D, Cox A, Smith C, Griffin M. Cell surface localization of tissue transglutaminase is dependent on a fibronectin-binding site in its N-terminal beta-sandwich domain. *J Biol Chem.* 1999;274(43):30707–30714.
52. Chau DY, Collighan RJ, Verderio EA, Addy VL, Griffin M. The cellular response to transglutaminase-cross-linked collagen. *Biomaterials.* 2005;26(33):6518–6529.
53. Maeda Y, Davé V, Whitsett JA. Transcriptional control of lung morphogenesis. *Physiol Rev.* 2007;87(1):219–244.
54. Telci D, Collighan RJ, Basaga H, Griffin M. Increased TG2 expression can result in induction of transforming growth factor beta1, causing increased synthesis and deposition of matrix proteins, which can be regulated by nitric oxide. *J Biol Chem.* 2009; 284(43):29547–29558.
55. Melino G, Annicchiarico-Petruzzelli M, Piredda L, Candi E, Gentile V, Davies PJ, Piacentini M. Tissue transglutaminase and apoptosis: sense and antisense transfection studies with human neuroblastoma cells. *Mol Cell Biol.* 1994;14(10):6584–6596.
56. Jones RA, Kotsakis P, Johnson TS, Chau DY, Ali S, Melino G, Griffin M. Matrix changes induced by transglutaminase 2 lead to inhibition of angiogenesis and tumor growth. *Cell Death Differ.* 2006;13(9):1442–1453.
57. Balajthy Z, Csomós K, Vámosi G, Szántó A, Lanotte M, Fésüs L. Tissue-transglutaminase contributes to neutrophil granulocyte differentiation and functions. *Blood.* 2006;108(6):2045–2054.
58. Nadalutti C, Viiri KM, Kaukinen K, Mäki M, Lindfors K. Extracellular transglutaminase 2 has a role in cell adhesion, whereas intracellular transglutaminase 2 is involved in regulation of endothelial cell proliferation and apoptosis. *Cell Prolif.* 2011;44(1): 49–58.
59. Dardik R, Inbal A. Complex formation between tissue transglutaminase II (tTG) and vascular endothelial growth factor receptor 2 (VEGFR-2): proposed mechanism for modulation of endothelial cell response to VEGF. *Exp Cell Res.* 2006;312(16): 2973–2982.
60. Dardik R, Loscalzo J, Inbal A. Factor XIII (FXIII) and angiogenesis. *J Thromb Haemost.* 2006;4(1):19–25.
61. Thuringer D, Maulon L, Frelin C. Rapid transactivation of the vascular endothelial growth factor receptor KDR/Flk-1 by the bradykinin B2 receptor contributes to endothelial nitric-oxide synthase activation in cardiac capillary endothelial cells. *J Biol Chem.* 2002;277(3):2028–2032.
62. Kaplan F, Ledoux P, Kassamali FQ, Gagnon S, Post M, Koehler D, Deimling J, Sweezey NB. A novel developmentally regulated gene in lung mesenchyme: homology to a tumor-derived trypsin inhibitor. *Am J Physiol.* 1999;276(6):L1027–L1036.
63. Robertson NG, Hamaker SA, Patriub V, Aster JC, Morton CC. Subcellular localisation, secretion, and post-translational processing of normal cochlin, and of mutants causing the sensorineural deafness and vestibular disorder, DFNA9. *J Med Genet.* 2003; 40(7):479–486.
64. Vogt DL, Gray CD, Young WS III, Orellana SA, Malouf AT. ARHGAP4 is a novel RhoGAP that mediates inhibition of cell motility and axon outgrowth. *Mol Cell Neurosci.* 2007;36(3): 332–342.
65. Grabski R, Szul T, Sasaki T, Timpl R, Mayne R, Hicks B, Sztul E. Mutations in COCH that result in non-syndromic autosomal dominant deafness (DFNA9) affect matrix deposition of cochlin. *Hum Genet.* 2003;113(5):406–416.
66. Ahsan M, Ohta K, Kuriyama S, Tanaka H. Novel soluble molecule, Akhirin, is expressed in the embryonic chick eyes and exhibits heterophilic cell-adhesion activity. *Dev Dyn.* 2005; 233(1):95–104.
67. Nadeau K, Jankov RP, Tanswell AK, Sweezey NB, Kaplan F. Lgl1 is suppressed in oxygen toxicity animal models of bronchopulmonary dysplasia and normalizes during recovery in air. *Pediatr Res.* 2006;59(3):389–395.
68. Zhang H, Sweezey NB, Kaplan F. LGL1 modulates proliferation, apoptosis, and migration of human fetal lung fibroblasts. *Am J Physiol Lung Cell Mol Physiol.* 2015;308(4):L391–L402.
69. Oyewumi L, Kaplan F, Gagnon S, Sweezey NB. Antisense oligodeoxynucleotides decrease LGL1 mRNA and protein levels and inhibit branching morphogenesis in fetal rat lung. *Am J Respir Cell Mol Biol.* 2003;28(2):232–240.
70. Lan J, Ribeiro L, Mandeville I, Nadeau K, Bao T, Cornejo S, Sweezey NB, Kaplan F. Inflammatory cytokines, goblet cell hyperplasia and altered lung mechanics in Lgl1+/- mice. *Respir Res.* 2009;10(1):83.

Appendix B: The science of steroids

Seminars in Fetal and Neonatal Medicine 24 (2019) 170–175

Contents lists available at ScienceDirect

Seminars in Fetal and Neonatal Medicine

journal homepage: www.elsevier.com/locate/siny

The science of steroids

Timothy J. Cole[a,b,*], Kelly L. Short[a], Stuart B. Hooper[c,d]

[a] Department of Biochemistry and Molecular Biology, Monash University, Melbourne, Vic, 3800, Australia
[b] Division of Endocrinology & Metabolism, Hudson Institute, Monash Medical Centre, Clayton, Vic, Australia
[c] The Richie Centre, Hudson Institute, Monash Medical Centre, Clayton, Vic, Australia
[d] Department of Obstetrics & Gynaecology, Monash Medical Centre, Clayton, Vic, Australia

ARTICLE INFO

Keywords:
Steroids
Glucocorticoids
Betamethasone
Glucocorticoid receptor
Fetal lung development

ABSTRACT

Steroids are complex lipophilic molecules that have many actions in the body to regulate cellular, tissue and organ functions across the life-span. Steroid hormones such as cortisol, aldosterone, estradiol and testosterone are synthesised from cholesterol in specialised endocrine cells in the adrenal gland, ovary and testis, and released into the circulation when required. Steroid hormones move freely into cells to activate intracellular nuclear receptors that function as multi-domain ligand-dependent transcriptional regulators in the cell nucleus. Activated nuclear receptors modify expression of hundreds to thousands of specific target genes in the genome. Steroid hormone actions in the fetus include developmental roles in the respiratory system, brain, and cardiovascular system. The synthetic glucocorticoid steroid betamethasone is used antenatally to reduce the complications of preterm birth. Development of novel selective partial glucocorticoid receptor agonists may provide improved therapies to treat the respiratory complications of preterm birth and spare the deleterious effects of postnatal glucocorticoids in other organs.

1. Introduction

Steroids are complex four-ringed organic molecules that serve many roles and functions in multicellular organisms. They are structural components of cell membranes exemplified by the important dietary steroid cholesterol and have many functional regulatory roles as modified structural forms of cholesterol to function as endogenous endocrine hormones. In all organisms, hormones *in vivo* play key regulatory roles in mediating communication and regulation of important functions and processes within and between cells, and across tissues, to connect all organs of the body [1]. Endocrine hormones circulate in the bloodstream and allow communication between cells and organs separated by relatively large distances. Hydrophilic or water-soluble hormones act primarily at the cell surface by binding to protein receptors embedded in the plasma membrane. In contrast, hydrophobic hormones circulate primarily bound to carrier plasma proteins and are able to freely defuse across cell membranes to activate specific intracellular hormone receptors [1].

This review will focus on the biology and actions of the lipophilic steroid hormones and some of the important synthetic steroid compounds, developed over the past 50 years to treat human disease, that act as specific agonists or antagonists to steroid hormone receptors *in vivo*. It will summarize current knowledge on the action of physiological steroid hormones in fetal development and the use of synthetic steroids to treat the postnatal complications associated with preterm birth.

2. Steroid biosynthesis and turnover

All steroids in the body are derived from cholesterol via a tightly regulated biosynthetic enzymatic pathway that operates predominantly in specific endocrine organs, including the adrenal gland, ovary, and testis. Further modifications of the steroid structure and resulting function can occur in many tissues and organs of the body such as in the liver, skin epidermis, brain and prostate [2].

In the steroidogenic cells of the adrenal gland, ovary and testis, cholesterol is first converted to pregnenolone by the cholesterol side-chain cleavage enzyme, $P450_{SSC}$, a cytochrome P450 enzyme, and this step represents the key regulatory point for synthesis of the majority of endogenous steroid hormones. Most of the enzymes in the steroid biosynthetic pathway are either cytochrome P450 enzymes or specialised hydroxysteroid dehydrogenase (HSD) enzymes, which belong to the short-chain alcohol dehydrogenase reductase (SDR) enzyme super family [3].

Adrenal steroid biosynthesis occurs in the outer cortex of the adrenal gland. The cortex is divided into three layers where specific

* Corresponding author. Department of Biochemistry and Molecular Biology, Monash University, Melbourne, Vic, 3800, Australia.
E-mail address: tim.cole@monash.edu (T.J. Cole).

https://doi.org/10.1016/j.siny.2019.05.005

steroids are produced, dependent on expression of specific biosynthetic enzymes. The outer zona glomerulosa specifically expresses the Cyp11B2 P450 enzyme aldosterone synthase to generate the cardiovascular steroid aldosterone. The centrally located zona fasciculata specifically expresses a closely related homologous Cyp11B1 P450 enzyme called 11β-hydroxylase to produce the glucocorticoid steroids cortisol and corticosterone. The inner zona reticularis produces the adrenal androgens, dihydroepiandrosterone (DHEA), DHEA-sulphate (DHEAS), androstenedione and testosterone, via the actions of the enzymes 3βHSD3, AKR1C3 and Sulfotransferase 2A1. These adrenal androgens circulate in the bloodstream and act as precursors for more biologically active reproductive steroids that are produced at higher levels in the gonads. There is some evidence, primarily at the RNA level, that some of these steroid biosynthetic enzymes are also expressed in other tissues and organs such as heart and brain, although it seems unlikely that these sites produce any significant levels of bioactive steroid [4].

Human plasma and tissue extracts can contain a large number of different steroid compounds, many of which are biologically inactive. This is because many active steroids are continually modified by other enzymes, particularly in the liver, to produce inactive steroid metabolites. Most steroids are inactivated by hydroxylation or sulphation, which render the structure unable to activate receptors or downstream intracellular signalling pathways, and these modifications also increase the solubility of the steroid for renal excretion. Common hepatic modifications include 6β-hydroxylation, 5β-reduction of C_{21} and C_{19} steroids and 4-hydroxylation of estrogens.

The steroid sulfotransferases (SULT) enzymes are a large family of enzymes that transfer a sulphate moiety to the steroid ring from a donor molecule called 3′-phosphoadenine-5′-phosphosulphate [5]. Important SULT enzymes include SULT2A1 that converts DHEA to DHEAS in the adrenal cortex, and SULT1E1 that sulphonates and inactivates estradiol for excretion. The hydroxysteroid dehydrogenases (HSDs) are also a large and important family of enzymes that are involved in steroid biosynthesis and inactivation. The steroid cortisol can be modified by two related HSDs, 11βHSD1 and 11βHSD2, which interconvert the keto/hydroxy side-chain on the 11th carbon of the cortisol steroid ring. 11βHSD1 is a bidirectional enzyme but is predominantly a reductase with the production of active cortisol in many metabolic tissues, such as the liver, and also the brain, regions of the kidney, and white adipose, thereby amplifying glucocorticoid-mediated signalling in target cells [6]. 11βHSD2 is a unidirectional dehydrogenase and inactivates cortisol to cortisone in tissues and is the key enzyme protecting the mineralocorticoid receptor (MR) from inappropriate activation by cortisol [7]. Loss of function mutations in the human 11βHSD2 gene causes the condition of 'apparent mineralocorticoid excess' that is characterised by early-onset hypertension and cardiovascular complications in very young children [8]. 11βHSD1 antagonists have been explored recently as a potential treatment for metabolic syndrome by blunting or attenuating the metabolic effects of cortisol, although unwanted side-effect profiles have been an issue in early clinical trials [6].

3. Steroids as physiological hormones

Endogenous steroid hormones have been long recognised as physiological regulators of development, growth, reproduction and systemic homeostasis. The majority of physiological steroid hormones are derived from the precursor steroid cholesterol and synthesised in specialised endocrine cells within specific endocrine glands [2]. The key important physiological endogenous steroid hormones are listed in Table 1, and include the adrenal steroids cortisol and aldosterone, the adrenal androgen precursors DHEA and DHEAS, and the reproductive steroids estradiol, testosterone and dihydrotestosterone. The physiological sex steroids comprise estradiol, which is predominantly synthesised in the female ovary, and testosterone and dihydrotestosterone that are synthesised predominantly in the male testis. These endocrine glands are composed of steroid synthesising cells that contain complex steroid biosynthetic pathways that involve a large number of intracellular steroid intermediates some of which are now thought to potentially have physiological roles in abnormal states or in complex genetic disease [2,9]. The biosynthetic enzymes modify chemical groups and sidechains across the four-ringed structure giving each steroid intermediate or final product a specificity of interaction with other enzymes and with intracellular receptor proteins (Fig. 1A and B). Mutations in the genes encoding key biosynthetic enzymes, such as the enzyme 21α-Hydroxylase or 17α-Hydroxylase can cause common endocrine conditions such as congenital adrenal hyperplasia (CAH) [10]. Careful measurement of the levels of endogenous steroids and steroid metabolites in body fluids such as urine and blood by mass spectrometry is now the mainstay diagnostic technique to detect steroid abnormalities that may indicate the presence of disease [11].

3.1. The reproductive steroids

The estrogenic and androgenic classes of steroid hormones collectively control determination of secondary gender characteristics and the regulation of reproduction in males and females. Reproductive steroids are primarily synthesised in the adult gonads following puberty and are responsible for the majority of secondary sex characteristics, the physiological changes that occur during puberty and the regulation of the reproductive phases of gonadal function.

Bioactive estradiol is produced from testosterone in the Granulosa cells of the ovary by the action of the P450 enzyme aromatase [12]. Ovarian theca cells also synthesise androstenedione and testosterone from cholesterol to provide androgenic precursors to the granulosa cell [2]. The enzyme aromatase is also expressed in other parts of the body including white adipose tissue and individuals with significant amounts of white fat can synthesise a high level of local estradiol that can contribute to higher systemic circulating estradiol levels. For example, this can lead to precocious puberty in very young girls that are overweight or obese [13]. Elevated aromatase expression in breast tissue can also drive breast tumour growth via increased local production of oestradiol that stimulates cell proliferation [12].

In the testis, Leydig cells produce androstenedione and testosterone from cholesterol via a five-step biosynthetic pathway. The more potent androgen dihydrotestosterone (DHT) is produced by the action of the enzyme 5α-Reductase that is predominantly expressed in peripheral tissues such as in the liver, brain, skin and the male prostate [14].

3.2. The cardiovascular steroids

The main role of the adrenal steroid aldosterone *in vivo* is the regulation of solute and fluid homeostasis primarily in the kidney and colon [15]. In the collecting duct of the kidney, aldosterone promotes the reabsorption of sodium, excretion of potassium, water uptake and therefore increased fluid volume, thereby maintaining systemic blood pressure. Synthesis and release of aldosterone from the adrenal gland is tightly regulated by the renin-angiotensin system. The renin secreting juxtaglomerular cells of the kidney sense volume, and low-volume (with low-sodium) stimulates secretion of renin, a protease enzyme, that cleaves circulating angiotensinogen to release angiotensin peptides thereby stimulating the adrenal zona glomerulosa to synthesise and secrete aldosterone [16]. Elevated plasma potassium is also able to directly stimulate aldosterone release from adrenal glomerulosa cells. The actions of aldosterone in collecting duct cells (and other epithelia) is mediated by the mineralocorticoid receptor (MR), a member of the nuclear receptor superfamily (described below).

A complication is that the MR is also activated by the related steroid cortisol that normally circulates at much higher concentrations in the bloodstream. However, inappropriate activation of the MR by cortisol in most MR expressing cells is prevented by the presence of the enzyme 11βHSD2 that converts cortisol to inactive cortisone thereby preventing

Table 1
List of the important physiological endogenous steroid hormones and synthetic steroid hormone agonists.

Steroid	Endogenous (E) or Synthetic (S)	Cell Receptor	Major functional roles in development or clinical importance
Cortisol/Corticosterone	E	GR, MR	Fetal organ development, metabolism, anti-stress and anti-immune responses
Aldosterone	E	MR	Postnatal renal function, fluid homeostasis and blood pressure control
Estradiol	E	ERα, ERβ	Puberty, female reproduction
Testosterone/Dihydrotestosterone	E	AR	Puberty, male reproduction
Progesterone	E	PR	Maintenance of pregnancy
DHEA/DHEAS	E	AR	Adrenal androgen precursor
Betamethasone	S	GR, MR	Prematurity, preterm birth
Dexamethasone	S	GR, MR	Prematurity, preterm birth, anti-inflammatory, lymphocyte apoptosis
Prednisolone	S	GR, MR	Anti-inflammatory; arthritis, autoimmune disease
Budesonide	S	GR, MR	Ant-inflammatory; asthma, COPD

DHEA, dihydroepiandrosterone; DHEAS, dihydroepiandrosterone-sulphate; GR; Glucocorticoid Receptor, MR, Mineralocorticoid Receptor, ER; Estrogen Receptor, AR; Androgen Receptor, PR; Progesterone Receptor. COPD; Chronic Obstructive Pulmonary Disease.

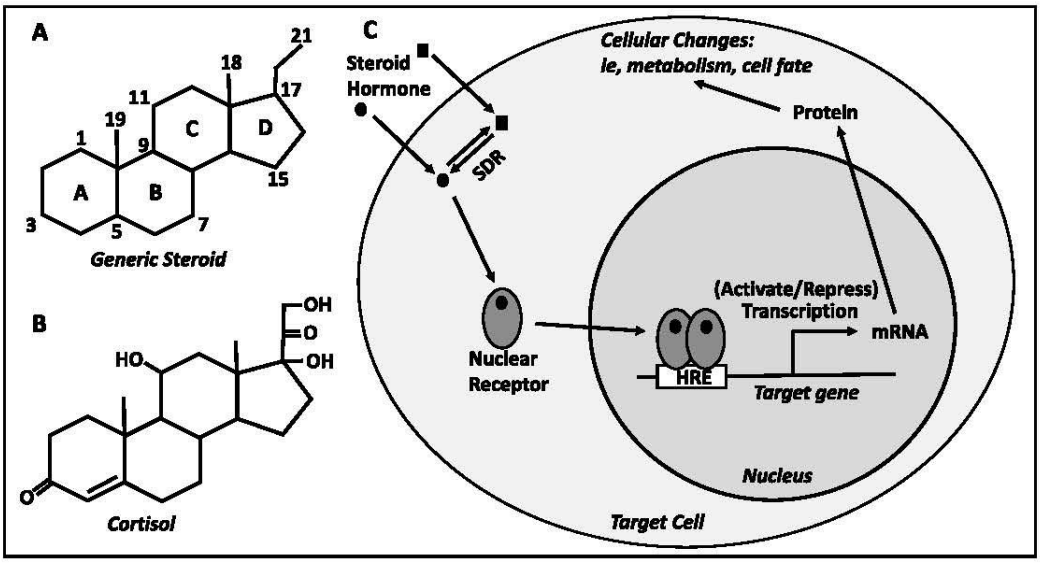

Fig. 1. The mechanism of action of intracellular nuclear receptors that mediate steroid signalling in cells. Nuclear receptors (NRs) bind lipophilic steroid hormones primarily in the cytosol of the cell, undergo a confirmation change, dimerise and translocate into the nucleus where they bind specific hormone response elements (HREs) close to specific target genes within the genome. The steroid hormone may require enzymatic modification by short-chain alcohol dehydrogenase reductase (SDR) enzymes to adopt their active confirmation. Activation or repression of gene expression alters cellular protein levels thereby initiating changes in cell function, such as metabolic activity and cell fate.

activation of inappropriate sodium and fluid uptake [17]. Very high levels of cortisol such as in conditions like Cushing's disease can overwhelm 11βHSD2 and cause in-appropriate hypertension. Treatments for hypertension have been developed that target the MR and this cardiovascular condition can now be well-controlled by specific MR antagonist drugs such as spironolactone and a newer drug eplerenone [18,19]. Aldosterone may also have other functional roles in tissues such as the brain where the MR is expressed in neural centres controlling thirst and appetite, but the mechanisms involved are not well understood [20].

3.3. The glucocorticoid steroids

The steroid cortisol is an essential mediator of the systemic stress response, yet plays major roles in many different physiological contexts and at different times during fetal and adult life [21]. Cortisol has a powerful effect on various arms of the immune system, and the development of strong synthetic glucocorticoid compounds such as dexamethasone and prednisolone more than 50 years ago have made them a mainstay for the clinical treatment of a range of inflammatory and autoimmune conditions [22]. Cortisol circulates in the bloodstream in a circadian fashion, with levels high in the morning and low in the evening, and release from the adrenal is tightly controlled by direct negative feedback to the hypothalamus and anterior pituitary where there is inhibition of corticotrophin-releasing hormone and adrenocorticotropic hormone, respectively.

Glucocorticoid steroids contribute to metabolic regulation as a catabolic hormone. They stimulate protein breakdown to release amino acids that can be utilised in hepatic gluconeogenesis to produce glucose, the breakdown of glycogen and the release of fatty acids from adipose depots. However, inappropriately elevated circulating cortisol (ie, in a 'Cushingoid' state) or synthetic glucocorticoids (eg, prednisolone) can stimulate excess hepatic glucose output leading to hyperglycemia and the development of diabetic states. These broad actions of glucocorticoids are mediated by the ubiquitous expression of its cognate receptor, the glucocorticoid receptor (GR) [23]. This is in contrast to the MR which has a much more restricted expression pattern in the body. Chronic high levels of cortisol can therefore lead to systemic effects that represent Cushing's disease, with remodelling of adipose depots, hyperglycemia, type-2 diabetes, high blood pressure, muscle wasting and bone remodelling leading to osteoporosis.

As part of the response to stress, cortisol has a profound effect on the brain. Stress from a range of causes (trauma, infection, fear, pain etc.) triggers the hypothalamus-pituitary-adrenal axis to release cortisol [21]. Elevated circulating cortisol seems to play two major roles: 1) promoting or preparing permissive effects to respond to the stressor,

reductase (SDR) relationships: a large family with eight clusters common to human, animal, and plant genomes. Protein Sci Publ Protein Soc 2002;11(3):636–41.
[4] Young MJ, Clyne CD, Cole TJ, Funder JW. Cardiac steroidogenesis in the normal and failing heart. J Clin Endocrinol Metab 2001;86(11):5121–6.
[5] Falany CN. Enzymology of human cytosolic sulfotransferases. FASEB J : Offic Publ Fed Am Soc Exp Biol 1997;11(4):206–16.
[6] Gathercole LL, Lavery GG, Morgan SA, Cooper MS, Sinclair AJ, Tomlinson JW, Stewart PM. 11beta-hydroxysteroid dehydrogenase 1: translational and therapeutic aspects. Endocr Rev 2013;34(4):525–55.
[7] Cole TJ. Cloning of the mouse 11 beta-hydroxysteroid dehydrogenase type 2 gene: tissue specific expression and localization in distal convoluted tubules and collecting ducts of the kidney. Endocrinology 1995;136(10):4693–6.
[8] Wilson RC, Krozowski ZS, Li K, Obeyesekere VR, Razzaghy-Azar M, Harbison MD, Wei JQ, Shackleton CH, Funder JW, New MI. A mutation in the HSD11B2 gene in a family with apparent mineralocorticoid excess. J Clin Endocrinol Metab 1995;80(7):2263–6.
[9] Miller WL. Steroidogenesis: unanswered questions. Trends Endocrinol Metabol: TEM 2017;28(11):771–93.
[10] White PC, Speiser PW. Congenital adrenal hyperplasia due to 21-hydroxylase deficiency. Endocr Rev 2000;21(3):245–91.
[11] Shackleton C, Pozo OJ, Marcos J. GC/MS in recent years has defined the normal and clinically disordered steroidome: will it soon Be surpassed by LC/tandem MS in this role? J Endocr Soc 2018;2(8):974–96.
[12] Simpson ER, Mahendroo MS, Means GD, Kilgore MW, Hinshelwood MM, Graham-Lorence S, Amarneh B, Ito Y, Fisher CR, Michael MD, et al. Aromatase cytochrome P450, the enzyme responsible for estrogen biosynthesis. Endocr Rev 1994;15(3):342–55.
[13] Simpson ER, Mahendroo MS, Means GD, Kilgore MW, Corbin CJ, Mendelson CR. Tissue-specific promoters regulate aromatase cytochrome P450 expression. J Steroid Biochem Mol Biol 1993;44(4–6):321–30.
[14] Russell DW, Wilson JD. Steroid 5 alpha-reductase: two genes/two enzymes. Annu Rev Biochem 1994;63:25–61.
[15] Rogerson FM, Fuller PJ. Mineralocorticoid action. Steroids 2000;65(2):61–73.
[16] Hattangady NG, Olala LO, Bollag WB, Rainey WE. Acute and chronic regulation of aldosterone production. Mol Cell Endocrinol 2012;350(2):151–62.
[17] Funder JW, Pearce PT, Smith R, Smith AI. Mineralocorticoid action: target tissue specificity is enzyme, not receptor, mediated. Science 1988;242(4878):583–5.
[18] Pitt B, Zannad F, Remme WJ, Cody R, Castaigne A, Perez A, Palensky J, Wittes J. The effect of spironolactone on morbidity and mortality in patients with severe heart failure. Randomized aldactone evaluation study investigators. N Engl J Med 1999;341(10):709–17.
[19] Zannad F, McMurray JJ, Krum H, van Veldhuisen DJ, Swedberg K, Shi H, Vincent J, Pocock SJ, Pitt B, Group E-HS. Eplerenone in patients with systolic heart failure and mild symptoms. N Engl J Med 2011;364(1):11–21.
[20] Geerling JC, Loewy AD. Aldosterone in the brain. Am J Physiol Renal Physiol 2009;297(3):F559–76.
[21] Sapolsky RM, Romero LM, Munck AU. How do glucocorticoids influence stress responses? Integrating permissive, suppressive, stimulatory, and preparative actions. Endocr Rev 2000;21(1):55–89.
[22] Barnes PJ. Anti-inflammatory actions of glucocorticoids: molecular mechanisms. Clin Sci 1998;94(6):557–72.
[23] Lu NZ, Cidlowski JA. Glucocorticoid receptor isoforms generate transcription specificity. Trends Cell Biol 2006;16(6):301–7.
[24] Liggins GC. The role of cortisol in preparing the fetus for birth. Reprod Fertil Dev 1994;6(2):141–50.
[25] Bird AD, McDougall AR, Seow B, Hooper SB, Cole TJ. Glucocorticoid regulation of lung development: lessons learned from conditional GR knockout mice. Mol Endocrinol 2015;29(2):158–71.
[26] Robinson-Rechavi M, Escriva Garcia H, Laudet V. The nuclear receptor superfamily. J Cell Sci 2003;116(Pt 4):585–6.
[27] Linja MJ, Porkka KP, Kang Z, Savinainen KJ, Janne OA, Tammela TL, Vessella RL, Palvimo JJ, Visakorpi T. Expression of androgen receptor coregulators in prostate cancer. Clin Cancer Res : Offic J Am Associat Canc Res 2004;10(3):1032–40.
[28] Amoutzias GD, Pichler EE, Mian N, De Graaf D, Imsiridou A, Robinson-Rechavi M, Bornberg-Bauer E, Robertson DL, Oliver SG. A protein interaction atlas for the nuclear receptors: properties and quality of a hub-based dimerisation network. BMC Syst Biol 2007;1:34.
[29] Mullican SE, Dispirito JR, Lazar MA. The orphan nuclear receptors at their 25-year reunion. J Mol Endocrinol 2013;51(3):T115–40.
[30] Greaves RF, Wudy SA, Badoer E, Zacharin M, Hirst JJ, Quinn T, Walker DW. A tale of two steroids: the importance of the androgens DHEA and DHEAS for early neurodevelopment. J Steroid Biochem Mol Biol 2019;188:77–85.
[31] Vuksan-Cusa B, Sagud M, Rados I. The role of dehydroepiandrosterone (DHEA) in schizophrenia. Psychiatr Danub 2016;28(1):30–3.
[32] Carvalho O, Goncalves C. Expression of oestrogen receptors in foetal lung tissue of mice. Anat Histol Embryol 2012;41(1):1–6.
[33] Plante J, Simard M, Rantakari P, Cote M, Provost PR, Poutanen M, Tremblay Y. Epithelial cells are the major site of hydroxysteroid (17beta) dehydrogenase 2 and androgen receptor expression in fetal mouse lungs during the period overlapping the surge of surfactant. J Steroid Biochem Mol Biol 2009;117(4–5):139–45.
[34] Simard M, Plante J, Boucher M, Provost PR, Tremblay Y. Type 2 and 5 17beta-hydroxysteroid dehydrogenases and androgen receptor in human fetal lungs. Mol Cell Endocrinol 2010;319(1–2):79–87.
[35] Boucher E, Provost PR, Tremblay Y. C21-steroids inactivation and glucocorticoid synthesis in the developing lung. J Steroid Biochem Mol Biol 2015;147:70–80.
[36] Wallace MJ, Hooper SB, Harding R. Role of the adrenal glands in the maturation of lung liquid secretory mechanisms in fetal sheep. Am J Physiol 1996;270(1 Pt 2):R33–40.
[37] Oakley RH, Cidlowski JA. The biology of the glucocorticoid receptor: new signaling mechanisms in health and disease. J Allergy Clin Immunol 2013;132(5):1033–44.
[38] Seow BKL, McDougall ARA, Short KL, Wallace MJ, Hooper SB, Cole TJ. Identification of betamethasone regulated target genes and cell pathways in fetal rat lung mesenchymal fibroblasts. Endocrinology 2019. in press Accepted May 20. pii: en.2018-01071. doi: 10.1210/en.2018-01071.
[39] Sangild PT. Stimulation of gastric proteases in the neonatal pig by a rise in adrenocortical secretion at parturition. Reprod Fertil Dev 1995;7(5):1293–8.
[40] Sangild PT, Sjostrom H, Noren O, Fowden AL, Silver M. The prenatal development and glucocorticoid control of brush-border hydrolases in the pig small intestine. Pediatr Res 1995;37(2):207–12.
[41] Dallman MF, Engeland WC, Rose JC, Wilkinson CW, Shinsako J, Siedenburg F. Nycthemeral rhythm in adrenal responsiveness to ACTH. Am J Physiol 1978;235(5):R210–8.
[42] Buttgereit F, Brand MD, Burmester GR. Equivalent doses and relative drug potencies for non-genomic glucocorticoid effects: a novel glucocorticoid hierarchy. Biochem Pharmacol 1999;58(2):363–8.
[43] Liggins GC, Howie RN. A controlled trial of antepartum glucocorticoid treatment for prevention of the respiratory distress syndrome in premature infants. Pediatrics 1972;50(4):515–25.
[44] Cheong JL, Burnett AC, Lee KJ, Roberts G, Thompson DK, Wood SJ, Connelly A, Anderson PJ, Doyle LW. Victorian Infant Collaborative Study G. Association between postnatal dexamethasone for treatment of bronchopulmonary dysplasia and brain volumes at adolescence in infants born very preterm. J Pediatr 2014;164(4):737–43. e731.
[45] Crowley PA. Antenatal corticosteroid therapy: a meta-analysis of the randomized trials, 1972 to 1994. Am J Obstet Gynecol 1995;173(1):322–35.
[46] Guidelines-Panel. Antenatal corticosteroids given to women prior to birth to improve fetal, infant, child and adult health: clinical Practice Guidelines. Auckland. New Zealand: Liggins Institute, The University of Auckland; 2015.
[47] Bird AD, Tan KH, Olsson PF, Zieba M, Flecknoe SJ, Liddicoat DR, Mollard R, Hooper SB, Cole TJ. Identification of glucocorticoid-regulated genes that control cell proliferation during murine respiratory development. J Physiol 2007;585(Pt 1):187–201.
[48] Bird AD, Choo YL, Hooper SB, McDougall AR, Cole TJ. Mesenchymal glucocorticoid receptor regulates the development of multiple cell layers of the mouse lung. Am J Respir Cell Mol Biol 2014;50(2):419–28.
[49] Carson R, Monaghan-Nichols AP, DeFranco DB, Rudine AC. Effects of antenatal glucocorticoids on the developing brain. Steroids 2016;114:25–32.
[50] Fortin-Pellerin E, Petersen C, Lefebvre F, Barrington KJ, Janvier A. Evolving neonatal steroid prescription habits and patient outcomes. Acta Paediatr 2013;102(8):799–804.
[51] Dalziel SR, Rea HH, Walker NK, Parag V, Mantell C, Rodgers A, et al. Long term effects of antenatal betamethasone on lung function: 30 year follow up of a randomised controlled trial. Thorax 2006;61(8):678–83.